

Lipids and Membranes

CHAPTER 12

1 Lipid Classification

- A. Fatty Acids
- B. Triacylglycerols
- C. Glycerophospholipids
- D. Sphingolipids
- E. Cholesterol

2 Properties of Lipid Aggregates

- A. Micelles and Bilayers
- B. Liposomes
- C. Bilayer Dynamics

3 Biological Membranes

- A. Membrane Proteins
- B. Lipid-Linked Proteins
- C. Fluid Mosaic Model of Membrane Structure
- D. The Erythrocyte Membrane
- E. Blood Groups
- F. Gap Junctions
- G. Channel-Forming Proteins

4 Membrane Assembly and Protein Targeting

- A. Lipid Distributions in Membranes
- B. The Secretory Pathway
- C. Vesicle Formation
- D. Vesicle Fusion
- E. Protein Targeting to Mitochondria

5 Lipoproteins

- A. Lipoprotein Structure
- B. Lipoprotein Function
- C. Lipoprotein Dysfunction in Atherosclerosis and Alzheimer's Disease

Membranes function to organize biological processes by compartmentalizing them. Indeed, the cell, the basic unit of life, is essentially defined by its enveloping plasma membrane. Moreover, in eukaryotes, many subcellular organelles, such as nuclei, mitochondria, chloroplasts, the endoplasmic reticulum, and the Golgi apparatus (Fig. 1-5), are likewise membrane bounded.

Biological membranes are organized assemblies of lipids and proteins with small amounts of carbohydrate. Yet they are not impermeable barriers to the passage of materials. Rather, they regulate the composition of the intracellular medium by controlling the flow of nutrients, waste products, ions, etc., into and out of the cell. They do this through membrane-embedded “pumps” and “gates” that transport specific substances against an electrochemical gradient or permit their passage with such a gradient (Chapter 20).

Many fundamental biochemical processes occur on or in a membranous scaffolding. For example, electron transport and oxidative phosphorylation (Chapter 22), processes that oxidize nutrients with the concomitant generation of ATP, are mediated by an organized battery of enzymes that are components of the inner mitochondrial membrane. Likewise, photosynthesis, in which light energy powers the chemical combination of H₂O and CO₂ to form carbohydrates (Chapter 24), occurs in the inner membranes of chloroplasts. The processing of information, such as sensory stimuli or intercellular communications, is generally a membrane-based phenomenon. Thus nerve impulses are mediated by nerve cell membranes (Section 20-5) and the presence of certain substances such as hormones and nutrients is detected by specific membrane-bound receptors (Chapter 19).

In this chapter, we examine the compositions, structures, and formation of biological membranes and related substances. Specific membrane-based biochemical processes, such as those mentioned above, are dealt with in later chapters.

1 LIPID CLASSIFICATION

Lipids (Greek: *lipos*, fat) are substances of biological origin that are soluble in organic solvents such as chloroform and methanol but are only sparingly soluble, if at all, in water. Hence, they are easily separated from other biological materials by extraction into organic solvents and may be further fractionated by such techniques as adsorption chromatography, thin layer chromatography, and reverse-phase chromatography (Section 6-3D). Fats, oils, certain vitamins and hormones, and most nonprotein membrane components are lipids. In this section, we discuss the structures and physical properties of the major classes of lipids.

A. Fatty Acids

Fatty acids are carboxylic acids with long-chain hydrocarbon side groups (Fig. 12-1). They are rarely free in nature but, rather, occur in esterified form as the major components of the various lipids described in this chapter. The more common biological fatty acids are listed in Table 12-1. In higher plants and animals, the predominant fatty acid residues are those of the C₁₆ and C₁₈ species **palmitic**, **oleic**, **linoleic**, and **stearic acids**. Fatty acids with <14 or >20 carbon atoms are uncommon. *Most fatty acids have an even number of carbon*

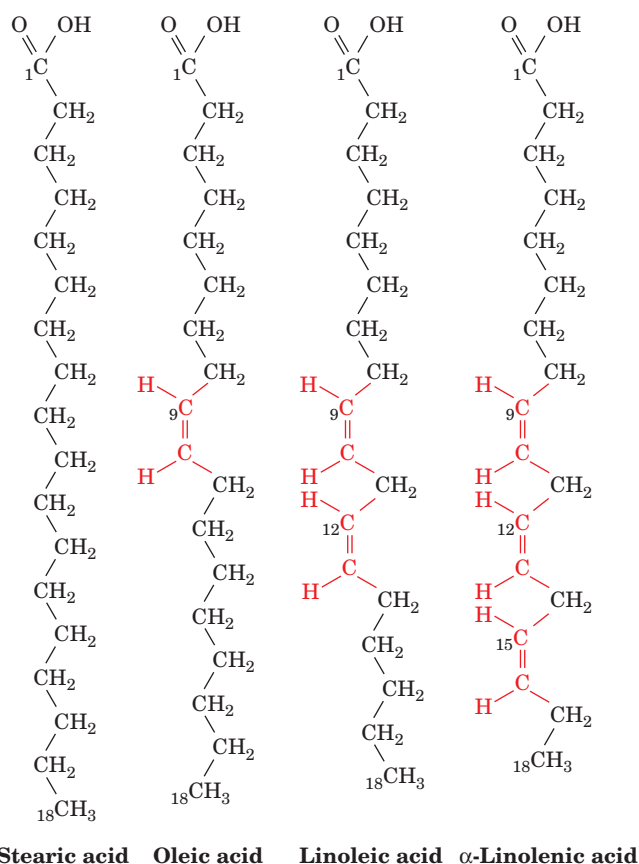


Figure 12-1 Structural formulas of some C_{18} fatty acids. The double bonds all have the cis configuration.

atoms because they are usually biosynthesized by the concatenation of C_2 units (Section 25-4C). Over half of the fatty acid residues of plant and animal lipids are unsaturated (contain double bonds) and are often polyunsaturated (contain two or more double bonds). Bacterial fatty acids are rarely polyunsaturated but are commonly branched, hydroxylated, or contain cyclopropane rings. Unusual fatty acids also occur as components of the oils and **waxes** (esters of fatty acids and long-chain alcohols) produced by certain plants.

a. The Physical Properties of Fatty Acids Vary with Their Degree of Unsaturation

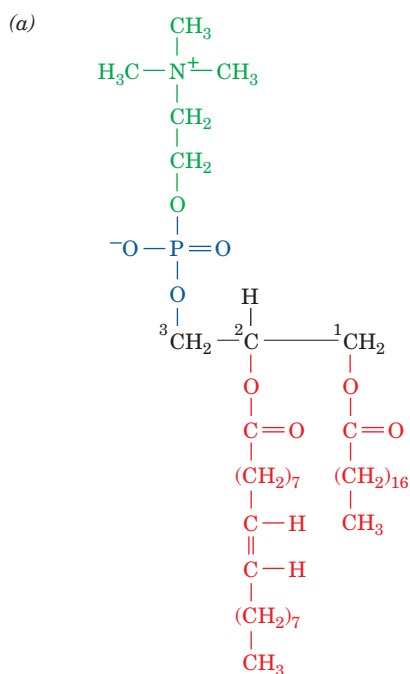
Table 12-1 indicates that the first double bond of an unsaturated fatty acid commonly occurs between its C_9 and C_{10} atoms counting from the carboxyl C atom (a Δ^9 - or 9-double bond). In polyunsaturated fatty acids, the double bonds tend to occur at every third carbon atom toward the methyl terminus of the molecule (such as $-\text{CH}=\text{CH}-\text{CH}_2-\text{CH}=\text{CH}-$). Double bonds in polyunsaturated fatty acids are almost never conjugated (as in $-\text{CH}=\text{CH}-\text{CH}=\text{CH}-$). Triple bonds rarely occur in fatty acids or any other compound of biological origin. Two important classes of polyunsaturated fatty acids are denoted $n-3$ (or $\omega-3$) and $n-6$ (or $\omega-6$) fatty acids. This nomenclature identifies the last double-bonded carbon atom as counted from the methyl terminal (ω) end of the chain.

Saturated fatty acids are highly flexible molecules that can assume a wide range of conformations because there is relatively free rotation about each of their $C-C$ bonds. Nevertheless, their fully extended conformation is that of minimum energy because this conformation has the least amount of

Table 12-1 The Common Biological Fatty Acids

Symbol ^a	Common Name	Systematic Name	Structure	mp (°C)
Saturated fatty acids				
12:0	Lauric acid	Dodecanoic acid	$\text{CH}_3(\text{CH}_2)_{10}\text{COOH}$	44.2
14:0	Myristic acid	Tetradecanoic acid	$\text{CH}_3(\text{CH}_2)_{12}\text{COOH}$	52
16:0	Palmitic acid	Hexadecanoic acid	$\text{CH}_3(\text{CH}_2)_{14}\text{COOH}$	63.1
18:0	Stearic acid	Octadecanoic acid	$\text{CH}_3(\text{CH}_2)_{16}\text{COOH}$	69.6
20:0	Arachidic acid	Eicosanoic acid	$\text{CH}_3(\text{CH}_2)_{18}\text{COOH}$	75.4
22:0	Behenic acid	Docosanoic acid	$\text{CH}_3(\text{CH}_2)_{20}\text{COOH}$	81
24:0	Lignoceric acid	Tetracosanoic acid	$\text{CH}_3(\text{CH}_2)_{22}\text{COOH}$	84.2
Unsaturated fatty acids (all double bonds are cis)				
16:1 $n-7$	Palmitoleic acid	9-Hexadecenoic acid	$\text{CH}_3(\text{CH}_2)_5\text{CH}=\text{CH}(\text{CH}_2)_7\text{COOH}$	-0.5
18:1 $n-9$	Oleic acid	9-Octadecenoic acid	$\text{CH}_3(\text{CH}_2)_7\text{CH}=\text{CH}(\text{CH}_2)_7\text{COOH}$	13.4
18:2 $n-6$	Linoleic acid	9,12-Octadecadienoic acid	$\text{CH}_3(\text{CH}_2)_4(\text{CH}=\text{CHCH}_2)_2(\text{CH}_2)_6\text{COOH}$	-9
18:3 $n-3$	α -Linolenic acid	9,12,15-Octadecatrienoic acid	$\text{CH}_3\text{CH}_2(\text{CH}=\text{CHCH}_2)_3(\text{CH}_2)_6\text{COOH}$	-17
18:3 $n-6$	γ -Linolenic acid	6,9,12-Octadecatrienoic acid	$\text{CH}_3(\text{CH}_2)_4(\text{CH}=\text{CHCH}_2)_3(\text{CH}_2)_3\text{COOH}$	
20:4 $n-4$	Arachidonic acid	5,8,11,14-Eicosatetraenoic acid	$\text{CH}_3(\text{CH}_2)_4(\text{CH}=\text{CHCH}_2)_4(\text{CH}_2)_2\text{COOH}$	-49.5
20:5 $n-3$	EPA	5,8,11,14,17-Eicosapentaenoic acid	$\text{CH}_3\text{CH}_2(\text{CH}=\text{CHCH}_2)_5(\text{CH}_2)_2\text{COOH}$	-54
22:6 $n-3$	DHA	4,7,10,13,16,19-Docosahexenoic acid	$\text{CH}_3\text{CH}_2(\text{CH}=\text{CHCH}_2)_6\text{CH}_2\text{COOH}$	
24:1 $n-9$	Nervonic acid	15-Tetracosenoic acid	$\text{CH}_3(\text{CH}_2)_7\text{CH}=\text{CH}(\text{CH}_2)_{13}\text{COOH}$	39

^aNumber of carbon atoms: number of double bonds. For unsaturated fatty acids, n is the number of carbon atoms, $n-x$ is the double-bonded carbon atom, and x is the number of that carbon atom counting from the methyl terminal (ω) end of the chain.



1-Stearoyl-2-oleoyl-3-phosphatidylcholine

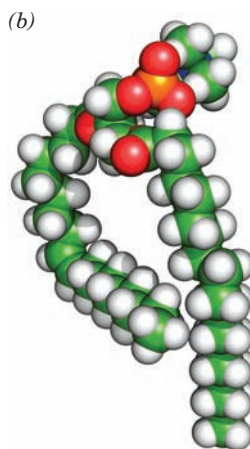
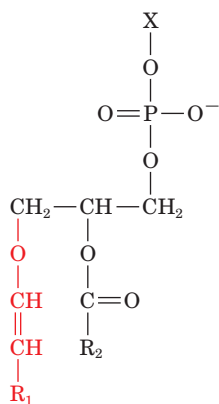


Figure 12-4 The glycerophospholipid 1-stearoyl-2-oleoyl-3-phosphatidylcholine. (a) Molecular formula in Fischer projection. (b) Energy-minimized space-filling model with C green, H white, N blue, O red, and P orange. Note how the unsaturated oleyl chain (left) is bent compared to the saturated stearoyl chain. [Based on coordinates provided by Richard Venable and Richard Pastor, NIH, Bethesda, Maryland.]

occur at the C1 position of glycerophospholipids, and the C2 position is often occupied by an unsaturated C₁₆ to C₂₀ fatty acid. Glycerophospholipids are, of course, also named according to the identities of these fatty acid residues (Fig. 12-4). Some glycerophospholipids have common names. For example, phosphatidylcholines are known as **lecithins**; diphosphatidylglycerols, the “double” glycerol phospholipids, are known as **cardiolipins** (because they were first isolated from heart muscle).

Plasmalogens



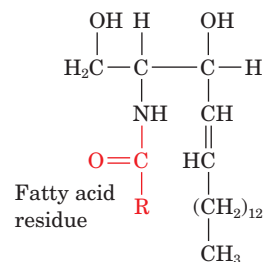
A plasmalogen

are glycerophospholipids in which the C1 substituent to the glycerol moiety is bonded to it via an α,β -unsaturated ether linkage in the *cis* configuration rather than through

an ester linkage. **Ethanolamine, choline,** and serine form the most common plasmalogen head groups.

D. Sphingolipids

Sphingolipids, which are also major membrane components, are derivatives of the C₁₈ amino alcohols **sphingosine, dihydrosphingosine** (Fig. 12-5), and their C₁₆, C₁₇, C₁₉, and C₂₀ homologs. Their *N*-acyl fatty acid derivatives, **ceramides**,



A ceramide

occur only in small amounts in plant and animal tissues but form the parent compounds of more abundant sphingolipids:

1. Sphingomyelins, the most common sphingolipids, are ceramides bearing either a phosphocholine (Fig. 12-6) or a phosphoethanolamine moiety, so that they can also be classified as **sphingophospholipids**. *Although sphingomyelins*

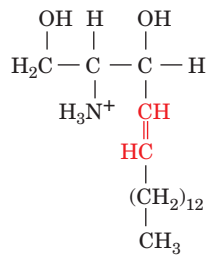
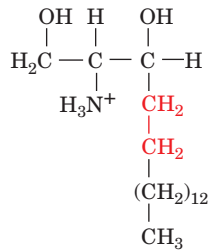
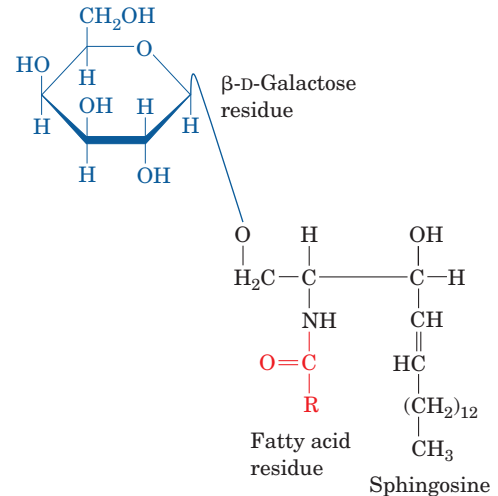
**Sphingosine****Dihydrosphingosine**

Figure 12-5 Molecular formulas of sphingosine and dihydrosphingosine. The chiral centers at C2 and C3 of sphingosine and dihydrosphingosine have the configurations shown in Fischer projection. The double bond in sphingosine has the trans configuration.

differ chemically from phosphatidylcholine and phosphatidylethanolamine, their conformations and charge distributions are quite similar. The membranous myelin sheath that surrounds and electrically insulates many nerve cell axons (Section 20-5Bc) is particularly rich in sphingomyelin.

2. Cerebrosides, the simplest **sphingoglycolipids** (alternatively **glycosphingolipids**), are ceramides with head groups that consist of a single sugar residue. **Galactocerebrosides**, which are most prevalent in the neuronal cell membranes of the brain, have a β -D-galactose head group.

**A galactocerebroside**

Glucocerebrosides, which instead have a β -D-glucose residue, occur in the membranes of other tissues. *Cerebrosides, in contrast to phospholipids, lack phosphate groups and hence are most frequently nonionic compounds.* The galactose residues of some galactocerebrosides, however, are sulfated at their C3 positions to form ionic compounds known as **sulfatides**. More complex sphingoglycolipids have unbranched oligosaccharide head groups of up to four sugar residues.

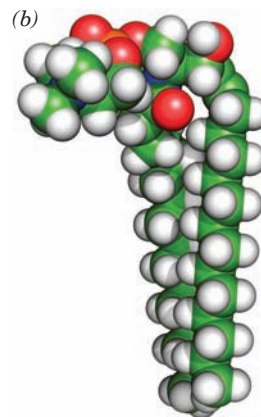
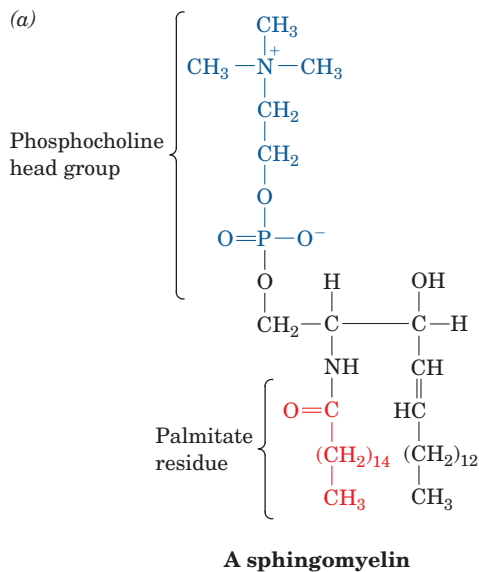


Figure 12-6 A sphingomyelin. (a) Molecular formula in Fischer projection. (b) Energy-minimized space-filling model with C green, H white, N blue, O red, and P orange. Note its conformational resemblance to glycerophospholipids (Fig. 12-4). [Based on coordinates provided by Richard Venable and Richard Pastor, NIH, Bethesda, Maryland.]

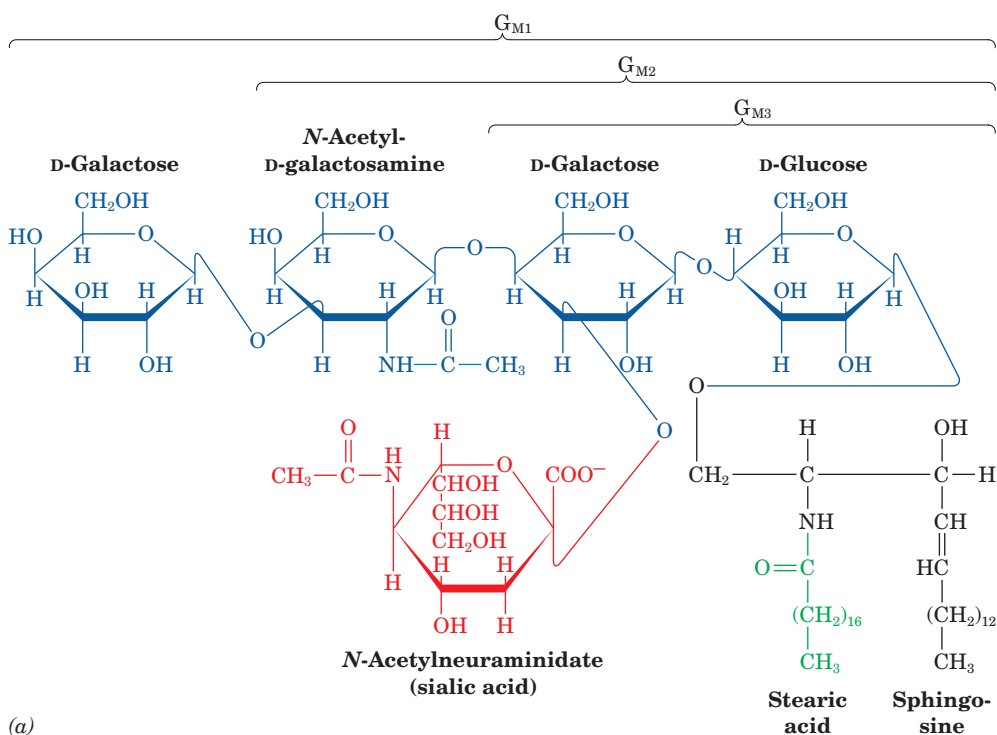


Figure 12-7 Ganglioside G_{M1} . (a) Structural formula with its sphingosine residue in Fischer projection. (b) Energy-minimized space-filling model with C green, H white, N blue, O red, and P orange. Gangliosides G_{M2} and G_{M3} differ from G_{M1} only by the

sequential absences of the terminal D-galactose and *N*-acetyl-D-galactosamine residues. Other gangliosides have different oligosaccharide head groups. [Based on coordinates provided by Richard Venable and Richard Pastor, NIH, Bethesda, Maryland.]

3. Gangliosides form the most complex group of sphingoglycolipids. They are ceramide oligosaccharides that include among their sugar groups at least one sialic acid residue (*N*-acetylneuraminic acid and its derivatives; Section 11-1Cc). The structures of gangliosides G_{M1} , G_{M2} , and G_{M3} , three of the hundreds that are known, are shown in Fig. 12-7. Gangliosides are primarily components of cell-surface membranes and constitute a significant fraction (6%) of brain lipids. Other tissues also contain gangliosides but in lesser amounts.

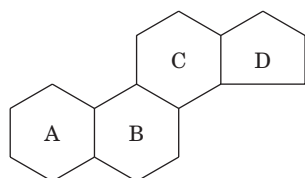
Gangliosides have considerable physiological and medical significance. Their complex carbohydrate head groups, which extend beyond the surfaces of cell membranes, act as specific receptors for certain pituitary glycoprotein hor-

mones that regulate a number of important physiological functions (Section 19-1). Gangliosides are also receptors for bacterial protein toxins such as cholera toxin (Section 19-2Cd). There is considerable evidence that gangliosides are specific determinants of cell-cell recognition, so they probably have an important role in the growth and differentiation of tissues as well as in carcinogenesis (cancer generation). Disorders of ganglioside breakdown are responsible for several hereditary **sphingolipid storage diseases**, such as **Tay-Sachs disease**, which are characterized by an invariably fatal neurological deterioration (Section 25-8Ce).

E. Cholesterol

Steroids, which are mostly of eukaryotic origin, are derivatives of **cyclopentanoperhydrophenanthrene** (Fig. 12-8). The much maligned **cholesterol** (Fig. 12-9), the most abundant steroid in animals, is further classified as a **sterol** because of its C3-OH group and its branched aliphatic side chain of 8 to 10 carbon atoms at C17.

Cholesterol is a major component of animal plasma membranes, where it is typically present at 30 to 40 mol %, and occurs in lesser amounts in the membranes of their subcellular organelles. Its polar OH group gives it a weak amphiphilic character, whereas its fused ring system provides it with greater rigidity than other membrane lipids. Cholesterol is therefore an important determinant of membrane



Cyclopentanoperhydrophenanthrene

Figure 12-8 Cyclopentanoperhydrophenanthrene, the parent compound of steroids. It consists of four fused saturated rings. The standard ring labeling system is indicated.

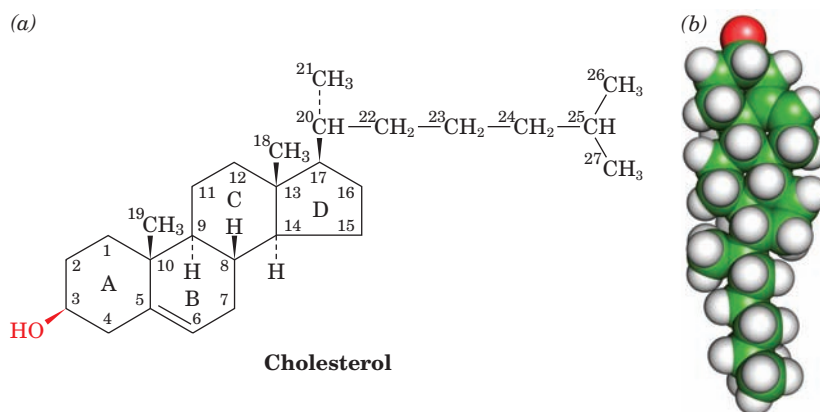
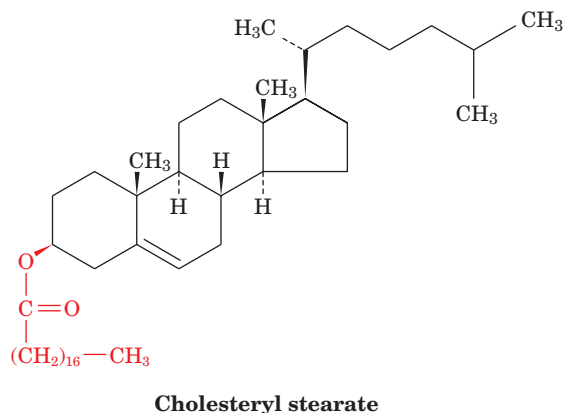


Figure 12-9 Cholesterol. (a) Structural formula with the standard numbering system. (b) Energy-minimized space-filling model with C green, H white, O red, and P orange. Cholesterol's rigid ring system makes it far less conformationally flexible than are

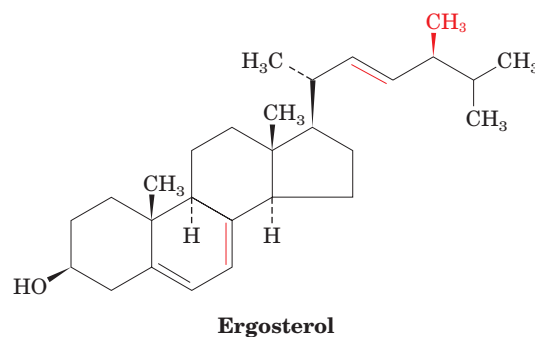
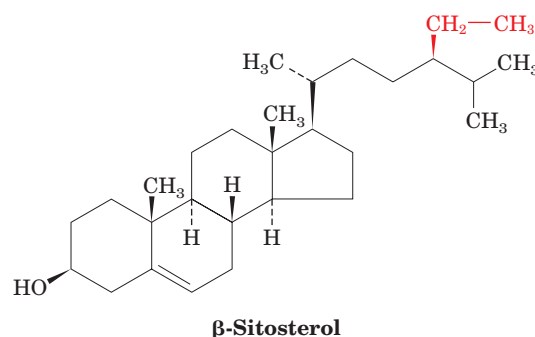
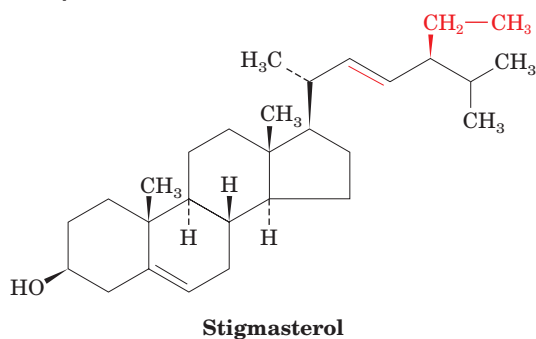
membrane lipids: Its cyclohexane rings can adopt either the boat or the chair conformations (Fig. 11-6) but the chair conformation is highly preferred. [Based on coordinates provided by Richard Venable and Richard Pastor, NIH, Bethesda, Maryland.]

properties. It is also abundant in blood plasma lipoproteins (Section 12-5), where ~70% of it is esterified to long-chain fatty acids to form **cholesteryl esters**.



Cholesterol is the metabolic precursor of **steroid hormones**, substances that regulate a great variety of physiological functions including sexual development and carbohydrate metabolism (Section 19-1G). The much-debated role of cholesterol in heart disease is examined in Section 12-5C. Cholesterol metabolism and the biosynthesis of steroid hormones are discussed in Section 25-6.

Plants contain little cholesterol. Rather, the most common sterol components of their membranes are **stigmasterol** and **β -sitosterol**



which differ from cholesterol only in their aliphatic side chains. Yeast and fungi have yet other membrane sterols such as **ergosterol**, which has a C7 to C8 double bond. Prokaryotes, with the exception of mycoplasmas (Section 1-1B), contain little, if any, sterol.

2 PROPERTIES OF LIPID AGGREGATES

The first recorded experiments on the physical properties of lipids were made in 1774 by the American statesman and scientist Benjamin Franklin. In investigating the well-known (at least among sailors) action of oil in calming waves, Franklin wrote:

At length being at Clapham [in London] where there is, on the common, a large pond, which I observed to be one day very

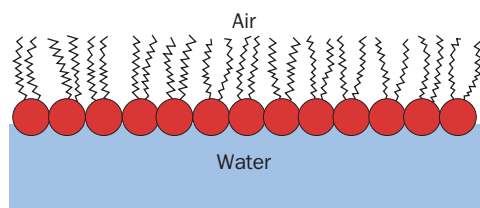


Figure 12-10 An oil monolayer at the air–water interface. The hydrophobic tails of the lipids avoid association with water by extending into the air.

rough with the wind, I fetched out a cruet of oil [probably olive oil] and dropt a little of it in the water. I saw it spread itself with surprising swiftness upon the surface. . . . I then went to the windward side, where [the waves] began to form; and there the oil, though not more than a teaspoonful, produced an instant calm over a space several yards square, which spread amazingly, and extended itself gradually till it reached the lee side, making all that quarter of the pond, perhaps half an acre, as smooth as a looking glass.

This is sufficient information to permit the calculation of the oil layer's thickness (although there is no indication that Franklin made this calculation, we can; see Problem 4). We now know that oil forms a monomolecular layer on the surface of water in which the polar heads of the amphiphilic oil molecules are immersed in the water and their hydrophobic tails extend into the air (Fig. 12-10).

The calming effect of oil on rough water is a consequence of a large reduction in the water's surface tension. An oily surface film has the weak intermolecular cohesion characteristic of hydrocarbons rather than the strong intermolecular attractions of water responsible for its normally large surface tension. Oil, nevertheless, calms only smaller waves; it does not, as Franklin later observed, affect the larger swells.

In this section, we discuss how lipids aggregate to form micelles and bilayers. We shall also be concerned with the physical properties of lipids in bilayers because these aggregates form the structural basis for biological membranes.

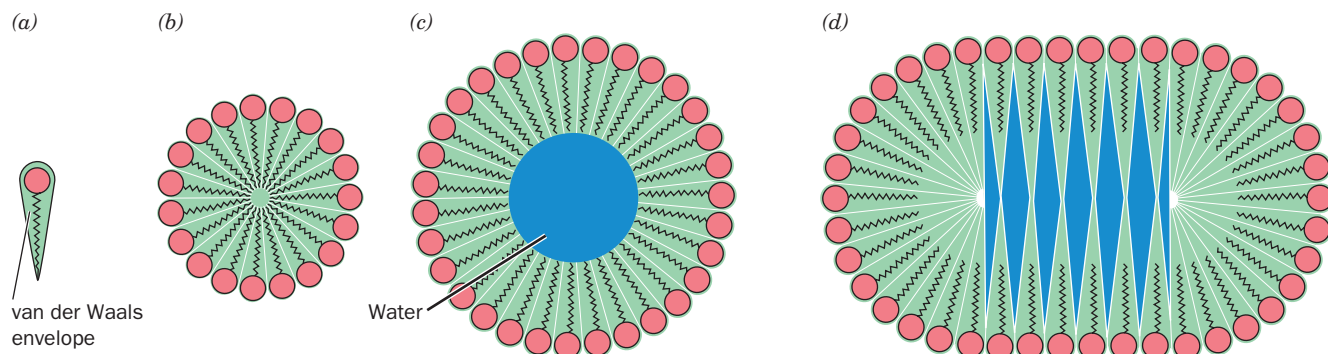


Figure 12-11 Aggregates of single-tailed lipids. The conical van der Waals envelope of single-tailed lipids (a) permits them to pack efficiently in forming a spheroidal micelle (b). The diameters of these micelles and hence their lipid population largely depend on the length of the tails. Spheroidal micelles

A. Micelles and Bilayers

In aqueous solutions, amphiphilic molecules, such as soaps and detergents, form micelles (globular aggregates whose hydrocarbon groups are out of contact with water; Section 2-1Ba). This molecular arrangement eliminates unfavorable contacts between water and the hydrophobic tails of the amphiphiles and yet permits the solvation of the polar head groups. Micelle formation is a cooperative process: An assembly of just a few amphiphiles cannot shield its tails from contact with water. Consequently, dilute aqueous solutions of amphiphiles do not form micelles until their concentration surpasses a certain **critical micelle concentration (cmc)**. Above the cmc, almost all the added amphiphile aggregates to form micelles. The value of the cmc depends on the identity of the amphiphile and the solution conditions. For amphiphiles with relatively small single tails, such as dodecyl sulfate ion, $\text{CH}_3(\text{CH}_2)_{11}\text{OSO}_3^-$, the cmc is $\sim 1 \text{ mM}$. Those of biological lipids, most of which have two large hydrophobic tails, are generally $< 10^{-6} \text{ M}$.

a. Single-Tailed Lipids Tend to Form Micelles

The approximate size and shape of a micelle can be predicted from geometrical considerations. Single-tailed amphiphiles, such as soap anions, form spheroidal or ellipsoidal micelles because of their conical shapes (their hydrated head groups are wider than their tails; Fig. 12-11a,b). The number of molecules in such micelles depends on the amphiphile, but for many substances, it is on the order of several hundred. For a given amphiphile, these numbers span a narrow range: Less would expose the hydrophobic core of the micelle to water, whereas more would give the micelle an energetically unfavorable hollow center (Fig. 12-11c). Of course, a large micelle could flatten out to eliminate this hollow center, but the resulting decrease of curvature at the flattened surfaces would also generate empty spaces (Fig. 12-11d).

b. Glycerophospholipids and Sphingolipids Tend to Form Bilayers

The two hydrocarbon tails of glycerophospholipids and sphingolipids give these amphiphiles a more or less cylindrical

composed of many more lipid molecules than the optimal number would have an unfavorable water-filled center (blue) (c). Such micelles could flatten out to collapse the hollow center, but as such ellipsoidal micelles become elongated they also develop water-filled spaces (d).

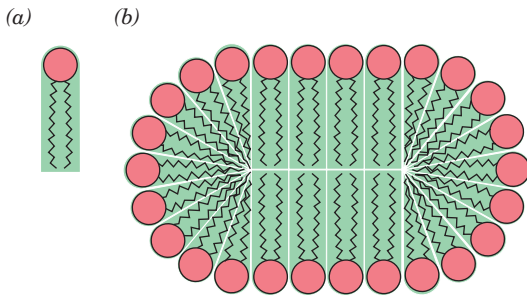
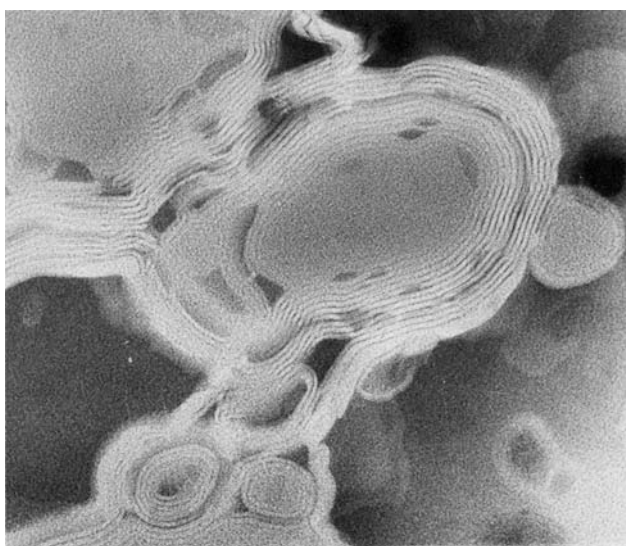


Figure 12-12 Bilayer formation by phospholipids. The cylindrical van der Waals envelope of phospholipids (a) causes them to form extended disklike micelles (b) that are better described as lipid bilayers.

shape (Fig. 12-12a). The steric requirements of packing such molecules together yields large disklike micelles (Fig. 12-12b) that are really extended bimolecular leaflets. The existence of such **lipid bilayers** was first proposed in 1925 by Evert Gorter and François Grendel, on the basis of their observation that lipids extracted from erythrocytes covered twice the area when spread as a monolayer at the air–water interface (Fig. 12-10) than in the erythrocyte plasma membrane (the erythrocyte’s only membrane). Lipid bilayers typically have thicknesses of $\sim 60 \text{ \AA}$, as measured by electron microscopy and X-ray diffraction techniques. Since their two head group layers are each expected to be $\sim 15 \text{ \AA}$ thick, their $\sim 15\text{-\AA}$ -long hydrocarbon tails must be nearly fully extended. We shall see below that *lipid bilayers form the structural basis of biological membranes*.



(a)

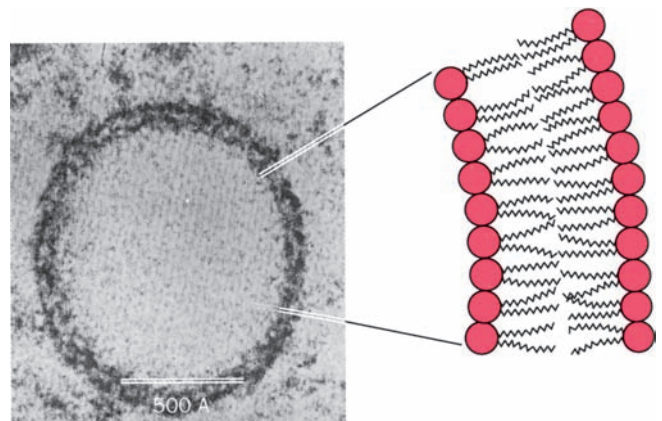
Figure 12-13 Lipid bilayers. (a) An electron micrograph of a multilamellar phospholipid vesicle in which each layer is a lipid bilayer. [Courtesy of Alec D. Bangham, Institute of Animal Physiology, Cambridge, U.K.] (b) An electron micrograph of a

B. Liposomes

A suspension of phospholipids in water forms multilamellar vesicles that have an onionlike arrangement of lipid bilayers (Fig. 12-13a). On **sonication** (agitation by ultrasonic vibrations), these structures rearrange to form **liposomes**—closed, self-sealing, solvent-filled vesicles that are bounded by only a single bilayer (Fig. 12-13b). They usually have diameters of several hundred Ångstroms and, in a given preparation, are rather uniform in size. Liposomes with diameters of $\sim 1000 \text{ \AA}$ can be made by injecting an ethanolic solution of phospholipid into water or by dissolving phospholipid in a detergent solution and then dialyzing out the detergent. Once formed, liposomes are quite stable and, in fact, may be separated from the solution in which they reside by dialysis, gel filtration chromatography, or centrifugation. Liposomes with differing internal and external environments can therefore be readily prepared. *Biological membranes consist of lipid bilayers with which proteins are associated* (Section 12-3A). Liposomes composed of synthetic lipids and/or lipids extracted from biological sources (e.g., lecithin from egg yolks) have therefore been extensively studied as models for biological membranes.

a. Lipid Bilayers Are Impermeable to Most Polar Substances

Since biological membranes form cell and organelle boundaries, it is important to determine their ability to partition two aqueous compartments. The permeability of a lipid bilayer to a given substance may be determined by forming liposomes in a solution containing the substance of interest, changing the external aqueous solution, and then measuring the rate at which the substance appears in the new external solution. It has been found in this way that *lipid bilayers are extraordinarily impermeable to ionic and polar substances and that the permeabilities of such substances increase with their solubilities in nonpolar solvents*. This suggests that to penetrate a lipid bilayer, a solute molecule must shed its hydration shell and become solvated by



(b)

liposome. Its wall, as the accompanying diagram indicates, consists of a bilayer. [Courtesy of Walter Stoeckenius, University of California at San Francisco.]

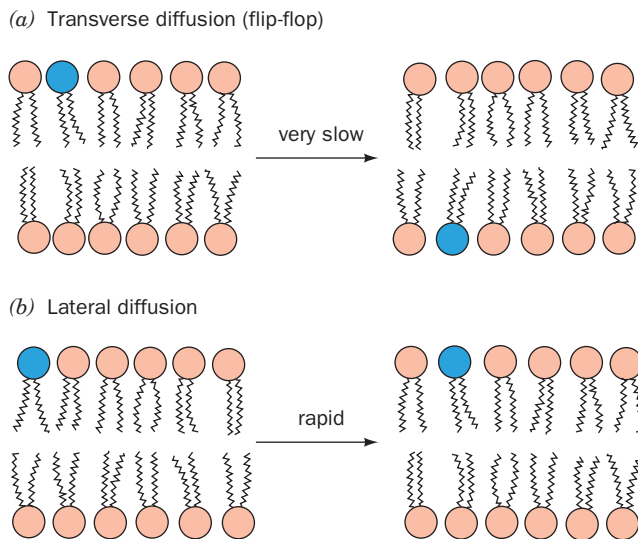


Figure 12-14 Phospholipid diffusion in a lipid bilayer.

(a) Transverse diffusion (flip-flop) is defined as the transfer of a phospholipid molecule from one bilayer leaflet to the other.
 (b) Lateral diffusion is defined as the pairwise exchange of neighboring phospholipid molecules in the same bilayer leaflet.

the bilayer's hydrocarbon core. Such a process is highly unfavorable for polar molecules, so that even the $\sim 30\text{-}\text{\AA}$ thickness of a lipid bilayer's hydrocarbon core forms an effective barrier for polar substances. However, measurements using tritiated water indicate that lipid bilayers are appreciably permeable to water. Despite the polarity of water, its small molecular size makes it significantly soluble in the hydrocarbon core of lipid bilayers and therefore able to permeate them.

The stability of liposomes and their impermeability to many substances make them promising vehicles for the delivery of therapeutic agents, such as drugs, enzymes, and genes

(for gene therapy), to particular tissues. Liposomes are absorbed by many cells through fusion with their plasma membranes. If methods can be developed for targeting liposomes to specific cell populations, then the desired substances could be directed toward particular tissues through liposome microencapsulation. Indeed, a number of liposome-delivered anticancer agents and antibiotics are already in use.

C. Bilayer Dynamics

a. Lipid Bilayers Are Two-Dimensional Fluids

The transfer of a lipid molecule across a bilayer (Fig. 12-14a), a process termed **transverse diffusion** or a **flip-flop**, is an extremely rare event. This is because a flip-flop requires the polar head group of the lipid to pass through the hydrocarbon core of the bilayer. The flip-flop rates of phospholipids, as measured by several techniques, are characterized by half-times that are minimally several days.

In contrast to their low flip-flop rates, *lipids are highly mobile in the plane of the bilayer (lateral diffusion, Fig. 12-14b)*. The X-ray diffraction patterns of bilayers at physiological temperatures have a diffuse band, centered at a spacing of 4.6 \AA , whose width is a measure of the distribution of lateral spacings between the hydrocarbon chains in the bilayer plane. This band, which resembles one in the X-ray diffraction patterns of liquid paraffins, is indicative that *the bilayer is a two-dimensional fluid in which the hydrocarbon chains undergo rapid fluxional (continuously changing) motions involving rotations about their C—C bonds*.

The lateral diffusion rate of lipid molecules can be quantitatively determined from the rate of **fluorescence recovery after photobleaching (FRAP; Fig. 12-15)**. A fluorescent group (**fluorophore**) is specifically attached to a bilayer component, and an intense laser pulse focused on a very small area ($\sim 3\text{ }\mu\text{m}^2$) is used to destroy (bleach) the fluorophore there. The rate at which the bleached area recovers its fluorescence, as monitored by fluorescence microscopy,

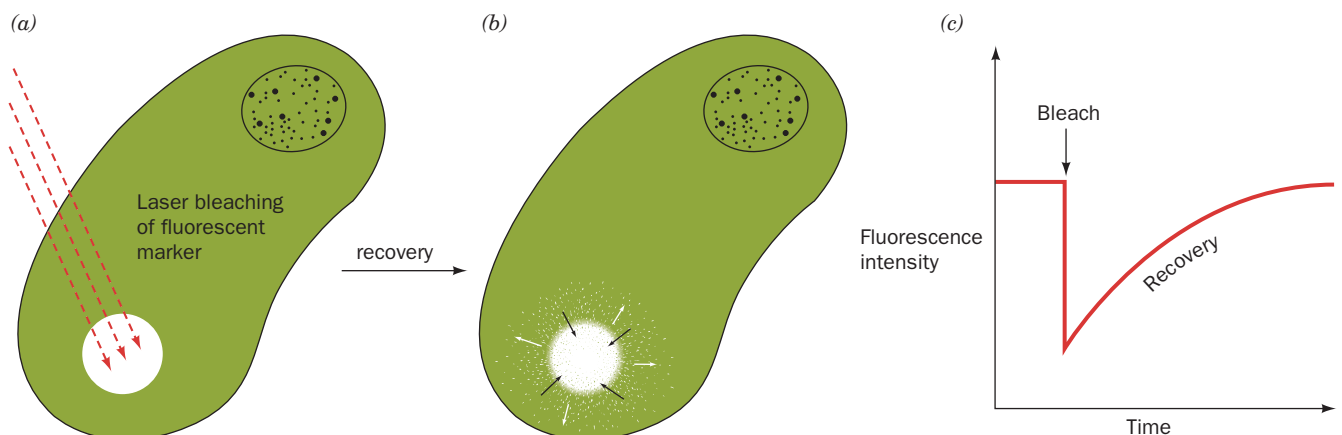


Figure 12-15 The fluorescence recovery after photobleaching (FRAP) technique. (a) An intense laser light pulse bleaches the fluorescent markers (green) from a small region of an immobilized cell that has a fluorescence-labeled membrane component. (b) The fluorescence of the bleached area, as monitored by

fluorescence microscopy, recovers as the bleached molecules laterally diffuse out of it and intact fluorescence-labeled molecules diffuse into it. (c) The fluorescence recovery rate depends on the diffusion rate of the labeled molecule. **See Guided Exploration 11: Membrane structure and the fluid mosaic model**

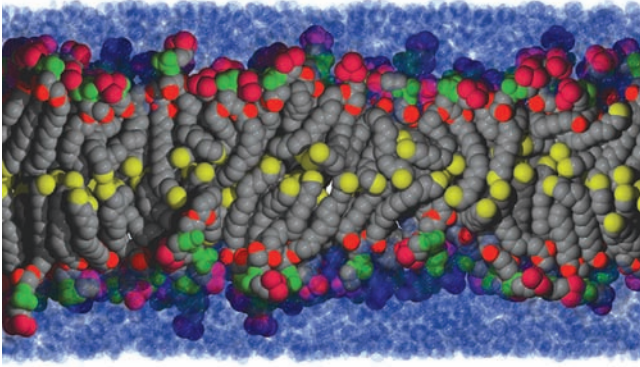



Figure 12-16 Model (snapshot) of a lipid bilayer at an instant in time. The conformations of dipalmitoylphosphatidylcholine molecules in a bilayer surrounded by water were modeled by computer. Atom colors are chain and glycerol C gray except terminal methyl C yellow, ester O red, phosphate P and O green, and choline C and N magenta. Water molecules are represented by translucent blue spheres (those near the bilayer appear dark because they overlap head group atoms). [Courtesy of Richard Pastor and Richard Venable, NIH, Bethesda, Maryland.]  **See Guided Exploration 11: Membrane structure and the fluid mosaic model**

indicates the rate at which unbleached and bleached fluorescence-labeled molecules laterally diffuse into and out of the bleached area, respectively. Such observations indicate, as do magnetic resonance measurements, that lipids in bilayers have lateral mobilities similar to those of the molecules in a light machine oil. Lipids in bilayers can therefore diffuse the $1\text{-}\mu\text{m}$ length of a bacterial cell in ~ 1 s. Methods for tracking the motions of single molecules in membranes have also been developed that link the molecule of interest to a small latex bead, colloidal gold particle, or fluorescent group, and then observe the movement of the label using high speed video techniques.

Molecular dynamics simulations (Section 9-4a) of lipid bilayers (Fig. 12-16) indicate that their lipid tails are highly

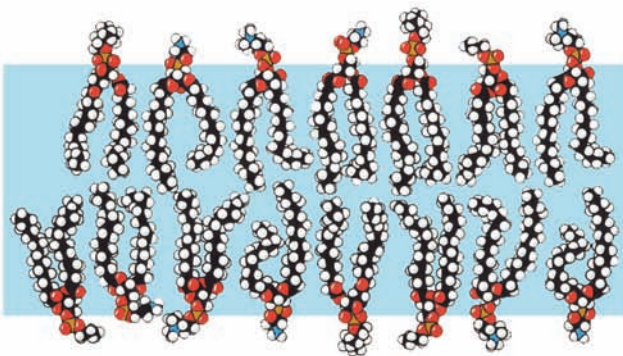
conformationally mobile due to rotations about their C—C bonds. However, the viscosity of these tails sharply increases closer to the lipid head groups because their lateral mobilities are more constrained by interactions with the more rigid head groups. Note that the methyl ends of the tails from opposite leaflets of the bilayer are frequently interdigitated rather than forming entirely separate layers, as Fig. 12-14 might be taken to suggest. This is particularly true in biological membranes because their various lipid molecules have tails of different lengths and/or are kinked due to the presence of double bonds. Molecular dynamics simulations also indicate that a lipid bilayer is flanked by several layers of ordered water molecules. Moreover, as Fig. 12-16 indicates, water molecules commonly penetrate well below the level of the head groups and glycerol residues. Hence, *a lipid bilayer typically consists of an $\sim 30\text{-}\text{\AA}$ -thick hydrocarbon core bounded on both sides by $\sim 15\text{-}\text{\AA}$ -thick interface regions containing rapidly fluctuating conglomerations of head groups, water, glycerol, carbonyl, and methylene groups.*

b. Bilayer Fluidity Varies with Temperature

As a lipid bilayer cools below a characteristic **transition temperature**, it undergoes a sort of phase change, termed an **order–disorder transition**, in which it becomes a gel-like solid (Fig. 12-17); that is, it loses its fluidity. Below the transition temperature, the diffuse $4.6\text{-}\text{\AA}$ X-ray diffraction band characteristic of the lateral spacing between hydrocarbon chains in a liquid-crystalline bilayer is replaced by a sharp $4.2\text{-}\text{\AA}$ band similar to that exhibited by crystalline paraffins. This indicates that the hydrocarbon chains in a bilayer become fully extended and packed in a hexagonal array as in crystalline paraffins.

The transition temperature of a bilayer increases with the chain length and the degree of saturation of its component fatty acid residues for the same reasons that the melting temperatures of fatty acids increase with these quantities. The transition temperatures of most biological membranes are

(a) Above transition temperature



(b) Below transition temperature

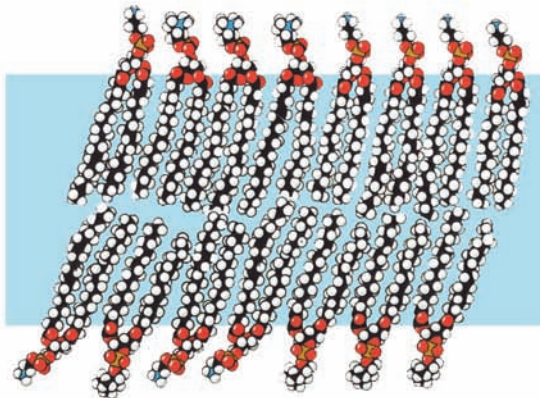


Figure 12-17 Order–disorder transition in a lipid bilayer.

(a) Above the transition temperature, both the lipid molecules as a whole and their nonpolar tails are highly mobile in the plane of the bilayer. Such a state of matter, which is ordered in some

directions but not in others, is called a liquid crystal. (b) Below the transition temperature, the lipid molecules form a much more orderly array to yield a gel-like solid. [After Robertson, R.N., *The Lively Membranes*, pp. 69–70, Cambridge University Press (1983).]

Table 12-3 Lipid Compositions of Some Biological Membranes^a

Lipid	Human		Beef Heart	
	Erythrocyte	Human Myelin	Mitochondria	<i>E. coli</i>
Phosphatidic acid	1.5	0.5	0	0
Phosphatidylcholine	19	10	39	0
Phosphatidylethanolamine	18	20	27	65
Phosphatidylglycerol	0	0	0	18
Phosphatidylinositol	1	1	7	0
Phosphatidylserine	8.5	8.5	0.5	0
Cardiolipin	0	0	22.5	12
Sphingomyelin	17.5	8.5	0	0
Glycolipids	10	26	0	0
Cholesterol	25	26	3	0

^aThe values given are weight percent of total lipid.

Source: Tanford, C., *The Hydrophobic Effect*, p. 109, Wiley (1980).

in the range 10 to 40°C. *Cholesterol, which by itself does not form a bilayer, decreases membrane fluidity near the membrane surface because cholesterol's rigid steroid ring system interferes with the motions of the fatty acid tails causing them to become more ordered.* However, because cholesterol does not extend into the membrane as far as most lipids, it also acts as a spacer that facilitates the increased mobility of the fatty acid tails near their methyl ends. Cholesterol also broadens the temperature range of the order–disorder transition and in high concentrations totally abolishes it. This behavior occurs because cholesterol inhibits the crystallization (cooperative aggregation into ordered arrays) of fatty acid tails by fitting in between them. Thus cholesterol functions as a kind of membrane plasticizer.

The fluidity of biological membranes is one of their important physiological attributes since it permits their embedded proteins to interact (Section 12-3C). The transition temperatures of mammalian membranes are well below body temperatures and hence these membranes all have a

fluidlike character. Bacteria and poikilothermic (cold-blooded) animals such as fish modify (through lipid biosynthesis and degradation) the fatty acid compositions of their membrane lipids with the ambient temperature so as to maintain membrane fluidity. For example, the membrane viscosity of *E. coli* at its growth temperature remains constant as the growth temperature is varied from 15 to 43°C.

c. Gaseous Anesthetics Alter Neuronal Membrane Structures

Gaseous anesthetics, such as diethyl ether, cyclopropane, **isoflurane** (CF₃—CHCl—O—CHF₂), and the noble gas Xe, act by interfering with the transmission of nerve impulses in the central nervous system. Since the body excretes these general anesthetics unchanged, it appears that they do not act by chemical means. Rather, experimental evidence, such as the linear correlation of their anesthetic effectiveness with their lipid solubilities, suggests that these nonpolar substances alter the structures of membranes by

Table 12-4 Compositions of Some Biological Membranes

Membrane	Protein (%)	Lipid (%)	Carbohydrate (%)	Protein to Lipid Ratio
Plasma membranes:				
Mouse liver cells	46	54	2–4	0.85
Human erythrocyte	49	43	8	1.1
Amoeba	52	42	4	1.3
Rat liver nuclear membrane	59	35	2.0	1.6
Mitochondrial outer membrane	52	48	(2–4) ^a	1.1
Mitochondrial inner membrane	76	24	(1–2) ^a	3.2
Myelin	18	79	3	0.23
Gram-positive bacteria	75	25	(10) ^a	3.0
<i>Halobacterium</i> purple membrane	75	25		3.0

^aDeduced from the analyses.

Source: Guidotti, G., *Annu. Rev. Biochem.* **41**, 732 (1972).

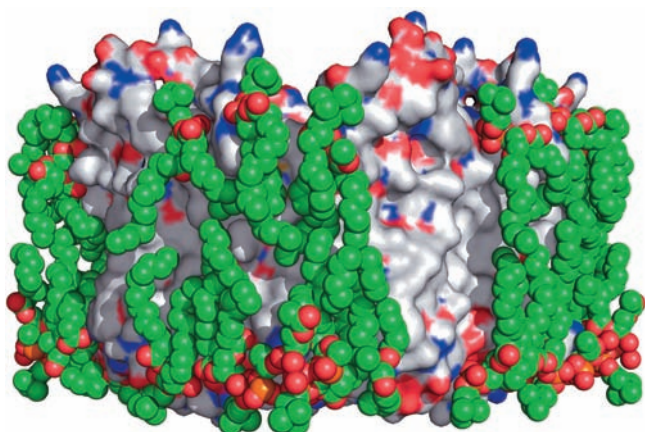


Figure 12-18 X-ray structure of the integral membrane protein aquaporin-0 (AQP0) in association with lipids. The protein is represented by its surface diagram, which is colored according to charge (red negative, blue positive, and white uncharged). Tightly bound molecules of dimyristoylphosphatidylcholine are drawn in space-filling form with C green, O red, and P orange. Note how the lipid tails closely conform to the nonpolar surface of the protein, thereby solvating it. The arrangement of the two rows of lipid molecules, with phosphorus–phosphorus distances of ~ 35 Å, matches the dimensions of a lipid bilayer. [Based on an electron crystallographic structure by Stephen Harrison and Thomas Walz, Harvard Medical School. PDBid 2B6O.]

dissolving in their hydrocarbon cores. Nerve impulse transmission, which is a membrane-based phenomenon (Section 20-5), is disrupted by these structural changes to which neuronal membranes seem particularly sensitive.

3 BIOLOGICAL MEMBRANES

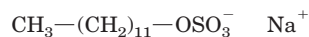
Biological membranes are composed of proteins associated with a lipid bilayer matrix. Their lipid fractions consist of complex mixtures that vary according to the membrane source (Table 12-3) and, to some extent, with the diet and environment of the organism that produced the membrane. Membrane proteins carry out the dynamic processes associated with membranes, and therefore specific proteins occur only in particular membranes. Protein-to-lipid ratios in membranes vary considerably with membrane function, as is indicated by Table 12-4, although most membranes are at least one-half protein. The myelin membrane, which functions passively as an insulator around certain nerve fibers (Section 20-5Bc), is a prominent exception to this generalization in that it contains only 18% protein.

In this section, we discuss the properties of membrane proteins and their behavior in biological membranes. Following this, we examine specific aspects of biological membranes, namely, the erythrocyte cytoskeleton, the nature of blood groups, gap junctions, and channel-forming proteins. We consider how membranes are assembled and how their component proteins are directed to them in Section 12-4.

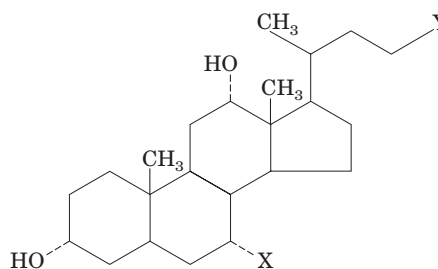
A. Membrane Proteins

Membrane proteins are operationally classified according to how tightly they are associated with membranes:

1. Integral or intrinsic proteins are tightly bound to membranes by hydrophobic forces (Fig. 12-18) and can only be separated from them by treatment with agents that disrupt membranes. These include organic solvents, detergents (e.g., those in Fig. 12-19), and chaotropic agents (ions that disrupt water structure; Section 8-4E). Integral proteins



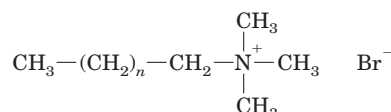
Sodium dodecyl sulfate (SDS)



X = H, Y = $\text{COO}^- \text{Na}^+$ **Sodium deoxycholate**

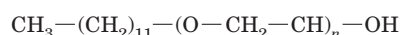
X = OH, Y = $\text{COO}^- \text{Na}^+$ **Sodium cholate**

X = OH, Y = $\text{CO}-\text{NH}-(\text{CH}_2)_3-\text{N}^+(\text{CH}_3)_2-(\text{CH}_2)_3-\text{SO}_3^-$ **CHAPS**



$n = 10$ **Dodecyltriethylammonium bromide (DTAB)**

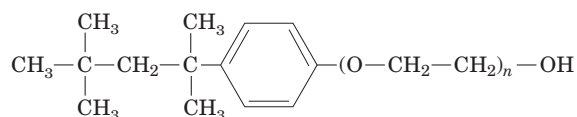
$n = 15$ **Cetyltrimethylammonium bromide (CTAB)**



Polyoxyethylenelauryl ether

$n = 4$ **Brij 30**

$n = 25$ **Brij 35**



Polyoxyethylene-*p*-isooctylphenyl ether

$n = 5$ **Triton X-20**

$n = 10$ **Triton X-100**

Figure 12-19 A selection of the detergents used in biochemical manipulations. Note that they may be anionic, cationic, zwitterionic, or uncharged. Ionic detergents are strongly amphiphilic and therefore tend to denature proteins, whereas neutral detergents are unlikely to do so.

tend to aggregate and precipitate in aqueous solutions unless they are solubilized by detergents or water-miscible organic solvents such as butanol or glycerol. Some integral proteins bind lipids so tenaciously that they can be freed from them only under denaturing conditions. Solubilized integral proteins can be purified by many of the protein fractionation methods discussed in Chapter 6.

2. Peripheral or extrinsic proteins are dissociated from membranes by relatively mild procedures that leave the membrane intact, such as exposure to high ionic strength salt solutions (e.g., 1M NaCl), metal chelating agents, or pH changes. Peripheral proteins, for example, cytochrome *c*, are stable in aqueous solution and do not bind lipid. They associate with a membrane by binding at its surface to its lipid head groups and/or its integral proteins through electrostatic and hydrogen bonding interactions. Membrane-free peripheral proteins behave as water-soluble globular proteins and can be purified as such (Chapter 6).

In this subsection we concentrate on integral proteins.

a. Integral Proteins Are Asymmetrically Oriented Amphiphiles

All biological membranes contain integral proteins, which typically comprise ~25% of the proteins encoded by a genome. Their locations on a membrane may be determined through **surface labeling**, a technique employing agents that react with proteins but cannot penetrate membranes. For example, an integral protein on the outer

surface of an intact cell membrane binds antibodies elicited against it, but a protein on the membrane's inner surface can do so only if the membrane has been ruptured. Membrane-impermeable protein-specific reagents that are fluorescent or radioactively labeled may be similarly employed. Using such surface-labeling reagents, it has been shown that *some integral proteins are exposed only to a specific surface of a membrane, whereas others, known as transmembrane proteins, span the membrane.* However, no protein is known to be completely buried in a membrane; that is, all have some exposure to the aqueous environment. Such studies have also established that *biological membranes are asymmetric in that a particular membrane protein is invariably located on only one particular face of a membrane or, in the case of a transmembrane protein, oriented in only one direction with respect to the membrane* (Fig. 12-20).

Integral proteins are amphiphilic; the protein segments immersed in a membrane's nonpolar interior have predominantly hydrophobic surface residues, whereas those portions that extend into the aqueous environment are by and large sheathed with polar residues. For example, proteolytic digestion and chemical modification studies indicate that the erythrocyte transmembrane protein **glycophorin A** (Fig. 12-21) has three domains: (1) a 72-residue externally located *N*-terminal domain that bears 16 carbohydrate chains; (2) a 19-residue sequence, consisting almost entirely of hydrophobic residues, that spans the erythrocyte cell membrane; and (3) a 40-residue cytoplasmic C-terminal

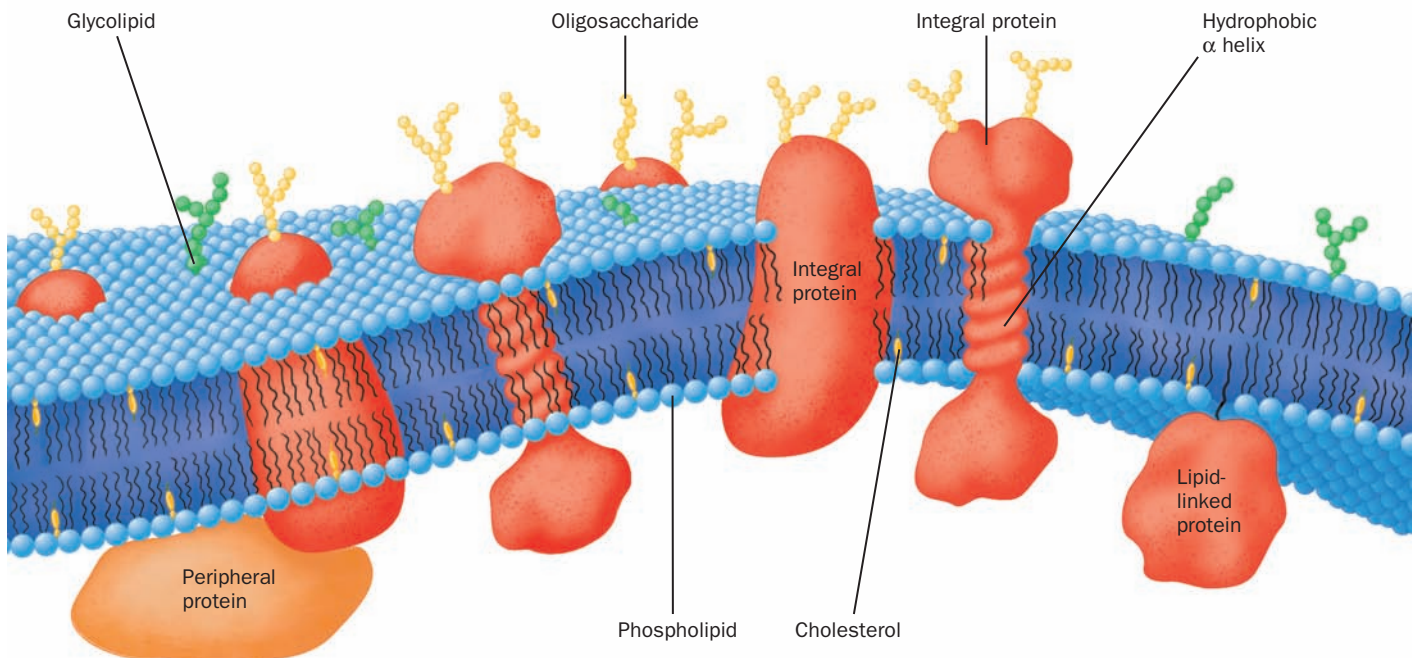



Figure 12-20 Diagram of a plasma membrane. Integral proteins (orange) are embedded in a bilayer composed of phospholipids (blue spheres with two wiggly tails) and cholesterol (yellow). The carbohydrate components of glycoproteins (yellow beaded chains) and glycolipids (green beaded chains) occur only

on the external face of the membrane. Most biological membranes have a higher proportion of protein than is drawn here.  See Guided Exploration 11: Membrane structure and the fluid mosaic model

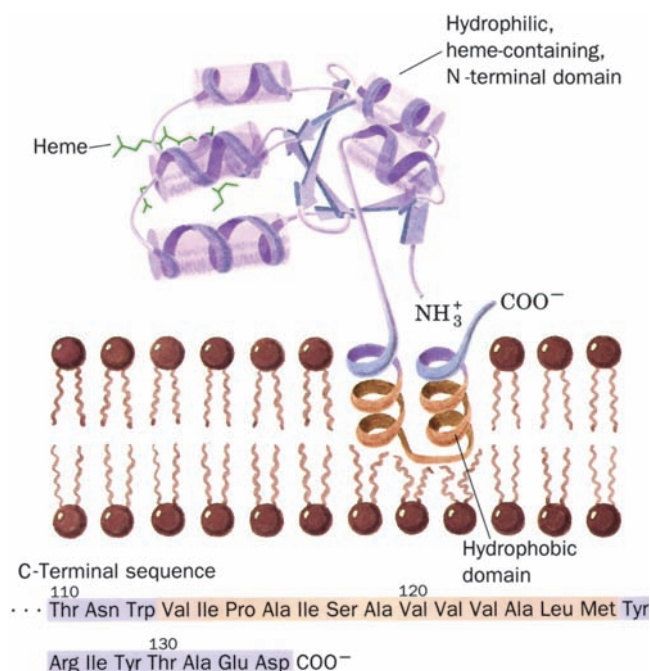
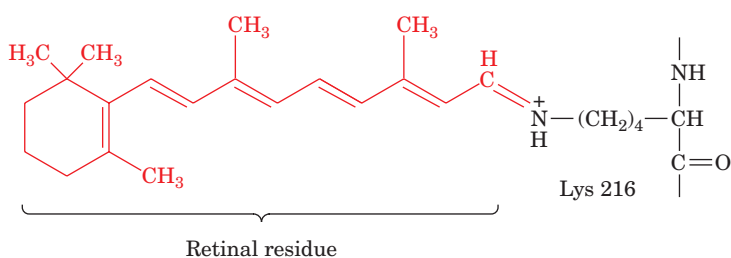


Figure 12-23 Liver cytochrome *b*₅ in association with a membrane. The protein's enzymatically active N-terminal domain (purple), whose X-ray structure has been determined, is anchored in the membrane by a hydrophobic and presumably α helical C-terminal segment (brown) that begins and ends with hydrophilic segments (purple). The amino acid sequence of the horse enzyme indicates that this hydrophobic anchor consists of a 13-residue segment ending 9 residues from the polypeptide's C-terminus (below). [Ribbon diagram of the N-terminal domain after a drawing by Jane Richardson, Duke University. Amino acid sequence from Ozols, J. and Gerard, C., *J. Biol. Chem.* **253**, 8549 (1977).]

(Fig. 12-23). The asymmetric orientation of integral proteins in the membrane is maintained by their infinitesimal flip-flop rates (even slower than those of lipids), which result from the greater sizes of the membrane protein "head groups" in comparison to those of lipids. The origin of this asymmetry is discussed in Section 12-4.

Relatively few integral proteins have yet been crystallized—and then usually in the presence of detergents, which are but poor substitutes for lipid bilayers. Thus, despite their biological abundance, only ~0.8% of the proteins of known structure are integral proteins (>80% of which are bacterial proteins). A database of these proteins



is maintained at http://blanco.biomol.uci.edu/Membrane_Proteins_xtal.html. In the remainder of this subsection, we discuss the structures of four integral proteins: bacteriorhodopsin, the bacterial photosynthetic reaction center, porins, and fatty acid amide hydrolase.

b. Bacteriorhodopsin Contains a Bundle of Seven Hydrophobic Helical Rods

One of the structurally most studied integral proteins is **bacteriorhodopsin (BR)** from the halophilic (salt loving) bacterium *Halobacterium salinarium* that inhabits such salty places as the Dead Sea (it grows best in 4.3M NaCl and is nonviable below 2.0M NaCl; seawater contains 0.6M NaCl). Under low O₂ conditions, its cell membrane develops ~0.5- μ m-wide patches of **purple membrane** whose only protein component is BR. This 247-residue protein is a light-driven proton pump; it generates a proton concentration gradient across the membrane that powers the synthesis of ATP (by a mechanism discussed in Section 22-3Bh). Bacteriorhodopsin's light-absorbing element, **retinal**, is covalently bound to its Lys 216 (Fig. 12-24). This **chromophore** (light-absorbing group), which is responsible for the membrane's purple color, is also the light-sensitive element in vision.

The purple membrane, which is 75% protein and 25% lipid, has an unusual structure compared to most other membranes (Section 12-3C): Its BR molecules are arranged in a highly ordered two-dimensional array (a two-dimensional crystal). This permitted Richard Henderson and Nigel Unwin, through **electron crystallography** (a technique they devised, resembling X-ray crystallography, in which the electron beam of an electron microscope is used to elicit diffraction from two-dimensional crystals), to determine the structure of BR to near-atomic resolution (3.0 Å). The more recently determined 1.9-Å-resolution X-ray structure of BR, based on single crystals of BR dissolved in lipidic cubic phases (mixtures of lipids and water that form a highly convoluted but continuous bilayer that is interpenetrated by aqueous channels), closely resembles that determined by electron crystallography.

Bacteriorhodopsin forms a homotrimer. Each of its subunits consists mainly of a bundle of seven ~25-residue α helical rods that each span the lipid bilayer in directions almost perpendicular to the bilayer plane (Fig. 12-25). BR is therefore said to be **polytopic** (multispanning; Greek: *topos*, place). The ~20-Å spaces between the protein molecules in the purple membrane are occupied by this bilayer (Fig. 12-25b). Adjacent α helices, which are largely

Figure 12-24 Molecular formula of retinal. Retinal, the prosthetic group of bacteriorhodopsin, forms a Schiff base with Lys 216 of the protein. A similar linkage occurs in **rhodopsin**, the photoreceptor of the eye (Section 19-2B).

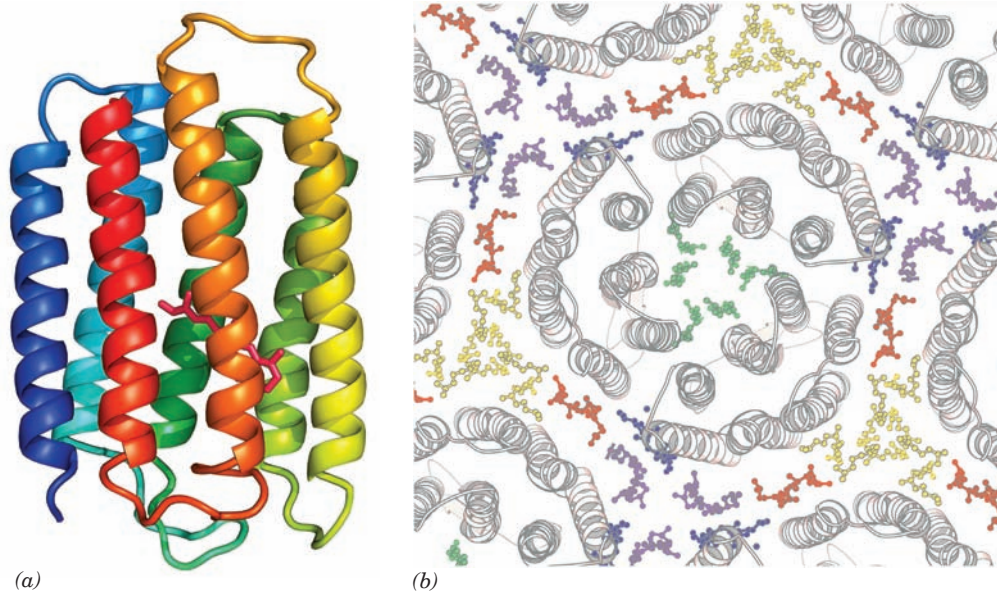



Figure 12-25 Structure of bacteriorhodopsin. (a) The protein is shown in ribbon form as viewed from within the membrane plane and colored in rainbow order from its N-terminus (*blue*) to its C-terminus (*red*). Its covalently bound retinal is drawn in stick form (*magenta*). [Based on an X-ray structure by Nikolaus Grigorieff and Richard Henderson, MRC Laboratory of Molecular Biology, Cambridge, U.K. PDBid 2BRD.] (b) The X-ray structure of a bacteriorhodopsin trimer with portions of its surrounding trimers as viewed from the extracellular side of the membrane. The protein molecules are shown in ribbon form (*gray*) and their associated lipid tails are shown in ball-and-stick

form in different colors with symmetry-related lipid tails the same color (the lipid head groups are disordered and hence not seen). Only the lipids in the extracellular leaflet are shown; those in the cytoplasmic leaflet have a similar distribution. Note how the seven antiparallel α helices in each BR monomer are cyclically arranged in two layers of four and three helices with helices adjacent in sequence also adjacent in space (the N to C direction circulates clockwise in this view). [Courtesy of Eva Pebay-Peyroula, Université Joseph Fourier, Grenoble, France. PDBid 1AP9.]  See Kinemage Exercise 8-1

hydrophobic in character, are connected in a head-to-tail fashion by short polypeptide loops. This arrangement places the protein's charged residues near the surfaces of the membrane in contact with the aqueous solvent. The internal charged residues line the center of the helix bundle of each monomer so as to form a hydrophilic channel that facilitates the passage of protons. Other membrane pumps and channels (Chapter 20) have similar structures.

c. The Photosynthetic Reaction Center Contains Eleven Transmembrane Helices

The primary photochemical process of photosynthesis in purple photosynthetic bacteria is mediated by the so-called **photosynthetic reaction center (PRC)** (Section 24-2B), a transmembrane (TM) protein consisting of at least three nonidentical ~ 300 -residue subunits that collectively bind four **chlorophyll** molecules, four other chromophores, and a nonheme Fe(II) ion. The 1187-residue photosynthetic reaction center of *Rhodospseudomonas (Rps.) viridis*, whose X-ray structure was determined in 1984 by Hartmut Michel, Johann Deisenhofer, and Robert Huber, was the first TM protein to be described in atomic detail (Fig. 12-26). The polytopic protein's TM portion consists of 11 α helices that form a 45-Å-long flattened cylinder with the expected hydrophobic surface. In later chapters

we shall see that the transmembrane portions of most TM proteins consist of bundles of one to >20 helices, most of which are closely perpendicular to the membrane although some may be obliquely oriented and/or not fully traverse the membrane.

d. Porins Are Channel-Forming Proteins That Contain Transmembrane β Barrels

The outer membranes of gram-negative bacteria (Section 11-3B) protect them from hostile environments but must nevertheless be permeable to small polar solutes such as nutrients and waste products. These outer membranes consequently contain embedded channel-forming proteins called **porins**, which are usually trimers of identical 30- to 50-kD subunits that permit the passage of solutes of less than ~ 600 D. Porins also occur in eukaryotes in the outer membranes of mitochondria and chloroplasts (thereby providing a further indication that these organelles are descended from bacteria; Section 1-2A).

The X-ray structures of several different porins have been elucidated, among them the *Rhodobacter (Rb.) capsulatus* porin, determined by Georg Schulz, and the *E. coli* **OmpF** and **PhoE** porins, determined by Johan Jansonius. The 340- and 330-residue OmpF and PhoE porins share 63% sequence identity but have little sequence similarity with the 301-residue *Rb. capsulatus* porin. Nevertheless, all

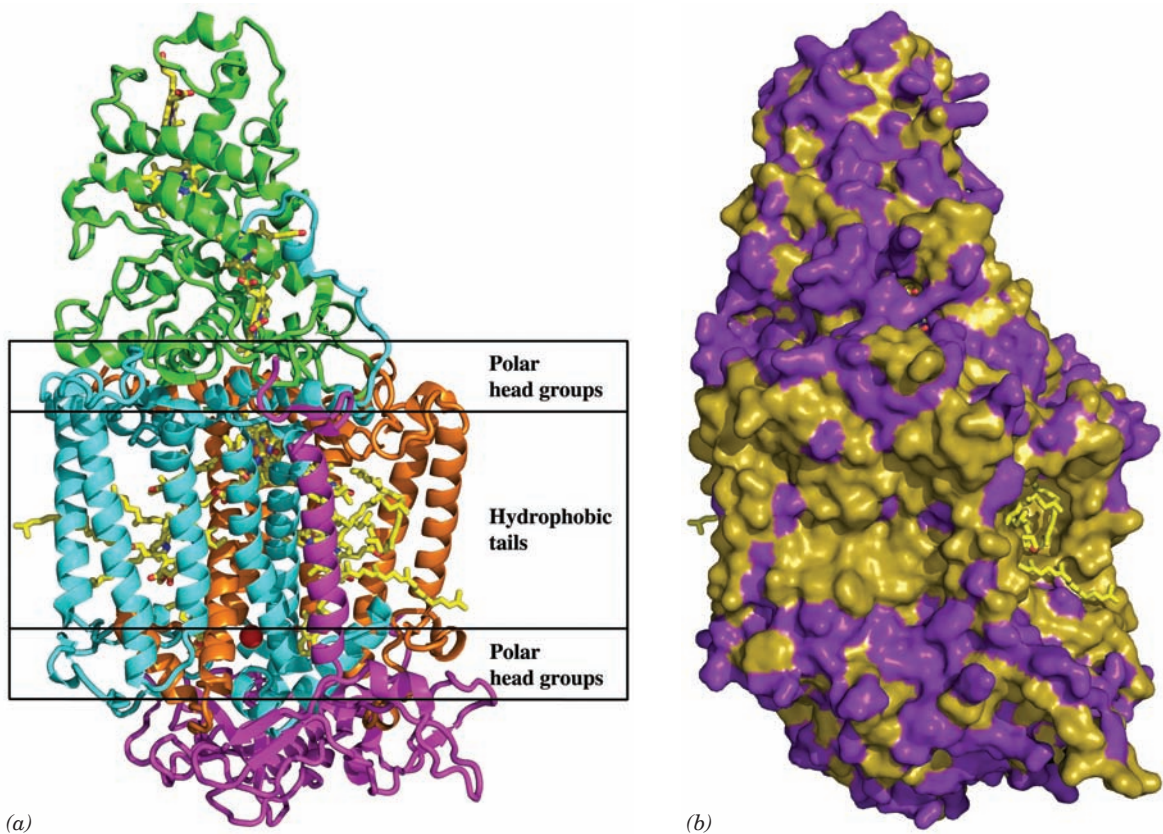


Figure 12-26 X-ray structure of the photosynthetic reaction center of *Rps. viridis*. (a) The H, M, and L subunits, which are respectively shown as pink, blue, and orange ribbons, collectively have 11 transmembrane helices. The four-heme *c*-type cytochrome (green), which does not occur in all species of photosynthetic bacteria, is bound to the external face of the complex. The prosthetic groups are drawn in stick form with C yellow, N blue, and O red with a bound Fe(II) ion represented by a red sphere. The position that the transmembrane protein is

thought to occupy in the lipid bilayer is indicated schematically. (b) A surface diagram, viewed as in Part a, in which hydrophobic residues are tan and polar residues are purple. Note how few polar groups are externally exposed in the portion of the protein that is immersed in the nonpolar region of the lipid bilayer.

[Based on an X-ray structure by Johann Deisenhofer, Robert Huber, and Hartmut Michel, Max-Planck-Institut für Biochemie, Martinsreid, Germany. PDBid 1PRC.]  See Kinemage

Exercise 8-2

three porins have closely similar structures. Each monomer of these homotrimeric proteins predominantly consists of a 16-stranded antiparallel β barrel which forms a solvent-accessible pore along the barrel axis that has a length of ~ 55 Å and a minimum diameter of ~ 7 Å (Fig. 12-27; although note that β barrel membrane proteins with 8, 10, 12, 14, 18, 19, 22, and 24 strands are also known). In the OmpF and PhoE porins, the N- and C-termini associate via a salt bridge in the 16th β strand, thereby forming a pseudocyclic structure (Fig. 12-27a). Note that a β barrel fully satisfies the polypeptide backbone's hydrogen bonding potential, as does an α helix. As expected, the side chains at the protein's membrane-exposed surface are nonpolar, thereby forming an ~ 25 -Å-high hydrophobic band encircling the trimer (Fig. 12-27c). In contrast, the side chains at the solvent-exposed surface of the protein, including those lining the walls of the aqueous channel, are polar. Possible mechanisms for solute selectivity by these porins are discussed in Section 20-2D.

e. Fatty Acid Amide Hydrolase Binds to Only One Bilayer Leaflet

Not all integral proteins are TM proteins. For example, the enzyme **fatty acid amide hydrolase (FAAH)** is an integral protein that binds to the cytoplasmic leaflet of the plasma membrane. It is therefore said to be **monotopic** as is cytochrome b_5 (Fig. 12-23). FAAH's X-ray structure, determined by Raymond Stevens and Benjamin Cravatt, reveals that each 537-residue subunit of this homodimer consists of an 11-stranded mixed β sheet surrounded by 28 α helices of various lengths (Fig. 12-28). Its membrane-binding segment consists of a helix-turn-helix motif, whose surface faces outward from the body of the protein to form a hydrophobic plateau. Its component nonpolar residues, many of which are aromatic, are interspersed with several basic residues, which presumably interact electrostatically with the membrane's phospholipid head groups. The structure of this hydrophobic motif resembles that observed in the X-ray structures of two other monotopic integral proteins,

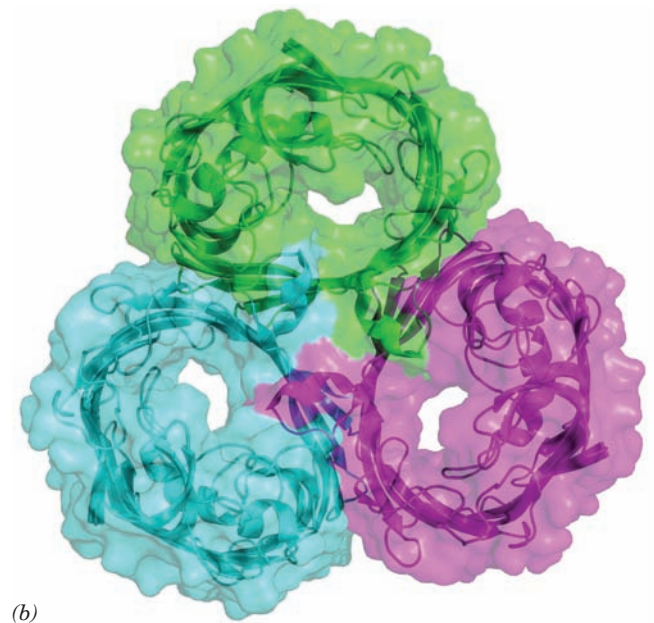
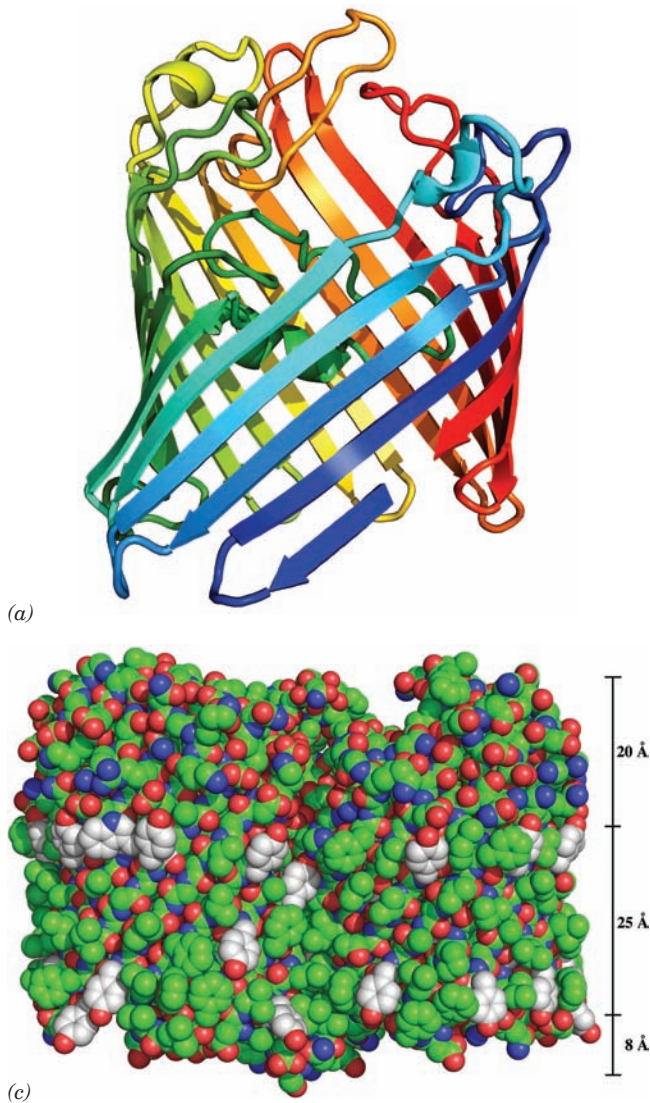



Figure 12-27 X-ray crystal structure of the *E. coli* OmpF porin. (a) A ribbon diagram of the monomer colored in rainbow order from its N-terminus (blue) to its C-terminus (red). Each strand of this 16-stranded antiparallel β barrel is inclined by $\sim 45^\circ$ to the barrel axis. Its C-terminal strand is continued by the N-terminal segment (bottom right), thereby forming a pseudo-continuous strand. All porins of known structure have similar structural properties. (b) Ribbon diagram of the trimer embedded in its semitransparent surface and viewed along its threefold axis of symmetry from the cell's exterior showing the pore through each subunit. Each subunit is differently colored. Adjacent β strands in adjoining subunits extend essentially perpendicularly to each other. (c) A space-filling model of the trimer viewed perpendicular to its 3-fold axis. N atoms are blue, O atoms are red, and C atoms are green, except those of Trp and Tyr side chains, which are white. These latter groups delimit an ~ 25 -Å-high hydrophobic band (scale at right) that is immersed in the nonpolar portion of the bacterial outer membrane (with the cell's exterior at the tops of Parts a and c). Compare the hydrophobic band in this figure with that in Fig. 12-26b. [Based on an X-ray structure by Johan Janssonius, University of Basel, Switzerland. PDBid 1OPF.]  See Kinemage Exercise 8-3

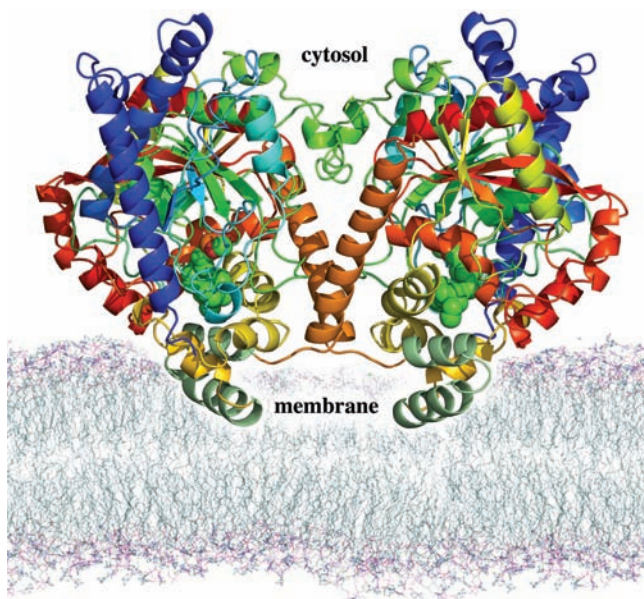


Figure 12-28 X-ray structure of rat liver fatty acid amide hydrolase indicating its proposed disposition in the cytoplasmic leaflet of the plasma membrane. This homodimeric enzyme is viewed along the plane of the membrane with its 2-fold axis of symmetry vertical. It is drawn in ribbon form with each subunit colored in rainbow order from its N-terminus (blue) to its C-terminus (red) except for its putative membrane-binding motif, which is dark green. The enzyme's bound inhibitor, methyl arachidonyl fluorophosphonate, is drawn in space-filling form with C green, O red, and P orange. The membrane model was generated by a molecular dynamics simulation of a palmitoyloleoylphosphatidylethanolamine bilayer. [Based on an X-ray structure by Raymond Stevens and Benjamin Cravatt, Scripps Research Institute, La Jolla, California. PDBid 1MT5.]

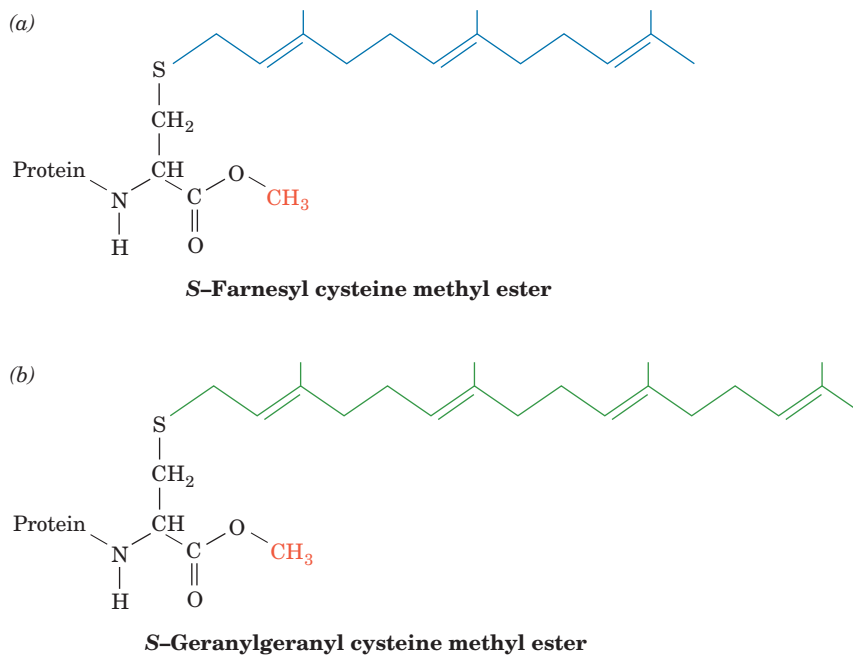


Figure 12-29 Prenylated proteins. (a) A farnesylated protein and (b) a geranylgeranylated protein. In both cases, the protein is synthesized with the C-terminal sequence CaaX, where C is Cys, “a” is often an aliphatic amino acid, and X is any amino acid. After the prenyl group is appended to the protein in thioether

linkage with the Cys residue, the aaX tripeptide is hydrolytically cleaved away and the new carboxyl terminus is methyl esterified. When X is Ala, Met, or Ser, the protein is farnesylated and when X is Leu, it is geranylgeranylated.

observations suggest that prenylated proteins may interact with specific membrane-bound receptor proteins and hence that *prenylation also facilitates protein–protein interactions*. This idea is corroborated by the observation that, in certain proteins involved in intracellular signaling [for example, **Ras** (Section 19-3Cf) and the so-called **G proteins** (Section 19-2)], prenylation and carboxyl methylation enhance the intersubunit associations that mediate signal transmission.

b. Fatty Acylated Proteins

Two fatty acids are known to be covalently linked to eukaryotic proteins:

1. Myristic acid, a biologically rare saturated C_{14} fatty acid (Table 12-1), which is appended to a protein in amide linkage to the α -amino group of an N-terminal Gly residue. Myristoylation almost always occurs cotranslationally (as the protein is being synthesized), and this attachment is stable, that is, the myristoyl group has a half-life similar to that of the protein to which it is appended.

2. Palmitic acid, a biologically common saturated C_{16} fatty acid, which is joined to a protein in thioester linkage to a specific Cys residue. In some cases, the palmitoylated protein is also prenylated. For example, Ras must be farnesylated and carboxyl methylated as described above before it is palmitoylated at a Cys residue that precedes the protein’s C-terminus by several residues. Palmitoylation occurs post-translationally in the cytosol and is reversible.

Fatty acyl groups are thought to function as membrane anchors for proteins, much as do prenyl groups. However, the requirement of many proteins for specific fatty acyl residues suggests that these groups also participate in targeting their attached proteins to specific cellular locations. Indeed, palmitoylated proteins occur almost exclusively on the cytoplasmic face of the plasma membrane, whereas myristoylated proteins are found in a number of subcellular compartments including the cytosol, endoplasmic reticulum, Golgi apparatus, plasma membrane, and nucleus. Many fatty acylated proteins participate in intracellular signaling processes through protein–protein interactions in a manner similar to prenylated proteins. Since the membrane affinities and biological activities of many proteins are enhanced by palmitoylation, the reversibility of palmitoylation appears to be involved in controlling intracellular signaling processes.

c. GPI-Linked Proteins

Glycosylphosphatidylinositol (GPI) groups function to anchor a wide variety of proteins to the exterior surface of the eukaryotic plasma membrane. There is no obvious relationship among the numerous proteins that have GPI anchors, which include enzymes, receptors, immune system proteins, and recognition antigens. Evidently, *GPI groups simply provide an alternative to transmembrane polypeptide domains in binding proteins to the plasma membrane.*

The core structure of GPI anchors consists of phosphatidylinositol (Table 12-2) glycosidically linked to a linear tetrasaccharide composed of three mannose residues

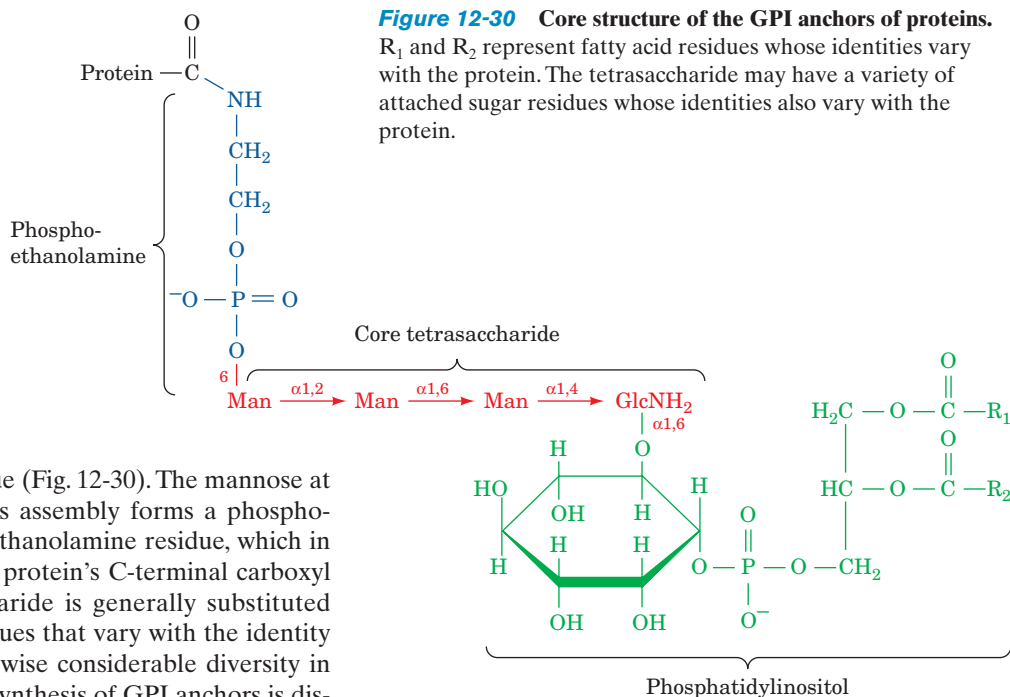



Figure 12-30 Core structure of the GPI anchors of proteins. R₁ and R₂ represent fatty acid residues whose identities vary with the protein. The tetrasaccharide may have a variety of attached sugar residues whose identities also vary with the protein.

and one glucosaminyl residue (Fig. 12-30). The mannose at the nonreducing end of this assembly forms a phosphoester bond with a phosphoethanolamine residue, which in turn, is amide-linked to the protein's C-terminal carboxyl group. The core tetrasaccharide is generally substituted with a variety of sugar residues that vary with the identity of the protein. There is likewise considerable diversity in the fatty acid residues. The synthesis of GPI anchors is discussed in Section 23-3Bk.

GPI-anchored proteins occur on the exterior surface of the plasma membrane for the same reason as do the carbohydrate residues of glycoproteins (which we discuss in Section 12-4Ca). Proteins destined to be GPI-anchored are synthesized with membrane-spanning C-terminal sequences of 20 to 30 hydrophobic residues (as described in Section 12-4Ba) that are removed during GPI addition. This is corroborated by the observation that GPI-anchored proteins are released from the plasma membrane by treatment with phosphatidylinositol-specific **phospholipases** (Section 19-4B), thereby demonstrating that the mature polypeptides are not embedded in the lipid bilayer.

C. Fluid Mosaic Model of Membrane Structure

 **See Guided Exploration 11: Membrane structure and the fluid mosaic model** *The demonstrated fluidity of artificial lipid bilayers suggests that biological membranes have similar properties.* This seminal idea was proposed in 1972 by S. Jonathan Singer and Garth Nicolson in their unifying theory of membrane structure known as the **fluid mosaic model**. The theory postulates that integral proteins resemble “icebergs” floating in a two-dimensional lipid “sea” (Fig. 12-20) and that these proteins freely diffuse laterally in the lipid matrix unless their movements are restricted by associations with other cell components.

a. The Fluid Mosaic Model Has Been Verified Experimentally

The validity of the fluid mosaic model has been established in several ways. Perhaps the most vivid is an experiment by Michael Edidin (Fig. 12-31). Cultured mouse cells were fused with human cells by treatment with **Sendai virus** to yield a hybrid cell known as a **heterokaryon**. The mouse cells were labeled with mouse protein-specific

antibodies to which a green-fluorescing dye had been covalently linked (**immunofluorescence**). The proteins on the human cells were similarly labeled with a red-fluorescing marker. On cell fusion, the mouse and human proteins, as seen under the fluorescence microscope, were segregated on the two halves of the heterokaryon. After 40 min at 37°C, however, these proteins had thoroughly intermingled. The addition of substances that inhibit metabolism or protein synthesis did not slow this process, but lowering the temperature below 15°C did. These observations indicate that the mixing process is independent of both metabolic energy and the insertion into the membrane of newly synthesized proteins. Rather, it is a result of the diffusion of existing proteins throughout the fluid membrane, a process that slows as the temperature is lowered.

Fluorescence photobleaching recovery measurements (Fig. 12-15) indicate that membrane proteins vary in their lateral diffusion rates. Some 30 to 90% of these proteins are freely mobile; they diffuse at rates only an order of magnitude or so slower than those of the much smaller lipids, so that they typically take from 10 to 60 min to diffuse the 20-μm length of a eukaryotic cell. Other proteins diffuse more slowly, and some, because of submembrane attachments, are essentially immobile.

The distribution of proteins in membranes may be visualized through electron microscopy using the **freeze-fracture** and **freeze-etch** techniques. In the freeze-fracture procedure, which was devised by Daniel Branton, a membrane specimen is rapidly frozen to near liquid nitrogen temperatures (−196°C). This immobilizes the sample and thereby minimizes its disturbance by subsequent manipulations. The specimen is then fractured with a cold microtome knife, which often splits the bilayer into monolayers (Fig. 12-32). Since the exposed membrane itself would be

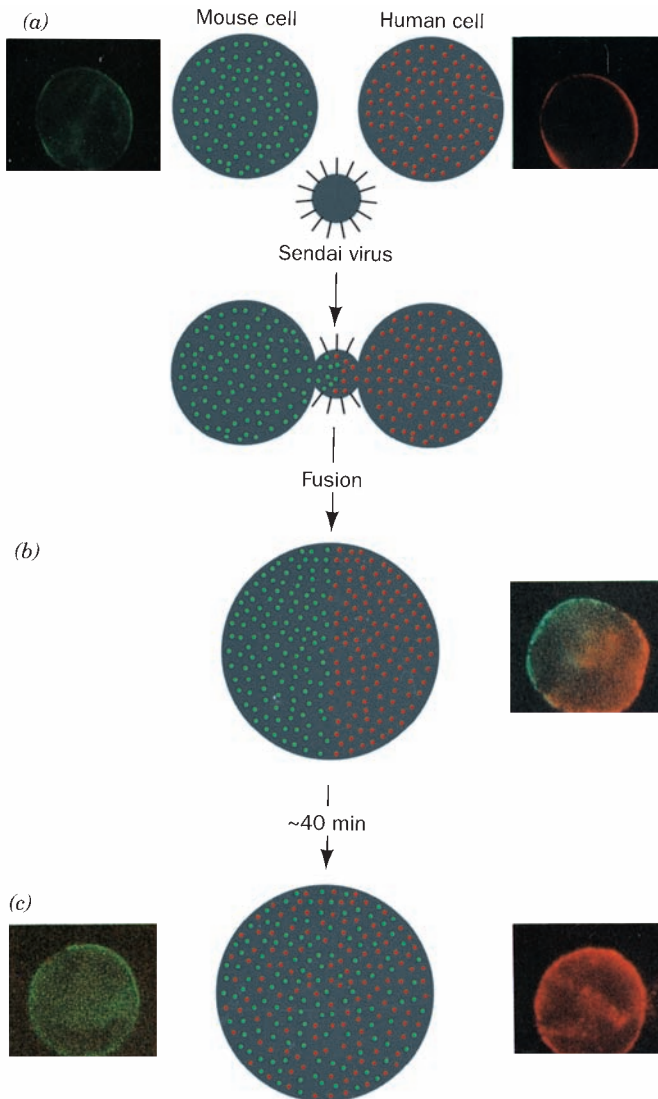


Figure 12-31 Sendai virus–induced fusion of a mouse cell with a human cell and the subsequent intermingling of their cell-surface components as visualized by immunofluorescence. Human and mouse antigens are labeled with red and green fluorescent markers, respectively. (a) The membrane-encapsulated Sendai virus specifically binds to cell-surface receptors on both types of cells and subsequently fuses to their cell membranes. (b) This results in the formation of a cytoplasmic bridge between the cells that expands so as to form a heterokaryon. (c) After 40 min, the red and green markers are fully intermingled. The photomicrographs were taken through filters that allowed only red or green light to reach the camera; that in Part *b* is a double exposure and those in Part *c* are of the same cell. [Immunofluorescence photomicrographs courtesy of Michael Edidin, Johns Hopkins University.]

destroyed by an electron beam, its metallic replica is made by coating the membrane with a thin layer of carbon, shadowing it (covering it by evaporative deposition under high vacuum) with platinum, and removing the organic matter by treatment with acid. Such a metallic replica can be examined by electron microscopy. In the freeze-etch procedure, the external surface of the membrane adjacent to the

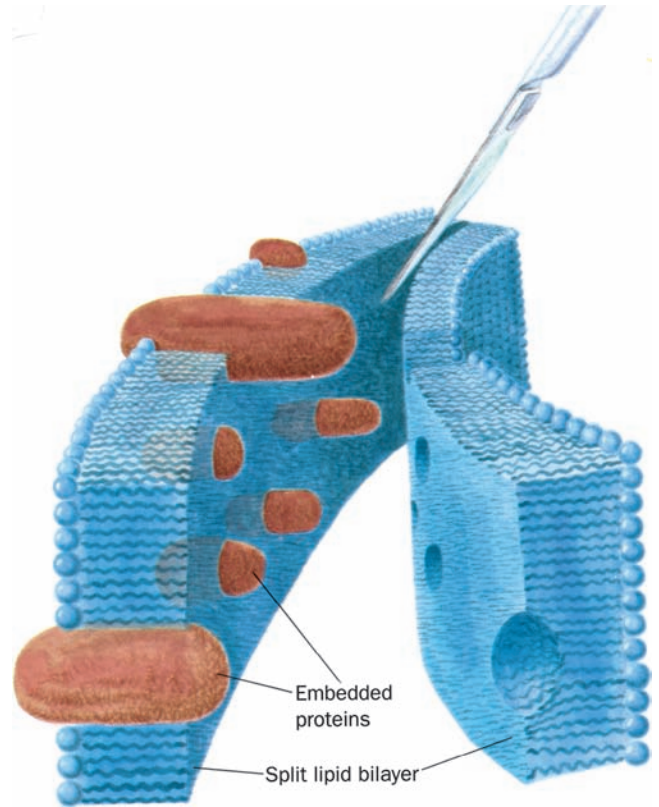


Figure 12-32 The freeze-fracture technique. A membrane that has been split by freeze-fracture, as is schematically diagrammed, exposes the interior of the lipid bilayer and its embedded proteins.

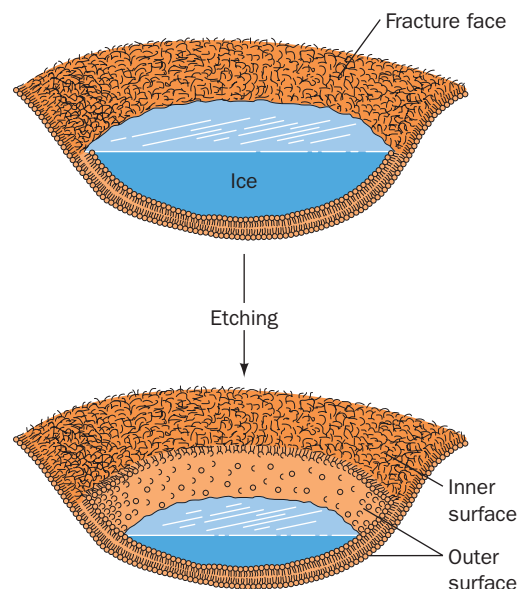


Figure 12-33 The freeze-etch procedure. The ice that encases a freeze-fractured membrane (*top*) is partially sublimated away so as to expose the outer membrane surface (*bottom*) for electron microscopy.

cleaved area revealed by freeze fracture may also be visualized by first sublimating (etching) away, at -100°C , some of the ice in which it is encased (Fig. 12-33).

Freeze-etch electron micrographs of most biological membranes show an inner fracture face that is studded with embedded 50- to 85-Å-diameter globular particles (Fig. 12-34) that appear to be distributed randomly. These particles correspond to membrane proteins, as is demonstrated by their disappearance when the membrane is treated with proteases before its freeze fracture. This is further corroborated by the observation that the myelin membrane, which has a low protein content, as well as liposomes composed of only lipids, have smooth inner fracture faces. Outer membrane surfaces also have a relatively smooth appearance (Fig. 12-34) because integral proteins tend not to protrude very far beyond them. The distributions of individual external proteins may be visualized by staining procedures, such as the use of ferritin-labeled antibodies, to yield electron micrographs similar in appearance to Fig. 11-36.

b. Membrane Lipids and Proteins Are Unevenly Distributed

The distribution of lipids between the different sides of biological membranes has been established through the use of phospholipid-hydrolyzing enzymes known as **phospholipases**. Phospholipases cannot pass through membranes, so that only phospholipids on the external surfaces of intact cells are susceptible to their action. Such studies indicate that *the lipids in biological membranes, like the proteins, are asymmetrically distributed between the leaflets of a bilayer* (e.g., Fig. 12-35). Carbohydrates, as we have seen (Section 11-3Cd), are located almost exclusively on the external surfaces of plasma membranes.

Lipids and proteins in plasma membranes may also be laterally organized. Thus, the plasma membranes of most cells have two or more distinct domains that have different functions. For example, the plasma membranes of **epithelial cells** (the cells lining body cavities and free surfaces) have an **apical domain**, which faces the lumen of the cavity and often has a specialized function (e.g., the absorption of nutrients in intestinal brush border cells; Section 20-4A), and a **basolateral domain**, which covers the remainder of the cell. These two domains, which do not intermix, have different compositions of both lipids and proteins.

A variety of measurements indicate that the hundreds of different lipids and proteins within a given plasma membrane domain are not uniformly mixed but instead often seg-

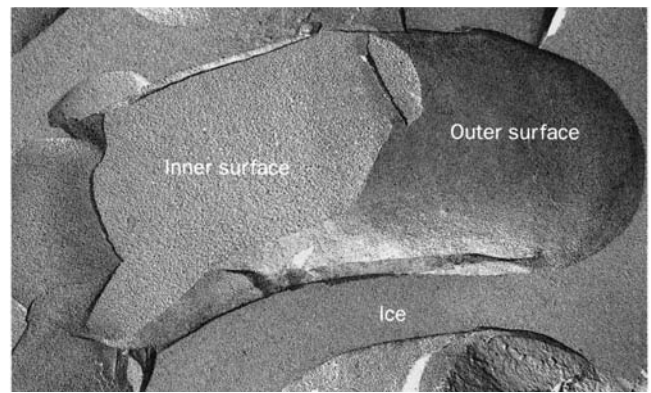


Figure 12-34 Freeze-etch electron micrograph of a human erythrocyte plasma membrane. The exposed interior face of the membrane is studded with numerous globular particles that are integral proteins (see Fig. 12-32). The outer surface of the membrane appears smoother than the inner surface because proteins do not project very far beyond the outer membrane surface. [Courtesy of Vincent Marchesi, Yale University.]

regate to form **microdomains** that contain only certain types of lipids and proteins. This may occur for several reasons:

1. Certain integral proteins associate to form aggregates or patches in the membrane (e.g., BR), which in turn may preferentially associate with specific lipids. Alternatively, some integral proteins are localized by attachments to elements of the cytoskeleton (which underlies the plasma membrane; Section 1-2A) or are trapped within the spaces enclosed by the resulting “fences.”

2. Integral proteins may specifically interact with particular lipids. For example, mismatches between the length of an integral protein’s hydrophobic TM band and the average thickness of a lipid bilayer may result in the selective accumulation of certain phospholipids around the protein in an annulus of 10 to 20 layers.

3. Divalent metal ions, notably Ca^{2+} , selectively ligate negatively charged head groups such as those of phosphatidylserine, thereby causing these phospholipids to aggregate in the membrane. Such metal ion-induced phase separations are known to regulate the activities of certain membrane-bound enzymes.

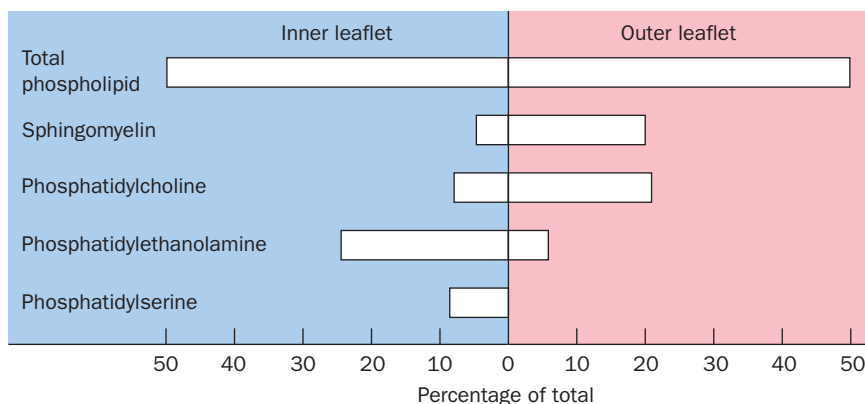


Figure 12-35 Asymmetric distribution of phospholipids in the human erythrocyte membrane. The phospholipid content is expressed as mole percent. [After Rothman, J.E. and Lenard, J., *Science* **194**, 1744 (1977).]

4. Glycosphingolipids (which occur only in the outer leaflet of the plasma membrane) and cholesterol pack together to form mobile **rafts** and ~75-nm-diameter flask-shaped indentations named **caveolae** (Latin for small caves) with which specific proteins preferentially associate. Glycosphingolipids, by themselves, do not form bilayers because their large head groups prevent the requisite close packing of their predominantly saturated hydrophobic tails. Conversely, cholesterol by itself does not form a bilayer due to its small head group. It therefore appears that the glycosphingolipids in these microdomains associate laterally via weak interactions between their carbohydrate head groups with the voids between their tails filled in by cholesterol. The sphingolipid–cholesterol rafts and caveolae are not solubilized at 4°C by uncharged detergents such as Triton X-100 (Fig. 12-19). The low density of the resulting **detergent-resistant membranes (DRMs)** allows their isolation by sucrose density gradient ultracentrifugation (Section 6-5Ba), thereby permitting their associated proteins to be identified. Many of the proteins that participate in transmembrane signaling processes (Chapter 19), including GPI-linked proteins, preferentially associate with DRMs. Caveolae, which appear to be rafts with which one or more homologous proteins named **caveolins** are associated, are likewise enriched with proteins that participate in signaling.

It should be noted that all of these aggregates are highly dynamic structures that rapidly exchange both proteins and lipids with their surrounding membrane as a consequence of the weak and transient interactions between membrane components and their interactions with the underlying cytoskeleton. In fact, single molecule tracking techniques (Section 12-2Ca) have demonstrated that lipid molecules in biological membranes undergo a series of short random motions over short time periods (~10 ms) interspersed by large hops (Fig. 12-36), a process called **hop diffusion**. Evidently, *biological membranes are partitioned rather than continuous two-dimensional fluids.*

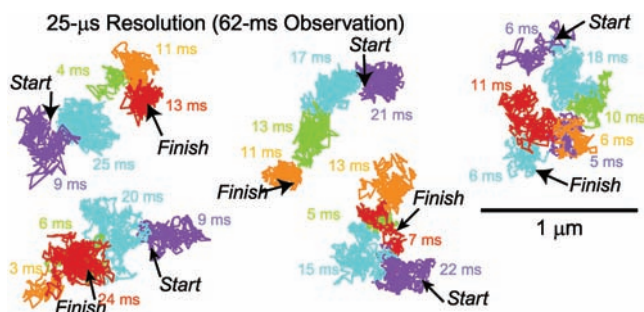


Figure 12-36 Hop diffusion of individual colloidal gold-tagged dioleoylphosphatidylethanolamine molecules in a plasma membrane. The position of each particle was determined at 25- μ s intervals (a video frame rate of 40,500 frames \cdot s $^{-1}$) over a period of 62 ms (2500 steps). Colored lines connect successive positions of the particle, with differently colored segments representing the various plausible regions in the plasma membrane to which the particle appears to have been transiently confined (in the order purple, blue, green, orange, and red). [Courtesy of Akihiro Kasumi, Nagoya University, Japan.]

D. The Erythrocyte Membrane

The erythrocyte membrane's relative simplicity, availability, and ease of isolation have made it the most extensively studied and best understood biological membrane. It is therefore a model for the more complex membranes of other cell types. A mature mammalian erythrocyte is devoid of organelles and carries out few metabolic processes; it is essentially a membranous bag of hemoglobin. Erythrocyte membranes can therefore be obtained by osmotic lysis, which causes the cell contents to leak out. The resultant membranous particles are known as erythrocyte **ghosts** because, on return to physiological conditions, they reseal to form colorless particles that retain their original shape. Indeed, by transferring sealed ghosts to another medium, their contents can be made to differ from the external solution.

a. Erythrocyte Membranes Contain a Variety of Proteins

The erythrocyte membrane has a more or less typical plasma membrane composition of about half protein, somewhat less lipid, and the remainder carbohydrate (Table 12-4). Its proteins may be separated by SDS–polyacrylamide gel electrophoresis (Section 6-4C) after first solubilizing the membrane in a 1% SDS solution. The resulting electrophoretogram for a human erythrocyte membrane exhibits seven major and many minor bands when stained with Coomassie brilliant blue (Fig. 12-37). If the electrophoretogram is instead treated with **periodic acid–Schiff's reagent (PAS)**, which stains carbohydrates, four so-called PAS bands become evident. The polypeptides corresponding to bands 1, 2, 4.1, 4.2, 5, and 6 are readily extracted from the

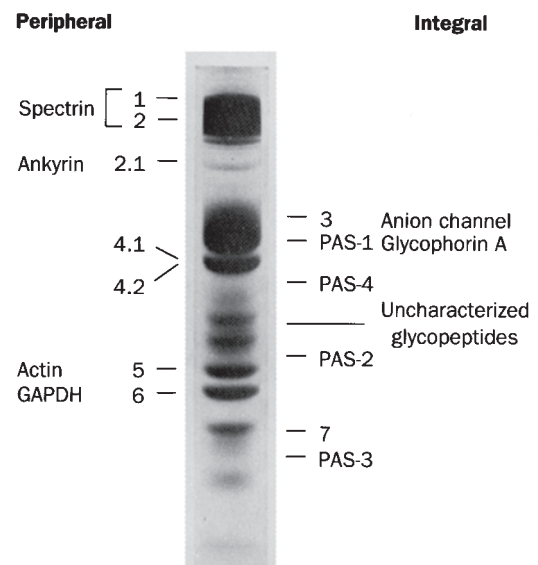


Figure 12-37 SDS–PAGE electrophoretogram of human erythrocyte membrane proteins as stained by Coomassie brilliant blue. The bands designated 4.1 and 4.2 are not separated with the 1% SDS concentration used. The minor bands are not labeled for the sake of clarity. The positions of the four sialoglycoproteins that would be revealed by PAS staining are indicated. [Courtesy of Vincent Marchesi, Yale University.]

membrane by changes in ionic strength or pH and hence are peripheral proteins. These proteins are located on the inner side of the membrane, as is indicated by the observation that they are not altered by the incubation of intact erythrocytes or sealed ghosts with proteolytic enzymes or membrane-impermeable protein labeling reagents. These proteins are altered, however, if “leaky” ghosts are so treated.

In contrast, bands 3, 7, and all four PAS bands correspond to integral proteins; they can be released from the membrane only by extraction with detergents or organic solvents. Of these, band 3 and PAS bands 1 and 2 correspond to TM proteins, as indicated by their different labeling patterns when intact cells are treated with membrane-impermeable protein-labeling reagents and when these reagents are introduced inside sealed ghosts. The PAS band 1 is a dimer of glyophorin A, which is formed through an SDS-resistant association between the TM helices of the polypeptide chains (Fig. 12-21); this dimer is the protein’s native form. The PAS band 2 protein is the monomeric form of glyophorin A.

The transport of CO_2 in blood (Section 10-1C) requires that the erythrocyte membrane be permeable to HCO_3^- and Cl^- (the maintenance of electroneutrality requires that for every HCO_3^- that enters a cell, a Cl^- or some other anion must leave the cell; Section 10-1Cb). The rapid transport of these and other anions across the erythrocyte membrane is mediated by a specific **anion channel** of which there are ~ 1 million/cell (comprising $>30\%$ of the membrane protein). Band 3 protein (929 residues and 5–8% carbohydrate) specifically reacts with anionic protein-labeling reagents that block the anion channel, thereby indicating that the anion channel is composed of band 3 protein. Furthermore, cross-linking studies with bifunctional reagents (Section 8-5Ca) demonstrate that the anion channel is at least a dimer. Hemoglobin and the glycolytic (glucose metabolizing) enzymes **aldolase**, **phosphofructokinase (PFK)**, and the band 6 protein **glyceraldehyde-3-phosphate dehydrogenase (GAPDH)**; Section 17-2F) all specifically and reversibly bind to band 3 protein on the cytoplasmic side of the membrane. The functional significance of this observation is unknown.

b. The Erythrocyte’s Cytoskeleton Is Responsible for Its Shape and Flexibility

A normal erythrocyte’s biconcave disklike shape (Fig. 7-19a) assures the rapid diffusion of O_2 to its hemoglobin molecules by placing them no farther than $1\ \mu\text{m}$ from the cell surface. However, the rim and the dimple regions of an erythrocyte do not occupy fixed positions on the cell membrane. This can be demonstrated by anchoring an erythrocyte to a microscope slide by a small portion of its surface and inducing the cell to move laterally with a gentle flow of isotonic buffer. A point originally on the rim of the erythrocyte will move across the dimple to the rim on the opposite side of the cell from where it began. Evidently, the membrane rolls across the cell while maintaining its shape, much like the tread of a tractor. This remarkable mechanical property of the erythrocyte membrane results from the presence of a submembranous network of proteins that function as a membrane “skeleton”—the cell’s cytoskeleton. Indeed, this property is partially duplicated by a

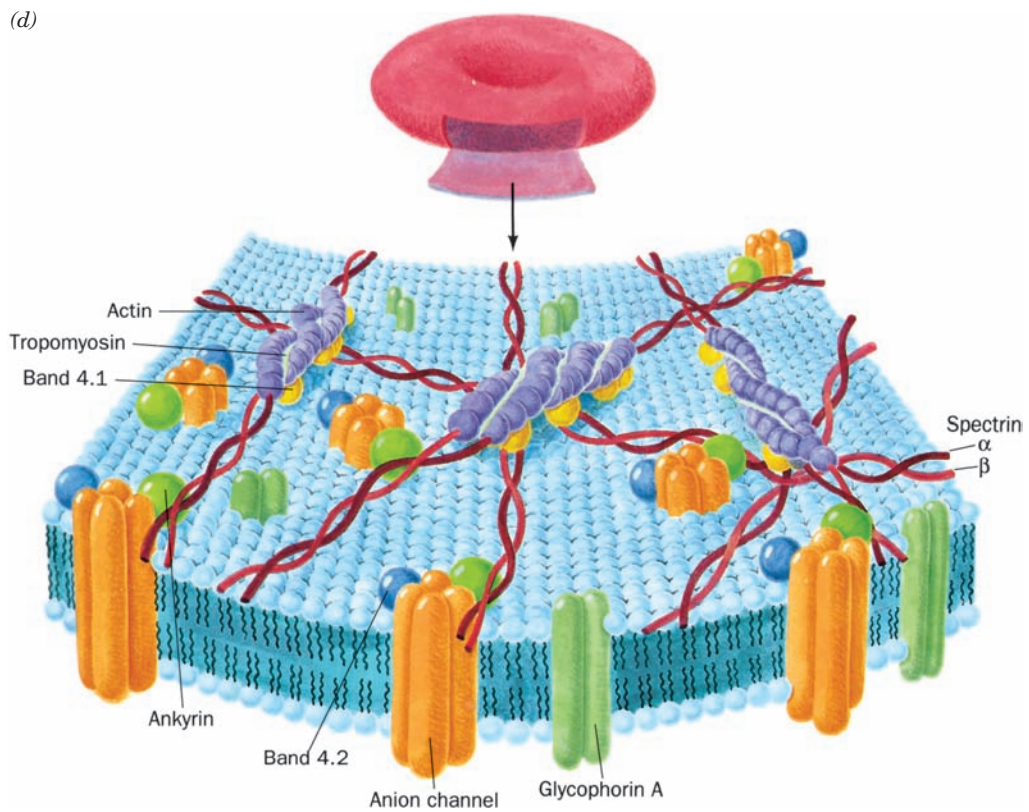
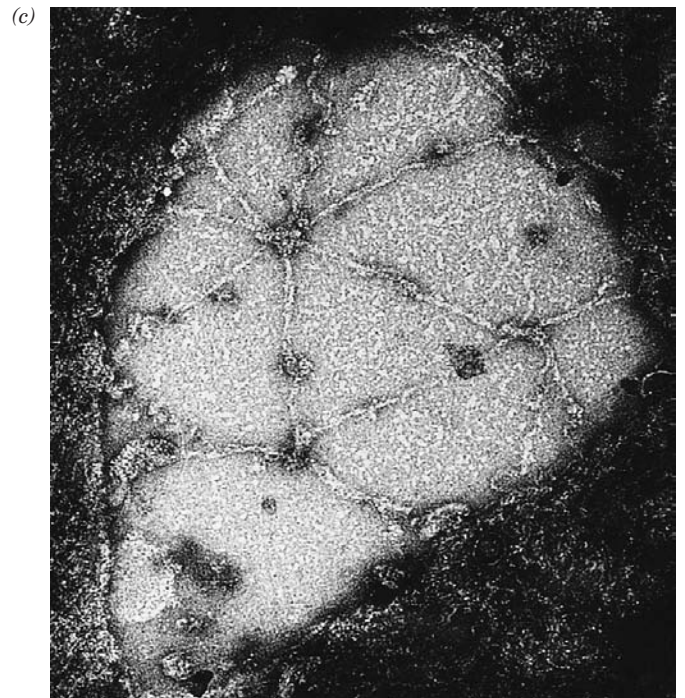
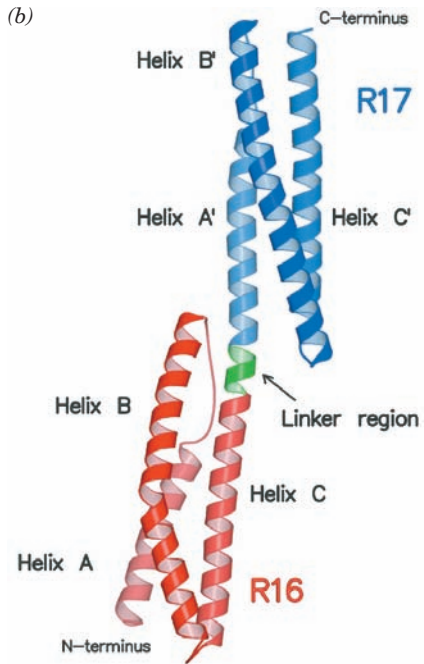
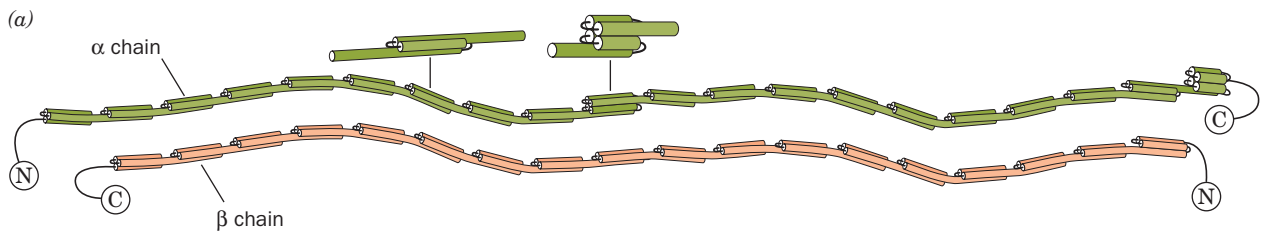
mechanical model consisting of a geodesic sphere (a spheroidal cage) that is freely jointed at the intersections of its struts but constrained from collapsing much beyond a flat surface. When placed inside an evacuated plastic bag, this cage also assumes a biconcave disklike shape.

The fluidity and flexibility imparted to an erythrocyte by its cytoskeleton has important physiological consequences. A slurry of solid particles of a size and concentration equal to that of red cells in blood has the flow characteristics approximating that of sand. Consequently, in order for blood to flow at all, much less for its erythrocytes to squeeze through capillary blood vessels smaller in diameter than they are, erythrocyte membranes, together with their cytoskeletons, must be fluidlike and easily deformable.

The protein **spectrin**, so called because it was discovered in erythrocyte ghosts, accounts for $\sim 75\%$ of the erythrocyte cytoskeleton. It is composed of two similar polypeptide chains, band 1 (α subunit; 2418 residues) and band 2 (β subunit; 2137 residues), which sequence analysis indicates each consist of repeating 106-residue segments that are predicted to fold into triple-stranded α helical coiled coils (Fig. 12-38a,b). Electron microscopy indicates that these large polypeptides are loosely intertwined to form a flexible wormlike $\alpha\beta$ dimer that is $\sim 1000\ \text{\AA}$ long (Fig. 12-38c). Two such heterodimers further associate in a

Figure 12-38 (Opposite) The human erythrocyte cytoskeleton.

(a) Structure of an $\alpha\beta$ dimer of spectrin. Both of these antiparallel polypeptides contain multiple 106-residue repeats, which are thought to form flexibly connected triple helical bundles. Two of these heterodimers join, head to head, to form an $(\alpha\beta)_2$ heterotetramer. [After Speicher, D.W. and Marchesi, V., *Nature* **311**, 177 (1984).] (b) X-ray structure of two consecutive repeats of chicken brain α -spectrin. Each of these 106-residue repeats consists of a down-up-down triple helical bundle in which the C-terminal helix of first repeat (R16; red) is continuous, via a 5-residue helical linker (green), with the N-terminal helix of the second repeat (R17; blue). The helices within each triple helical bundle wrap around each other in a gentle left-handed supercoil that is hydrophobically stabilized by the presence of nonpolar residues at the *a* and *d* positions of heptad repeats on all three of its component α helices (Fig. 8-26). Despite the expected rigidity of α helices, there is considerable evidence that spectrin is a flexible wormlike molecule. [Courtesy of Alfonso Mondragón, Northwestern University, PDBid 1CUN.] (c) Electron micrograph of an erythrocyte cytoskeleton that has been stretched to an area 9 to 10 times greater than that of the native membrane. Stretching makes it possible to obtain clear images of the cytoskeleton, which in its native state is so densely packed and irregularly flexed that it is difficult to pick out individual molecules and to ascertain how they are interconnected. Note the predominantly hexagonal network composed of spectrin tetramers cross-linked by junctions containing actin and band 4.1 protein. [Courtesy of Daniel Branton, Harvard University.] (d) Model of the erythrocyte cytoskeleton. The so-called junctional complex, which is magnified in this drawing, contains actin, **tropomyosin** (which, in muscle, also associates with actin; Section 35-3Ac), and band 4.1 protein, as well as **adducin**, **dematin**, and **tropomodulin** (not shown). [After Goodman, S.R., Krebs, K.E., Whitfield, C.F., Riederer, B.M., and Zagen, I.S., *CRC Crit. Rev. Biochem.* 23, 196 (1988).]



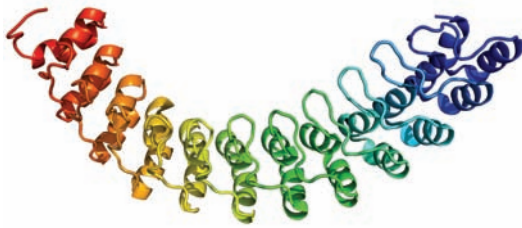


Figure 12-39 X-ray structure of human ankyrin repeats 13 to 24. The polypeptide is shown in ribbon form colored in rainbow order from its N-terminus (*blue*, repeat 13) to its C-terminus (*red*, repeat 24). [Based on an X-ray structure by Peter Michaely, University of Texas Southwestern Medical Center, Dallas, Texas. PDBid 1N11.]

head-to-head manner to form an $(\alpha\beta)_2$ heterotetramer. These tetramers, of which there are $\sim 100,000/\text{cell}$, are cross-linked at both ends by attachments to bands 4.1 and 5 to form a dense and irregular protein meshwork that underlies the erythrocyte plasma membrane (Fig. 12-38*c,d*). Band 5, a globular protein that forms filamentous oligomers, has been identified as **actin**, a common cytoskeletal element in other cells (Section 1-2Ae) and a major component of muscle (Section 35-3Ac). Spectrin also associates with band 2.1, an 1880-residue monomer known as **ankyrin**, which, in turn, binds to band 3, the anion channel protein. This attachment anchors the cytoskeleton to the membrane. Indeed, on solubilization of spectrin and actin by low ionic strength solutions, the erythrocyte ghosts' biconcave shape is lost and their integral proteins, which normally occupy fixed positions in the membrane plane, become laterally mobile.

Ankyrin's N-terminal 798-residue segment consists almost entirely of 24 tandem ~ 33 -residue repeats known as **ankyrin repeats** (Fig. 12-39), which also occur in a variety of other proteins. Each ankyrin repeat consists of two short (8- or 9-residue) antiparallel α helices followed by a long loop. These structures are arranged in a right-handed superhelical stack. The entire assembly forms an elongated concave surface that is postulated to bind various integral proteins as well as spectrin. Immunochemical studies have revealed spectrinlike, ankyrinlike, and band 4.1-like proteins in the cytoskeletons of a variety of tissues.

c. Hereditary Spherocytosis and Elliptocytosis Arise from Defects in the Erythrocyte Cytoskeleton

Individuals with **hereditary spherocytosis** have spherical erythrocytes that are relatively fragile and inflexible. These individuals suffer from hemolytic anemia because the spleen, a labyrinthine organ with narrow passages that normally filters out aged erythrocytes (which lose flexibility toward the end of their ~ 120 -day lifetime), prematurely removes spherocytotic erythrocytes. The hemolytic anemia may be alleviated by the spleen's surgical removal. However, the primary defects in spherocytotic cells are reduced

synthesis of spectrin, the production of an abnormal spectrin that binds band 4.1 protein with reduced affinity, or the absence of band 4.1 protein.

Hereditary elliptocytosis (having elongated or elliptical red cells; also known as **hereditary ovalocytosis**), a condition that is common in certain areas of Southeast Asia and Melanesia, confers resistance to malaria in heterozygotes (but apparently is lethal in homozygotes). This condition arises from defects in the erythrocyte anion channel. A common such defect consists of a 9-residue deletion that inactivates this TM protein. The consequent reduced capacity of red cells to import phosphate or sulfate ions may inhibit the intraerythrocytic growth of rapidly developing malarial parasites.

The camel, the renowned "ship of the desert," provides a striking example of adaptation involving the erythrocyte membrane. This remarkable animal is still active after a loss of water constituting 30% of its body weight and, when thus dehydrated, can drink sufficient water in a few minutes to become fully rehydrated. The rapid uptake of such a large amount of water by the blood, which must deliver it to the cells, would lyse the erythrocytes of most animals. Yet camel erythrocytes, which have the shape of flattened ellipsoids rather than biconcave disks, are resistant to osmotic lysis. Camel spectrin binds to its membrane with particular tenacity, but on spectrin removal, which requires a strong denaturing agent such as guanidinium chloride, camel erythrocytes assume a spherical shape.

E. Blood Groups

The outer surfaces of erythrocytes and other eukaryotic cells are covered with complex carbohydrates that are components of plasma membrane glycoproteins and glycolipids. They form a thick, fuzzy cell coating, the **glycocalyx** (Fig. 12-40), which contains numerous identity markers that function in various recognition processes. Human erythrocytes have 30 genetically distinct blood group systems comprised of >600 known **blood group determinants**, although many of these determinants are rare or occur only in certain ethnic groups. Of these systems, only two—the **ABO blood group system** (discovered in 1900 by Karl

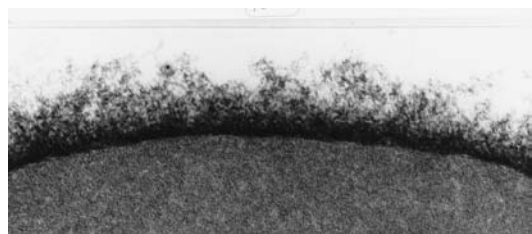


Figure 12-40 The erythrocyte glycocalyx as revealed by electron microscopy using special staining techniques. It is up to 1400 \AA thick and composed of closely packed, 12- to 25-\AA -diameter oligosaccharide filaments linked to plasma membrane-associated proteins and lipids. [Courtesy of Harrison Latta, UCLA.]

Landsteiner) and the **rhesus (Rh) blood group system**—have major clinical importance. The various blood groups are identified by means of suitable antibodies or by specific plant lectins.

a. ABO Blood Group Substances Are Carbohydrates

The ABO system consists of three blood group substances, the **A, B, and H antigens**, which are components of erythrocyte surface sphingoglycolipids. [Antigens are characteristic constellations of chemical groups on macromolecules that elicit the production of specific antibodies when introduced into an animal (Section 35-2Aa). Each antibody molecule can specifically bind to at least two of its corresponding antigen molecules, thereby cross-linking them.] Individuals with type A cells have A antigens on their cell surfaces and carry anti-B antibodies in their serum; those with type B cells, which bear B antigens, carry anti-A antibodies; those with type AB cells, which bear both A and B antigens, carry neither anti-A nor anti-B antibodies; and type O individuals, whose cells bear neither antigen, carry both anti-A and anti-B antibodies. Consequently, the transfusion of type A blood into a type B individual, for example, causes an anti-A antibody–A antigen reaction, which agglutinates (clumps together) the transfused erythrocytes, resulting in an often fatal blockage of blood vessels. The H antigen is discussed below. Anti-A and anti-B antibodies, which are not present at birth, appear to arise through an immune response to A-like and B-like antigens in food and/or to the colonization of the infant gut by bacteria that produce such antigens [the immune system normally suppresses the production of antibodies directed against the body's own antigens (Section 35-2Ac) so, for example, a type A individual does not produce anti-A antibodies].

The ABO blood group substances are not confined to erythrocytes but also occur in the plasma membranes of many tissues as glycolipids of considerable diversity. In fact, in the ~80% of the population known as secretors, these antigens are secreted as *O*-linked components of glycoproteins into various body fluids, including saliva, milk, seminal fluid, gastric juice, and urine. These diverse molecules, which are 85% carbohydrate by weight and have molecular masses ranging up to thousands of kilodaltons, consist of multiple oligosaccharides attached to a polypeptide chain.

The A, B, and H antigens differ only in the sugar residues at their nonreducing ends (Table 12-5). The H antigen occurs in type O individuals; it is also the precursor oligosaccharide of A and B antigens. Type A individuals have a 303-residue glycosyltransferase that specifically adds an *N*-acetylgalactosamine residue to the terminal position of the H antigen, whereas in type B individuals, this enzyme, which differs by four amino acid residues from that of type A individuals, instead adds a galactose residue. In type O individuals, the enzyme is inactive because its synthesis terminates after its 115th residue.

Do the different blood groups confer any biological advantages or disadvantages? Epidemiological studies indicate

Table 12-5 Structures of the A, B, and H Antigenic Determinants in Erythrocytes

Type	Antigen
H	Galβ(1 → 4)GlcNAc... ↑ 1,2 L-Fucα
A	GalNAcα(1 → 3)Galβ(1 → 4)GlcNAc... ↑ 1,2 L-Fucα
B	Galα(1 → 3)Galβ(1 → 4)GlcNAc... ↑ 1,2 L-Fucα

Abbreviations: Gal = galactose, GalNAc = *N*-acetylgalactosamine, GlcNAc = *N*-acetylglucosamine, L-Fuc = L-fucose.

that type A and B individuals are less susceptible to cholera infections than are type O individuals, with the relatively rare type AB individuals being highly resistant to this deadly disease. Apparently, type A and B oligosaccharides block a receptor for the bacterium causing cholera, *Vibrio cholera* (Section 19-2Cd). In addition, type O individuals, particularly nonsecretors, have a higher incidence of peptic (stomach) ulcers. However, type A individuals have a higher incidence of stomach cancer, heart disease, and pernicious anemia (Section 25-2Ee).

F. Gap Junctions

Most cells in multicellular organisms are in metabolic and electrical as well as physical contact with neighboring cells. This contact is brought about by tubular particles, named **gap junctions**, that join discrete regions of neighboring plasma membranes much like hollow rivets (Fig. 12-41). Indeed, these intercellular channels are so widespread that many whole organs are continuous from within. Thus gap junctions are important intercellular communication channels. For example, the synchronized contraction of heart muscle is brought about by flows of ions through gap junctions (heart muscle is not innervated as is skeletal muscle). Likewise, gap junctions serve as conduits for some of the substances that mediate embryonic development; blocking gap junctions with antibodies that bind to them causes developmental abnormalities in species as diverse as hydras, frogs, and mice. Gap junctions also function to nourish cells that are distant from the blood supply, such as bone and lens cells. Thus, it is not surprising that, in humans, defects in gap junctions are associated with certain neurodegenerative diseases, cataracts, deafness, several skin diseases, and developmental anomalies.

Gap junctions consist of a single sort of protein subunit known as a **connexin**. A single gap junction consists of two apposed hexagonal rings of connexins, called **connexons**, one from each of the adjoining plasma membranes

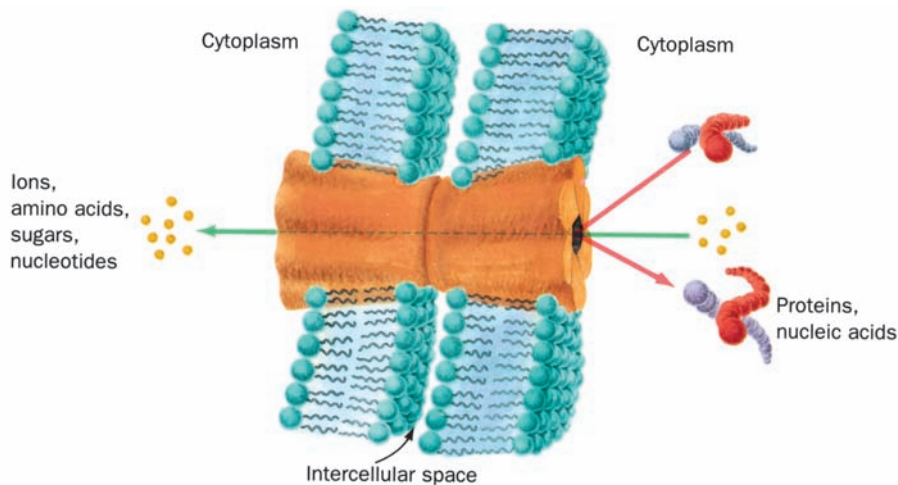


Figure 12-41 Model of a gap junction. Gap junctions between adjacent cells consist of two apposed plasma membrane–embedded hexagonal studs that bridge the gap between the cells.

Gap junctions hold cells a fixed distance apart—the gap. Small molecules and ions, but not macromolecules, can pass between cells via the gap junction’s central channel.

(Fig. 12-41). Cells are normally connected by clusters of hundreds to thousands of connexons. A given animal expresses numerous genetically distinct connexins, with humans, for example, expressing 21 different connexins ranging in molecular mass from 25 to 50 kD. Many types of cells simultaneously express several different species of connexins, and in cells that do so, there is considerable evidence that at least some connexons may be formed from two or more species of connexins. Moreover, the gap junctions joining two cells may consist of two different types of connexons. These various types of gap junctions presumably differ in their selectivities for the substances they transmit.

Mammalian gap junction channels are minimally 16 to 20 Å in diameter, which Werner Loewenstein established by microinjecting single cells with fluorescent molecules of various sizes and observing with a fluorescence microscope whether the fluorescent probe passed into neighboring cells. The molecules and ions that can pass freely between neighboring cells are limited in molecular mass to a maximum of ~1000 D; macromolecules such as proteins and nucleic acids cannot leave a cell via this route.

The diameter of a gap junction channel varies with Ca^{2+} concentration: The channels are fully open when the Ca^{2+} level is $<10^{-7} M$ and narrow as the Ca^{2+} concentration increases until, above $5 \times 10^{-5} M$, they close. This shutter system is thought to protect communities of interconnected cells from the otherwise catastrophic damage that would result from the death of even one of their members. Cells generally maintain very low cytosolic Ca^{2+} concentrations ($<10^{-7} M$) by actively pumping Ca^{2+} out of the cell as well as into their mitochondria and endoplasmic reticulum (Section 20-3B; Ca^{2+} is an important intracellular messenger whose cytosolic concentration is precisely regulated). Ca^{2+} floods back into leaky or metabolically depressed

cells, thereby inducing closure of their gap junctions and sealing them off from their neighbors.

a. Connexins Contain Transmembrane Four-Helix Bundles

The X-ray structure of the gap junction formed by the 226-residue human **connexin 26 (Cx26)**, determined by Tomitake Tsukihara, reveals a 12-mer with D_6 symmetry, a height of 155 Å, and a maximal diameter of 92 Å that encloses a central channel (Fig. 12-42a). The extracellular portion of each connexon extends 23 Å from the extracellular surface and interdigitates with the opposite connexon by 6 Å to span an intercellular gap of 40 Å. Each Cx26 subunit forms an up–down–up–down four-helix bundle in which both the N- and C-termini occupy the cytosol. The central channel has a diameter of ~40 Å at its cytosolic entrance that funnels down to 14 Å near the extracellular surface of the membrane and then widens to 25 Å in the extracellular space (Fig. 12-42b). The positively charged funnel entrance would attract negatively charged molecules. However, the region of maximal channel constriction is negatively charged, which should also affect the channel’s charge selectivity.

G. Channel-Forming Proteins

A number of bacterial toxins are synthesized as water-soluble monomers that, on interacting with their target membrane via a specific receptor protein, spontaneously insert into the membrane as a TM pore. This process, which for many such **channel-forming toxins (CFTs)** requires their oligomerization, causes the leakage of small ions and molecules from the target cell, thereby killing it through loss of osmotic balance. The formation of only one CFT-based pore is often sufficient to kill a cell.

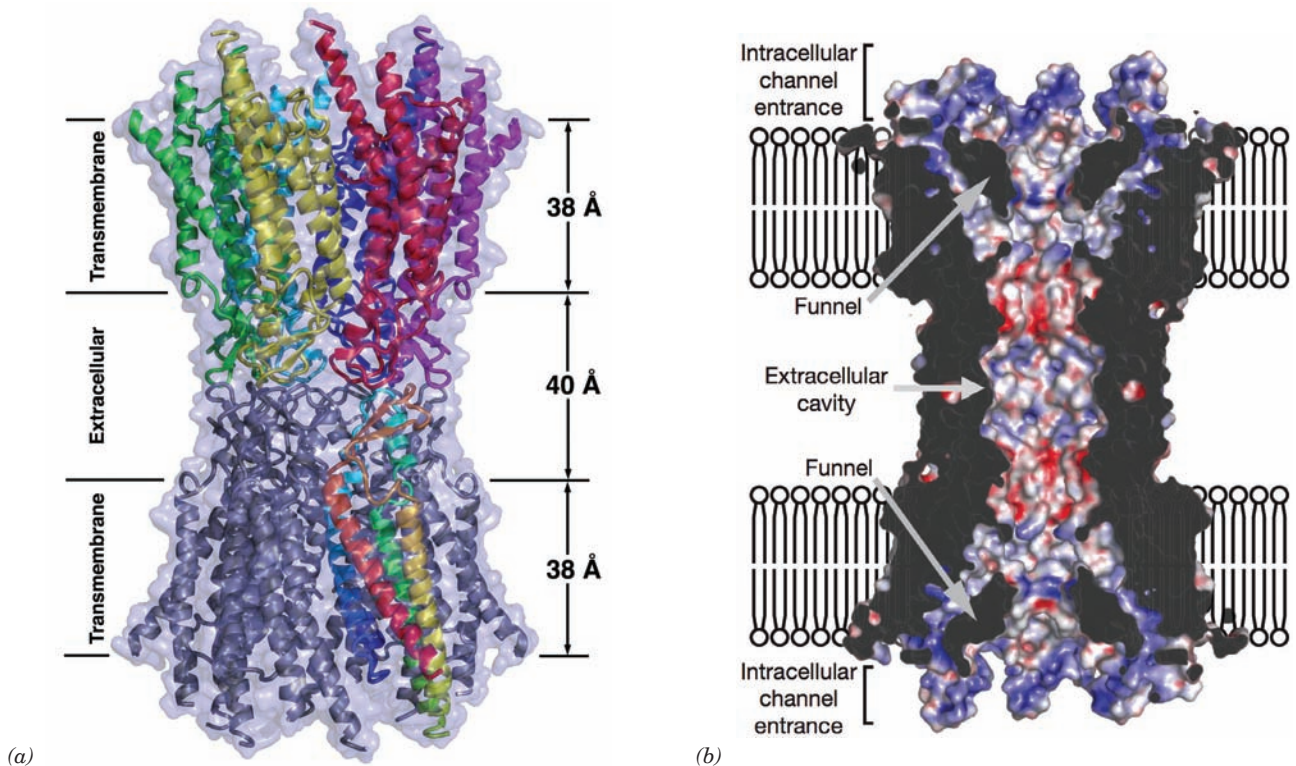


Figure 12-42 X-ray structure of the connexin 26 gap junction. (a) View perpendicular to the protein's 6-fold axis (parallel to the planes of the membranes) in which the protein is drawn in ribbon form embedded in its semitransparent molecular surface. Each connexin of the upper connexon has a different color, whereas one connexin in the lower connexon is colored in rainbow order from its N-terminus (blue) to its C-terminus (red) with the remaining connexins purple. The extent of the

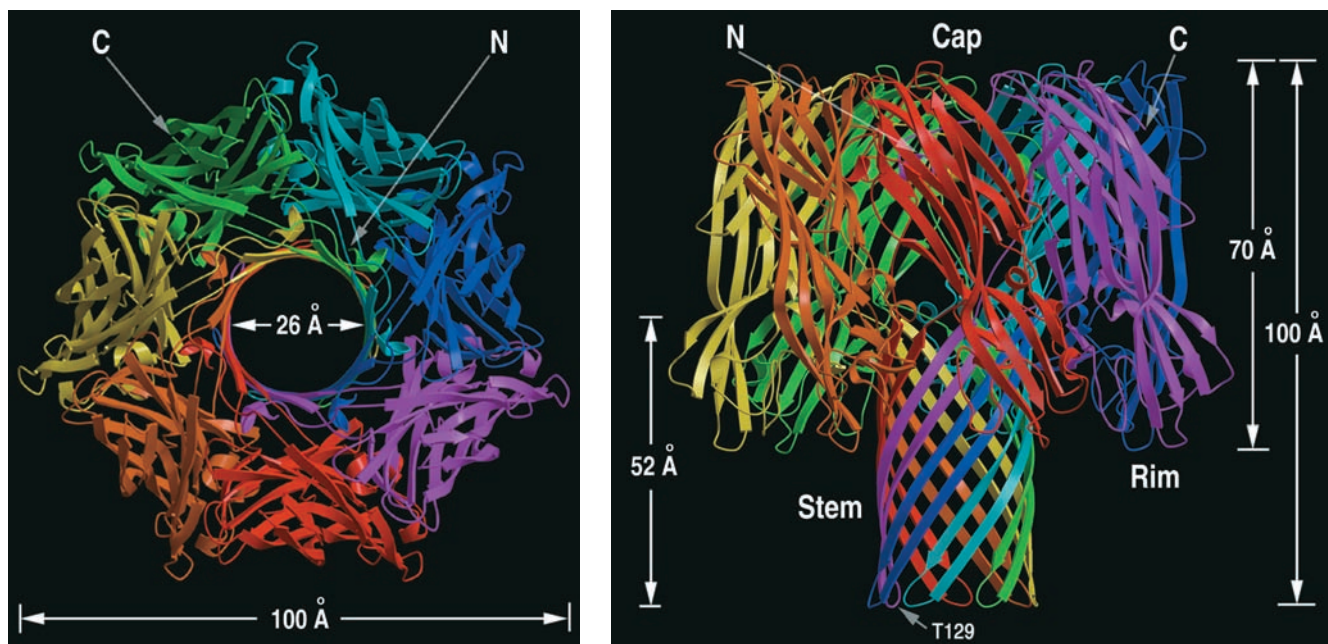
transmembrane region was deduced from the distribution of hydrophobic and aromatic residues (Section 12-3Af). (b) Cutaway drawing through the surface diagram of the gap junction channel. The channel surface is colored according to its electrostatic potential with red positive, blue negative, and white neutral. [Part a based on an X-ray structure by, and Part b courtesy of Tomitake Tsukihara, University of Osaka, Japan. PDBid 2ZW3.]

One of the best characterized CFTs is **α -hemolysin**, which the human pathogen *Staphylococcus aureus* secretes as a water-soluble 293-residue monomer and which spontaneously inserts into the membranes of erythrocytes and several other types of cells in the form of heptameric pores. Even though the α -hemolysin monomer is water-soluble and lacks clearly hydrophobic segments, the heptamer acts as a typical TM protein in that it is not released from the membrane by treatment with high salt, low pH, or chaotropic agents but, instead, requires treatment with detergents for this to occur.

The X-ray structure of detergent-solubilized α -hemolysin, determined by Eric Gouaux, reveals a striking mushroom-shaped heptameric complex that is 100 Å in height and 100 Å in diameter (Fig. 12-43a,b). A 14- to 46-Å-diameter solvent-filled channel, which runs along the protein's 7-fold axis, forms a TM pore. The stem of the mushroom, the protein's TM segment, consists of a 52-Å-high and 26-Å-diameter, porinlike, 14-stranded, antiparallel β barrel composed of seven 2-stranded antiparallel β sheets, one from each subunit (Fig. 12-43b). The remainder of each subunit

consists of a β sandwich domain and a rim domain, which together form a 70-Å-long ellipsoid (Fig. 12-43c). Seven of these ellipsoids are distributed in a ring, thereby forming the mushroom's cap and rim. The rim domain projects toward and probably interacts with the membrane's phospholipid head groups via the basic and aromatic residues that extend from the crevice between the top of the stem and rim.

A variety of experimental evidence indicates that the spontaneous formation of the heptameric TM pore occurs via several discrete steps: (1) the binding of the aqueous monomer to the membrane surface, probably through the interaction of the protein's polypeptide loops with the surface groups of the lipid bilayer; (2) the formation of the heptamer on the surface of the membrane; and (3) the insertion of the 14-stranded β barrel through the membrane to form the TM pore. The structural details of this process are as yet unknown, although it seems clear that there is little change in the monomers' secondary structure on their assembly to form the heptameric TM pore. The reason why monomers do not form heptamers in aqueous solution is



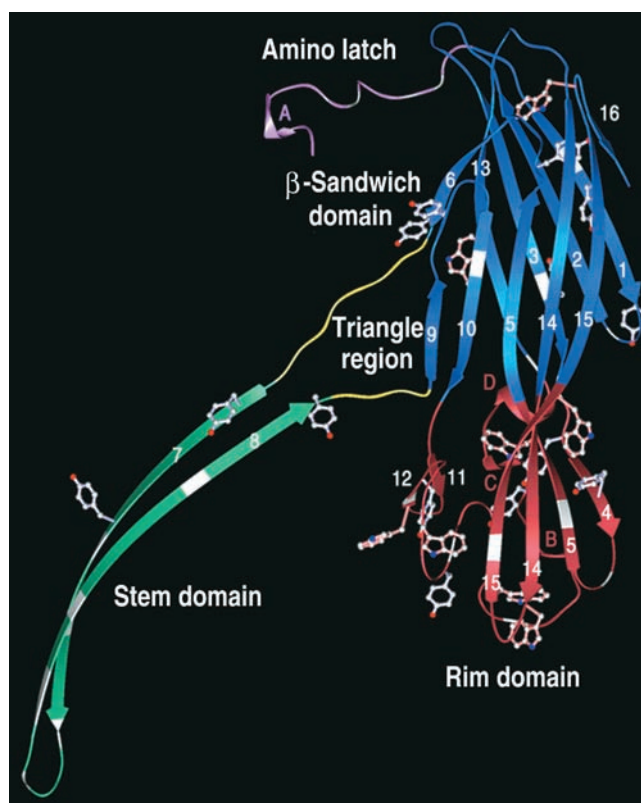
(a) (b)
Figure 12-43 X-ray structure of α -hemolysin. Views (a) along and (b) perpendicular to the heptameric transmembrane pore's 7-fold axis. Each subunit is drawn with a different color. (c) The monomer unit with its three domains drawn in different colors. [Courtesy of Eric Gouaux, Columbia University. PDBid 7AHL.]

probably due to differences between the strengths of the intrasubunit interactions in the monomer in aqueous solution and the intersubunit interactions in the heptamer in the membrane.

Not all CFTs form pores using β barrels. Rather, a variety of CFTs, notably several *E. coli* proteins known as **colicins**, form pores that are lined with α helices. Most such pores consist of monomers.

4 MEMBRANE ASSEMBLY AND PROTEIN TARGETING

As cells grow and divide, they synthesize new membranes. How are such asymmetric membranes generated? One way in which this might occur is through self-assembly. Indeed, when the detergent used to disperse a biological membrane is removed, liposomes form in which functional integral proteins are embedded. In most cases, however, these model membranes are symmetrical, both in their lipid distribution between the inner and outer leaflets of the bilayer and in the orientations of their embedded proteins. An alternative hypothesis of membrane assembly is that it occurs on the scaffolding of preexisting membranes; that is, membranes are generated by the expansion of old ones rather than by the creation of new ones. In this section we shall see that this is, in fact, how biological membranes are generated. In doing so, we shall consider how proteins



(c)

are inserted into and passed through membranes as well as how portions of membranes in the form of vesicles pinch off from one membrane and fuse with another, thereby transporting proteins and lipids between these membranes. These highly complex processes are indicative of the intricacies of biological processes in general.

1. Membranes contain proteins known as **flippases** that catalyze the flip-flops of specific phospholipids. These proteins tend to equilibrate the distribution of their corresponding phospholipids across a bilayer; that is, the net transport of a phospholipid is from the side of the bilayer with the higher concentration of the phospholipid to the opposite side. Such a process, as we shall see in Section 20-2, is a form of **facilitated diffusion**.

2. Membranes contain proteins known as **phospholipid translocases** that transport specific phospholipids across a bilayer in a process that is driven by ATP hydrolysis. These proteins can transport certain phospholipids from the side of a bilayer that has the lower concentration of the phospholipids being translocated to the opposite side, thereby establishing a nonequilibrium distribution of the phospholipids. Such a process, as we shall see in Section 20-2, is a form of **active transport**.

The observed distribution of phospholipids across membranes (e.g., Fig. 12-35) therefore appears to arise from the membrane orientations of the enzymes that synthesize phospholipids combined with the countervailing tendencies of ATP-dependent phospholipid translocases to generate asymmetric phospholipid distributions and those of flippases to randomize these distributions.

b. A Membrane's Characteristic Lipid Composition Can Arise in Several Ways

In eukaryotic cells, lipids are synthesized on the cytoplasmic face of the endoplasmic reticulum, from where they are transported to other membranes. Perhaps the most important mechanism of lipid transport is the budding off of membranous vesicles from the ER and their subsequent fusion with other membranes (Sections 12-4C and 12-4D). However, this mechanism does not explain the different lipid compositions of the various membranes in a cell. Lipids may also be transported between membranes by the **phospholipid exchange proteins** present in many cells. These proteins spontaneously transfer specific phospholipids, one molecule at a time, between two membranes separated by an aqueous medium. A membrane's characteristic lipid composition may also arise through on-site remodeling and/or selective degradation of its component lipids through the action of specific enzymes (Section 25-8A).

B. The Secretory Pathway

Membrane proteins, as are all proteins, are ribosomally synthesized under the direction of messenger RNA templates such that each polypeptide grows from its N-terminus to its C-terminus by the stepwise addition of amino acid residues (Section 5-4B). Cytologists have long noted two classes of eukaryotic ribosomes, those free in the cytosol and those bound to the endoplasmic reticulum (**ER**) so as to form the **rough endoplasmic reticulum (RER)**, so called because of the knobby appearance its bound ribosomes give it; Fig. 1-5). Both classes of ribosomes are nevertheless structurally identical; they differ only in the nature of the polypeptide they are synthesizing. *Free*

ribosomes synthesize mostly soluble and mitochondrial proteins, whereas membrane-bound ribosomes manufacture TM proteins and proteins destined for secretion, operation within the ER, or incorporation into lysosomes (membranous organelles containing a battery of hydrolytic enzymes that function to degrade and recycle cell components; Section 1-2Ad). These latter proteins initially appear in the RER.

a. The Secretory Pathway Accounts for the Targeting of Many Secreted and Membrane Proteins

How are RER-destined proteins differentiated from other proteins? And how do these large, relatively polar molecules pass through the RER membrane? These processes occur via the **secretory pathway**, which was first described by Günter Blobel, César Milstein, and David Sabatini around 1975. Since ~25% of the different species of proteins synthesized by all types of cells are integral proteins and many others are secreted, ~40% of the various types of proteins that a cell synthesizes must be processed via the secretory pathway or some other protein targeting pathway (e.g., that which directs proteins to the mitochondrion; Section 12-4E). In this subsection, we first present an overview of the secretory pathway and then discuss its various aspects in detail. The secretory pathway is outlined in Fig. 12-46:

1. All secreted, ER-resident, and lysosomal proteins, as well as many TM proteins, are synthesized with leading (*N*-terminal) 13- to 36-residue **signal peptides**. These signal peptides consist of a 6- to 15-residue hydrophobic core flanked by several relatively hydrophilic residues that usually include one or more basic residues near the N-terminus (Fig. 12-47). Signal peptides otherwise have little sequence similarity. However, a variety of evidence indicates they form α helices in nonpolar environments.

2. When the signal peptide first protrudes beyond the ribosomal surface (when the polypeptide is at least ~40 residues long), the **signal recognition particle (SRP)**, a 325-kD complex of six different polypeptides and a 300-nucleotide RNA molecule, binds to both the signal peptide and the ribosome accompanied by replacement of the SRP's bound GDP by GTP. The SRP's resulting conformational change causes the ribosome to arrest further polypeptide growth, thereby preventing the RER-destined protein from being released into the cytosol as well as averting premature protein folding that would preclude the protein from entering the ER (see below).

3. The SRP-ribosome complex diffuses to the RER surface, where it is bound by the **SRP receptor (SR)** in complex with the **translocon**, a protein pore in the ER membrane through which the growing polypeptide will be extruded. In forming the SR-translocon complex, the SR's bound GDP is replaced by GTP.

4. The SRP and SR stimulate each other to hydrolyze their bound GTP to GDP (which is energetically equivalent to ATP hydrolysis), resulting in conformational changes that cause them to dissociate from each other and

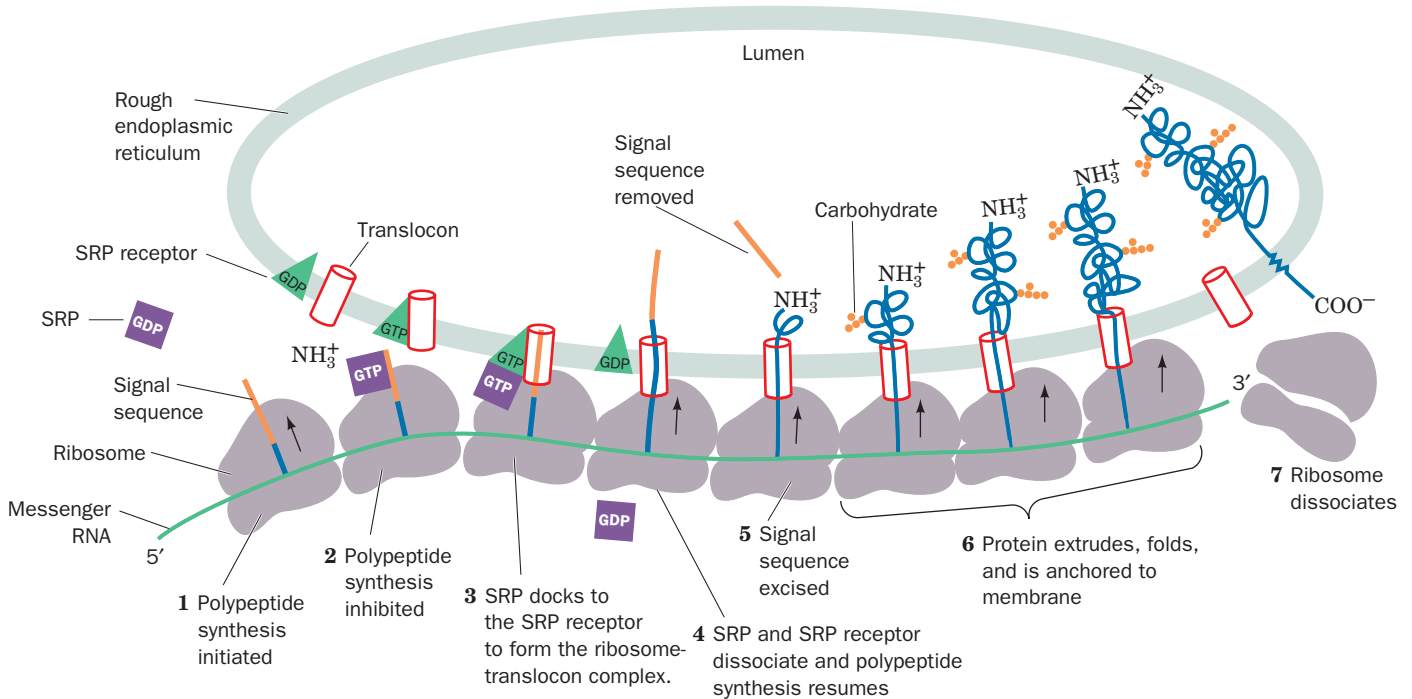


Figure 12-46 The ribosomal synthesis, membrane insertion, and initial glycosylation of an integral protein via the secretory pathway. (1) Protein synthesis is initiated at the N-terminus of the polypeptide, which consists of a 13- to 36-residue signal sequence. (2) A signal recognition particle (SRP) binds to the ribosome and the signal sequence emerging from it, thereby arresting polypeptide synthesis. (3) The SRP is bound by the transmembrane SRP receptor (SR) in complex with the translocon, thereby bringing together the ribosome and the translocon. (4) The SRP and SR hydrolyze their bound GTPs, causing them to dissociate from the ribosome–translocon complex. The ribosome then resumes the synthesis of the polypeptide, which passes through the translocon into the

of the ER. (5) Shortly after the entrance of the signal sequence into the lumen of the endoplasmic reticulum, it is proteolytically excised. (6) As the growing polypeptide chain passes into the lumen, it commences folding into its native conformation, a process that is facilitated by its interaction with the chaperone protein BiP (not shown). Simultaneously, enzymes initiate the polypeptide’s specific glycosylation. Once the protein has folded, it cannot be pulled out of the membrane. At points determined by its sequence, the polypeptide becomes anchored in the membrane (proteins destined for secretion pass completely into the ER lumen). (7) Once polypeptide synthesis is completed, the ribosome dissociates into its two subunits. See the Animated Figures

from the ribosome–translocon complex. This permits the bound ribosome to resume polypeptide synthesis such that the growing polypeptide’s N-terminus passes through the

translocon into the lumen of the ER. Most ribosomal processes, as we shall see in Section 32-3, are driven by GTP hydrolysis.

		Signal peptidase cleavage site
Bovine growth hormone	M M A A G P R T S LLLAFAALLCLP W T Q V V G	A F P
Bovine proalbumin	M K W V T FISLLLLF S S A Y S	R G V
Human proinsulin	M A L W M R L L P L L A L L A L W G P D P A A A	F V N
Human interferon γ	M K Y T S Y I L A F Q L C I Y L G S L G	C Y C
Human α -fibrinogen	M F S M R I V C L V L S V V G T A W T	A D S
Human IgG heavy chain	M E F G L S W L F L V A I L K G V Q C	E V Q
Rat amylase	M K F V L L L S L I G F C W A	Q Y D
Murine α -fetoprotein	M K W I T P A S L I L L L L H F A A S K	A L H
Chicken lysozyme	M R S LL I L V L C F L P L A A L G	K V F
<i>Zea mays</i> rein protein 22.1	M A T K I L A L L A L L A L L V S A T N A	F I I

Figure 12-47 N-Terminal sequences of some eukaryotic secretory preproteins. The hydrophobic cores (brown) of most

signal peptides are preceded by basic residues (blue). [After Watson, M.E.E., *Nucleic Acids Res.* **12**, 5147–5156 (1984).]

5. Shortly after the signal peptide enters the ER lumen, it is specifically cleaved from the growing polypeptide by a membrane-bound **signal peptidase** (polypeptide chains with their signal peptide still attached are known as **preproteins**; signal peptides are alternatively called **presequences**).

6. The nascent (growing) polypeptide starts to fold to its native conformation, a process that is facilitated by its interaction with an ER-resident chaperone protein Hsp70 (Section 9-2C). Enzymes in the ER lumen then initiate **post-translational modification** of the polypeptide, such as the specific attachments of “core” carbohydrates to form glycoproteins (Section 23-3B); the formation of disulfide bonds as facilitated by protein disulfide isomerase (Section 9-2A), an ER-resident protein; and the attachment of GPI anchors (Section 23-3Bk).

7. When polypeptide synthesis is completed, the protein is released from both the ribosome and the translocon, and the ribosome dissociates from the RER. Secretory, ER-resident, and lysosomal proteins pass completely through the RER membrane into the lumen. TM proteins, in contrast, contain one or more hydrophobic ~22-residue TM sequences that remain embedded in the membrane.

The secretory pathway also occurs in prokaryotes for the insertion of certain proteins into the cell membrane (whose exterior is equivalent to the ER lumen). Indeed, all forms of life yet tested have homologous SRPs and SRs. However, in bacteria, the binding of the SRP to the ribosome does not arrest translation.

b. The Cryo-Electron Microscopy Structure of the SRP in Complex with a Translating Ribosome Reveals How the SRP Binds Signal Peptide and Arrests Translation

Mammalian SRPs consist of six polypeptides known as **SRP9**, **SRP14**, **SRP19**, **SRP54**, **SRP68**, and **SRP72** (where the numbers are their molecular masses in kilodaltons) and an ~300-nucleotide (nt) 7S RNA [Fig. 12-48; RNAs are often classified according to their sedimentation rate in Svedberg units (S), which increases with their molecular mass (Section 6-5Aa)]. Many prokaryotic SRPs are much simpler; that in *E. coli* consists of a single polypeptide named **Ffh** that is homologous to SRP54 (Ffh for *Fifty-four* homolog) and a 4.5S RNA (114 nt) that, in part, is predicted to have a secondary structure similar to that portion of the 7S RNA to which SRP54 binds. Indeed, replacing SRP54 with Ffh or vice versa yields functional SRPs, at least *in vitro*, thereby suggesting that the Ffh–4.5S RNA complex is a structurally minimized version of the eukaryotic SRP.

The 12-Å resolution cryo-electron microscopy (cryo-EM)-based structure of canine SRP in complex with a wheat germ ribosome containing a nascent (growing) polypeptide chain was determined by Joachim Frank and Roland Beckmann. The structure reveals that the so-called S domain of the ~270-Å-long SRP binds at the base of the large (60S) ribosomal subunit next to the exit of the tunnel through which newly synthesized polypeptide emerges, whereas the Alu domain bends around the large subunit to contact the ribosome at the interface between its large and small (40S) subunits (Fig. 12-49).

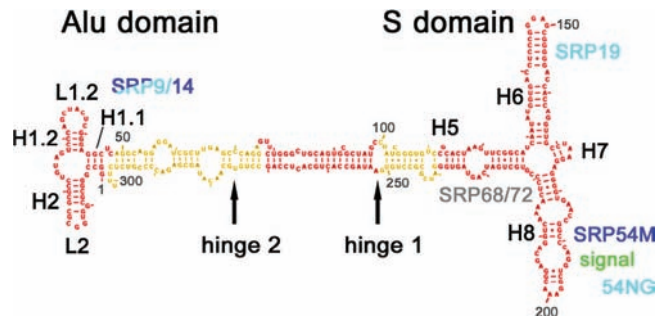


Figure 12-48 Sequence and secondary structure of canine 7S RNA. Its various double helical segments (denoted H1 through H8) and loops (denoted L1 and L1.2), are drawn in red and yellow with Watson–Crick base pairs represented by connecting lines and non-Watson–Crick base pairs indicated by dots. The positions at which the various SRP proteins bind to the 7S RNA are indicated in cyan, blue, and gray. [Courtesy of Roland Beckmann, Humboldt University of Berlin, Germany.]

The ribosome–SRP structure was modeled by fitting the much higher resolution X-ray structures of the yeast ribosome (Section 32-3Af) and various SRP fragments to the cryo-EM-derived electron density (Figs. 12-49d and 12-50). The model indicates that the 7S RNA consists mainly of a long double helical rod that is bent at two positions named hinge 1 and hinge 2 (RNA, as does DNA, can form a base-paired double helix, although its conformation is distinctly different from that of B-DNA; Section 29-1Bc). The signal sequence exiting the ribosome, which was modeled as an α helix, binds to SRP54, which contacts the ribosome near the mouth of its peptide exit tunnel.

SRP54 consists of three domains: the N-terminal N domain; the central G domain, which contains the SRP’s GTPase function and together with the N domain mediates the SRP’s interaction with the SRP receptor; and the C-terminal M domain, which is rich in methionine (25 of its 209 residues in humans). The N domain forms a bundle of four antiparallel α helices that closely associates with the G domain, which consists of an open β sheet (Section 8-3Bi) that structurally resembles those of other GTPases. The M domain contains a deep groove that binds the helical signal sequence. The groove is lined almost entirely with hydrophobic residues including many of SRP54’s Met residues (the Met side chain has physical properties similar to that of an *n*-butyl group). Its flexible unbranched Met side chain “bristles” presumably provide the groove with the plasticity to bind a variety of different signal sequences so long as they are hydrophobic and form an α helix.

Ribosomes, as we shall see in Section 32-3Dk, employ protein **elongation factors** to deliver aminoacyl-tRNAs and to motivate the sequence of reactions that appends an amino acid residue to the growing polypeptide chain. The eukaryotic SRP’s Alu domain, which is required for translational arrest, contacts the ribosome’s intersubunit region at the same positions to which the ribosomal elongation factors bind. This suggests that the Alu domain arrests translation by binding to the ribosome with sufficient affinity to block the binding of the ribosome’s required elongation factors. This is corroborated by the observation that

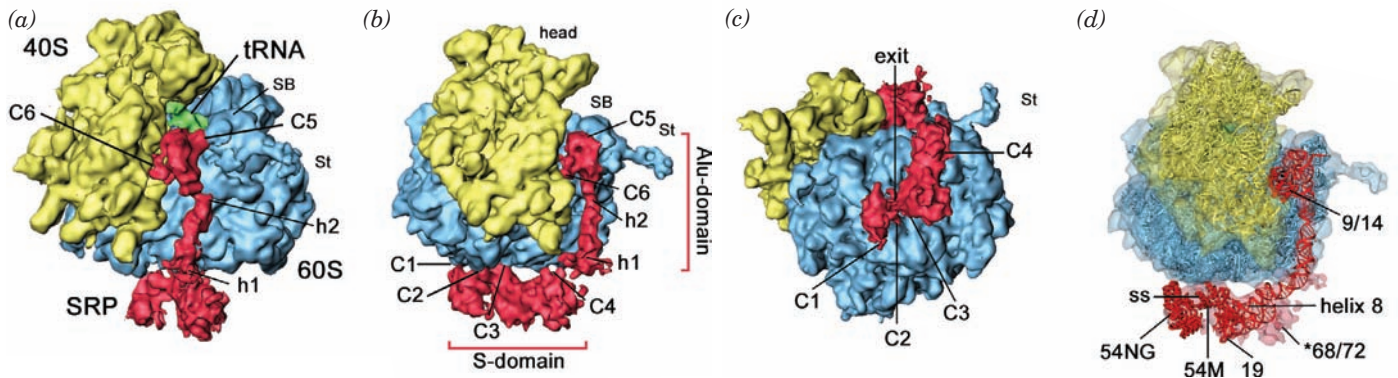


Figure 12-49 Cryo-EM structure of a translating wheat germ ribosome in complex with canine SRP at 12 Å resolution.

(a) Surface diagram showing the small (40S) ribosomal subunit in yellow, the large (60S) ribosomal subunit in blue, the SRP in red, and the tRNA occupying the ribosomal P-site (to which the growing polypeptide chain is covalently linked; Fig. 5-28) in green. C1 to C6 indicate the six positions at which the SRP

contacts the ribosome and h1 and h2 indicate the 7S RNA's hinge positions. St and SB stand for stalk and stalk base. (b) As in Part a but rotated 70° about the vertical axis. (c) As in Part a but rotated 90° about the horizontal axis. (d) As in Part b but with transparent surfaces showing the molecular models of the ribosome and SRP. [Courtesy of Roland Beckmann, Humboldt University of Berlin, Germany.]

bacterial SRP's, which do not arrest translation on binding to a ribosome, lack Alu domains.

c. Secretory Pathway Initiation Is Driven by GTP Hydrolysis

In eukaryotes, the SRP receptor is a heterodimer of subunits named **SR α** and **SR β** . SR β is a 271-residue integral protein that has an N-terminal TM segment, whereas SR α is a 638-residue peripheral protein that is apparently membrane-bound through the association of its N-terminal segment with SR β . Both SR α and SR β are GTPases.

In *E. coli*, the SR consists of a single 497-residue subunit named **FtsY**, whose C-terminal portion is homologous to that of SR α , although their N-terminal portions have no

sequence similarity. Curiously, the X-ray structure of the C-terminal portion of FtsY closely resembles that of the N and G domains of SRP54, with which it shares ~34% identity.

The targeting of the SRP-ribosome complex to the ER membrane is mediated by the GTPase functions of SRP54, SR α , and SR β . In numerous biological systems, mainly those mediating translation (Section 32-3), vesicle transport (Sections 12-4C and 12-4D), and signal transduction (Section 19-2), GTPases function as molecular switches that endow the system with unidirectionality and specificity. These so-called **G proteins** have at least two stable conformations: GDP-bound and GTP-bound. Interconversion between these states only occurs in a unidirectional cycle due to the irreversibility of GTP hydrolysis. In most cases, a G protein must interact with other proteins in order to change conformational states. Thus, GTP hydrolysis often requires stimulation by a specific **GTPase activating protein (GAP)**, and the exchange of bound GDP for GTP may require the assistance of a specific **guanine nucleotide exchange factor (GEF; Section 19-2Ca)**. The need for these particular factors confers specificity on the system.

The GEF for the SRP is the complex of the newly emerged signal sequence with the M domain of SRP54, which induces the adjoining G domain to exchange its bound GDP for GTP (Fig. 12-46, Stage 2). The formation of the resulting SRP · GTP complex results in a conformational change that locks the SRP to the ribosome, which, in turn, induces translational arrest. The GEF for the SR appears to be an empty translocon, which thereby associates with the resulting SR · GTP complex to which the SRP · GTP-ribosome complex then binds (Fig. 12-46, Stage 3). Evidently, the SRP and SR, both in their GTP forms, act as “molecular matchmakers” to bring together an empty translocon with a ribosome synthesizing a signal sequence-bearing polypeptide. The SRP and the SR then reciprocally stimulate each other's GTPase functions (act as mutual GAPs; neither protein alone has significant GTPase activity) followed by their dissociation, yielding free SRP · GDP and SR · GDP complexes ready to participate in a new

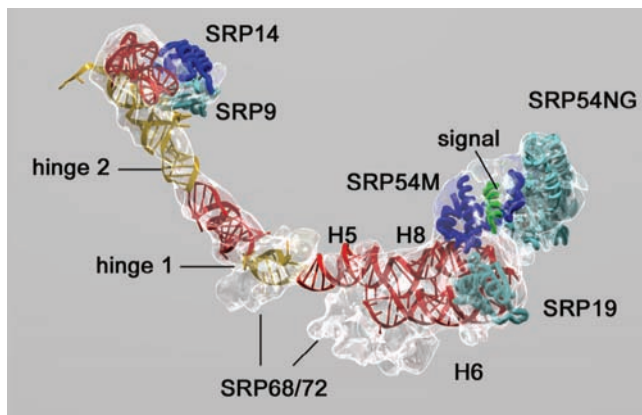


Figure 12-50 Molecular model of the SRP. The transparent cryo-EM-based electron density is shown in white and the ribbon diagrams of the X-ray structures of SRP proteins and RNA fragments that have been docked into it are colored as is indicated in Fig. 12-48. The signal sequence, modeled as an α helix, is green. Note that no atomic resolution structure of the SRP68/72 heterodimer is available. [Courtesy of Roland Beckmann, Humboldt University of Berlin, Germany. PDBid 2G05.]

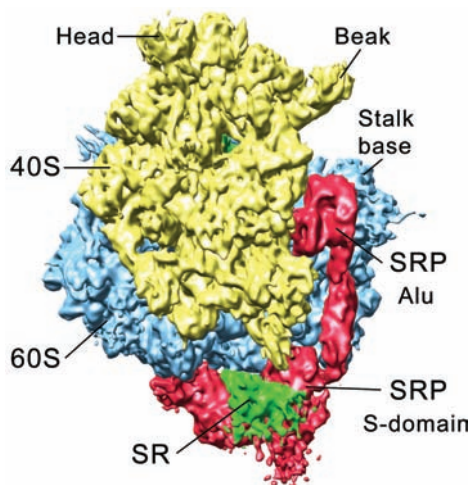


Figure 12-51 Cryo-EM structure of the eukaryotic SR-SRP-ribosome complex at 8 Å resolution. The complex is oriented and colored as in Fig. 12-49*b* with the SR colored green. [Courtesy of Roland Beckmann, Humboldt University of Berlin, Germany.]

round of the secretory pathway (Fig. 12-46, Stage 4). The release of the SRP and SR permits the now translocon-associated ribosome to recommence translation, thereby extruding the polypeptide it is synthesizing into or through the ER membrane as described below.

In the structure of the SRP-ribosome complex (Fig. 12-49), the S domain of the SRP blocks the binding of the translocon at the mouth of the peptide exit tunnel. However, the cryo-EM-based structure of the SR-SRP-ribosome complex (but lacking SRβ's TM segment), determined by Irmgard Sinning and Beckmann, reveals that the SR contacts both the large ribosomal subunit and the S domain of the SRP (Fig. 12-51) in a way that pushes the SRP's S domain in the SRP-ribosome complex away from the peptide exit site. This allows the translocon access to its ribosomal binding site and presumably positions it such that the M domain-bound signal sequence can readily be transferred to it. The position of the eukaryotic SRP's Alu domain on the ribosome is unaffected by the binding of the SR.

d. The Translocon Forms a Transmembrane Pore

How are preproteins transported across or inserted into the RER membrane? In 1975, Blobel postulated that these processes are mediated by a TM channel. However, it was not until 1991 that he was able to show that these channels actually exist through electrophysiological measurements indicating that the RER membrane contains ion-conducting channels. These increase in number when the ribosome-bearing side of the RER is treated with **puromycin** (an antibiotic that causes the ribosome to prematurely release the growing polypeptide; Section 32-3Df), thereby suggesting that the channels are usually plugged by the presence of the polypeptides. By linking fluorescent dyes whose fluorescence is sensitive to the polarity of their environment to a nascent polypeptide, Arthur Johnson demonstrated

that these channels, now called translocons, enclose aqueous pores that completely span the ER membrane.

The various ER transmembrane proteins that comprise the translocon were identified through the use of photoactivatable groups that were attached to signal sequences and mature regions of preproteins. On exposure to light of the proper wavelength, the photoactivatable groups react with nearby proteins to form covalent cross-links, thereby permitting the identification of these proteins. The central component of the translocon, named **Sec61** (Sec for *secretion*) in eukaryotes and the **SecY** complex in prokaryotes, is a heterotrimeric protein. Its α and γ subunits, but not its β subunit, are essential for channel function and are conserved across all kingdoms of life (these subunits are respectively named Sec61α, Sec61β, and Sec61γ in eukaryotes and SecY, SecE, and SecG in bacteria).

The X-ray structure of the SecY complex from the archaeon *Methanococcus jannaschii*, determined by Stephen Harrison and Tom Rapoport, reveals that its α, β, and γ subunits, respectively, have 10, 1, and 1 TM α helices (Fig. 12-52*a,b*). The α subunit's TM helices are wrapped around an hourglass-shaped channel whose minimum diameter is ~3 Å (Fig. 12-52*c*). The channel is blocked at its extracellular end by a short, relatively hydrophilic helix (blue unnumbered helix in Fig. 12-52*a,b* and yellow helix in Fig. 12-52*c*). A variety of evidence indicates that this helix functions as a plug to prevent small molecules and ions from leaking across the membrane in the absence of a translocating polypeptide and that an incoming signal peptide pushes this helix aside. The γ subunit extends diagonally across the back of the α subunit so as to buttress it. The β subunit makes relatively tenuous contacts with the α subunit, which likely explains why the β subunit is dispensable for translocon function.

A cryo-EM-based structure of a mammalian ribosome-Sec61 complex (Fig. 12-53*a*), determined by Rapoport and Christopher Akey at 11 Å resolution, reveals that a single Sec61 channel is positioned over the ribosome's peptide exit tunnel with Sec61's 6/7 and 8/9 loops extending into the peptide exit tunnel (Fig. 12-53*b*). Indeed, mutating the positively charged residues of the 6/7 and 8/9 loops, which presumably bind to negatively charged ribosomal RNA, abolishes ribosome binding.

How wide is the SecY complex's **protein-conducting channel (PCC)** when it is translocating a polypeptide? At minimum, it would have to be ~7 Å across (the diameter of an extended anhydrous polypeptide), although if a TM sequence assumed its helical conformation while still in the PCC, the PCC would have to be at least ~12 Å wide. Such widening could be accomplished by movements of the helices from which the pore ring side chains emanate. The maximum dimensions of the PCC, as estimated from a consideration of the SecY structure (Fig. 12-52), are 15 × 20 Å. Such movements are supported by molecular dynamics calculations (Section 9-4a). Despite the large pore size of an active translocon, the ER membrane's permeability barrier is largely maintained. Evidently, the pore ring fits around the translocating polypeptide chain like a gasket, thereby preventing the passage of small molecules and ions during polypeptide translocation.

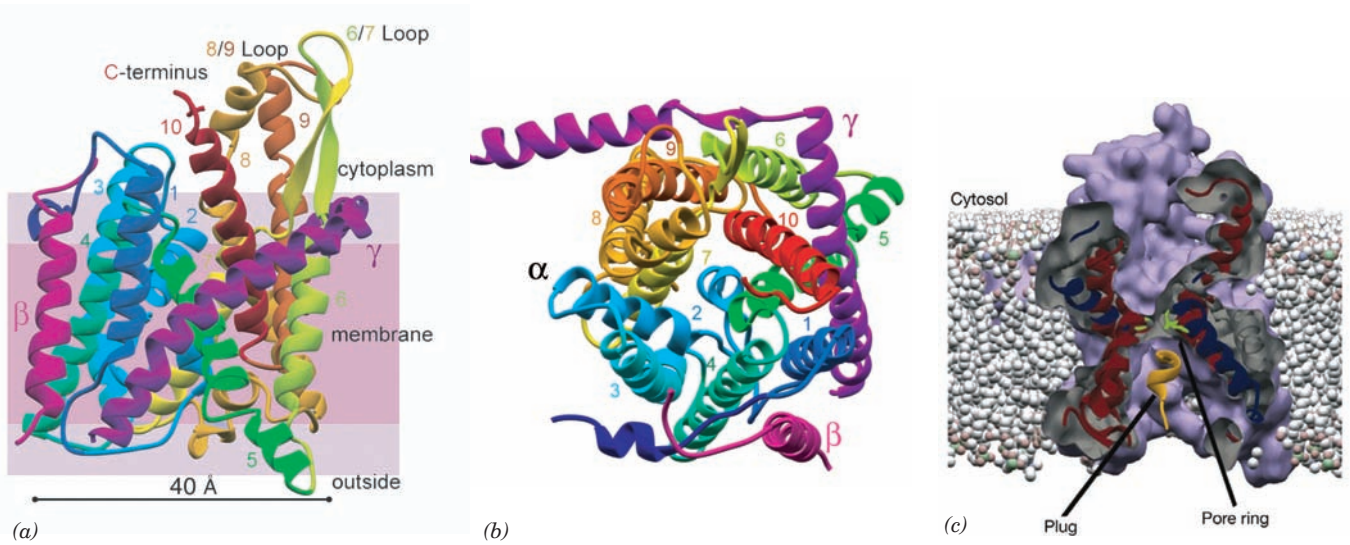


Figure 12-52 X-ray structure of the *M. jannaschii* SecY complex. (a) X-ray structure of the complex, with shading indicating the positions of membrane phospholipid head groups (violet) and hydrocarbon tails (pink). The α subunit of SecY (436 residues) is colored in rainbow order and its helices are numbered from its N-terminus (dark blue) to its C-terminus (red), the β subunit (74 residues) is magenta, and the γ subunit (53 residues) is purple. (b) View of SecY from the cytosol. The

translocon's putative lateral gate is on the left between helices 2 and 7. (c) Cross-section of the protein-conducting channel as viewed from the bottom of Part b. The helix that plugs the channel is yellow and the six hydrophobic side chains that form the narrowest part of the channel, the so-called pore ring, are green. [Courtesy of Stephen Harrison and Tom Rapoport, Harvard Medical School. PDBid 1RH5.]

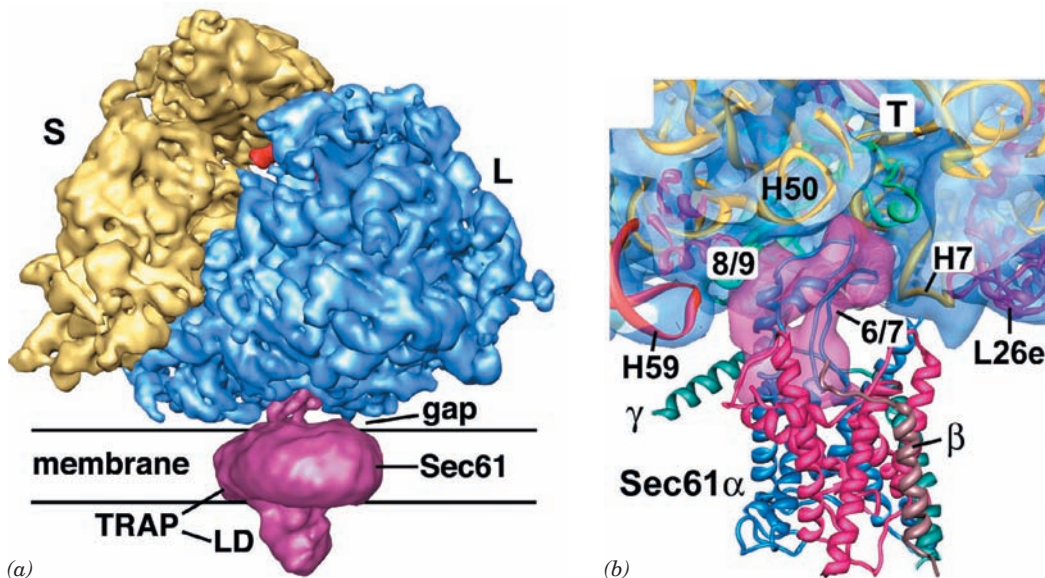


Figure 12-53 Cryo-EM structure of a canine ribosome-Sec61-TRAP complex at 11 Å resolution. (a) A surface diagram viewed parallel to the ER membrane. The ribosome's small (S) and large (L) subunits are yellow and blue, a tRNA occupying the ribosome's exit site (Section 32-3Bd) is red, and the Sec61-TRAP complex is magenta. LD is TRAP's lumenal domain. (b) A thin slab showing the interface between the ribosome and Sec61. The modeled structures of the ribosome

and Sec61, shown as ribbons, are embedded in their transparent surface diagrams, which are colored as in Part a. Note how loops 6/7 and 8/9 of Sec61 are inserted into the ribosome's peptide exit tunnel (T), where they interact with RNA helices H7 and H50. L26e is a protein subunit. [Courtesy of Tom Rapoport, Harvard Medical School; and Christopher Akey, Boston University School of Medicine. PDBid 3DKN.]

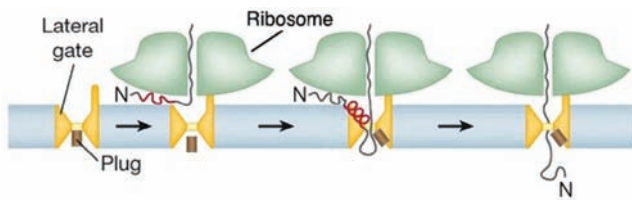


Figure 12-54 The stages of polypeptide translocation of a secretory protein. The red line represents the hydrophobic portion of the signal sequence. The process begins with the insertion of the nascent peptide as a loop into the PCC (left). The signal sequence then binds as an ~ 2 -turn helix between the SecY/Sec61 α subunit's helices 2 and 7, which helps displace the plug helix (middle). Finally, the signal sequence is excised by the signal protease (not shown) and the nascent peptide enters the ER through the PCC (right). [Courtesy of Tom Rapoport, Harvard Medical School.]

The translocation of a secretory protein begins with its insertion as a loop into the PCC (Fig. 12-54, left). This was established by using a mutant protein whose signal sequence is not excised by the signal protease and showing, through proteolysis experiments, that the protein's N- and C-termini both remained on the ER membrane's cytoplasmic side. Subsequently, as was shown by photo-cross-linking experiments, the signal sequence forms an ~ 2 -turn helix that inserts between TM helices 2 and 7 of Sec61 α (Fig. 12-54, middle). The separation of helices 2 and 7 (the lateral gate; Fig. 12-52b) helps displace the plug helix, which following signal sequence excision, allows the nascent polypeptide pass through the PCC into the ER (Fig. 12-54, right).

Additional components of the mammalian translocon are named **translocating chain-associated membrane protein (TRAM, ~ 375 residues; predicted to have 8 TM helices with both its N- and C-termini in the cytosol)** and **translocon-associated membrane protein (TRAP; an ~ 800 -residue heterotetramer with its α , β , and δ subunits each having one TM helix and its γ subunit having four TM helices)**. Through the use of Sec61-containing liposomes that either did or did not also contain TRAM, Rapoport demonstrated that TRAM is required for the translocation and membrane integration of most but not all preproteins into the liposome. Whether or not a given preprotein requires TRAM for translocation depends on its signal sequence, although no particular characteristic of this sequence appears to be critical for TRAM dependence. TRAP, which is seen in Fig. 12-53a, functions similarly to increase the translocational efficiency of proteins with certain signal sequences.

e. The Translocon Laterally Inserts Transmembrane Helices Into the ER Membrane

In addition to forming a conduit for soluble proteins to enter the ER, the translocon must insert an integral protein's TM segments into the ER membrane. The translocon, in concert with the ribosome, recognizes these TM segments and installs them into the lipid bilayer via a lateral gate between helices 2 and 7 in the SecY/Sec61 α subunit (Fig. 12-55).

Monotopic (alternatively, **single-pass**) TM proteins fall into one of three classes:

1. Type I proteins have cleavable N-terminal signal sequences. They are inserted into the membrane much like secretory proteins (Fig. 12-54) but have an ~ 22 -residue hydrophobic **stop-transfer anchor sequence** that the translocon laterally inserts into the membrane as a helix. Hence a type I protein has its N-terminus in the ER.

2. Type II proteins lack a cleavable N-terminal signal sequence. However, they have an ~ 22 -residue hydrophobic **signal-anchor sequence**, not necessarily near the protein's N-terminus, that is recognized by the SRP. The SRP then passes the nascent polypeptide to the translocon, which laterally inserts the signal-anchor sequence into the membrane oriented such that the protein's N-terminus is in the cytoplasm. This requires the polypeptide to loop around inside the translocon before being inserted into the membrane (Fig. 12-56, lower portion). The C-terminal segment of a type II protein is presumably extruded into the gap between the ribosome and the translocon (Fig. 12-53a) before being passed through the translocon.

3. Type III proteins, like type II proteins, lack a cleavable N-terminal signal sequence and have a signal-anchor sequence that is not necessarily near the protein's N-terminus. However, the orientation of these signal-anchor sequences in the membrane is opposite to that of type II proteins. Hence the way that type III proteins are inserted into the membrane resembles that of type I proteins (Fig. 12-56, upper portion). They differ, however, in that the transfer of a type III protein's N-terminal segment across the membrane cannot be initiated until after its signal-anchor sequence has been synthesized.

For polytopic (alternatively, **multipass** or **type IV**) TM proteins, looping must occur each time an additional helix is to be installed in the membrane. Evidently, the PCC of the

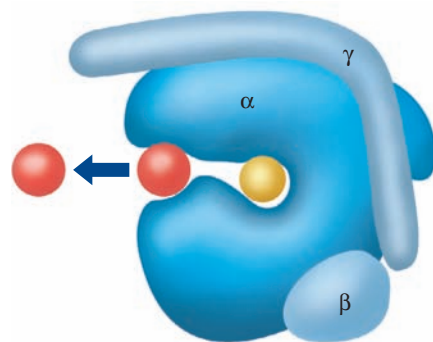


Figure 12-55 Model for the insertion of a TM helix into a membrane. The translocon (blue) is viewed as in Fig. 12-52b. A polypeptide chain (yellow) is shown bound in the translocon's pore during its translocation through the membrane, and a TM helix (red) is shown passing through the translocon's lateral gate and being released into the membrane (arrow). [Based on a drawing by Dobberstein, B. and Sinning, I., *Science* **303**, 320 (2004).]

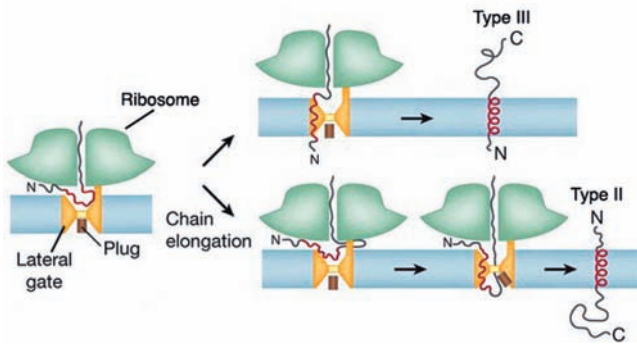


Figure 12-56 The generation of types II and III proteins.

Here, the red line represents a signal-anchor sequence. The N-terminus of a type III protein must pass through the translocon before its succeeding TM helix is laterally installed in the membrane (*top*). However, for a type II protein, whose N-terminus is retained in the cytoplasm (*bottom*), the subsequently synthesized polypeptide (represented by the loop between the ribosome and the translocon) must pass through the PCC. For polytopic TM proteins, these two processes alternate. [Based on a drawing by Tom Rapoport, Harvard Medical School.]

active translocon has sufficient room for successive TM segments to reverse their direction prior to being inserted into the ER membrane. Helices may be inserted into the membrane either singly or in pairs, depending on their hydrophobicity and their ability to form stable helix–helix interactions.

What controls the orientations of the helices in a TM protein, that is, its **topogenesis**? Most TM proteins, as Gunnar von Heijne pointed out, adopt an orientation such that their cytoplasmically exposed ends, those that are not translocated across the membrane, are more positively charged (have more Arg and Lys residues) than their lumenally exposed ends—the **positive-inside rule**. This appears mainly due to the charge distribution within the translocon, which is oriented with its more positive face on the cytoplasmic side of the membrane (in accordance with the positive-inside rule). In fact, mutating certain charged residues of Sec61 α so as to reverse their charge (e.g., changing an Arg to Glu), inverts the orientation of the TM helices it installs in the membrane. Another important influence on the orientation of a TM helix is its hydrophobicity gradient: The more hydrophobic end of a TM helix is preferentially translocated across the membrane.

Despite the foregoing, one might reasonably expect that the membrane orientation of the N-terminal TM helix of a polytopic TM protein dictates the orientations of the succeeding TM helices (many, if not all, of which have yet to be synthesized at the time the N-terminal helix is inserted into the membrane). However, the deletion or insertion of a TM helix from/into a polypeptide does not necessarily change the membrane orientations of the succeeding TM helices: When two successive TM helices have the same preferred orientation, one of them may be forced out of the membrane. Moreover, the topological organization of TM proteins is influenced by the membrane lipid composition.

This suggests that the translocon's lateral gate frequently opens and closes so as to allow its transiting peptide to sample the outside lipid environment and only inserts a peptide segment into the lipid bilayer if it is thermodynamically favorable to do so; that is, helix insertion may be considered as a partitioning between the aqueous environment in the translocon and that of the membrane.

Polytopic TM proteins can fold to their native conformations only after all their TM helices have been inserted into the membrane. This process is guided by packing interactions between helices as well as specific interactions with membrane lipids. Thus, although a TM protein's sequence determines its topology, it does so for a specific membrane lipid environment. Evidently, the lipid composition of a membrane and the topologies of its embedded TM proteins have coevolved.

f. Protein Folding in the ER Is Monitored by Molecular Chaperones

The ER, as does the cytosol, contains a battery of molecular chaperones that assist in protein folding and act as agents of quality control. The best characterized of these is the Hsp70 homolog (Section 9-2C) **BiP** (for *binding protein*). BiP associates with many secretory and TM proteins although, if folding proceeds normally, these interactions are weak and short-lived. However, proteins that are improperly folded, incorrectly glycosylated, or improperly assembled form stable complexes with BiP that are often exported, via a poorly understood process involving the translocon called **retrotranslocation**, to the cytosol where they are proteolytically degraded (Section 32-6). The entire process is named **ERAD** (for *ER-associated degradation*). Two other notable ER-resident chaperones are **calreticulin** and **calnexin**, homologous proteins that participate in facilitating and monitoring the folding and assembly of glycoproteins (Section 23-3Bf). The ER also contains protein disulfide isomerases (PDIs; Section 9-2A) and peptidyl prolyl cis–trans isomerases (PPIs; Section 9-2B).

Abnormalities of protein folding and assembly are important mechanisms of disease (e.g., Section 9-5). For instance, **cystic fibrosis** is the most common life-threatening recessive genetic disease in the Caucasian population (affecting one in ~2000 individuals). It occurs in homozygotes for a defective **cystic fibrosis transmembrane regulator (CFTR) protein**, a 1480-residue glycoprotein with 12 TM helices that functions as a Cl[−] transporter in the plasma membrane of epithelial cells. Individuals with cystic fibrosis produce highly viscous mucus that, in its most damaging effects, blocks the small airways in the lungs. This leads to persistent infections, which cause severe progressive lung degeneration that is usually fatal by around age 30. Although cystic fibrosis is caused by any of more than 1000 known mutations in the CFTR gene, 70% of the cases arise from the deletion of Phe 508 (Δ F508), which is located in a cytoplasmic domain of the CFTR protein (which is initially inserted into the ER membrane). Although this mutant domain in Δ F508 folds to nearly its native conformation (Δ F508 retains almost full biological activity), it does so much more slowly than in the wild-type protein. This results in its retrotranslocation

and degradation by an, in this case, overly zealous proteolytic surveillance system (Section 32-6B).

g. Some Proteins Are Post-Translationally Transported through Membranes

The secretory proteins we discussed pass through the membrane as they are being synthesized by the ribosome, that is, their membrane translocation occurs cotranslationally. However, some secretory proteins are translocated only after they have been fully synthesized in the cytoplasm, that is, post-translationally. Nevertheless, both co- and post-translational translocation is mediated by the translocon. Yet, the translocon is a passive pore, that is, it does not provide the free energy that drives translocation. In cotranslational translocation, it is the ribosomally mediated extension of the polypeptide that pushes it through the translocon.

In eukaryotes, post-translationally translocated secretory proteins have signal sequences that are only moderately hydrophobic; they are not recognized by the SRP but still bind to Sec61. These proteins are bound by cytoplasmic chaperones, which keep them in a loosely folded or unfolded state that permits them to pass through the translocon. Their translocation is driven by a so-called **Brownian ratchet** mechanism that is mediated by the partnering of Sec61 with the tetrameric TM complex **Sec62/Sec63** and the luminal Hsp70-like chaperone BiP (Fig. 12-57). The polypeptide in the translocon randomly slides back and forth via Brownian motion. However, in the ER, the so-called J-domain (a homolog of the *E. coli* cochaperone DnaJ; Section 9-2C) on the luminal surface of Sec63 induces BiP to hydrolyze its bound ATP to ADP. The resulting BiP-ADP complex then binds the polypeptide emerging from the translocon, which prevents it from sliding back toward the cytoplasm. When the peptide again slides forward, another BiP-ADP complex binds to it, etc., until the entire polypeptide has entered the ER. BiP eventually exchanges

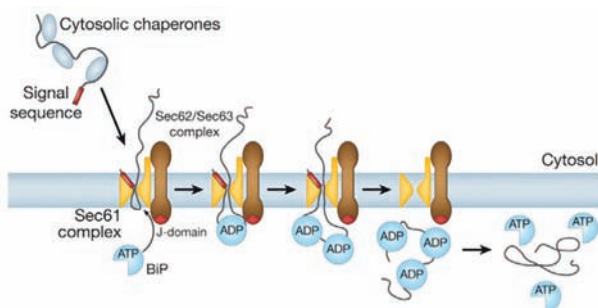


Figure 12-57 Scheme for post-translational translocation in eukaryotes. As the translocating polypeptide enters the ER through Sec61, the BiP-ATP complex binds to Sec63, whose J-domain induces BiP to hydrolyze its bound ATP to ADP. The resulting BiP-ADP complex binds to the emerging peptide so as to prevent its backsliding. As additional peptide segments emerge from Sec61, the process repeats until the entire protein has entered the ER. BiP eventually exchanges its bound ADP for ATP causing it to release the peptide, which then folds to its native conformation. [Courtesy of Tom Rapoport, Harvard Medical School.]

its ADP for ATP, which causes it to release the polypeptide, which then folds to its native conformation.

In bacteria, the motor that drives post-translational translocation is **SecA**, which binds to the cytoplasmic face of the SecY complex and pushes the polypeptide through the translocon via repeated cycles of ATP hydrolysis. SecA is aided in doing so by the cytosolic chaperone **SecB**, which prevents the polypeptide from folding in the cytoplasm.

C. Vesicle Formation

Shortly after their polypeptide synthesis is completed, the partially processed transmembrane, secretory, and lysosomal proteins appear in the Golgi apparatus (Fig. 1-5), a 0.5- to 1.0- μm -diameter organelle consisting of a stack of 3 to 6 or more (depending on the species) flattened and functionally distinct membranous sacs known as **cisternae**, where further post-translational processing, mainly glycosylation, occurs (Section 23-3Bg). The Golgi stack (Fig. 12-58) has two distinct faces, each comprised of a network of interconnected membranous tubules: the **cis Golgi network (CGN)**, which is opposite the ER and is the port through which proteins enter the Golgi apparatus; and the **trans Golgi network (TGN)**, through which processed proteins exit to their final destinations. The intervening Golgi stack contains at least three different types of sacs, the **cis**, **medial**, and **trans cisternae**, each of which contains different sets of glycoprotein processing enzymes.

Proteins transit from one end of the Golgi stack to the other while being modified in a stepwise manner, a process that is described in Section 23-3Bg. These proteins are transported via two mechanisms:

1. They are conveyed between successive Golgi compartments in the cis to trans direction as cargo within membranous vesicles that bud off of one compartment and fuse with a successive compartment, a process known as forward or **anterograde transport**.

2. They are carried as passengers in Golgi compartments that transit the Golgi stack, that is, the cis cisternae eventually become trans cisternae, a process called **cisternal progression** or **maturation**. This process is mediated through the backward or **retrograde transport** of Golgi-resident proteins from one compartment to the preceding one via membranous vesicles.

The cisternal progression mechanism has been clearly shown to occur but the significance of the anterograde transport mechanism is as yet unclear. In any case, on reaching the trans Golgi network, the now mature proteins are sorted and sent to their final cellular destinations.

a. Membrane, Secretory, and Lysosomal Proteins Are Transported in Coated Vesicles

The vehicles in which proteins are transported between the RER, the Golgi apparatus, and their final destinations, as well as between the different compartments of the Golgi apparatus, are known as **coated vesicles** (Fig. 12-59). This is because these 60- to 150-nm-diameter

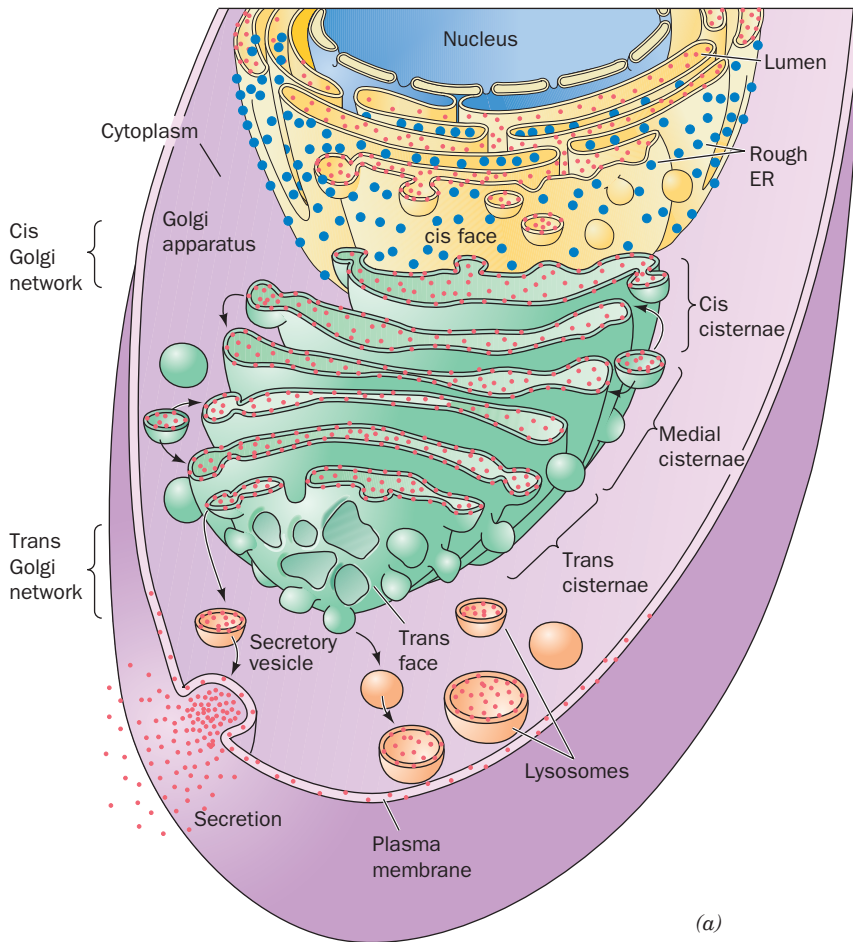
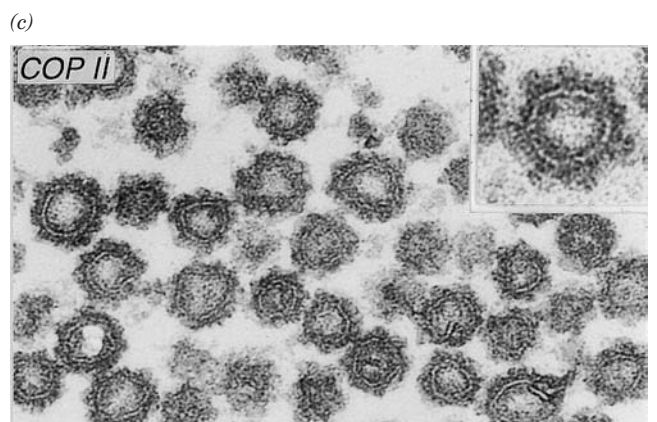
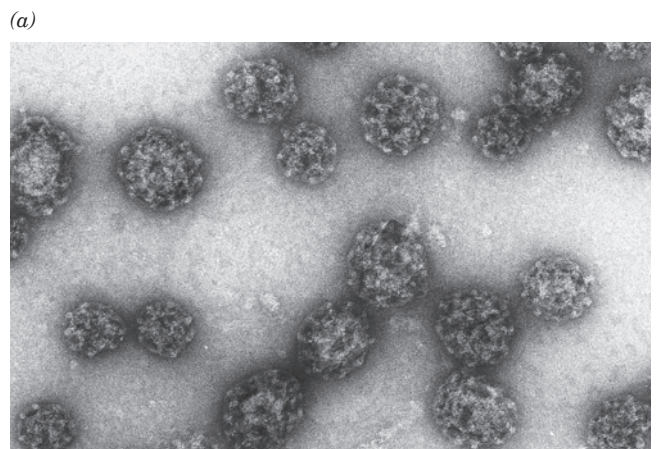
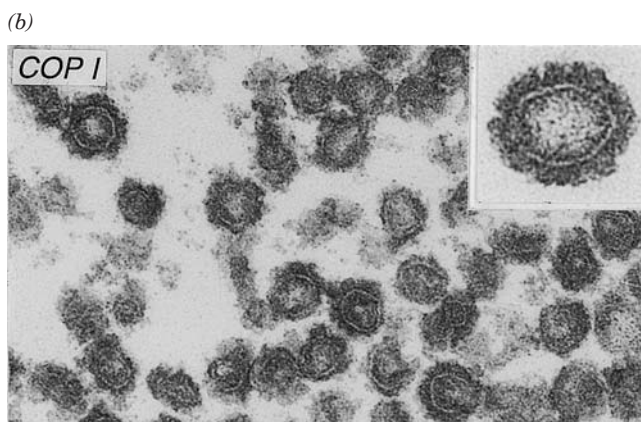


Figure 12-58 Post-translational processing of proteins. Proteins destined for secretion, insertion into the plasma membrane, or transport to lysosomes are synthesized by RER-associated ribosomes (blue dots; top). As they are synthesized, the proteins (red dots) are either translocated into the lumen of the ER or inserted into its membrane. After initial processing in the ER, the proteins are encapsulated in vesicles that bud off from the ER membrane and subsequently fuse with the cis Golgi network. The proteins are progressively processed in the cis, medial, and trans cisternae of the Golgi. Finally, in the trans Golgi network (bottom), the completed glycoproteins are sorted for delivery to their final destinations, the plasma membrane, **secretory vesicles**, or lysosomes, to which they are transported by yet other vesicles.

Figure 12-59 Electron micrographs of coated vesicles. (a) Clathrin-coated vesicles. Note their polyhedral character. [Courtesy of Barbara Pearse, Medical Research Council, Cambridge, U.K.] (b) COPI-coated vesicles. (c) COPII-coated vesicles. The insets in Parts b and c show the respective vesicles at higher magnification. [Courtesy of Lelio Orci, University of Geneva, Switzerland.]



membranous sacs are initially encased on their outer (cytosolic) faces by specific proteins that act as flexible scaffolding in promoting vesicle formation. A vesicle buds off from its membrane of origin and later fuses to its target membrane. *This process preserves the orientation of the transmembrane protein* (Fig. 12-60), so that the lumens of

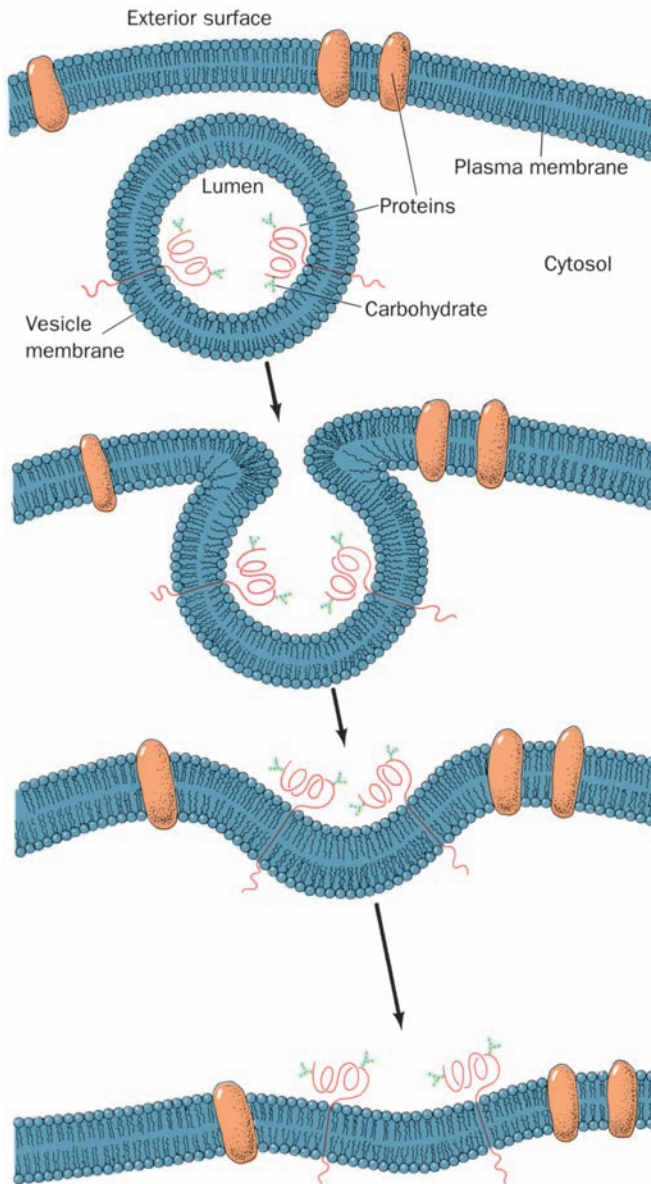


Figure 12-60 The fusion of a vesicle with the plasma membrane preserves the orientation of the integral proteins embedded in the vesicle bilayer. The inside of the vesicle and the exterior of the cell are topologically equivalent because the same side of the protein is always immersed in the cytosol. Note that any soluble proteins contained within the vesicle would be secreted. In fact, proteins destined for secretion are packaged in membranous secretory vesicles that subsequently fuse with the plasma membrane as shown.

the ER and the Golgi cisternae are topologically equivalent to the outside of the cell. This explains why the carbohydrate moieties of TM glycoproteins and the GPI anchors of GPI-linked proteins occur only on the external surfaces of plasma membranes.

The three best characterized types of coated vesicles are distinguished by their protein coats:

1. Clathrin (Fig. 12-59a), a protein that forms a polyhedral framework around vesicles that transport TM, GPI-linked, and secreted proteins from the Golgi to the plasma membrane. The clathrin cages, which were first characterized by Barbara Pearse, can be dissociated to flexible three-legged proteins known as **triskelions** (Fig. 12-61) that consist of three so-called heavy chains (**HC**, 1675 residues) that each bind one of two homologous light chains, **LCa** or **LCb** (~240 residues), at random.

2. COPI protein (Fig. 12-59b; COP for *coat protein*), which forms what appears to be a fuzzy rather than a polyhedral coating about vesicles that carry out both the anterograde and retrograde transport of proteins between successive Golgi compartments. In addition, COPI-coated vesicles return escaped ER-resident proteins from the Golgi to the ER (see below). COPI consists of seven different subunits (α , 160 kD; β , 110 kD; β' , 102 kD; γ , 98 kD; δ , 61 kD; ϵ , 31 kD; and ζ , 20 kD). The soluble complex comprising the COPI protomer is named **coatomer**.

3. COPII protein (Fig. 12-59c), which transports proteins from the ER to the Golgi. The COPII vesicle components are then recycled by COPI-coated vesicles for participation in another round of vesicle formation (the COPI vesicle components entering the ER are presumably recycled by COPII-coated vesicles). The COPII coat consists of the GTPase **Sar1**, the heterodimer **Sec23/24** in which Sec23 is a Sar1-specific GAP and Sec24 functions in cargo selection,

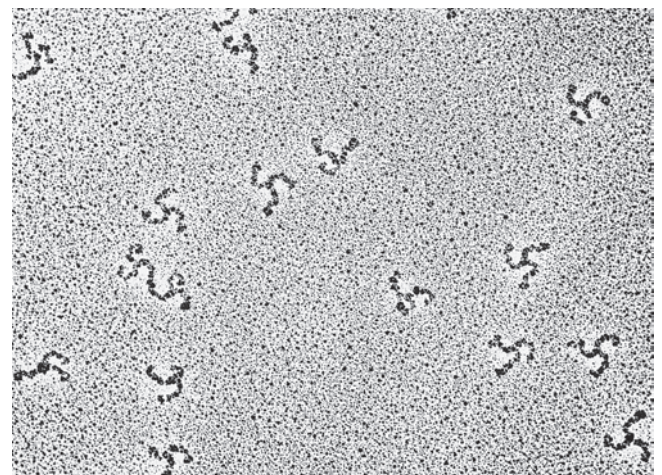


Figure 12-61 Electron micrograph of triskelions. The variable orientations of their legs are indicative of their flexibility. [Courtesy of Daniel Branton, Harvard University.]

and the heterodimer **Sec13/31**, which forms polyhedral cages (see below).

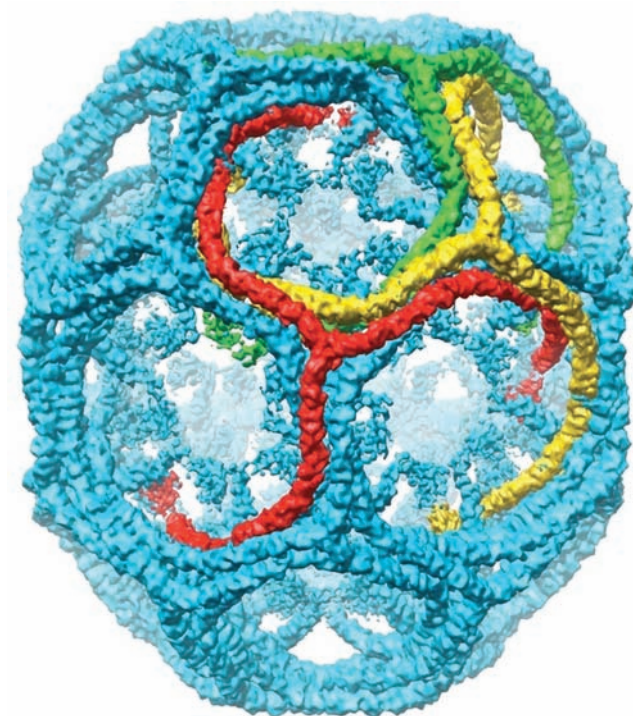
All of the above coated vesicles also carry receptors, which bind the proteins being transported, as well as **fusion proteins**, which mediate the fusion of these vesicles with their target membranes. We discuss these processes below and in Section 12-4D.

b. Clathrin Cages Are Formed by Overlapping Heavy Chains

Clathrin-coated vesicles (CCVs) are structurally and functionally better characterized than those coated with COPI or COPII. Clathrin forms polyhedral cages in which, as a cryo-EM study by Harrison, Tomas Kirchhausen, and Thomas Walz has shown most clearly (Fig. 12-62a), each vertex is the center (hub) of a triskelion, and its edges,

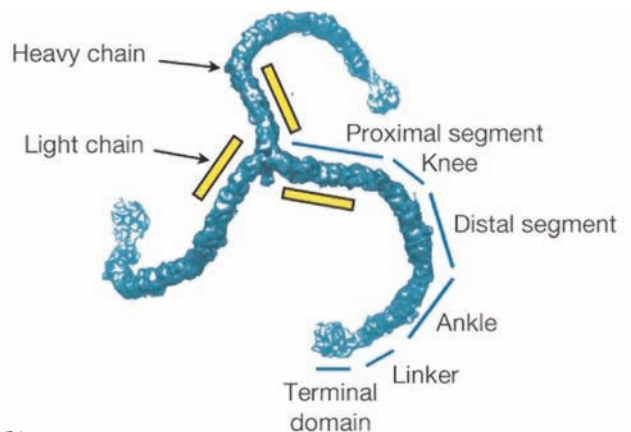
which are ~ 225 Å long, are each formed by the interdigitated legs of four triskelions—two antiparallel proximal segments and two distal segments (Fig. 12-62b). Such polyhedra (Fig. 12-62c), which have 12 pentagonal faces and a variable number of hexagonal faces (for geometric reasons explained in Section 33-2A), are the most parsimonious way of enclosing spheroidal objects in polyhedral cages. The volume enclosed by a clathrin polyhedron, of course, increases with its number of hexagonal faces (a “minicoat” is too small to contain a transport vesicle).

The triskelion’s ~ 475 -Å-long legs are each formed by the 1675-residue heavy chains (HCs), which trimerize via their C-terminal domains (Fig. 12-62b). In addition to projecting outward from its hub (vertex), each leg curls toward the center of the particle such that three ankles meet and interact ~ 75 Å below a hub that is two vertices away from each of their hubs.

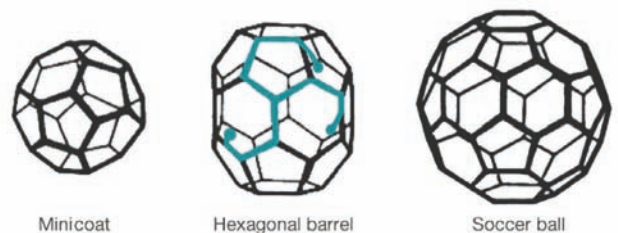


(a)

Figure 12-62 Anatomy of clathrin-coated vesicles. (a) A cryo-EM-based image of a light chain-free clathrin cage from bovine brain at 7.9 Å resolution. The particle shown, a so-called hexagonal barrel, which has D_6 symmetry, consists of 36 triskelions. Three of its interdigitated but symmetry-unrelated triskelions are drawn in red, yellow, and green. (b) A cryo-EM-based image of a triskelion labeled with the names of its various segments. The N-terminus of each heavy chain occupies the terminal domain and its C-terminus is located in the vertex joining the three heavy chains to form the triskelion. (c) Diagrams of the three polyhedral structures that are formed when triskelions assemble into clathrin cages *in vitro*. The minicoat



(b)



(c)

has tetrahedral (T) symmetry, the hexagonal barrel has D_6 symmetry, and the soccer ball has icosahedral (I) symmetry (symmetry is discussed in Section 8-5B). These polyhedra consist of 28, 36, and 60 triskelions, respectively. The arrangement of one triskelion within the hexagonal barrel is indicated in blue. *In vivo*, clathrin forms membrane-enclosing polyhedral cages with a large range of different sizes (number of hexagons). The hexagonal barrel seen in Part a is only ~ 700 Å in diameter, whereas clathrin-coated membranous vesicles are typically ~ 1200 Å in diameter or larger. [Courtesy of Stephen Harrison, Tomas Kirchhausen, and Thomas Walz, Harvard Medical School.]

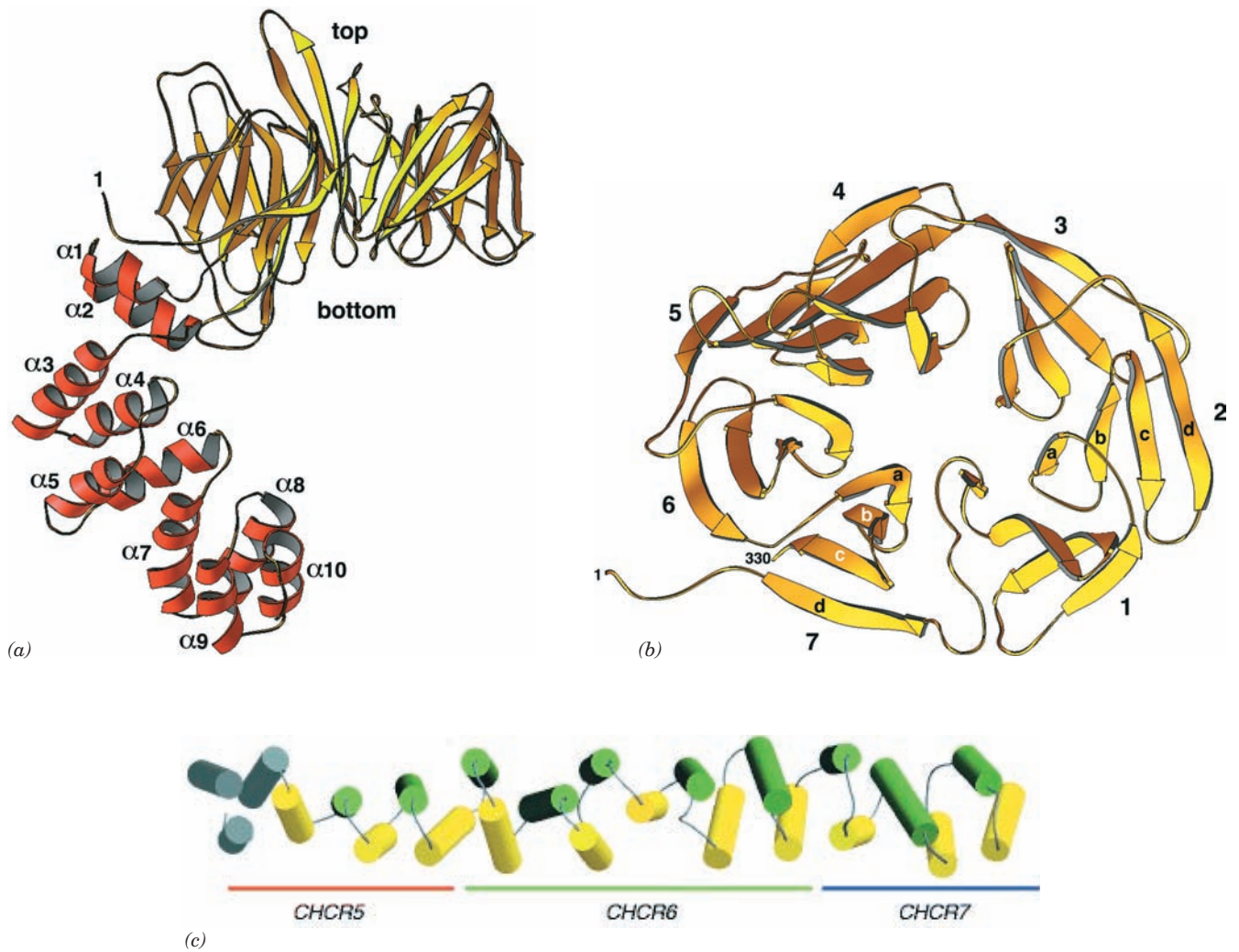
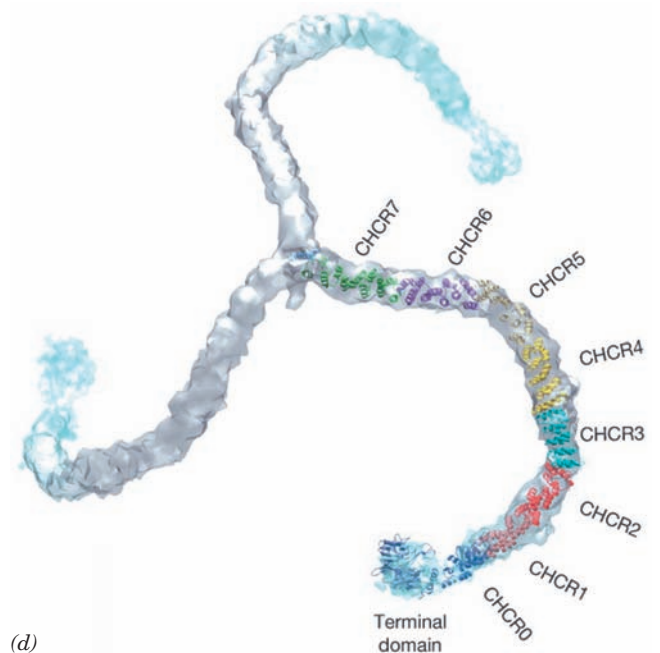


Figure 12-63 Structure of the clathrin heavy chain. (a) The X-ray structure of the N-terminal domain and part of the linker of rat HC. The N-terminal domain forms a seven-bladed β propeller (yellow) that is seen here in side view, and the linker (red) forms an α solenoid. (b) The β propeller as viewed from the top along its pseudo-7-fold axis. [Parts *a* and *b* courtesy of Tomas Kirchhausen, Harvard Medical School. PDBid 1BPO.] (c) The X-ray structure of bovine clathrin HC residues 1210 to 1516 as viewed with its N-terminus on the left. The helices are alternately colored yellow and green with the exception of the three N-terminal helices, which are colored gray to indicate that they are poorly resolved. The orange, green, and blue bars denote the regions of CHCR5, CHCR6, and CHCR7, respectively. [Courtesy of Peter Hwang, University of California at San Francisco. PDBid 1B89.] (d) A backbone model of a triskelion (residues 1–1597) generated by docking the foregoing X-ray structures together with homology models of the remaining CHCRs into the cryo-EM-determined electron density of a heavy chain (Fig. 12-62a). [Courtesy of Stephen Harrison, Tomas Kirchhausen, and Thomas Walz, Harvard Medical School. PDBid 1XI4.]



Although the X-ray structure of an entire HC has not been determined, those of its N-terminal portion and a part of its proximal segment have been elucidated:

1. The N-terminal segment (residues 1–494; Fig. 12-63*a,b*), whose structure was determined by Harrison and Kirchhausen, consists of two domains: (i) an N-terminal seven-bladed **β propeller** in which each structurally similar propeller blade is formed by a four-stranded antiparallel β sheet (Fig. 12-63*b*; the terminal domain) named the **WD40** sequence motif because it often contains the dipeptide WD and is ~ 40 residues long; and (ii) a C-terminal linker that consists of 10 α helices of variable lengths (2–4 turns) connected by short loops and arranged in an irregular right-handed helix (a helix of helices, that is, a **superhelix**) named an **α solenoid** (alternatively, an **α -zigzag**).

2. The proximal segment (residues 1210–1516; Fig. 12-63*c*), whose structure was determined by Peter Hwang and Robert Fletterick, consists of 24 linked α helices that are arranged similarly but more regularly than the above α solenoid to form a rod-shaped right-handed superhelix. The rigidity of this motif is attributed to its continuous hydrophobic core together with the efficient interdigitation of its side chains where its crossing antiparallel α helices come into contact (Section 8-3B).

Sequence and structural alignments indicate that HC residues 537 to 1566 consist of seven homologous ~ 145 -residue **clathrin heavy chain repeats (CHCRs)** that are arranged in tandem and which each contain 10 helices (the proximal segment consists of all of CHRC6 together with the C- and N-terminal portions of CHRC5 and CHRC7; Fig. 12-63*c*). This has permitted the generation of a backbone model of a triskelion by docking the foregoing X-ray structures and homology models of the CHCRs whose structures have not been experimentally determined in the cryo-EM-determined electron density (Fig. 12-63*d*; homology modeling is discussed in Section 9-3B). Each HC leg consists of an extended superhelix of linked α helices. Nevertheless, triskelion legs exhibit considerable flexibility (Fig. 12-61), a functional necessity for the formation of different sized vesicles as well as for the budding of a vesicle from a membrane surface, which is accompanied by a change in its curvature. The HC appears to flex mainly along its knee and ankle segments (Fig. 12-62*b*).

The proximal segment bears extensive hydrophobic surface patches that follow the grooves between adjacent helices. Apparently, the lengthwise association of two proximal segments in a clathrin cage (Fig. 12-62*a*) is stabilized by the burial of these hydrophobic patches through the complementary packing of the helices of one proximal leg in the grooves on another.

Light chains (LCs) are not required for clathrin cage assembly. Indeed, LCs inhibit heavy chain polymerization *in vitro*, which suggests that they have a regulatory role in preventing inappropriate clathrin cage assembly in the

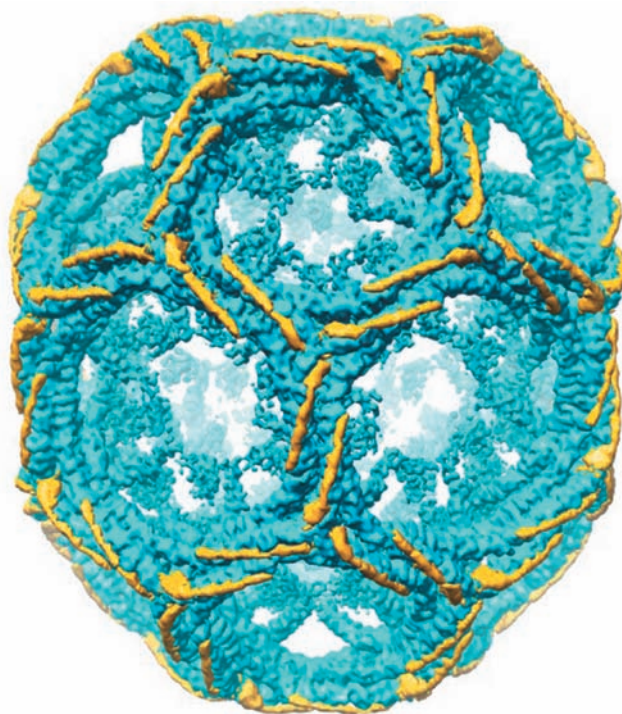


Figure 12-64 Arrangement of light chains on a clathrin cage.

The differences between the cryo-EM-determined electron densities of a hexagonal barrel with and without light chains are shown in yellow with the light chain-free electron density shown in blue. [Courtesy of Stephen Harrison, Tomas Kirchhausen, and Thomas Walz, Harvard Medical School.]

cytosol. Comparison of the cryo-EM structures of intact and LC-free hexagonal barrels reveals that the central portion of an LC consists of a 71-residue helix that binds to a surface formed by the interhelical loops along the HC proximal segment with the C-terminus of the LC closest to the triskelion hub (Fig. 12-64). The segments of the 60% identical LCa and LCb that differ in sequence are largely confined to their N- and C-terminal regions, which do not participate in HC binding and hence are likely to contain sites for the attachment of cytosolic factors that regulate vesicle uncoating.

c. Clathrin-Coated Vesicles Also Participate in Endocytosis

CCVs, as we have seen, transport TM and secretory proteins from the trans Golgi network (TGN) to the plasma membrane (Fig. 12-58). In addition, through a process known as **endocytosis** (discussed in Section 12-5Bc), they act to engulf specific proteins from the extracellular medium by the invagination of a portion of the plasma membrane and to transport them to intracellular destinations.

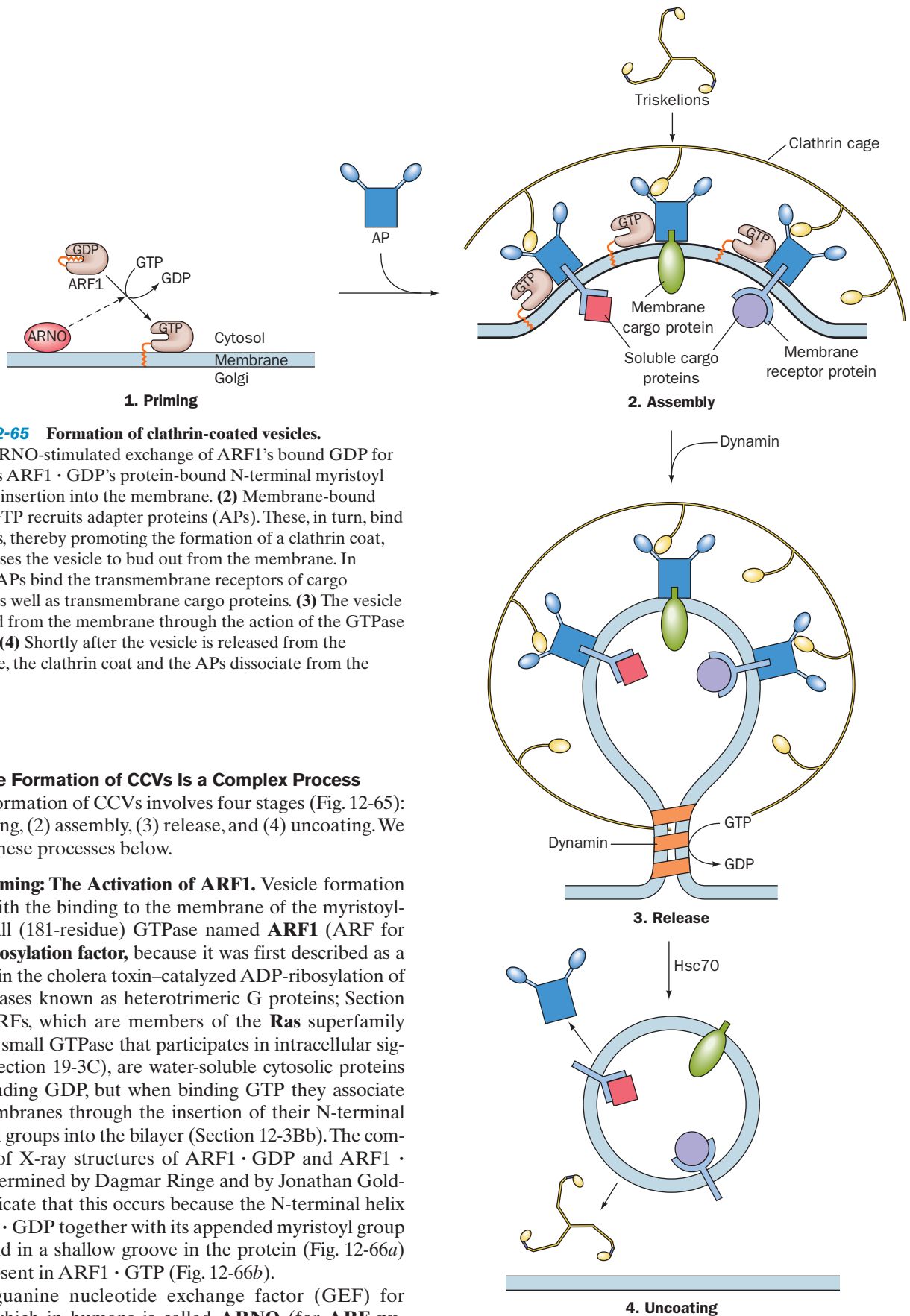


Figure 12-65 Formation of clathrin-coated vesicles.

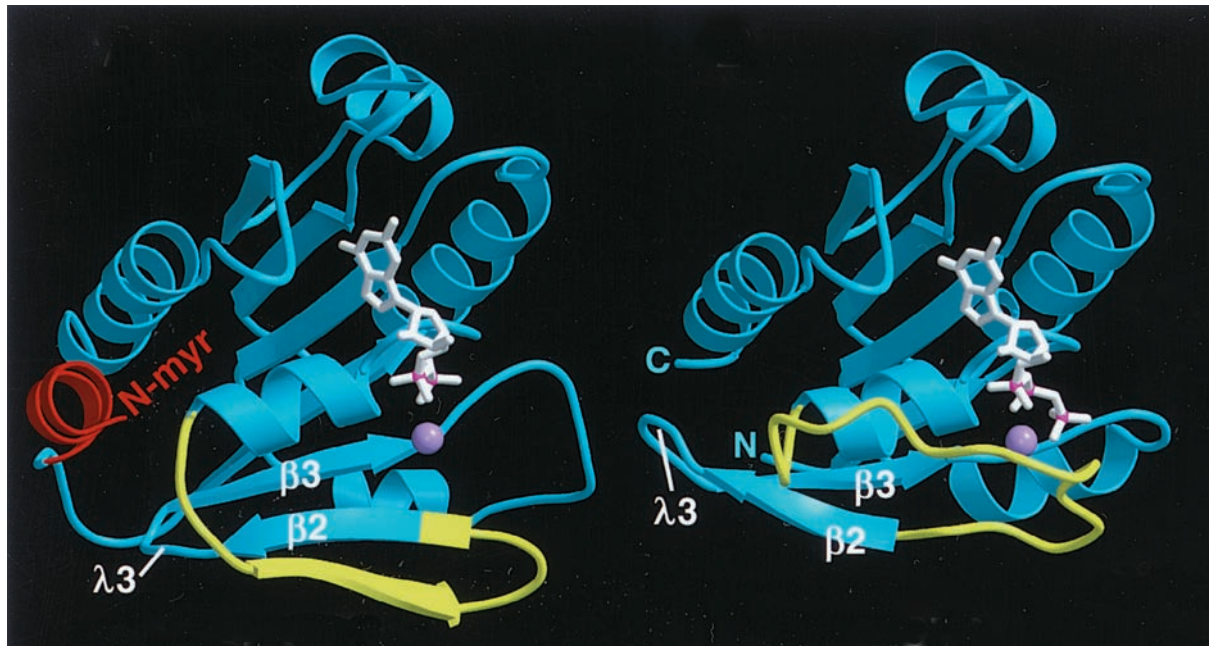
(1) The ARNO-stimulated exchange of ARF1's bound GDP for GTP frees ARF1 · GDP's protein-bound N-terminal myristoyl group for insertion into the membrane. (2) Membrane-bound ARF1 · GTP recruits adapter proteins (APs). These, in turn, bind triskelions, thereby promoting the formation of a clathrin coat, which causes the vesicle to bud out from the membrane. In addition, APs bind the transmembrane receptors of cargo proteins as well as transmembrane cargo proteins. (3) The vesicle is released from the membrane through the action of the GTPase dynamin. (4) Shortly after the vesicle is released from the membrane, the clathrin coat and the APs dissociate from the vesicle.

d. The Formation of CCVs Is a Complex Process

The formation of CCVs involves four stages (Fig. 12-65): (1) priming, (2) assembly, (3) release, and (4) uncoating. We outline these processes below.

1. Priming: The Activation of ARF1. Vesicle formation begins with the binding to the membrane of the myristoylated small (181-residue) GTPase named **ARF1** (ARF for **ADP-ribosylation factor**, because it was first described as a cofactor in the cholera toxin-catalyzed ADP-ribosylation of the GTPases known as heterotrimeric G proteins; Section 19-2). ARFs, which are members of the **Ras** superfamily (Ras is a small GTPase that participates in intracellular signaling; Section 19-3C), are water-soluble cytosolic proteins when binding GDP, but when binding GTP they associate with membranes through the insertion of their N-terminal myristoyl groups into the bilayer (Section 12-3Bb). The comparison of X-ray structures of ARF1 · GDP and ARF1 · GTP, determined by Dagmar Ringe and by Jonathan Goldberg, indicate that this occurs because the N-terminal helix of ARF1 · GDP together with its appended myristoyl group are bound in a shallow groove in the protein (Fig. 12-66a) that is absent in ARF1 · GTP (Fig. 12-66b).

The guanine nucleotide exchange factor (GEF) for ARF1, which in humans is called **ARNO** (for **ARF nucleotide-binding site opener**; 399 residues), contains an



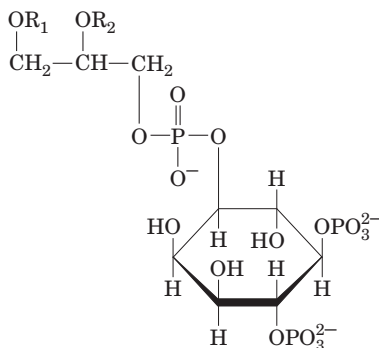
(a)

Figure 12-66 X-ray structures of (a) ARF1 · GDP and (b) ARF1 · GMPPNP. (GMPPNP is a nonhydrolyzable GTP analog in which the O atom linking GTP's β - and γ -phosphorus atoms is replaced by an NH group.) The bound nucleotides are drawn in stick form in white with their phosphorus atoms magenta and their bound Mg^{2+} ions shown as lavender spheres. In ARF1 · GDP, the protein's N-terminal helix (red) together with its covalently linked myristoyl group (not present in the X-ray structures) are bound in a shallow hydrophobic groove on the surface of the protein formed in part by the residues of loop $\lambda 3$.

(b)

However, the replacement of GDP by GMPPNP (and presumably GTP) induces a conformational change in residues 37 to 53 (yellow) that displaces strand $\beta 2$ by two residues along strand $\beta 3$, a shift of 7 Å. The resulting movement of loop $\lambda 3$ eliminates the binding site for the N-terminus, thereby making the myristoyl group available for membrane insertion (residues 1–17 of the GMPPNP complex are disordered). [Courtesy of Jonathan Goldberg, Memorial Sloan-Kettering Cancer Center, New York. The X-ray structure of ARF1 · GDP was determined by Dagmar Ringe, Brandeis University. PDBid 1HUR.]

~200-residue domain similar to the highly conserved yeast protein **Sec7**. When ARNO or its isolated Sec7 domain is incubated with myristoylated ARF1 · GDP, it fails to catalyze nucleotide exchange unless lipid micelles are also present, thereby suggesting that ARNO is activated only when localized to a membrane surface. Indeed, ARNO contains a **pleckstrin homology (PH) domain**, an ~100-residue module occurring in numerous proteins (Section 19-3Ce) that binds the minor membrane phospholipid **phosphatidylinositol-4,5-bisphosphate (PIP₂)**,



Phosphatidylinositol-4,5-bisphosphate (PIP₂)

which is also a precursor of compounds that participate in intracellular signaling (Section 19-4A).

2. Assembly: Adaptor Proteins Link Cargo Proteins to the Clathrin Coat. Membrane-bound ARF1 · GTP acts to recruit **adaptor proteins (APs)** to the membrane surface. APs bind clathrin HC together with TM proteins that are either receptors that selectively bind soluble cargo proteins inside the budding vesicle or are cargo proteins themselves. APs comprise the central cores of CCVs and, in fact, are the scaffolding on which clathrin cages form. The APs bind clathrin via its N-terminal β propeller domain (Fig. 12-63a), which forms the knobs that project inward from clathrin cages (Fig. 12-62a). The grooves between the propeller blades on the top face of the β propeller (Fig. 12-63b) probably form the AP binding sites.

AP1 is the most common AP contained in the coated vesicles originating from the TGN, whereas the homologous **AP2** predominates in endocytotic vesicles. Both APs are heterotetramers: AP1 consists of the subunits γ , $\beta 1$ (~110 kD each), $\mu 1$ (~50 kD), and $\sigma 1$ (~17 kD), whereas the corresponding subunits of the better characterized AP2 are named α , $\beta 2$, $\mu 2$, and $\sigma 2$ (Fig. 12-67). Electron microscopy and X-ray studies indicate that the large subunits each consist of a trunk and an appendage domain joined by

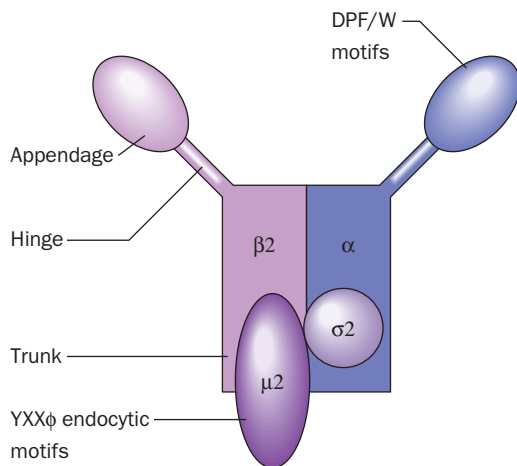


Figure 12-67 Schematic diagram of the AP2 heterotetramer. AP1 has a similar structure. [After Pearse, B.M., Smith, C.J., and Owen, D.J., *Curr. Opin. Struct. Biol.* **10**, 223 (2000).]

a flexible and proteolytically sensitive hinge region (Fig. 12-67). The AP2 hinge region of $\beta 2$ binds to the clathrin β propeller, whereas the cytoplasmic domains of target proteins bind most commonly to $\mu 2$ via YXX ϕ sequences (where ϕ is a bulky hydrophobic residue), but in some cases to its α and $\sigma 2$ subunits via [D/E]XXXL[L/I] sequences, which are known as **dileucine motifs**. This explains why the proteolytic excision of AP2's appendage domain prevents the assembly of clathrin coats, although the remaining AP2 trunk can still bind to membranes that contain proteins bearing a YXX ϕ internalization signal. In addition, both AP1 and AP2 bind PIP₂ and mutating their PIP₂-binding sites prevents them from localizing to their target membranes.

Mammals have two additional heterotetrameric APs, **AP3** and **AP4**, both of which function in the TGN. Moreover, database searches for AP homologs have identified a family of monomeric clathrin adapters named **GGAs** (for Golgi-localized γ -ear-containing ARF-binding proteins), whose C-terminal domain is homologous to the appendage or "ear" domain of AP1's γ subunit (and AP2's α subunit; Fig. 12-67). These various adapter proteins participate in the transport of their target proteins between different pairs of membranes so that CCVs are multifunctional entities.

3. Release: Vesicle Scission Is Mediated by Dynamin.

The budding of a CCV from its parent membrane appears to be mechanically driven by the formation of the clathrin cage. However, the actual scission of the coated bud from its parent membrane to form a coated vesicle requires the participation of **dynamin**, an ~870-residue GTPase. Dynamin contains a PIP₂-binding PH domain, which recruits dynamin to the membrane. On binding GTP, dynamin forms a helical oligomer that wraps about the base of the budding vesicle so as to squeeze this region down to a thin tube (Fig. 12-68). The oligomerization together with the presence of PIP₂ stimulates dynamin to hydrolyze its bound GTP (dynamin also contains a GAP domain), causing the helical oligomer to lengthen its pitch. However, the

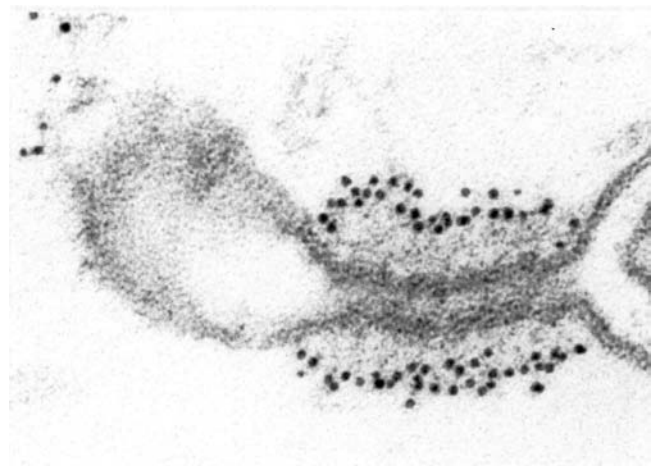


Figure 12-68 Electron micrograph of a budding coated vesicle. The vesicle was incubated with the nonhydrolyzable GTP analog **GTP γ S** (in which a terminal O atom on the γ -phosphorus of GTP is replaced by S) and then treated with gold-tagged anti-dynamin antibodies (*black dots*). Note that the dynamin surrounds a long narrow tube at the base of the budding vesicle that has not pinched off from the membrane. [Courtesy of Pietro De Camilli, Yale University School of Medicine.]

way in which this process releases the vesicle from the membrane is not well understood.

4. Uncoating: The Recycling of Clathrin and Adapter Proteins.

Shortly after the formation of a CCV, the clathrin is released as triskelions, thereby recycling them for participation in the formation of additional coated vesicles. This process is mediated by the ATPase **Hsc70** (Hsc for *heat shock cognate*), an ~650-residue homolog of the chaperone Hsp70 (Section 9-2C) present in all eukaryotic cells, which on ATP hydrolysis forms a complex with clathrin. Hsc70 is recruited to the appropriate sites on the clathrin lattice by the ~910-residue cochaperone **auxilin**, which binds to specific sites on the clathrin heavy chains. Auxilin contains a J-domain that induces Hsc70 to hydrolyze its bound ATP to ADP, thereby causing Hsc70 to bind to and dismantle the clathrin lattice. The cryo-EM structure of the clathrin "hexagonal barrel" in complex with Hsc70 and a J-domain-containing fragment of auxilin at 28 Å resolution, determined by Alasdair Steven, indicates that Hsc70 is located within diffuse rings inside the clathrin cage's pentagonal and hexagonal rings (Fig. 12-69). This suggests that triskelions are pried out of the clathrin lattice by the concerted action of up to six Hsc70 molecules. This may occur by a simple clockwise rotation of a triskelion as viewed in Fig. 12-62a. On the subsequent exchange of its bound ADP for ATP, the Hsc70 releases its bound triskelions.

Following clathrin release from newly formed vesicles, the APs are also released. This process may be initiated by the hydrolysis of ARF1's bound GTP to GDP, which would release ARF1 from the membrane and, presumably, from binding an AP. In any case, the coating and uncoating of vesicles by clathrin must be closely regulated processes since both occur simultaneously.

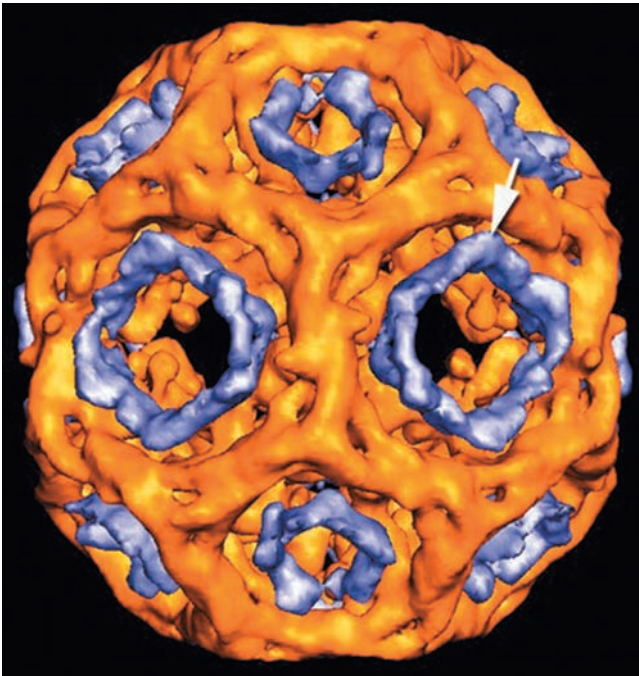


Figure 12-69 Cryo-EM-based image of a clathrin hexagonal barrel in complex with Hsc70 and a J-domain-containing fragment of auxilin at 28 Å resolution. The clathrin cage is gold and electron density attributable to the Hsc70 is blue. The white arrow indicates the position at which the Hsc70 most closely approaches the clathrin lattice. [Courtesy of Alasdair Steven, NIH, Bethesda, Maryland.]

A variety of regulatory and accessory proteins of largely unknown function have also been implicated in CCV formation. Moreover, many of the proteins described above are each present in several isoforms. Hence it is clear that our understanding of this process is far from complete.

e. The Assembly of COPI- and COPII-Coated Vesicles Resembles That of Clathrin-Coated Vesicles

COPI- and COPII-coated vesicles are both assembled in processes, elucidated in large part by Randy Schekman, that resemble CCV assembly:

1. Priming: COPI-coated vesicles are primed identically to CCVs: ARF1 is recruited to the membrane by the ARNO-promoted exchange of its bound GDP for GTP (Fig. 12-65, Step 1). COPII-coated vesicle assembly is similarly primed but by different proteins: **Sar1** (for secretion-associated and Ras-related protein-1) is the small ARF family GTPase that carries out this process, and the exchange of its GDP for GTP is mediated by the transmembrane GEF **Sec12**.

2. Assembly: ARF1 · GTP stoichiometrically recruits intact coatamers to form COPI-coated vesicles. Most of the seven COPI coatamer subunits have homologs in the clathrin system and function accordingly: The β -, γ -, δ -, and ζ -COPs correspond to the β 2, α , μ 2, and σ 2 subunits of AP2, respectively (Fig. 12-67), and the α - and ϵ -COPs correspond to the clathrin heavy and light chains. In COPII coat formation, Sar1 · GTP recruits the TM complex **Sec23/24**, which in turn recruits cargo proteins and **Sec13/31**, which forms the budding vesicle's polyhedral outer shell (see below).

3. Release: Both COPI- and COPII-coated vesicles spontaneously bud off from their parent membranes; these processes appear to have no requirement for an analog of dynamin as does CCV release.

4. Uncoating: As is the case for CCVs, COPI- and COPII-coated vesicles uncoat shortly after being released from their parent membranes. These processes appear to be initiated by the hydrolysis of the GTPs bound to ARF1 and Sar1, which thereby weaken the attachment of COPI and COPII to their respective vesicles. The GTPase activating protein (GAP) for COPI vesicles, a 415-residue protein named **ARF GAP**, appears to be a component of the COPI coat. In COPII vesicles, Sec23 is the GAP for Sar1.

f. The Components of COPII and Clathrin Cages Are Structurally Similar but Functionally Different

Cryo-EM studies of the COPII component Sec13/31 by Bridget Carragher and William Balch reveal that, *in vitro*, this heterodimer forms a 600-Å-diameter cuboctahedral cage (Fig. 12-70). A cuboctahedron has *O* symmetry (the symmetry of a cube; Section 8-5B) and has 24 edges of equal length; 12 vertices, each of which is formed by the

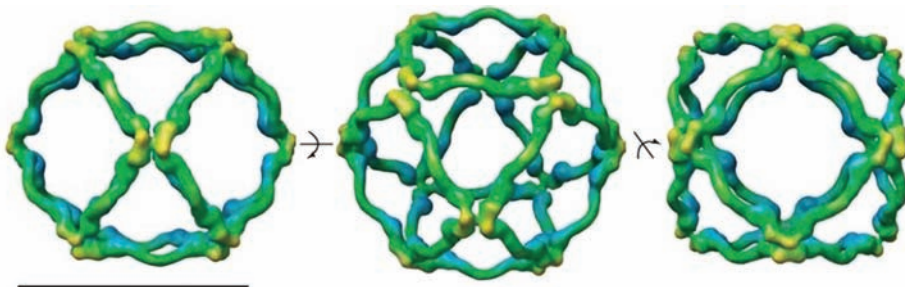


Figure 12-70 Cryo-EM structure of the human Sec13/31 COPII cage at 30 Å resolution. The views are along the cuboctahedral cage's 2-fold axis (left), its 3-fold axis (middle), and its 4-fold axis (right). The surfaces of the cage elements are

colored according to their distance from the center of the cage with blue nearest and yellow farthest. The scale bar is 500 Å long. [Courtesy of Bridget Carragher and William Balch, The Scripps Research Institute, La Jolla, California.]

interaction of four edges (in contrast to clathrin cages whose vertices are each formed by the intersection of three edges; Fig. 12-62c); and 14 faces, of which 8 are equilateral triangles and 6 are squares. *In vivo*, COPII vesicles are often larger than 600 Å in diameter. However, several larger polyhedra are known whose vertices are each formed by the intersection of four equal-length edges.

Although the full-length Sec13/31 complex has not been crystallized, its limited proteolysis led to two X-ray structures determined by Jonathan Goldberg:

1. That of the 297-residue Sec13 in complex with residues 1 to 411 of the 1297-residue Sec31 (Fig. 12-71a). Sec13 forms six blades of a β propeller and the Sec31 fragment forms a seven-bladed β propeller with its C-terminal segment contributing a seventh blade to the Sec13 β propeller. Each blade of these propellers consists of a WD40 repeat as do the blades of the clathrin β propeller.

2. That of the Sec13/31 edge element (Fig. 12-71b), which is a 2-fold symmetric heterotetramer that contains the full length Sec13 in complex with residues 370–763 of Sec31. As in the previous structure, Sec13 forms six blades of a β propeller with a seventh blade contributed by the here N-terminal segment of the Sec31 fragment. The remainder of the Sec31 fragment consists of an α solenoid with its N-terminal end folded back over itself and its C-terminal end overlapping the C-terminal end of another Sec31 fragment to form an interlocked dimer. Thus, the central portion of the complex consists of a double layer of α solenoids.

Since the same segment of Sec31 passes through Sec13 in both complexes and their Sec13 subunits are superimposable, this strongly suggests that the Sec13/31 complex contains the assembly unit shown in Fig. 12-71c. This assembly unit has been docked into the cryo-EM-determined struc-

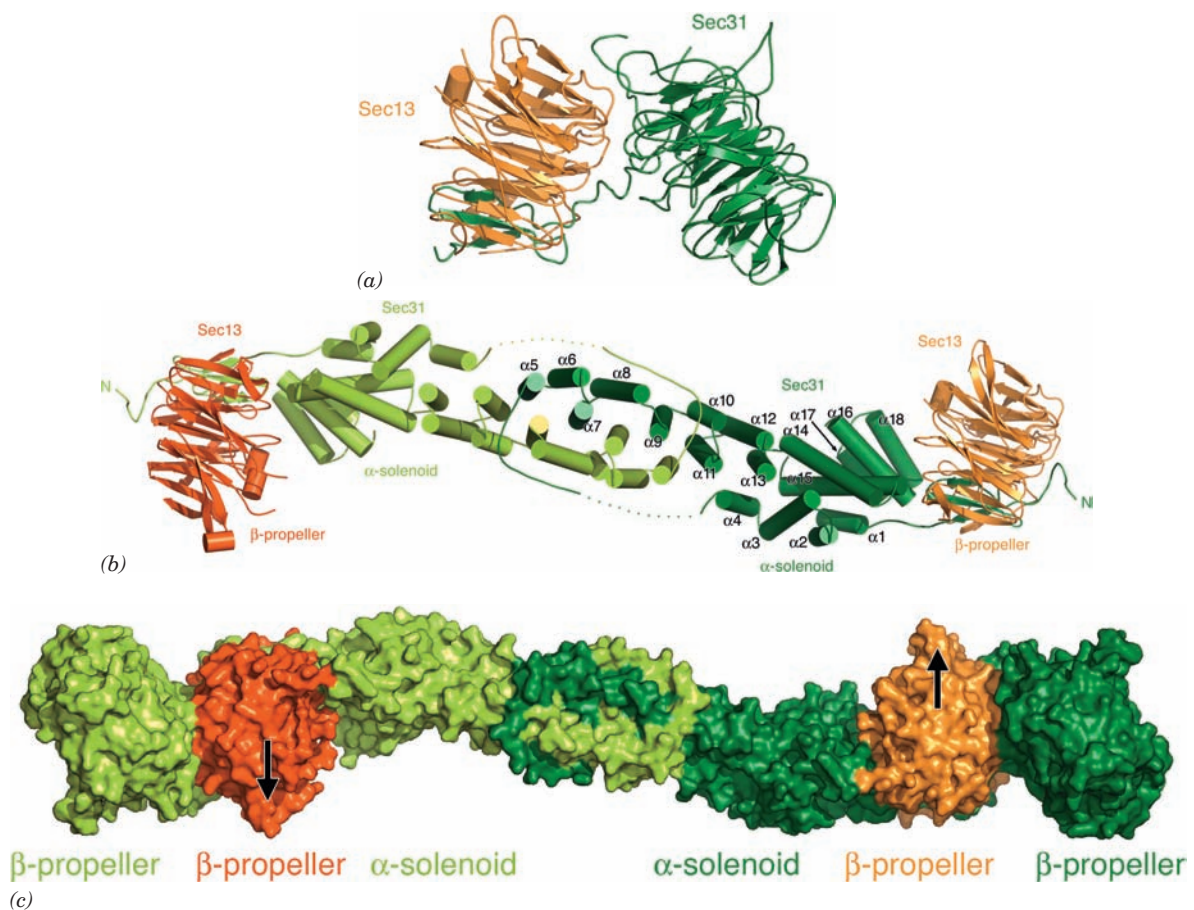


Figure 12-71 X-ray structures of portions of the Sec13/31 complex from yeast. (a) The Sec13/31 vertex element, which consists of Sec13 (orange) in complex with residues 1 to 411 of Sec31 (green). The complex forms two seven-bladed β propellers with one blade of the mainly Sec13 β propeller contributed by the C-terminal portion of the Sec31 fragment. (b) The Sec13/31 edge element, which is a heterotetramer composed of two molecules each of Sec13 (red and orange) and residues 370 to

763 of Sec31 (light and dark green). The complex is viewed along its 2-fold axis and oriented as in Part a. Here Sec13 forms β propellers as in Part a and the Sec31 fragment forms a 215-Å-long double layered α solenoid. (c) Molecular model of the Sec13/31 assembly unit drawn as a surface diagram that is colored and oriented as in Parts a and b. [Courtesy of Jonathan Goldberg, Memorial Sloan-Kettering Cancer Center, New York, New York. PDBids 2PM6 and 2PM9.]



Figure 12-72 Molecular model of the COPII cage viewed approximately along its 3-fold axis. Its 48 Sec13/31 subunits are drawn in worm form colored as in Fig. 12-71. Four Sec31 β propellers associate to form each vertex of the cuboctahedral cage with the remaining portions of the heterotetrameric Sec13/31 assembly units forming its edges. The inner diameter of the cage is ~ 520 Å. [Courtesy of Jonathan Goldberg, Memorial Sloan-Kettering Cancer Center, New York, New York.]

ture of the Sec13/31 cage (Fig. 12-70) to yield the model for the COPII cage drawn in Fig. 12-72.

It is instructive to consider the similarities and differences between COPII and clathrin cages. Both consist of seven-bladed β propellers and α solenoids. In COPII cages, all such motifs participate in forming its edges with four Sec31 β propellers associating to form each of its vertices. In contrast, clathrin cages are constructed entirely from their α solenoidal segments with three such segments associating to form each of its vertices and with their β propeller motifs located in the interior of the cage, where they interact with adapter proteins. Moreover, the ~ 40 -Å-diameter edges of COPII cages each consist of a double layer of α solenoids, whereas the ~ 120 -Å-diameter edges of clathrin cages each consist of the interdigitated α solenoidal segments from four triskelions. Evidently, evolution has molded the similar components of these cages to different functions. Sequence analysis of COPI coat proteins have identified α solenoid and β propeller motifs, which suggests that the clathrin-, COPI-, and COPII-coated vesicles arose from the same proto-coatamer.

The C-terminal segment of Sec31, which is not present in the forgoing X-ray structures, contains an apparently unstructured Pro-rich segment (residues 770–1110 are 20% Pro) that has been implicated in binding the Sar1–Sec23/24 complex (which initiates vesicle budding by binding to the cytoplasmic regions of cargo TM proteins). Based on the X-ray structure of the Sar1–Sec23/24 complex and the fact that a cuboctahedral Sec13/31 cage

has 48 binding sites for this complex, it would appear that the Sar1–Sec23/24 complex forms a 50-Å-thick layer beneath the surface of the COPII cage. Indeed, cryo-EM studies on COPII vesicles assembled from purified Sec13/31 and Sec23/24 complexes reveal that the Sec23/24 complexes form a cage that is concentric to and inside the Sec13/31 cage.

g. Proteins Are Directed to the Lysosome by Carbohydrate Recognition Markers

How are proteins in the ER selected for transport to the Golgi apparatus and from there to their respective membranous destinations? A clue as to the nature of this process is provided by the human hereditary defect known as **I-cell disease** (alternatively, **mulcolipidosis II**), which in homozygotes is characterized by severe progressive psychomotor retardation, skeletal deformities, and death by age 10. The lysosomes in the connective tissue of I-cell disease victims contain large inclusions (after which the disease is named) of glycosaminoglycans and glycolipids as a result of the absence of several lysosomal hydrolases. These enzymes are synthesized on the RER with their correct amino acid sequences but, rather than being dispatched to the lysosomes, are secreted into the extracellular medium. This misdirection results from the absence of a mannose-6-phosphate recognition marker on the carbohydrate moieties of these hydrolases because an enzyme required for mannose phosphorylation fails to recognize the lysosomal proteins. The mannose-6-phosphate residues are normally bound by a receptor in the coated vesicles that transport lysosomal hydrolases from the Golgi apparatus to the lysosomes (Section 23-3Bj). Other glycoproteins are directed to their intracellular destinations by similar carbohydrate markers.

h. ER-Resident Proteins Have the C-Terminal Sequence KDEL

Most soluble ER-resident proteins in mammals have the C-terminal sequences KDEL (HDEL in yeast), KKXX, or KXKXXX (where X represents any amino acid residue), whose alteration results in the secretion of the resulting protein. By what means are these proteins selectively retained in the ER? Since many ER-resident proteins freely diffuse within the ER, it seems unlikely that they are immobilized by membrane-bound receptors within the ER. Rather, it has been shown that ER-resident proteins, as do secretory and lysosomal proteins, readily leave the ER via COPII-coated vesicles but that ER-resident proteins are promptly retrieved from the Golgi and returned to the ER in COPI-coated vesicles. Indeed, coatamer binds the Lys residues in the C-terminal KKXX motif of transmembrane proteins, which presumably permits it to gather these proteins into COPI-coated vesicles. Furthermore, genetically appending KDEL to the lysosomal protease **cathepsin D** causes it to accumulate in the ER, but it nevertheless acquires an *N*-acetylglucosaminyl-1-phosphate group, a modification that is made in an early Golgi compartment. Presumably, a membrane-bound receptor in a post-ER compartment binds the KDEL signal and the

resulting complex is returned to the ER in a COPI-coated vesicle. **KDEL receptors** have, in fact, been identified in yeast and humans. However, the observation that former KDEL proteins whose KDEL sequences have been deleted are, nevertheless, secreted relatively slowly suggests that there are mechanisms for retaining these proteins in the ER by actively withholding them from the bulk flow of proteins through the secretory pathway.

D. Vesicle Fusion

Vesicles that travel only short distances ($<1 \mu\text{m}$) between their parent and target membranes (e.g., between neighboring Golgi cisternae) do so via simple diffusion, a process that typically takes from one to several minutes. However, vesicles that have longer distances to commute (e.g., from the TGN to the plasma membrane) are actively transported along cytoskeletal microtubules (Section 1-2A) by the motor proteins **dynein** and **kinesin**, which unidirectionally crawl along microtubule “tracks” in an ATP-driven process (Section 35-3H).

a. Vesicle Fusion Is Most Easily Studied in Yeast and in Synapses

On arriving at its target membrane, a vesicle fuses with it, thereby releasing its contents on the opposite side of the target membrane (Fig. 12-60). How do vesicles fuse and why do they fuse only with their target membranes and not other membranes? Progress in answering these questions has been made mainly by using two experimental approaches, the genetic dissection of this process in yeast and its biochemical analysis in **synapses**, the junctions between neurons (nerve cells) and between neurons and muscles (Fig. 12-73).

When a nerve impulse in the presynaptic cell reaches a synapse, it triggers the fusion of **neurotransmitter-containing synaptic vesicles** with the **presynaptic membrane** (a specialized section of the neuron’s plasma membrane), thereby releasing the neurotransmitter (a small molecule) into the $\sim 200\text{-\AA}$ -wide **synaptic cleft** (the process whereby membranous vesicles fuse with the plasma membrane to release their contents outside the cell is called **exocytosis**). The neurotransmitter rapidly diffuses across the synaptic cleft to the postsynaptic membrane, where it binds to specific receptors that then trigger the continuation of the nerve impulse in the postsynaptic cell (Section 20-5C). The homogenization of nerve tissue causes its presynaptic endings to pinch off and reseal to form **synaptosomes**, which can be readily isolated by density gradient ultracentrifugation for subsequent study.

b. Vesicle Fusion Requires the Coordinated Actions of Many Proteins

Biological membranes do not spontaneously fuse. Indeed, being negatively charged, they strongly repel one another at short distances. These repulsive forces must be overcome if biological membranes are to fuse. As we shall see below, we are just beginning to understand how this complicated process occurs.

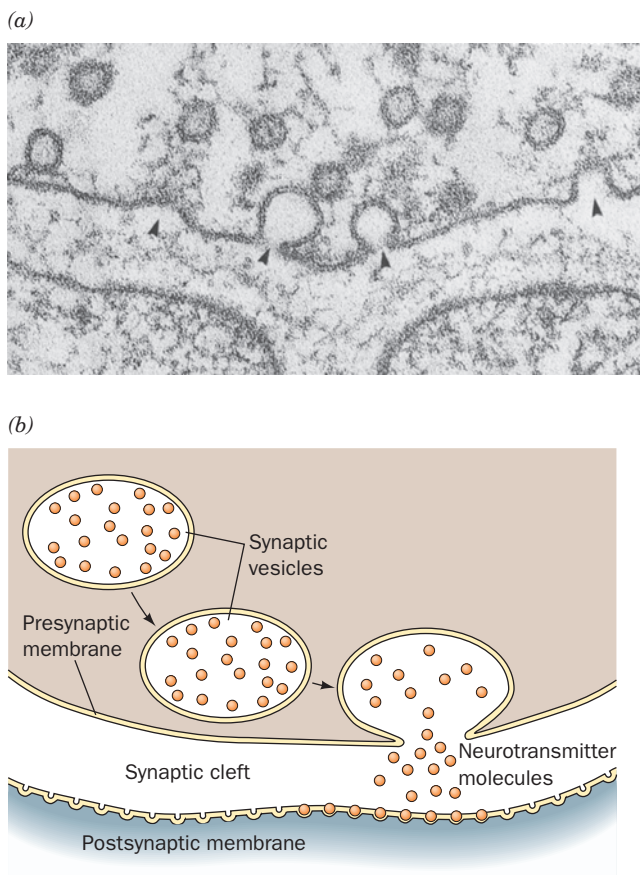
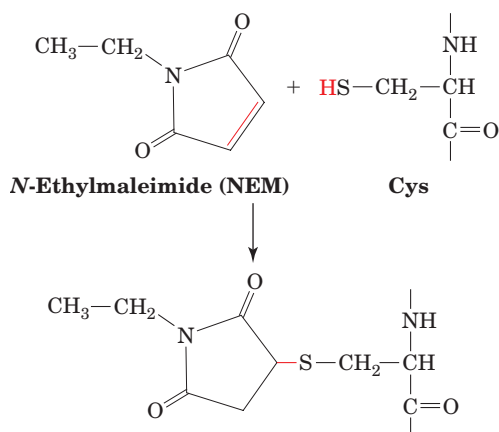


Figure 12-73 Transmission of nerve impulses across a synaptic cleft. (a) Electron micrograph of a frog neuromuscular junction in which the synaptic vesicles are undergoing exocytosis (arrows) with the presynaptic membrane (top). [Courtesy of John Heuser, Washington University School of Medicine, St. Louis, Missouri.] (b) The neurotransmitter, which is thereby discharged into the synaptic cleft, rapidly (in $<0.1 \text{ ms}$) diffuses to the postsynaptic membrane, where it binds to transmembrane receptors, triggering a new nerve impulse.

Studies of the mechanism of vesicle fusion were pioneered by Rothman, who demonstrated that the fusion process is blocked by low concentrations of the cysteine-alkylating agent ***N*-ethylmaleimide (NEM)**,



indicating the presence of an **NEM-sensitive fusion (NSF) protein**. NSF is a cytosolic ATPase that does not bind to membranes unless a **soluble NSF attachment protein (SNAP)** is also present. SNAPs bind to membranes in the absence of NSF, demonstrating that SNAPs bind before NSF. SNAPs bind to alkali-extracted membranes, which indicates that **SNAP receptors (SNAREs)** are integral or lipid-linked proteins.

Three classes of proteins appear to participate in all vesicle fusion reactions:

1. Rab proteins, which are small (20–29 kD) GTPases of the Ras superfamily that play a central role in directing vesicle transport. Cells express numerous Rab isoforms, 11 in yeast and 63 in humans, each localized to a specific membrane compartment. Rab proteins have two tandem Cys residues at their C-termini, both of which are geranylgeranylated (Section 12-3Ba). A soluble protein named **GDP dissociation inhibitor (GDI)** binds to Rab · GDP so as to mask its geranylgeranyl groups and thus maintain it in the cytoplasm. However, when Rab · GDP interacts with a cognate **Rab-GEF** on the surface of its target vesicle, the geranylgeranyl groups on the resulting Rab · GTP are unmasked and insert into the vesicle membrane—much like the anchoring of ARF1 · GTP to the Golgi membrane (Fig. 12-65). Rab · GTP then binds to rodlike proteins emanating from the vesicle's target membrane known as **tethering factors** to form a relatively loose association between the two membranes. After vesicle fusion, Rab hydrolyzes its bound GTP to GDP in a process induced by a specific **Rab-GAP** and the resulting Rab · GDP is extracted from the membrane by GDI, thereby recycling the system. Rab proteins are also implicated in initiating the actual membrane fusion step (see below) as well as in the vesicle interactions with the cytoskeleton that function in transporting vesicles to their proper destinations.

2. SNAREs, which form cognate combinations of membrane-associated proteins known as **R-SNAREs** and **Q-SNAREs** (because they contain conserved Arg and Gln residues in their cytoplasmic domains; they were originally named **v-SNAREs** and **t-SNAREs**, respectively, because they are mainly associated with the vesicle and target membranes). The best characterized SNAREs are those functioning at neuronal synapses: **Synaptobrevin** (alternatively, **VAMP** for vesicle associated membrane protein) is an R-SNARE, whereas **syntaxin** and **SNAP-25** (for synaptosome associated protein of 25 kD) are Q-SNAREs. *R-SNAREs and Q-SNAREs associate to firmly anchor the vesicle to its previously loosely tethered target membrane*, a process called “docking.” The docked complexes, which are described below, are eventually disassembled by NSF in association with a SNAP protein. (Note that SNAP-25 is not a SNAP protein; by curious coincidence, the two independently characterized proteins were assigned the same acronym before it was realized that they are functionally associated.)

3. The SM proteins (so called because they are named **Sec1** in yeast and **Munc18** in mammals), which in synapses bind to syntaxin so as to prevent synaptobrevin and SNAP-

25 from binding to it. Mutational studies indicate that these 65- to 70-kD hydrophilic proteins are essential for vesicle fusion.

c. SNAREs Form a Stable Four-Helix Bundle

The R-SNARE synaptobrevin and the Q-SNAREs syntaxin and SNAP-25 form a highly stable complex; boiling SDS solution is required to dissociate it. Synaptobrevin and syntaxin each have a C-terminal TM helix, and SNAP-25 is anchored to the membrane via palmitoyl groups that are linked to Cys residues in its central region. The X-ray structure of the associating portions of this complex (Fig. 12-74a), determined by Reinhard Jahn and Axel Brünger, reveals it to be a bundle of four parallel ~65-residue α helices with two of the helices formed by the N- and C-terminal segments of SNAP-25. Since synaptobrevin is anchored in the vesicle membrane and syntaxin and SNAP-25 are anchored in the target membrane, this so-called core complex firmly ties together the two membranes (Fig. 12-74b).

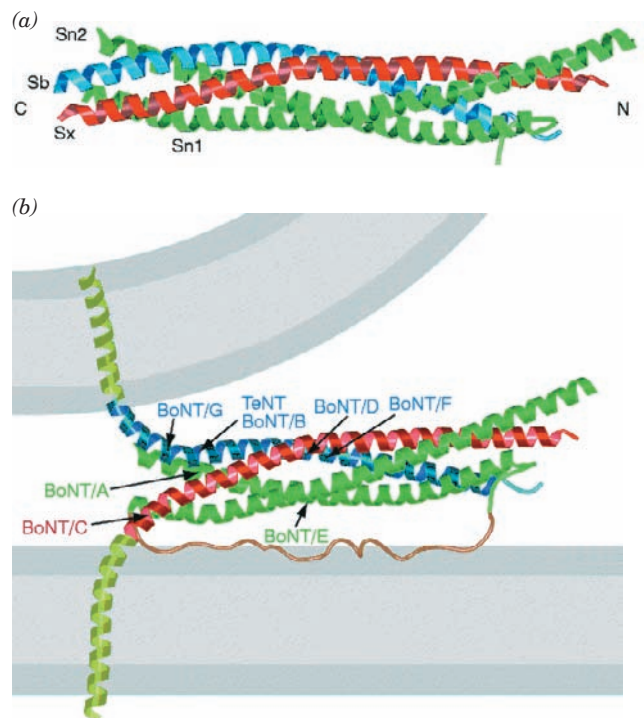


Figure 12-74 X-ray structure of the syntaxin–synaptobrevin–SNAP-25 core complex. (a) Ribbon diagram showing the syntaxin helix (Sx) in red, the synaptobrevin helix (Sb) in blue, and the N- and C-terminal helices of SNAP-25 (Sn1 and Sn2) in green. (b) Model of the synaptic fusion complex linking two membranes (gray). The helices of the core complex are colored as in Part a. The transmembrane C-terminal extensions of syntaxin and synaptobrevin are modeled as helices (light green). The loop connecting the N- and C-terminal helices of SNAP-25 is speculatively represented as an unstructured loop (brown). Recall that this loop is anchored to the membrane via Cys-linked palmitoyl groups (not shown). The cleavage sites for the various clostridial neurotoxins are indicated by the arrows. [Courtesy of Axel Brünger, Yale University. PDBid 1SFC.]

The four helices of the core complex wrap around each other with a gentle left-handed twist. For the most part, the sequence of each helix has the expected 7-residue repeat, $(a-b-c-d-e-f-g)_m$, with residues *a* and *d* hydrophobic (Section 8-2A; note that this property is characteristic of 4- and 3-helix bundles as well as of coiled coils). However, the central layer of side chains along the length of the 4-helix bundle consists of an Arg residue from synaptobrevin that is hydrogen bonded to three Gln side chains, one from syntaxin and one from each of the SNAP-25 helices. These highly conserved polar residues are sealed off from the aqueous environment such that their interactions are enhanced by the low dielectric constant of their environment. It therefore appears that these interactions serve to bring the four helices into proper register.

Since cells contain large numbers of different R-SNAREs and Q-SNAREs (25 in yeast and 36 in humans), it would seem likely that their interactions are at least partially responsible for the specificity that vesicles exhibit in fusing with their target membranes. Indeed, Rothman has shown this to be the case by determining, *in vitro*, the rate of fusion of liposomes bearing different SNAREs. In testing all the R-SNAREs in the yeast genome against Q-SNAREs known to be localized to the yeast Golgi, vacuole, and plasma membranes, he found that liposome fusion only occurs when the combinations of R- and Q-SNAREs correspond to those mediating membrane flow *in vivo*. Nevertheless, it seems likely that the *in vivo* specificity of vesicle fusion is augmented by other mechanisms such as the localization of cognate R- and Q-SNAREs to particular regions in the cell and by the actions of regulatory proteins including, as is indicated above and discussed below, Rab proteins.

d. Tetanus and Botulinus Toxins Specifically Cleave SNAREs

The frequently fatal infectious diseases **tetanus** (which arises from wound contamination) and **botulism** (a type of food poisoning) are caused by certain anaerobic bacteria of the genus *Clostridium*. These bacteria produce extremely potent protein neurotoxins that inhibit the release of neurotransmitters into synapses. In fact, botulinus toxins are the most powerful known toxins; they are ~ 10 millionfold more toxic than cyanide ($10^{-10} \text{ g} \cdot \text{kg}^{-1}$ will kill a mouse).

There are seven serologically distinct types of botulinus neurotoxins, designated **BoNT/A** through **BoNT/G**, and one type of tetanus neurotoxin, **TeTx**. Each of these homologous proteins is synthesized as a single ~ 150 -kD polypeptide chain that is cleaved by host proteases to yield an ~ 50 -kD L chain that remains disulfide-linked to the ~ 100 -kD H chain (Fig. 12-75). The H chains bind to specific types of neurons (via gangliosides and protein receptors), where they facilitate the uptake of the L chain by endocytosis. The L chains are proteases, and each cleaves its target SNARE at a specific site (Fig. 12-74b). This prevents the formation of the core complex and thereby halts the exocytosis of synaptic vesicles. The H chain of TeTx specifically binds to inhibitory neurons (which function to moderate excitatory nerve impulses) and is thereby responsible for the spastic paralysis characteristic of tetanus. The H chains of the BoNTs instead bind to motor neurons (which

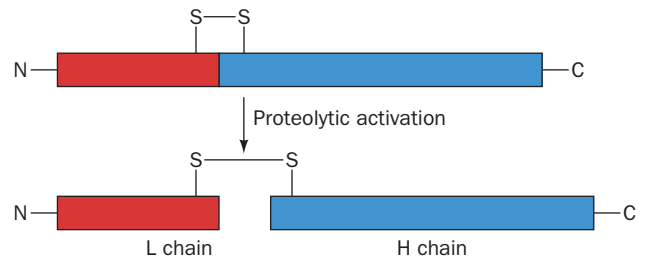


Figure 12-75 Model of clostridial neurotoxins and their activation by host proteases. The disulfide bond linking the L and H segments is cleaved after the neurotoxin is taken up by its target neuron.

innervate muscles) and thus cause the flaccid paralysis characteristic of botulism.

The administration of carefully controlled quantities of botulinus toxin (trade name Botox) is medically useful in relieving the symptoms of certain types of chronic muscle spasms. Moreover, this toxin is used cosmetically: Its injection into the skin relaxes the small muscles causing wrinkles and hence these wrinkles disappear for ~ 3 months.

e. Bilayer Fusion Is Mechanically Induced

The association of Q-SNAREs on a vesicle with an R-SNARE on its target membrane brings the two bilayers into close proximity, yielding a so-called **trans-SNARE complex**. But what induces the fusion of the juxtaposed bilayers? The answer, which is diagrammed in Fig. 12-76, is that the mechanical forces arising from the formation of a ring of several (estimated to be 5–10) trans-SNARE complexes pulls together apposing bilayers. This expels the contacting lipids between them so as to join their outer leaflets, a process known as **hemifusion**. Indeed, the pressure (force/area) within the ring of trans-SNARE complexes is estimated to be 100 to 1000 atm. In the resulting transient structure, no aqueous contact between the two membrane systems has yet been established. However, as the fusion process proceeds (the trans-SNAREs continue zipping up), the two inner leaflets of the now partially joined membranes come together to form a new bilayer, whose component lipids are subsequently similarly expelled to yield a **fusion pore**. The fusion pore then rapidly expands, thereby fully joining the two membranes as well as their contents. Thus, vesicle fusion is driven by the protein folding forming the trans-SNARE complexes.

As we discussed above, liposomes containing the corresponding Q- and R-SNAREs spontaneously fuse. However, this *in vitro* process takes 30 to 40 minutes whereas, for example, the *in vivo* fusion of a synaptic vesicle with the presynaptic membrane takes < 0.3 ms (Section 20-5C). This suggests that other proteins such as Rab proteins and/or their **effectors** (proteins with which they interact) participate in mediating the bilayer fusion process.

f. The Structure of the nSec1–Syntaxin Complex Suggests a Function for Rab Protein

The neuronal SM protein, which is named **nSec1**, binds to syntaxin with high affinity to form a complex that is mutually exclusive with the formation of the syntaxin–

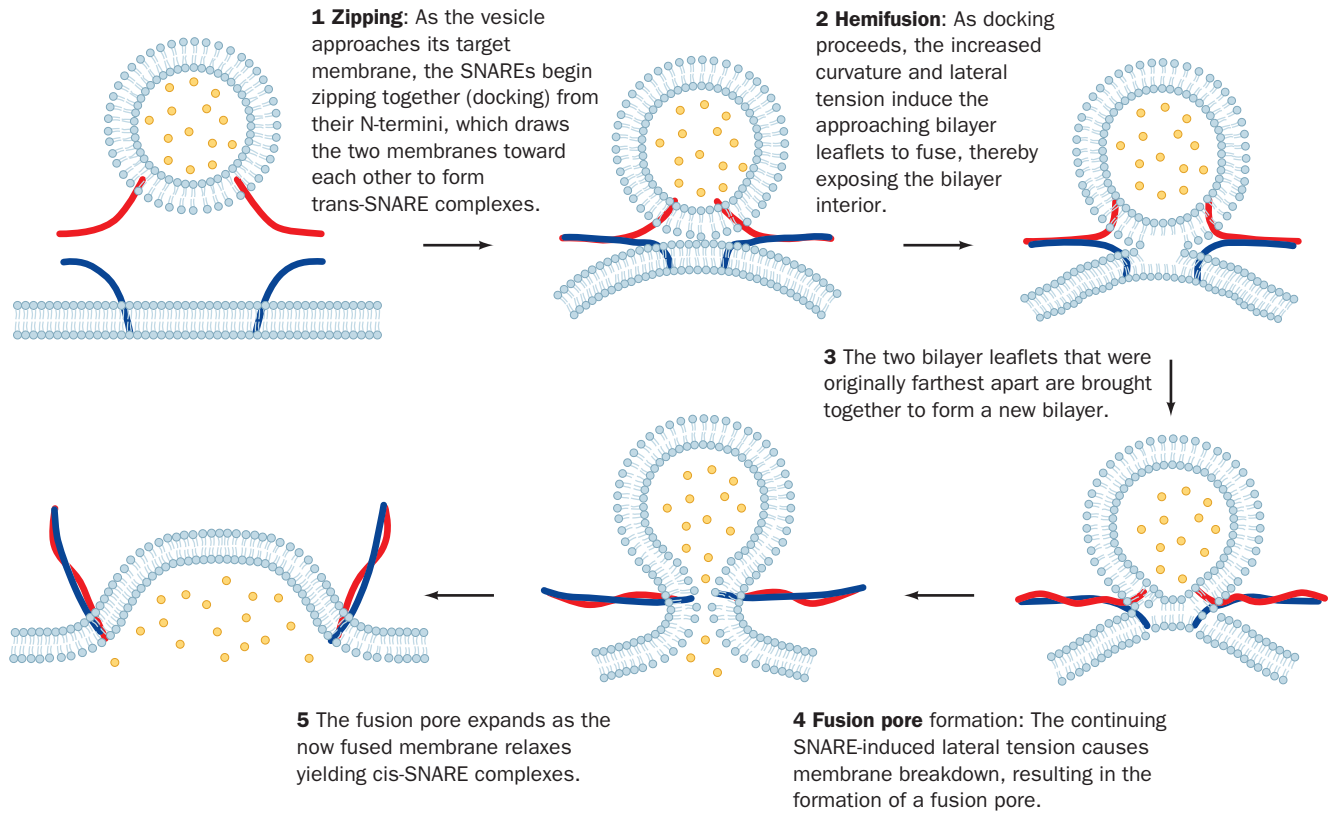


Figure 12-76 Model for SNARE-mediated vesicle fusion. Here the R-SNARE and the Q-SNAREs are schematically

represented by red and blue worms. [After a drawing by Chen, Y.A. and Scheller, R.H., *Nature Rev. Mol. Cell Biol.* **2**, 98 (2001).]

synaptobrevin–SNAP-25 complex. The X-ray structure of nSec1 in complex with the cytoplasmic domain of syntaxin (Fig. 12-77), determined by William Weis, reveals that this portion of the 288-residue syntaxin forms an N-terminal

up–down–up–down four-helix bundle. Syntaxin’s C-terminal helix (but lacking its TM portion) adopts a bent and somewhat irregular conformation, which differs from that in the core complex displayed in Fig. 12-74. In contrast, the

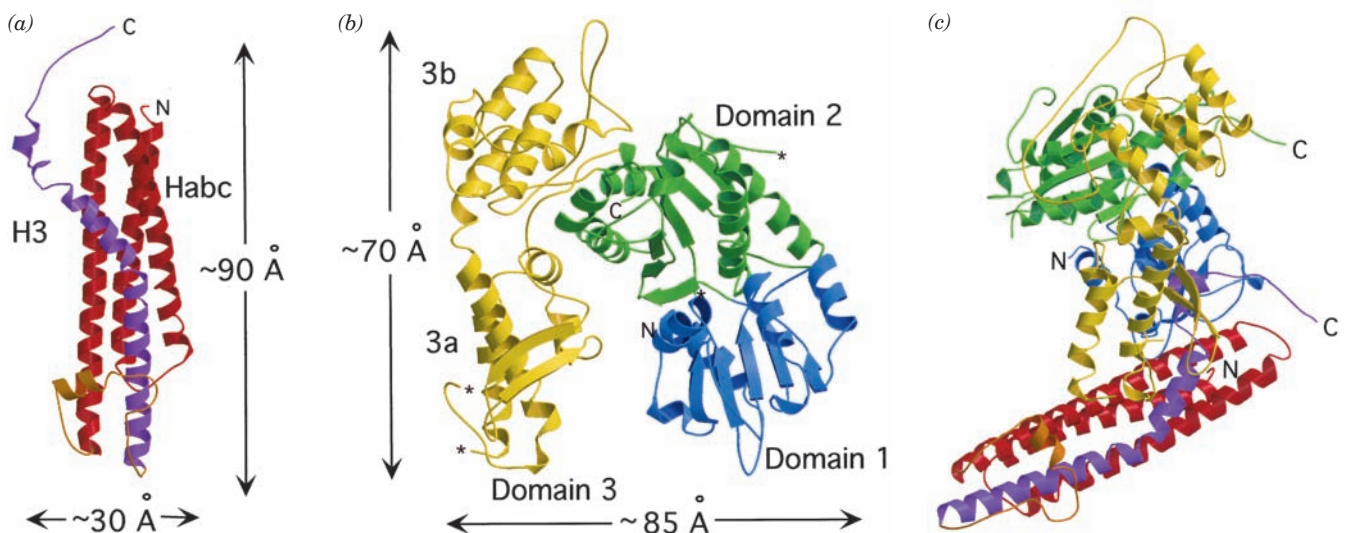


Figure 12-77 X-ray structure of the complex between nSec1 and syntaxin. (a) Ribbon diagram of syntaxin with its N-terminal 3-helix bundle (Habc) red and the cytoplasmic portion, its C-terminal helix (H3; the segment that forms a component of the core complex), purple. (b) Ribbon diagram of nSec1 with its

three domains differently colored. (c) The nSec1–syntaxin complex colored as in Parts a and b and viewed such that the nSec1 is rotated by 90° about the vertical axis relative to Part b. [Courtesy of William Weis, Stanford University School of Medicine. PDBid 1DN1.]

remaining N-terminal 3-helix bundle is closely superimposable on the NMR structure of this segment alone. The 594-residue nSec1 is an arch-shaped molecule that binds syntaxin, and in particular its C-terminal helix, in the cleft of the arch (Fig. 12-77c).

The formation of the syntaxin–synaptobrevin–SNAP-25 complex that mediates vesicle fusion requires that the nSec1–syntaxin complex dissociate and that syntaxin’s N-terminal 3-helix bundle release the C-terminal helix. Mutational studies indicate that a Rab protein and/or its effectors mediate this process. It has therefore been proposed that the binding of Rab and/or its effectors to the nSec1–syntaxin complex causes nSec1 to change conformation, which in turn induces syntaxin’s N-terminal 3-helix bundle to release the C-terminal helix, thereby permitting the SNARE complex to form. Thus Rab controls the availability of syntaxin.

g. NSF Mediates Core Complex Disassembly

The SNARE complex in the fused membranes, the so-called **cis-SNARE complex**, must eventually be dissociated in order for its component proteins to participate in a new round of vesicle fusion. This process is mediated by NSF, an ATP-dependent cytosolic protein that binds to SNAREs (SNAP receptors) through the intermediacy of adaptor proteins called SNAPs (soluble NSF attachment proteins). Although it was initially proposed that the NSF-mediated disassembly of the cis-SNARE complex somehow directly drove membrane fusion, it is now clear that NSF functions to recycle SNAREs after their participation in membrane fusion, that is, *NSF functions as an ATP-driven molecular chaperone*. However, since trans-SNARE complexes form spontaneously, *membrane fusion is indirectly driven by NSF-mediated ATP hydrolysis*.

NSF is a hexamer of identical 752-residue subunits. Sequence analysis and limited proteolysis studies indicate that each subunit consists of three domains:

1. An N-terminal so-called N domain (residues 1–205), which mediates NSF’s interactions with SNAPs and SNAREs.
2. A D1 domain (206–487), which binds ATP and catalyzes its hydrolysis in a process that drives the disassembly of the cis-SNARE complex.
3. A C-terminal D2 domain (488–752), which is homologous to D1. D2 binds ATP with a much higher affinity than does D1 but hydrolyzes it very slowly, if at all. D2 · ATP mediates the hexamerization of NSF, which is required for NSF activity.

The X-ray structure of the D2 domain of NSF was independently determined by Weis and by Jahn and Brünger. Its wedge-shaped subunits associate to form a 116-Å-diameter and 40-Å-high disk-shaped hexamer that has an ~18-Å-diameter central pore (Fig. 12-78). The ATP is bound near the interface between two subunits, where it presumably helps stabilize their association.

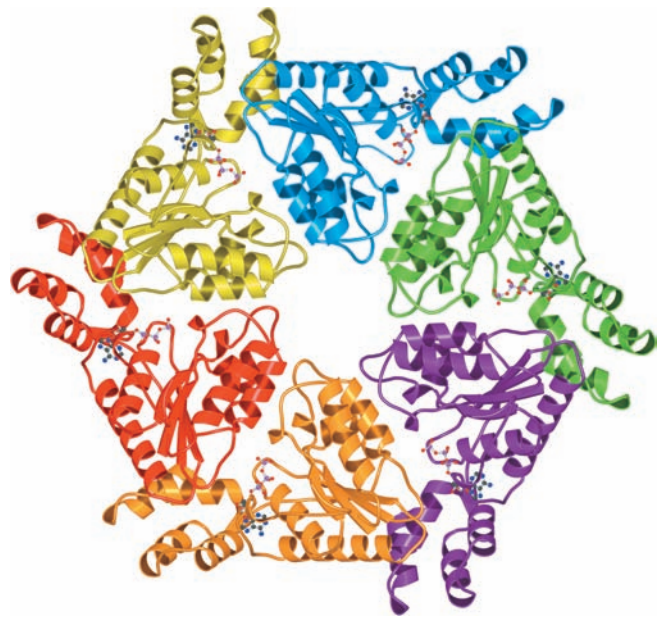


Figure 12-78 X-ray structure of the NSF D2 hexamer as viewed from its N-terminal end along its 6-fold axis. Each subunit is differently colored. The bound ATPs are drawn in ball-and-stick form. [Courtesy of Axel Brünger, Yale University. PDBid 1NSF.]

Electron micrographs by Jahn and John Heuser of intact NSF in the presence of ATP have the appearance of an ~120-Å-diameter hexagonal ring with a 30- to 50-Å central opening when seen in top view (Fig. 12-79a) and of a 120-Å by 150-Å rectangle when seen in side view (Fig. 12-79b). The length of the rectangle is about twice the height of the D2 disk, which suggests that D1 forms a D2-like hexagonal disk that stacks on D2. In the presence of ADP, NSF has an identical appearance, which suggests that D1 rapidly hydrolyzes its bound ATP to form ADP. However, in the presence of the nonhydrolyzable ATP analog ATP γ S (in which a terminal O atom on the γ -phosphorus atom of ATP is replaced by S), NSF displays six globular feet that are tightly packed around the somewhat smaller hexagonal ring (Fig. 12-79c). Since the hexagonal rings but not the globules are seen when D1–D2 constructs are imaged in the presence of ATP γ S, the globules must be the N domains. Evidently, the N domains are held tightly around the central disk of stacked D1 and D2 hexamers when D1 binds ADP but are released when D1 binds ATP.

The mechanism whereby NSF disassembles the cis-SNARE complex is largely unknown. The rod-shaped SNARE core complex (Fig. 12-74a), which is 20 to 25 Å in diameter, is too wide to fit inside the 18-Å-diameter central pore of the D2 hexamer (and presumably the similarly shaped D1 hexamer) without significant structural changes. It is therefore unlikely that the core complex binds inside NSF’s central cavity in a manner similar to the way that the GroEL–GroES chaperonin system binds its substrate proteins (Section 9-2Ca). Moreover, electron micrographs indicate that the complex of SNAP and the

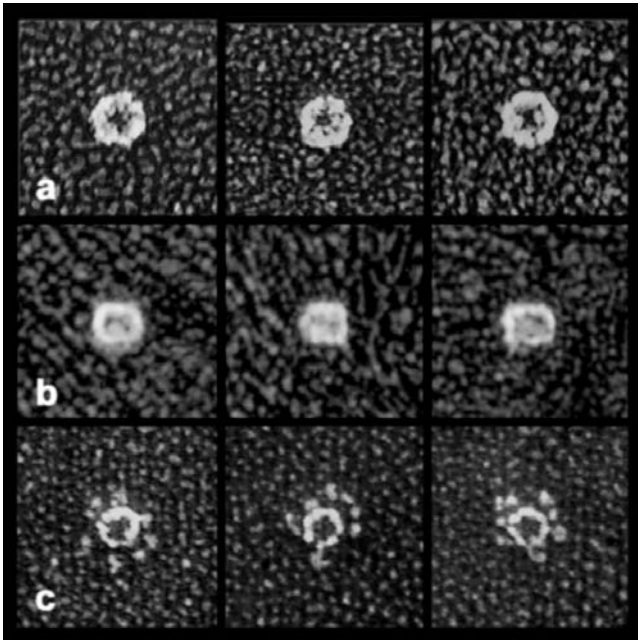


Figure 12-79 Quick-freeze/deep-etch electron micrographs of NSF hexamers. (a) Top and (b) side views in the presence of ATP. (c) Top view in the presence of ATP γ S. [Courtesy of John Heuser, Washington University School of Medicine, St. Louis, Missouri.]

three SNARE proteins binds to one end of NSF in the presence of ATP γ S (but not at all in the presence of ADP). Since NSF oligomers containing mixtures of active and inactive D1 domains are unable to disassemble SNARE complexes, it appears that the NSF subunits function in a cooperative manner.

E. Protein Targeting to Mitochondria

Although mitochondria contain functioning genetic and protein synthesizing systems, their genomes encode only a handful of inner membrane proteins (13 in humans; 8 in yeast). The vast majority of mitochondrial proteins (~99%), which comprise 10 to 20% of intracellular proteins, are encoded by nuclear genes and are synthesized by cytosolic ribosomes. They must therefore traverse one or both mitochondrial membranes (Section 1-2Ac) to reach their final destinations. In this subsection, we discuss how proteins are imported into mitochondria and are directed to their correct destinations [outer membrane, inner membrane, intermembrane space, or **matrix** (the space enclosed by the inner membrane)]. Our rapidly developing knowledge of this process was elucidated in large part through investigations in yeast and in the pink bread mold *Neurospora crassa* by Walter Neupert, Nikolaus Pfanner, Trevor Lithgow, and Gottfried Schatz. However, there is considerable evidence that this process is well conserved among all eukaryotes. The transport systems we describe

here and in Section 12-4B resemble those that mediate the import of proteins into chloroplasts (in which proteins must cross up to three membranes; Section 1-2Ag) and peroxisomes (Section 1-2Ad).

a. Proteins Must Be Unfolded for Import Into Mitochondria

Most nuclear-encoded mitochondrial proteins are fully synthesized by cytosolic ribosomes before they are imported into mitochondria; that is, they are post-translationally imported. One might expect, therefore, that mitochondrial proteins, many of which are integral proteins, would at least partially fold and/or nonspecifically aggregate in the cytosol before encountering the mitochondrial import system. Yet a variety of evidence indicates that *only unfolded proteins can pass through mitochondrial membranes*. For example, **dihydrofolate reductase (DHFR)**, a normally cytosolic enzyme, is imported into yeast mitochondria when it is preceded by the targeting sequence (see below) of a cytosolically synthesized mitochondrial protein. However, the importation of this chimeric protein is arrested by the presence of **methotrexate**, an analog of DHFR's normal substrate **dihydrofolate** (Section 28-3Be), which binds to DHFR with such high affinity that it stabilizes the protein's native conformation.

The import competence of mitochondrially destined proteins is maintained in the cytosol by a variety of ATP-dependent molecular chaperones. These include members of the Hsp70 family (Section 9-2C) and, in mammals, a protein named **mitochondrial import stimulation factor (MSF)**. Consequently, the genetically engineered shut-down of Hsp70 production in yeast causes the cells to cytosolically accumulate proteins that would otherwise be imported into the mitochondria. Moreover, the rate of the Hsp70-facilitated mitochondrial import of a protein is enhanced by its prior denaturation by urea. Evidently, Hsp70 functions in this process as an ATP-driven "protein unfoldase."

b. Translocation of Proteins Across the Outer Mitochondrial Membrane

Most cytosolically synthesized matrix proteins have cleavable N-terminal signal sequences that do not interact with the SRP. These presequences consist of 10 to 80 residues that form amphipathic helices with one face positively charged. However, many mitochondrial proteins, including most metabolite carrier proteins of the inner membrane (see below), have poorly characterized internal targeting sequences.

The protein subunits that participate in importing proteins across the outer mitochondrial membrane are called **TOM proteins** (for translocase of the outer mitochondrial membrane) and are named Tomxx, where xx is the molecular mass of the subunit in kilodaltons. Likewise, many of the proteins involved in translocating proteins across the inner mitochondrial membrane are called **TIM proteins** (for translocase of the inner mitochondrial membrane) and are named Timxx.

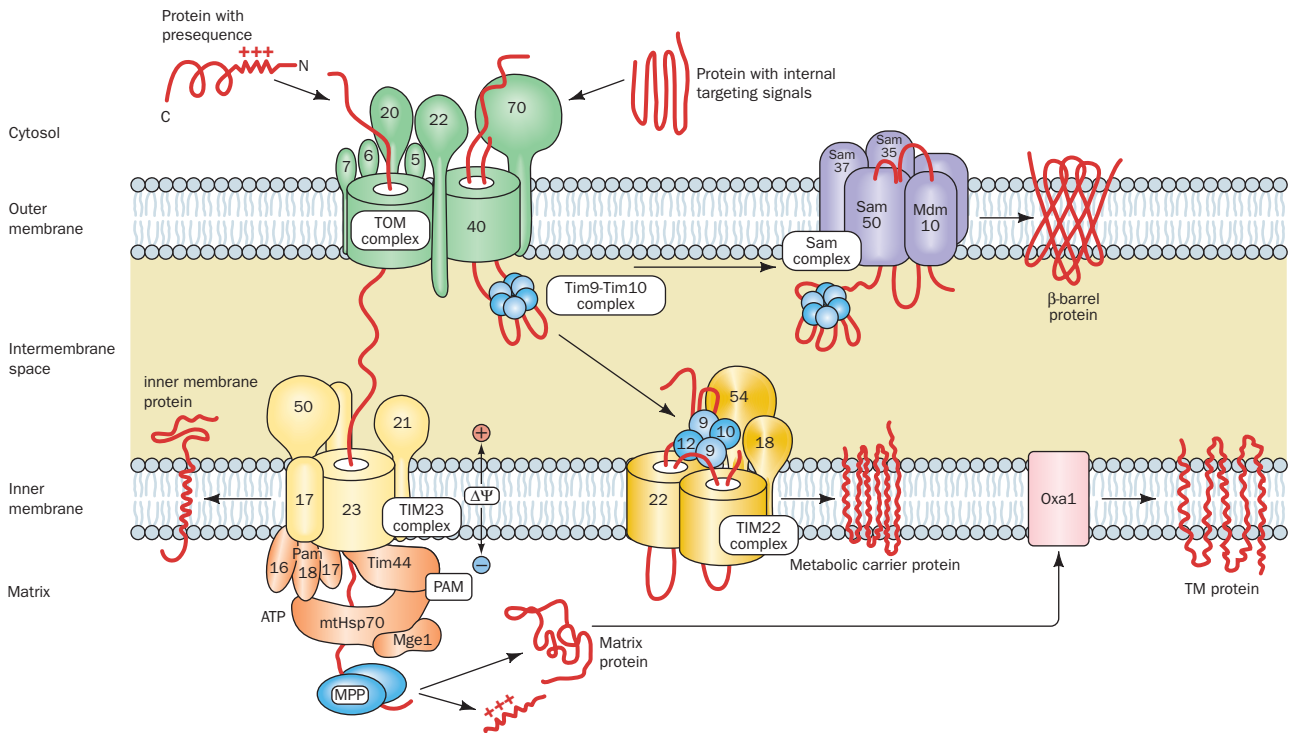


Figure 12-80 Schematic diagram of the mitochondrial protein import machinery in yeast. See the text for a description. The subunit compositions of these complexes in mitochondria from

other organisms are similar. [After Bolender, N., Sickmann, A., Wagner, R., Meisinger, C., and Pfanner, N., *EMBO Rep.* **9**, 42–49 (2008).]

The **TOM complex**, the machinery that imports all mitochondrial proteins through the outer mitochondrial membrane, does so as follows (Fig. 12-80, top left—green):

1. The signal sequences of unfolded preproteins associate with the cytoplasmic domains of mitochondrial receptor proteins: N-terminal signal sequences interact mainly with **Tom20** in complex with **Tom22**, whereas internal signal sequences interact mainly with **Tom70**. The NMR structure of a portion of Tom20's cytosolic domain in complex with an 11-residue segment of a presequence peptide (Fig. 12-81), determined by Toshiya Endo and Daisuke Kohda, reveals that the Tom20 domain consists mainly of five helices. Its two N-terminal helices form a nonpolar surface groove in which the helical presequence binds, mainly via hydrophobic interactions rather than ionic interactions. Evidently, Tom20 recognizes the presequence's amphipathic helix but not its positive charges. These positive charges, which are required for mitochondrial import, interact with Tom22.

2. Tom20 and Tom70 deliver preproteins to the **general import pore (GIP)**, so called because all nuclear-encoded mitochondrial proteins must pass through it. The GIP is formed by **Tom40**, a polytopic TM protein, which CD measurements indicate consists mainly of β sheets and hence has a TM β barrel structure that presumably resembles that of bacterial porins (Fig. 12-27). Electrophysiological measurements demonstrate that Tom40 contains a cation-selective hydrophilic channel through which precursor proteins are transported. Tom40 is closely associated with three small single pass TM subunits, **Tom5**, **Tom6**, and **Tom7**, to form

the **TOM core complex**. The deletion of any one of these small subunits has only minor effects but the deletion of all three is lethal. They appear to stabilize the TOM complex but their individual functions are largely unknown. Electron micrographs of the *Neurospora* TOM core complex (Fig. 12-82) reveal an ~ 70 -Å-high (~ 20 Å larger than the thickness of the lipid bilayer) and ~ 120 -Å-wide particle containing two ~ 21 -Å-diameter pores that presumably are the protein-conducting channels. This agrees with permeability experiments using cations of various sizes, which indicate that the Tom40 pore is ~ 22 Å in diameter.

3. The forces driving the translocation of polypeptides through the TOM complex remain largely enigmatic. A proposed mechanism, the **acid chain hypothesis**, is that the positively charged presequence is sequentially transferred between acidic (negatively charged) patches to which it binds with successively higher affinities. Such patches are present on the cytoplasmic faces of Tom20, Tom22, and Tom5, as well as on the intermembrane faces of Tom40 and Tom22.

At this stage, the import pathway for mitochondrial proteins splits several ways. We discuss these various pathways below.

c. Translocation of Proteins Into the Matrix

Polypeptides with N-terminal signal sequences, which include the precursors of all matrix-destined proteins, most inner membrane proteins, and many proteins that occupy the intermembrane space (**IMS**), are translocated across the inner mitochondrial membrane by the **TIM23 complex**

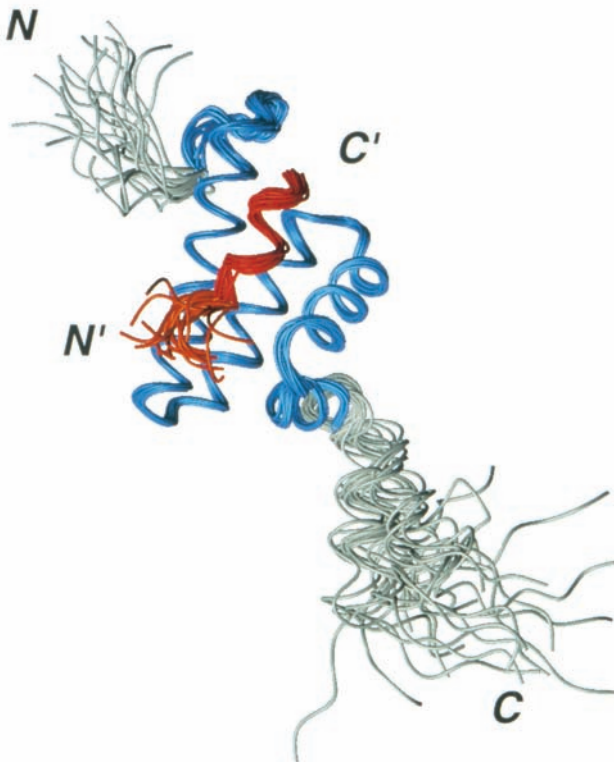


Figure 12-81 NMR structure of the cytoplasmic domain of rat **Tom20** in complex with the C-terminal 11-residue segment (GPRLSRLLSYA) of the 22-residue presequence of the rat mitochondrial enzyme aldehyde dehydrogenase. The diagram is a superposition of the 20 final structures in the NMR analysis (Section 8-3A) in which the residues used to make the superposition are blue (Tom20) and red (presequence) and the remaining residues are gray (Tom20) and orange (presequence). [Courtesy of Toshiya Endo, Nagoya University, Nagoya, Japan, and Daisuke Kohda, Biomolecular Engineering Research Institute, Osaka, Japan. PDBid 1OM2.]

(Fig. 12-80, *bottom left*—yellow). This complex contains a protein channel formed by **Tim23**, which is closely associated with **Tim17**. The peripheral protein **Tim50** binds the polypeptide emerging from the Tom40 channel and passes it to **Tim23**. Electron microscopy studies indicate that the TOM and TIM23 complexes are in apposition at sites where the inner and outer mitochondrial membranes approach each other most closely. Indeed, **Tim21** transiently associates with Tom22 across this contact site by displacing the emerging signal sequence.

In the presence of methotrexate, the above DHFR chimera becomes stuck in the membrane with the spacer that linked the enzyme to its N-terminal presequence simultaneously spanning the TOM and TIM23 complexes. The N-terminal end of the spacer is presumably trapped in the matrix through its association with **mtHsp70** (see below). Consequently, if the spacer is so short that it cannot span both membranes (less than ~ 40 residues), no stable translocation intermediate is formed. Thus, it appears that presequences make their way between the TOM and TIM23 complexes without the aid of chaperones.

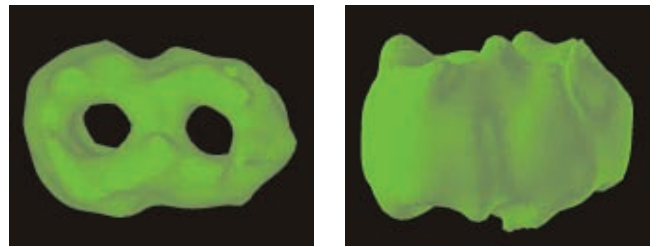


Figure 12-82 Electron microscopy-based image of the TOM core complex particles from *Neurospora*. The particles, which are shown in top view (*left*) and side view (*right*), contain two openings that presumably represent the mitochondrial outer membrane's protein-conducting channels. [Courtesy of Stephan Nussberger and Walter Neupert, Universität München, Germany.]

The translocation of a protein across the inner mitochondrial membrane requires energy in the form of both ATP and an electrostatic potential across the inner mitochondrial membrane. This so-called **membrane potential** (Section 20-1), $\Delta\Psi$, which is metabolically generated (Section 22-3Ba), apparently functions to electrophoretically transport the positively charged N-terminal signal sequence into the matrix (the matrix is negatively charged with respect to the cytosol).

The ATP is utilized by matrix Hsp70 (mtHsp70; alternatively, **mHsp70**), the central component of the **presequence translocase-associated motor (PAM; Fig. 12-80, bottom left—orange)**. This molecular chaperone binds to **Tim44** on the inner face of the inner mitochondrial membrane, where it is thought to mechanically pull the protein through the Tim23 pore via a Brownian ratchet mechanism (Section 12-4Bg). **Pam 18** (alternatively, **Tim14**), which associates with Tim44, has a J-domain that presumably recruits mtHsp70 and induces it to hydrolyze its bound ATP to ADP, thus activating it to bind the incoming polypeptide. **Pam16** (alternatively **Tim16**), which binds Tim14, is thought to act as a negative regulator of Tim14 by physically blocking its access to mtHsp70. **Pam17** is required for the assembly of the Pam18–Pam16 module. The matrix protein **Mge1** stimulates mtHsp70 to exchange its bound ADP for ATP, thus permitting it to participate in another cycle of the Brownian ratchet.

Once a preprotein, or at least its N-terminal segment, has entered the matrix, its N-terminal signal sequence is excised by **matrix processing peptidase (MPP)**, an essential protein. The imported protein then folds/assembles to its native state, a process that is facilitated by a battery of ATP-dependent chaperone proteins including mtHsp70 (only about 10% of which is associated with Tim44) and Hsp60/Hsp10 (homologs of the GroEL/ES system; Section 9-2C).

Some of the polypeptides that are translocated by the TIM23 complex have a stop-transfer anchor sequence. The TIM23 complex laterally inserts the resulting TM helix into the inner mitochondrial membrane (Fig. 12-80, *bottom, far left*) such that its N-terminal portion occupies the matrix, where MPP excises its N-terminal signal sequence.

d. Insertion of Metabolite Carrier Proteins Into the Inner Mitochondrial Membrane

The mitochondrial inner membrane is impermeable to nearly all polar substances and hence contains numerous (35 in yeast) **metabolite carrier proteins** to permit the acquisition of reactants and the delivery of products. The most abundant members of this family are the **ATP–ADP translocator** (which exchanges the ATP synthesized in the matrix for the ADP product of cytosolic ATP hydrolysis; Section 20-4C) and the **phosphate carrier** (which returns the phosphate product of cytosolic ATP hydrolysis to the matrix; Section 22-1Ba). All metabolite carrier proteins have six TM helices with both their N- and C-termini in the IMS.

Most members of the metabolite carrier family lack N-terminal signal sequences and are therefore translocated through the TOM complex via interactions with its Tom70 receptor. Curiously, however, the Tom20–Tom22 complex is the receptor for most other outer membrane proteins that have internal signal sequences. Metabolite carrier proteins are escorted across the IMS by a hexameric complex of the homologous proteins **Tim9** and **Tim10**, (Tim9)₃(Tim10)₃, which is thought to shield the hydrophobic domains of the metabolite carrier proteins (Fig. 12-80, *middle—blue*). Metabolite carrier proteins in a preparation of mitochondria depleted of Tim9 and Tim10 are not inserted into the GIP, as indicated by their failure to reach a protease-resistant state. This suggests that it is the binding of the Tim9–Tim10 complex to an unfolded metabolite carrier protein that drives its translocation across the outer mitochondrial membrane.

The Tim9–Tim10 complex delivers the metabolite carrier protein to the peripheral protein **Tim12** (a homolog of Tim9 and Tim10), which is associated with the integral proteins **Tim22** (which is homologous to Tim 23), **Tim54**, and **Tim18** to form the **TIM22 complex** (Fig. 12-80, *bottom middle—gold*). *Tim22 then mediates the lateral insertion of the metabolite carrier protein into the inner mitochondrial membrane, where it assembles to form homodimers.* This process occurs via an unknown but membrane potential-dependent mechanism. The functions of Tim54 and Tim18 are unknown.

e. Soluble Proteins Occupying the Intermembrane Space Are Imported via Three Mechanisms

Despite the fact that its width is around that of a membrane bilayer, the IMS contains a large collection of essential proteins. The precursors of some of these proteins are imported, as described above, such that they become anchored to the IMS by a single TM helix that has its N-terminal end in the matrix (Fig. 12-80, *bottom, far left*). Such a protein is then cleaved by an inner membrane protease on the C-terminal side of its TM helix, thereby releasing it into the IMS, where it folds to its native conformation. Since the mature protein lacks a signal sequence, it is no longer subject to importation into the matrix and hence remains in the IMS. **Coproporphyrinogen oxidase**, which participates in heme biosynthesis (Section 26-4Ae), is such a protein.

Many small proteins that lack N-terminal signal sequences are imported, via the TOM complex, into the IMS.

There they assume their native fold, thus trapping them in the IMS—the so-called **folding-trap mechanism**. Such proteins have conserved patterns of Cys and/or His residues that enable them to bind metal ion-containing cofactors in the IMS or to form disulfide bonds, both of which stabilize their native structures. [Note that the latter proteins are among the few intracellular proteins that have disulfide bonds (Section 8-4D). Evidently, the IMS has an oxidative environment.] For example, **apocytochrome c** (cytochrome *c* without its covalently attached heme group; Fig. 9-39) folds when the IMS-resident enzyme **cytochrome c heme lyase (CCHL)** catalyzes the attachment of its heme group, whereas Tim9, Tim10, and Tim12 each contain twin CX₃C motifs that form disulfide bonds.

A third class of IMS-resident proteins remain in the IMS through their association with the inner membrane, that is, they are peripheral proteins. CCHL is a member of this class of proteins.

f. Many Polytopic Inner Membrane Proteins Are First Imported to the Matrix

Many cytosolically synthesized polytopic proteins destined for insertion into the mitochondrion's inner membrane are first imported into the matrix as described above and then inserted into the inner membrane, an indirect routing that reflects the mitochondrion's bacterial origin [the primordial mitochondrion, being a gram-negative bacterium, synthesized all of its proteins in its cytoplasm (the primordial matrix) so that membrane-bound or intermembrane proteins had to be exported to these destinations]. These proteins, for the most part, are synthesized with bipartite N-terminal targeting sequences whose inner (more C-terminal) segments, once exposed by the removal of the above-described N-terminal presequence, direct the proteins to the inner membrane. The insertion of several such proteins into the inner mitochondrial membrane is mediated by the TM protein **Oxa1**, which also occupies the inner mitochondrial membrane (Fig. 12-80, *bottom right, pink*). Oxa1, which binds mitochondrial ribosomes on its matrix side, also inserts mitochondrially synthesized proteins into the inner mitochondrial membrane. As might be expected, Oxa1 is related to a protein that inserts proteins into the inner membrane of gram-negative bacteria.

g. Insertion of β Barrel Proteins Into the Outer Mitochondrial Membrane

The outer membranes of mitochondria and chloroplasts contain proteins, such as porins (Section 12-3Ad) and Tom40, that have TM β barrels. These are the only places in eukaryotic cells that TM β barrels occur, which also reflects the bacterial origins of these organelles (Sections 1-2Ac and 1-2Ag).

β barrel proteins are imported into the IMS by the TOM complex. There they are bound by the Tim9–Tim10 complex, which escorts them to the **SAM complex** (for sorting and assembly machinery; alternatively **TOB complex** for topogenesis of mitochondrial outer membrane β barrel), which in turn inserts them into the outer mitochondrial membrane (Fig. 12-80, *top right—purple*). The SAM complex

Table 12-6 Characteristics of the Major Classes of Lipoproteins in Human Plasma

	Chylomicrons	VLDL	IDL	LDL	HDL
Density ($\text{g} \cdot \text{cm}^{-3}$)	<0.95	<1.006	1.006–1.019	1.019–1.063	1.063–1.210
Particle diameter (\AA)	750–12,000	300–800	250–350	180–250	50–120
Particle mass (kD)	400,000	10,000–80,000	5000–10,000	2300	175–360
% Protein ^a	1.5–2.5	5–10	15–20	20–25	40–55
% Phospholipids ^a	7–9	15–20	22	15–20	20–35
% Free cholesterol ^a	1–3	5–10	8	7–10	3–4
% Triacylglycerols ^b	84–89	50–65	22	7–10	3–5
% Cholesteryl esters ^b	3–5	10–15	30	35–40	12
Major apolipoproteins	A-I, A-II, B-48, C-I, C-II, C-III, E	B-100, C-I, C-II, C-III, E	B-100, C-I, C-II, C-III, E	B-100	A-I, A-II, C-I, C-II, C-III, D, E

^aSurface components.^bCore lipids.

is formed by the TM β barrel-containing protein **Sam50** (alternatively, **Tob55** or **Tom55**) in association with **Sam37** (**Mas37/Tom37**), **Sam35** (**Tob35/Tom38**), and **Mdm10** (mitochondrial distribution and morphology 10). β barrel proteins are inserted into the outer membrane from its inner side, which presumably is also an evolutionary consequence of the mitochondrion's bacterial origin. Nevertheless, the TOM and SAM complexes are functionally coupled as indicated by the observation that when β barrel proteins are imported into mitochondria lacking Sam50, they accumulate in the TOM complex rather than in the IMS. Sam50 is homologous to the bacterial outer membrane protein **Omp85**, which participates in inserting β barrel proteins into the bacterial outer membrane.

5 LIPOPROTEINS

Lipids and proteins associate noncovalently to form **lipoproteins**, which function in the blood plasma as transport vehicles for triacylglycerols and cholesterol. In this section, we discuss the structure, function, and dysfunction of lipoproteins, and how eukaryotic cells take up lipoproteins and other specific proteins from their external medium through receptor-mediated endocytosis.

A. Lipoprotein Structure

Lipids, such as phospholipids, triacylglycerols, and cholesterol, are but sparingly soluble in aqueous solution. Hence, they are transported by the circulation as components of lipoproteins, globular micellelike particles that consist of a nonpolar core of triacylglycerols and cholesteryl esters surrounded by an amphiphilic coating of protein, phospholipid, and cholesterol. Lipoproteins have been classified into five broad categories on the basis of their functional and physical properties (Table 12-6):

1. Chylomicrons, which transport exogenous (externally supplied; in this case, dietary) triacylglycerols and cholesterol from the intestines to the tissues.

2–4. Very low density lipoproteins (VLDL), intermediate density lipoproteins (IDL), and low density lipoproteins (LDL), a group of related particles that transport endogenous (internally produced) triacylglycerols and cholesterol from the liver to the tissues (the liver synthesizes triacylglycerols from excess carbohydrates; Section 25-4).

5. High density lipoproteins (HDL), which transport endogenous cholesterol from the tissues to the liver.

Lipoprotein particles undergo continuous metabolic processing, so that they have variable properties and compositions (Table 12-6). Each contains just enough protein, phospholipid, and cholesterol to form an $\sim 20\text{-\AA}$ -thick monolayer of these substances on the particle surface (Fig. 12-83). Lipoprotein densities increase with decreasing particle diameter because the density of their outer coating is greater than that of their inner core.

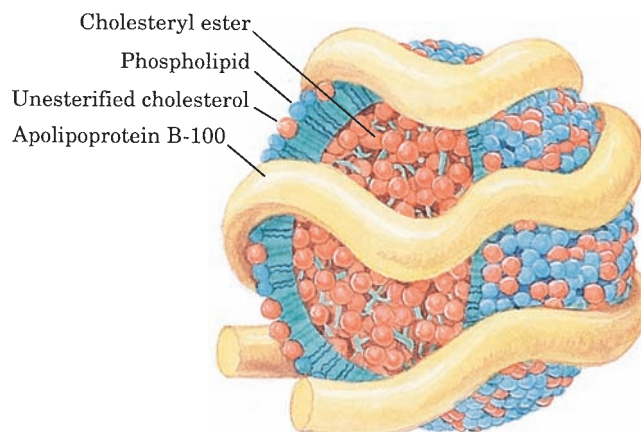


Figure 12-83 LDL, the major cholesterol carrier of the bloodstream. This spheroidal particle consists of some 1500 cholesteryl ester molecules surrounded by an amphiphilic coat of 800 phospholipid molecules, 500 cholesterol molecules, and a single 4536-residue molecule of apolipoprotein B-100.

Table 12-7 Properties of the Major Species of Human Apolipoproteins

Apolipoprotein	Number of Residues	Molecular Mass ^a (kD)	Function
A-I	243	29	Activates LCAT ^b
A-II	77	17	Inhibits LCAT, activates hepatic lipase
B-48	2152	241	Cholesterol clearance
B-100	4536	513	Cholesterol clearance
C-I	56	6.6	Activates LCAT?
C-II	79	8.9	Activates LPL ^c
C-III	79	8.8	Inhibits LPL, activates LCAT?
D	169	19	Unknown
E	299	34	Cholesterol clearance

^aAll apolipoproteins are monomers but apoA-II, which is a disulfide-linked dimer.

^bLCAT = lecithin-cholesterol acyltransferase.

^cLPL = lipoprotein lipase.

a. Apolipoproteins Have Amphipathic Helices That Coat Lipoprotein Surfaces

The protein components of lipoproteins are known as **apolipoproteins** or just **apoproteins**. At least nine apolipoproteins are distributed in significant amounts in the different human lipoproteins (Tables 12-6 and 12-7). Most of them are water-soluble and associate rather weakly with lipoproteins. Hence, they readily transfer between lipoprotein particles via the aqueous phase. CD measurements indicate that *apolipoproteins have a high helix content, which increases when they are incorporated in lipoproteins*. Apparently, the helices are stabilized by a lipid environment, presumably because helices fully satisfy the polypeptide backbone's hydrogen bonding potential in a lipoprotein's water-free interior.

b. The X-ray Structure of ApoA-I Mimics That in HDL

Apolipoprotein A-I (apoA-I) is HDL's major apoprotein. Sequence analysis indicates that apoA-I consists mainly of repeated amphipathic α helices of 11 or 22 residues that provide the protein's lipid-binding regions. *These putative α helices, as well as similar helices that occur in most other apolipoproteins, have their hydrophobic and hydrophilic residues on opposite sides of the helical cylinders* (Fig. 12-84). Furthermore, the polar helix face has a zwitterionic character in that its negatively charged residues project from the center of this face, whereas its positively charged residues are located at its edges. Indeed, a synthetic 22-residue polypeptide of high helix-forming propensity, which was designed by E. Thomas Kaiser to have this polarity distribution but to otherwise have minimal similarity to the repeating apoA-I sequences, behaves much like apoA-I in binding to egg lecithin liposomes. Evidently, the structural role of apoA-I, and probably most other apolipoproteins, is fulfilled by its helical segments rather than by any organized tertiary structure. This suggests that *lipoprotein α helices float on phospholipid surfaces, much like logs on water*. The phospholipids are presumably arrayed with their charged groups bound to

oppositely charged residues on the polar face of the helix and with the first few methylene groups of their fatty acid residues in hydrophobic association with the nonpolar face of the helix.

A variety of criteria indicate that apoA-I undergoes significant secondary structural changes on binding lipid. However, apo $\Delta(1-43)$ A-I, a truncation mutant that lacks residues 1 to 43 of the 243-residue human apoA-I, has a

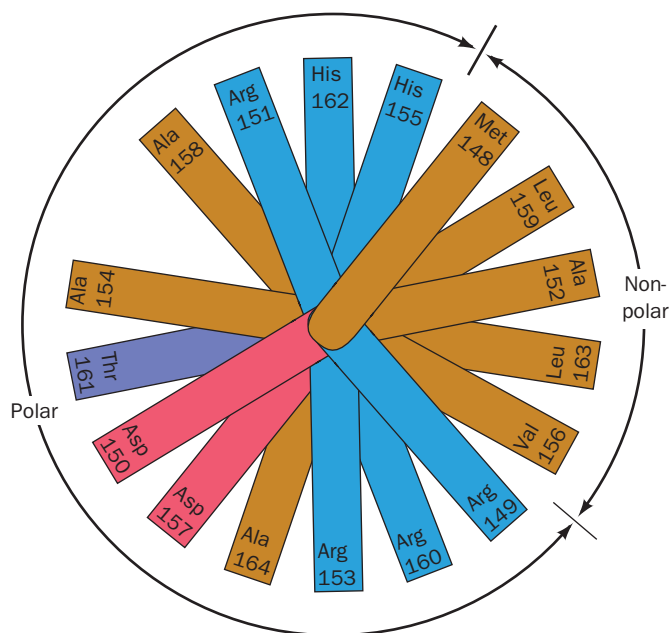
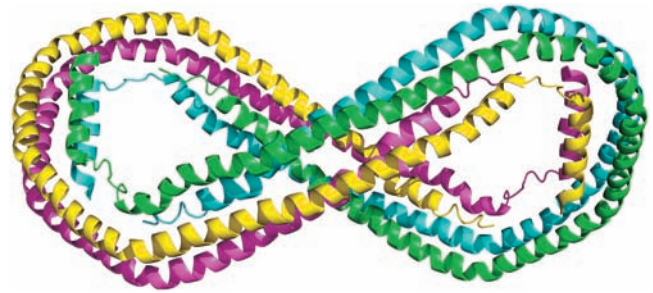


Figure 12-84 A helical wheel projection of the amphipathic α helix constituting residues 148 to 164 of apolipoprotein A-I. (In a helical wheel representation, the side chain positions are projected down the helix axis onto a plane.) Note the segregation of nonpolar, acidic, and basic residues to different sides of the helix. Other apolipoprotein helices have similar polarity distributions. [After Kaiser, E.T., in Oxender, D.L. and Fox, C.F. (Eds.), *Protein Engineering*, p. 194, Liss (1987).]



(a)

Figure 12-85 X-ray structure of human apo $\Delta(1-43)$ A-I. The four monomers of the D_2 -symmetric tetramer it forms are drawn in different colors. (a) View along the 2-fold axis relating the cyan and yellow subunits and the green and magenta subunits. (b) View from the top of Part a along the 2-fold axis relating the cyan and magenta subunits and the green and yellow subunits. The third pairings, cyan with green and magenta with yellow,



(b)

which interact along most of their lengths, probably maintain their identities in HDL particles, whereas the other pairings, whose interactions are less extensive, are unlikely to do so. [Based on an X-ray structure by David Borhani, Southern Research Institute, Birmingham, Alabama, and Christie Brouillette, University of Alabama Medical Center, Birmingham. PDBid 1AV1.]

conformation that closely resembles that of lipid-bound apoA-I, whether or not lipid is present. Lipid-free apo $\Delta(1-43)$ A-I is therefore likely to provide a valid structural model for lipid-bound apoA-I.

The X-ray structure of apo $\Delta(1-43)$ A-I (Fig. 12-85) was determined by David Borhani and Christie Brouillette. It revealed that, over most of its length, each polypeptide chain forms a pseudocontinuous amphipathic α helix that is punctuated by kinks at Pro residues that are spaced mainly at intervals of 22 residues to form 10 helical segments arranged in the shape of a twisted horseshoe. Two such monomers (e.g., the cyan and magenta monomers in Fig. 12-85) associate in an antiparallel fashion along most of their lengths to form a dimer that has the shape of a twisted elliptical ring. Two such dimers, in turn, associate via their hydrophobic surfaces to form an elliptical tetramer with D_2 symmetry that has outer dimensions of $135 \times 90 \text{ \AA}$ and an inner hole of $95 \times 50 \text{ \AA}$. The surface of this tetrameric ring, which consists of up-down-up-down 4-helix bundles over about three-fourths of its circumference, is hydrophilic with a uniform electrostatic potential, whereas the interior of each 4-helix bundle contains mainly Val and Leu side chains. Since, in this conformation, these hydrophobic residues are unavailable for binding to lipid, it is postulated that they associate in the lipid-free crystal so as to shelter the lipid-binding face of apo $\Delta(1-43)$ A-I dimers from contact with water (which fills the spaces in the crystal).

The sizes and shapes of the apo $\Delta(1-43)$ A-I dimer and tetramer seem ideal for wrapping around the 50- to 120- \AA -diameter HDL particles. Since HDL particles often contain two or four apoA-I monomers, it is proposed that when pairs of apoA-I monomers bind to HDL, they do so as the above-described antiparallel dimer. Its exposed nonpolar

side chains could then hydrophobically interact with the HDL particle's buried nonpolar groups. Two such dimers could associate on the surface of an HDL particle to form a tetramer, although, most probably, in a different manner than is seen in the structure of apo $\Delta(1-43)$ A-I.

B. Lipoprotein Function

The various lipoproteins have different physiological functions, as we discuss below.

a. Chylomicrons Are Delipidated in the Capillaries of Peripheral Tissues

Chylomicrons, which are assembled by the intestinal mucosa, function to keep exogenous triacylglycerols and cholesterol suspended in aqueous solution. These lipoproteins are released into the intestinal lymph (known as **chyle**), which is transported through the lymphatic vessels before draining into the large body veins via the thoracic duct. After a fatty meal, the otherwise clear chyle takes on a milky appearance.

Chylomicrons adhere to binding sites on the inner surface (endothelium) of the capillaries in skeletal muscle and adipose tissue. There, within minutes after entering the bloodstream, the chylomicron's component triacylglycerols are hydrolyzed through the action of **lipoprotein lipase (LPL)**, an extracellular enzyme that is activated by **apoC-II**. The tissues then take up the liberated monoacylglycerol and fatty acid hydrolysis products. The chylomicrons shrink as their triacylglycerols are progressively hydrolyzed until they are reduced to cholesterol-enriched **chylomicron remnants**. The chylomicron remnants reenter the circulation by dissociating from the capillary endothelium and are subsequently taken up by the liver, as is

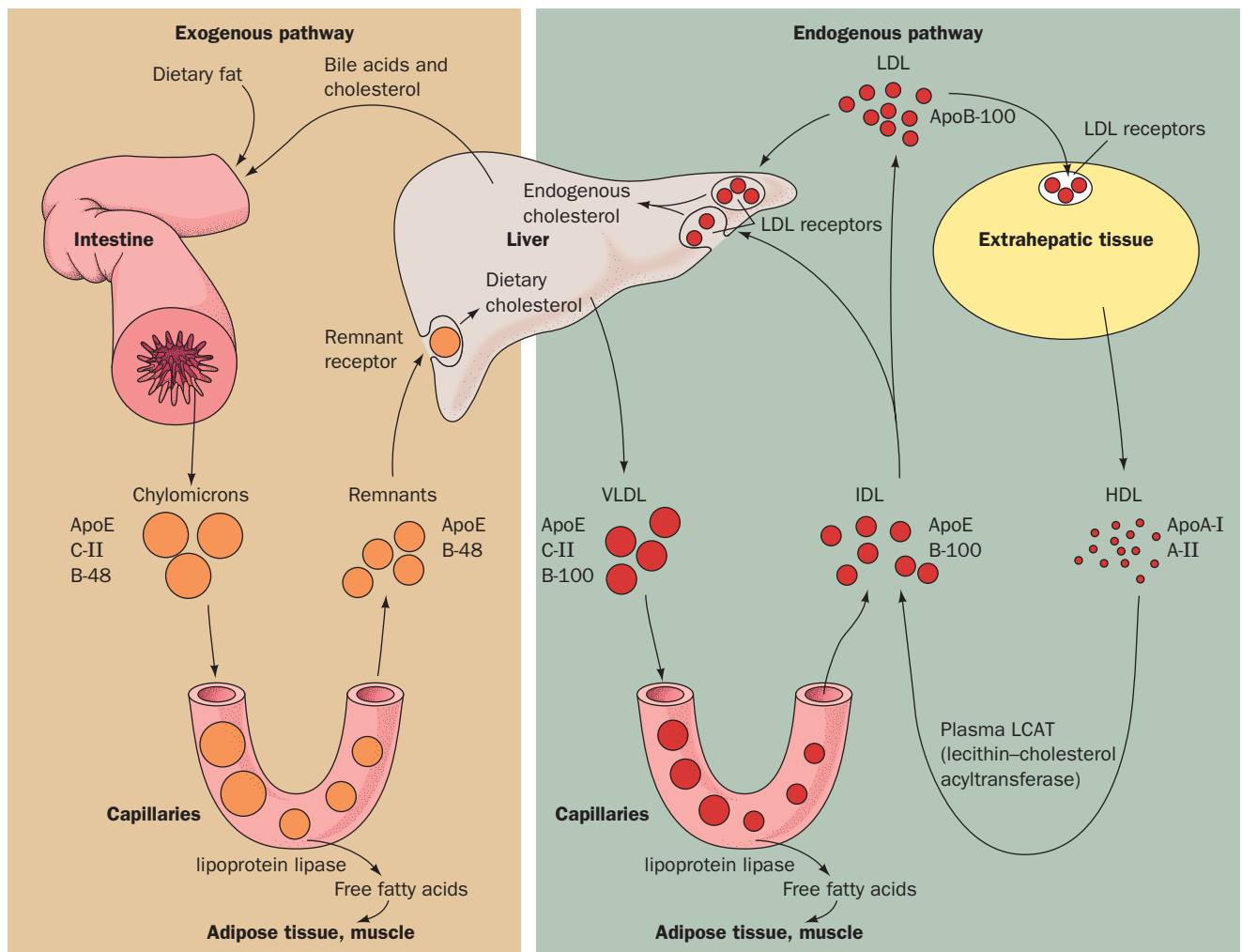


Figure 12-86 Model for plasma triacylglycerol and cholesterol transport in humans. [After Brown, M.S. and Goldstein, J.L., in Brunwald, E., Isselbacher, K.J., Petersdorf, R.G., Wilson, J.D.,

Martin, J.B., and Fauci, A.S. (Eds.), *Harrison's Principles of Internal Medicine* (11th ed.), p. 1652, McGraw-Hill (1987).]

 See the Animated Figures

explained below. *Chylomicrons therefore function to deliver dietary triacylglycerols to muscle and adipose tissue and dietary cholesterol to the liver* (Fig. 12-86, left).

b. VLDL Are Degraded Much Like Chylomicrons

VLDL, which are synthesized in the liver as lipid transport vehicles, are also degraded by lipoprotein lipase (Fig. 12-86, right). The VLDL remnants appear in the circulation, first as IDL and then as LDL. In the transformation of VLDL to LDL, all their proteins but **apoB-100** are removed and much of their cholesterol is esterified by the HDL-associated enzyme **lecithin-cholesterol acyltransferase (LCAT)**, as is discussed below. This enzyme transfers a fatty acid residue from atom C2 of lecithin to cholesterol with the concomitant formation of **lysolecithin** (Fig. 12-87).

ApoB-100, a 4536-residue monomeric glycoprotein (and thus one of the largest monomeric proteins known), has a hydrophobicity approaching that of integral proteins and contains relatively few amphipathic helices. Hence, in contrast

to the other, less hydrophobic plasma apolipoproteins, apoB-100 is neither water-soluble nor transferred between lipoprotein particles. Each LDL particle contains but one molecule of apoB-100, which immunoelectron microscopy indicates has an extended form that covers at least half of the particle surface (Fig. 12-83). Chylomicrons, however, contain **apoB-48**, a 2152-residue protein that is identical in sequence to the N-terminal 48% of apoB-100. Indeed, both proteins are encoded by the same gene. The remarkable mechanism by which this gene expresses different length proteins in liver and intestines is discussed in Section 31-4A.

c. Cells Take Up Cholesterol through Receptor-Mediated Endocytosis of LDL

Cholesterol, as we have seen, is an essential component of animal cell membranes. The cholesterol may be externally supplied or, if this source is insufficient, internally synthesized (Section 25-6A). Michael Brown and Joseph Goldstein have demonstrated that *cells obtain exogenous cholesterol*

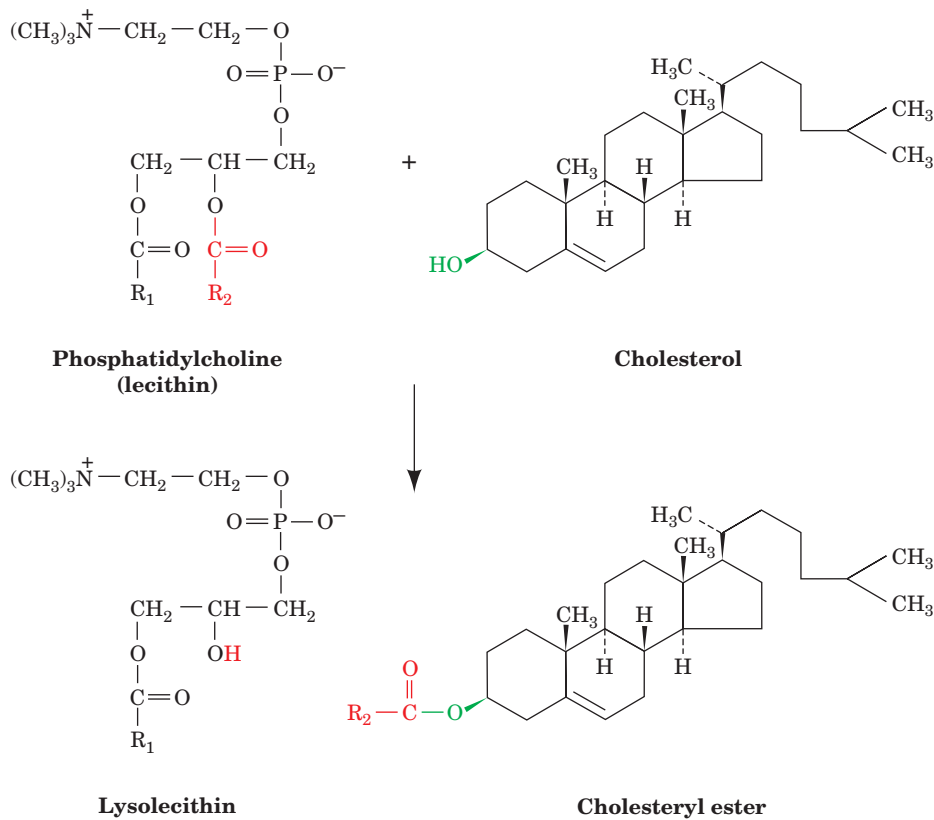


Figure 12-87 Reaction catalyzed by lecithin-cholesterol acyltransferase (LCAT). The transferred acyl group is most often a linoleic acid residue.

mainly through the endocytosis (engulfment) of LDL in complex with **LDL receptor (LDLR)**, a cell-surface transmembrane glycoprotein that specifically binds apoB-100. LDLR also binds chylomicron remnants via their apoE components.

LDLR is an 839-residue glycoprotein that has a 767-residue N-terminal ligand-binding **ectodomain** (extracellular domain; Greek: *ectos*, outside), a 22-residue TM segment that presumably forms an α helix, and a 50-residue C-terminal cytoplasmic domain. The X-ray structure of

LDLR's ectodomain, determined by Brown, Goldstein, and Deisenhofer at pH 5.3 (for reasons explained below), confirms the results of sequence studies indicating that this protein consists of, from N- to C-terminus, seven tandemly repeated \sim 40-residue Cys-rich modules, two \sim 40-residue EGF-like domains (EGF is the acronym for **epidermal growth factor**, a hormonally active polypeptide that stimulates cell proliferation; Section 19-3), a six-bladed β propeller domain, and an EGF-like domain (Fig. 12-88). The Cys-rich modules, designated R2 to R7 (R1 is disordered and hence unseen), are arranged in an \sim 140-Å-long arc that loops around to the EGF-like domains

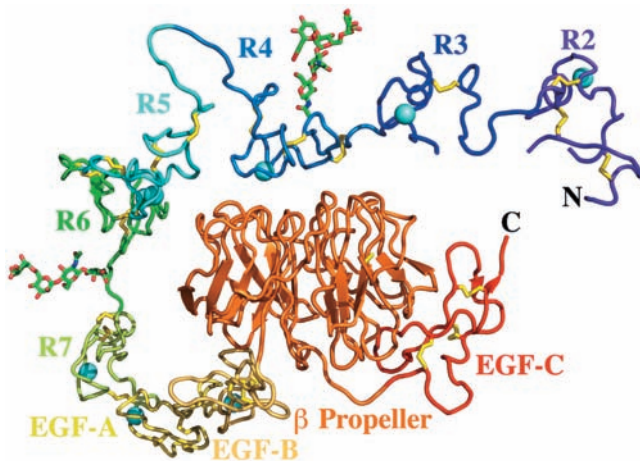


Figure 12-88 X-ray structure of the extracellular domain of the human LDL receptor at 3.7 Å resolution. The protein is drawn in ribbon form with each of its observed modules given a different color. Its eight bound Ca^{2+} ions are represented by cyan spheres, and two N-linked carbohydrates (a tetrasaccharide and a pentasaccharide) are shown in stick form with C green, N blue, and O red. Disulfide linkages are drawn in yellow. The Cys-rich modules are labeled R2 through R7 and the EGF-like domains are labeled EGF-A through EGF-C. The absence of the R1 module and the fragmented appearance of the R2 and R3 modules are due to the disorder of the missing segments. [After an X-ray structure by Michael Brown, Joseph Goldstein, and Johann Deisenhofer, University of Texas Southwest Medical Center, Dallas, Texas. PDBid 1N7D.]

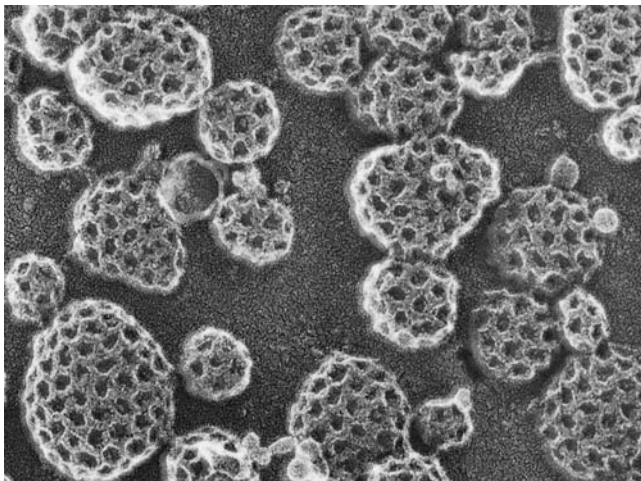


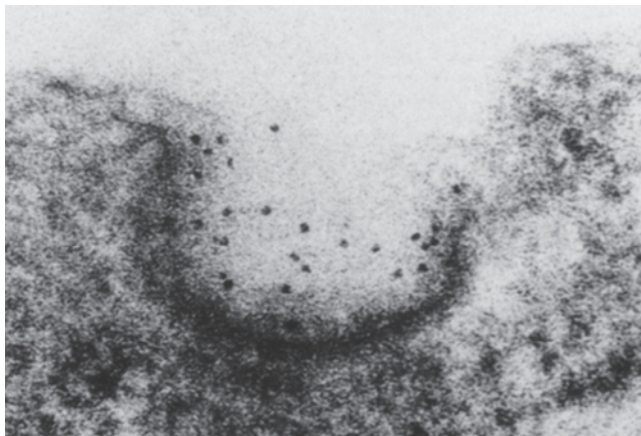
Figure 12-89 Freeze-etch electron micrograph of coated pits on the inner surface of a cultured fibroblast's plasma membrane. Compare this figure with that of clathrin-coated vesicles (Fig. 12-59a). [Courtesy of John Heuser, Washington University School of Medicine, St. Louis, Missouri.]

and the β propeller. Each Cys-rich module binds a Ca^{2+} ion and consists of two loops connected by three disulfide bonds. Note that they are devoid of regular secondary structure (helices and sheets). The EGF-like domains likewise each bind a Ca^{2+} ion (except for EGF-C), have three disulfide bonds, and lack regular secondary structure. Modules R4 and R5, which are critical for ligand binding, bind to one face of the β propeller via extensive and conserved side chain interactions. The Cys-rich modules each have a somewhat different conformation, which suggests that they are pliable. Moreover, modules R2, R3,

R6, and R7, and presumably R1, which are also implicated in LDL binding, appear to be unconstrained by interactions with the rest of the protein. This presumably explains why LDLR can bind lipoproteins of varying sizes and compositions.

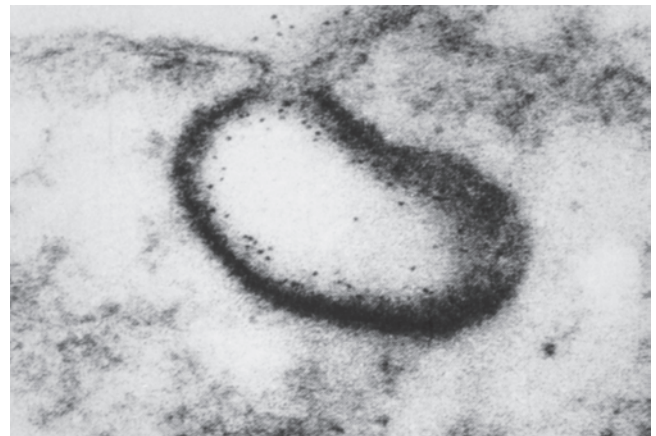
LDLRs cluster into **coated pits**, which serve to gather the cell-surface receptors that are destined for endocytosis while excluding other cell-surface proteins. The coated pits, which have a clathrin backing (Fig. 12-89), invaginate into the plasma membrane to form clathrin-coated vesicles (Fig. 12-90; Section 12-4C) that subsequently fuse with lysosomes. *Such receptor-mediated endocytosis* (Fig. 12-91) is a general mechanism whereby cells take up large molecules, each through a corresponding specific receptor. Indeed, the liver takes up chylomicron remnants in this manner through the mediation of a separate **remnant receptor** that specifically binds apoE.

At neutral pH, LDLR binds LDL via its Cys-rich modules, most importantly R4 and R5. However, in the acidic environment of the endosome, LDLR releases its bound LDL (Fig. 12-91). The X-ray structure of LDLR at pH 5.3 (Fig. 12-88), the pH of the endosome, suggests that this occurs via LDL's displacement from modules R4 and R5 by LDLR's β barrel domain. This model is bolstered by the observation that, at pH 5.3, the interface between modules R4 and R5 and the β barrel domain contains several conserved His-containing salt bridges that presumably form only when these His residues are protonated. Moreover, an LDLR construct in which the EGF-like domains and the β propeller domain have been deleted readily binds LDL but does not release it at acidic pH. Thus it is likely that at neutral pH, LDLR assumes an open and flexible conformation in which the R4 and R5 modules do not associate with the β barrel domain but, instead, are available to bind LDL.



(a)

Figure 12-90 Electron micrographs showing the endocytosis of LDL by cultured human fibroblasts. LDL was conjugated to ferritin so that it appears as dark dots. (a) LDL bound to a coated pit on the cell surface. (b) The coated pit invaginates and begins



(b)

to pinch off from the cell membrane to form a coated vesicle enclosing the bound LDL. [From Anderson, R.G.W., Brown, M.S., and Goldstein, J.L., *Cell* **10**, 356 (1977). Copyright © 1977 by Cell Press.]

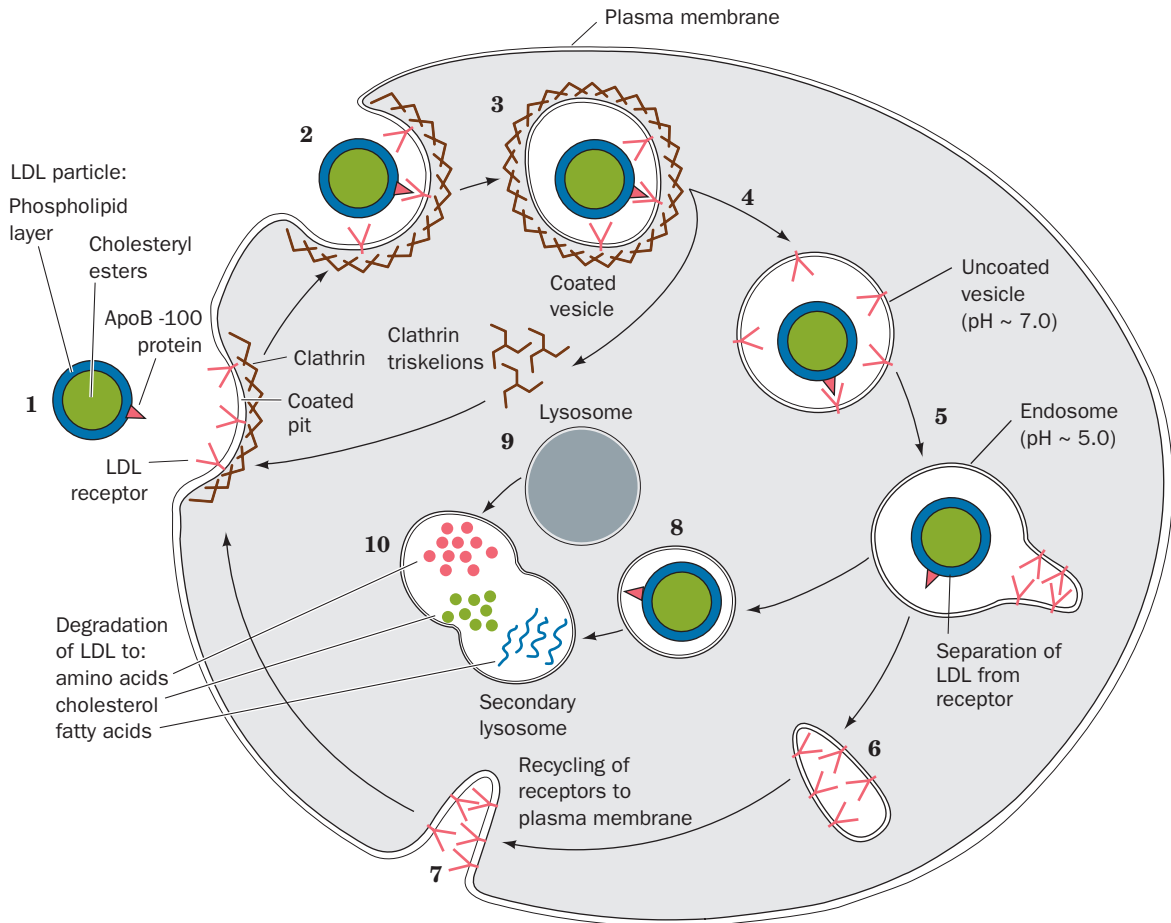


Figure 12-91 Sequence of events in the receptor-mediated endocytosis of LDL. LDL specifically binds to LDL receptors (LDLRs) on clathrin-coated pits (1). These bud into the cell (2) to form coated vesicles (3), whose clathrin coats depolymerize as triskelions, resulting in the formation of uncoated vesicles (4). These vesicles then fuse with vesicles called **endosomes** (5), which have an internal pH of ~ 5.0 . The acidity induces LDL to dissociate from LDLR. LDL accumulates in the vesicular portion of the endosome, whereas LDLR concentrates in the

membrane of an attached tubular structure, which then separates from the endosome (6) and subsequently recycles LDLR to the plasma membrane (7). The vesicular portion of the endosome (8) fuses with a lysosome (9), yielding a **secondary lysosome** (10), wherein the apoB-100 component of LDL is degraded to its component amino acids and the cholesteryl esters are hydrolyzed to yield cholesterol and fatty acids. An LDLR molecule cycles in and out of the cell every 10 to 20 minutes during its ~ 20 -hour lifetime.

In the lysosome, as demonstrated by radioactive labeling studies, LDL's apoB-100 is rapidly degraded to its component amino acids (Fig. 12-91). The cholesteryl esters are hydrolyzed by a lysosomal lipase to yield cholesterol, which is subsequently incorporated into the cell membranes. Any excess intracellular cholesterol is reesterified for storage within the cell through the action of **acyl-CoA:cholesterol acyltransferase (ACAT)**.

The overaccumulation of cellular cholesteryl esters is prevented by two feedback mechanisms:

1. High intracellular levels of cholesterol suppress the synthesis of LDLR, thus decreasing the rate of LDL accumulation by endocytosis (although LDLR cycles in and out

of the cell every 10 to 20 min, it is slowly degraded by the cell such that its half-life is ~ 20 h).

2. Excess intracellular cholesterol inhibits the biosynthesis of cholesterol (Section 25-6Bb).

d. ApoE's Receptor Binding Domain Contains a Four-Helix Bundle

ApoE is a 299-residue monomeric protein that consists of two independently folded domains: an N-terminal domain that binds strongly to LDLR but only weakly to lipid and a C-terminal domain that binds to the lipoprotein surface but lacks affinity for LDLR. Proteolysis of apoE yields fragments corresponding to apoE's N-terminal domain

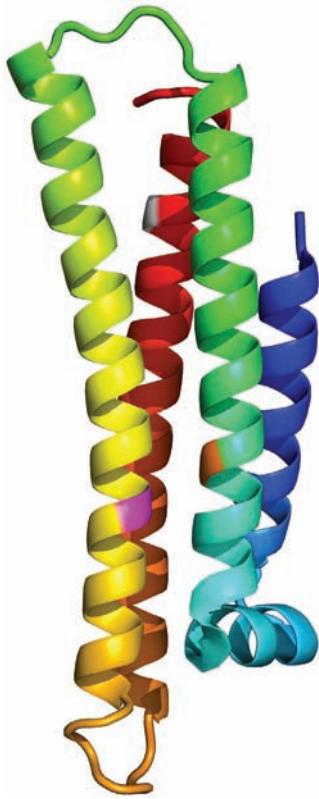


Figure 12-92 Ribbon diagram of the receptor-binding domain of human apolipoprotein E. The polypeptide chain is colored in rainbow order from its N-terminus (blue) to its C-terminus (red). Residues 61, 112, and 158 are colored orange, magenta, and gray, respectively. [Based on an X-ray structure by David Agard, University of California at San Francisco. PDBid 1LPE.]

(residues 1–191) and C-terminal domain (residues 216–299). Sequence analysis suggests that the C-terminal domain is largely composed of helices. The X-ray structure of the N-terminal domain (Fig. 12-92), determined by David Agard, reveals that it consists mainly of five α helices, four of which form an elongated (65 Å) up–down–up–down four-helix bundle. The helices of the four-helix bundle, as expected, are strongly amphipathic, with their hydrophobic residues sequestered inside the protein, out of contact with solvent, whereas their hydrophilic residues are solvent-exposed. The structure appears to be further stabilized by numerous salt bridges on the protein’s highly charged surface.

The C-terminal helix of the apoE N-terminal fragment contains nine closely spaced basic residues that are not involved in salt bridges, thereby producing a large positively charged patch on the protein surface. ApoE variants in which one of these basic residues is replaced by a neutral or acidic residue all display reduced affinity for LDLR, thereby suggesting that the patch forms apoE’s binding site for LDLR. Hence this C-terminal helix has been dubbed apoE’s receptor-binding helix.

LDLR binds apoB-100 and apoE with comparable affinities. ApoB-100 (but not apoB-48) contains a conserved segment that is similar to apoE’s receptor-binding

helix, although the two proteins otherwise have no apparent sequence similarity. In VLDL, the receptor-binding domain of apoB-100 is unavailable for receptor binding but is exposed on transformation of the VLDL to LDL.

e. HDL Transports Cholesterol from the Tissues to the Liver

HDL has essentially the opposite function of LDL: *It removes cholesterol from the tissues.* HDL is assembled in the plasma from components obtained largely through the degradation of other lipoproteins. *Circulating HDL acquires its cholesterol by extracting it from cell-surface membranes and converts it to cholesteryl esters through the action of LCAT, an enzyme that is activated by apoA-I. HDL therefore functions as a cholesterol scavenger.*

The liver is the only organ capable of disposing of significant quantities of cholesterol (by its conversion to bile acids; Section 25-6C). This occurs through the mediation of both LDLR and a specific HDL receptor named **SR-BI** (for scavenger receptor class B type I). About half of the VLDL, after its degradation to IDL and LDL, is taken up by the liver via LDLR-mediated endocytosis (Fig. 12-86, right). However, hepatocytes (liver cells) take up cholesteryl esters from HDL by an entirely different mechanism: Rather than being engulfed and degraded, the SR-BI-bound HDL selectively transfers its component cholesteryl esters to the cell. The lipid-depleted HDL then dissociates from the cell and reenters the circulation.

C. Lipoprotein Dysfunction in Atherosclerosis and Alzheimer’s Disease

Atherosclerosis, the most common form of **arteriosclerosis** (hardening of the arteries), is characterized by the presence of **atheromas** (Greek: *athera*, mush), arterial thickenings that, on sectioning, exude a pasty yellow deposit of almost pure cholesteryl esters (Fig. 12-93).

Atherosclerosis is a progressive disease that begins as intracellular lipid deposits in the smooth muscle cells of the inner arterial wall. These lesions eventually become fibrous, calcified plaques that narrow and even block the arteries. The resultant roughening of the arterial wall promotes the formation of blood clots, which may also occlude the artery. A blood flow stoppage, known as an **infarction**, causes the death of the deprived tissues. Although atheromas can occur in many different arteries, they are most common in the coronary arteries, the arteries supplying the heart. This results in **myocardial infarctions** or “heart attacks,” the most common cause of death in Western industrialized countries.

a. Deficient LDL Receptors Result in Atherosclerosis

The development of atherosclerosis is strongly correlated with the level of plasma cholesterol. This is particularly evident in individuals with **familial hypercholesterolemia (FH)**. Homozygotes with this inherited disorder have such high levels of the cholesterol-rich LDL (which is often referred to as “bad cholesterol”) in their plasma that their plasma cholesterol levels are three- to fivefold greater than the average level of $\sim 175 \text{ mg} \cdot 100 \text{ mL}^{-1}$. This situation results in the

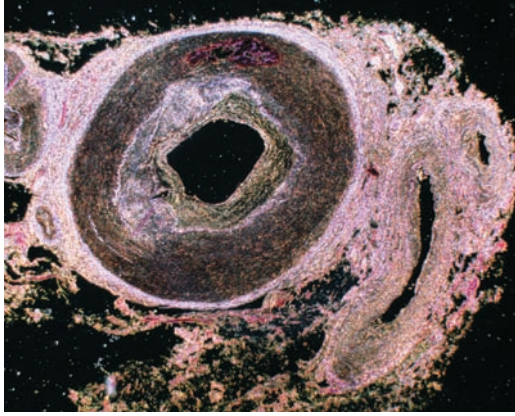


Figure 12-93 An atherosclerotic plaque in a coronary artery. The vessel wall is dramatically thickened as a result of lipid accumulation and activation of inflammatory processes. [© Eye of Science/Photo Researchers.]

deposition of cholesterol in their skin and tendons as yellow nodules known as **xanthomas**. However, far greater damage is caused by the rapid formation of atheromas that, in homozygotes, cause death from myocardial infarction as early as the age of 5. Heterozygotes, which comprise ~1 person in 500, are less severely afflicted; they develop symptoms of coronary artery disease after the age of 30.

Cells taken from FH homozygotes completely lack functional LDLR, whereas those taken from heterozygotes have about half of the normal complement. Homozygotes and, to a lesser extent, heterozygotes are therefore unable to utilize the cholesterol in LDL. Rather, their cells must synthesize most of the cholesterol for their needs. The high level of plasma LDL in these individuals results from two related causes:

1. Its decreased rate of degradation because of the lack of LDLR.
2. Its increased rate of synthesis from IDL due to the failure of LDLR to take up IDL.

Over 1000 mutations of LDLR that cause FH have been discovered. These mutants have been grouped into five classes depending on the nature of the defect in LDLR functioning they cause (Fig. 12-91): (1) failure to produce detectable amounts of protein; (2) partial or complete failure to be transported to the plasma membrane; (3) impaired ligand binding; (4) failure to localize to clathrin-coated pits and in internalization; and (5) defects in ligand release and recycling. Class 4 mutants are caused by changes in LDLR's so-called **sorting sequence**, NPXR, in its cytoplasmic domain, which binds to AP2 in clathrin-coated pits.

The long-term ingestion of a high-fat/high-cholesterol diet has an effect similar to although less severe than FH. A high intracellular level of cholesterol suppresses the synthesis of LDLR (Section 25-6Bb), thereby reducing the amount of LDL that a cell takes up from the circulation. Excessive dietary cholesterol, delivered to the tissues via chylomicrons, therefore contributes to high plasma LDL levels.

b. Scavenger Receptors Take Up Oxidized LDL

Atherosclerotic plaques in individuals with FH contain **macrophages** (a type of white blood cell that ingests and, if possible, destroys a variety of foreign and endogenous substances) that contain so much cholesterol that they are known as **foam cells**. How do macrophages take up cholesterol? Macrophages from both normal individuals and those with FH have few LDLRs and therefore take up little native LDL. However, they avidly take up, by endocytosis, LDL that has been chemically modified by the acetylation of its Lys residues (which eliminates this side chain's positive charge, thereby increasing LDL's negative charge). The macrophage cell-surface receptors that bind acetylated LDL are known as **scavenger receptors** because they also bind certain other polyanionic molecules.

Scavenger receptors avidly take up oxidized LDL. The unsaturated fatty acids of LDL are highly susceptible to chemical oxidation but, in the blood, are protected from oxidation by antioxidants. However, these antioxidants are thought to become depleted when LDL is trapped for an extended time within the artery walls (where it is thought to gain access by an injury to the arterial lining through which plasma leaks into the arterial wall). As a consequence, oxygen radicals convert LDL's unsaturated fatty acids to aldehydes and oxides that react with its Lys residues, thereby mimicking acetylation. The ingested LDL is degraded as described above and its cholesterol converted to cholesteryl esters, which accumulate as insoluble residues.

The physiological significance of this scenario has been demonstrated by the observations that antibodies against aldehyde-conjugated Lys residues stain atherosclerotic plaques, that LDL from atherosclerotic plaques binds to scavenger receptors and produces foam cells *in vitro*, and that antioxidants inhibit atherosclerosis in rabbits that have an animal counterpart of FH. It should be noted that tobacco smoke oxidizes LDL, which may explain why smoking leads to an increased incidence of atherosclerosis. High plasma levels of LDL, of course, also accelerate LDL uptake.

If this model of atheroma formation is correct, then the optimal level of plasma LDL is the lowest concentration that can adequately supply cholesterol to the cells. Such a level, which is thought to be ~25 mg of cholesterol · 100 mL⁻¹, occurs in various mammalian species that are not naturally susceptible to atherosclerosis as well as in newborn humans. Yet the plasma LDL level in adult Western men averages ~7-fold higher than this supposed optimal level. The reasons for such a high plasma cholesterol level are poorly understood (but see below), although it is clear that it is affected by diet and by environmental stress. Medical strategies for reducing the level of plasma cholesterol are considered in Section 25-6Bd.

c. Atherosclerosis Is a Multifactorial Disease

Epidemiological studies indicate that high plasma levels of HDL (which is often referred to as "good cholesterol") are strongly correlated with a low incidence of cardiovascular disease. Women have HDL levels higher than men and also less heart disease. Many of the factors that decrease the incidence of heart disease also tend to increase HDL

levels. These include strenuous exercise, weight loss, certain drugs such as alcohol, and female sex hormones known as **estrogens** (Section 19-1Gb). Conversely, cigarette smoking is inversely related to HDL concentration. Curiously, in communities that have a very low incidence of coronary artery disease, both the mean HDL and LDL concentrations are low. The reasons for these various effects are unknown.

There is also a strong inverse correlation in humans between the risk for atherosclerosis and the plasma level of apoA-I, HDL's major protein component, which is required for its assembly. To investigate whether apoA-I has a direct antiatherogenic effect, mice of a strain that develops diet-induced **fatty streak lesions** in their large blood vessels were genetically modified to express high plasma levels of human apoA-I (fatty streak lesions are the precursors of atherosclerotic plaques, which these mice have too short a lifetime to develop). These transgenic mice are significantly protected from developing fatty streak lesions. Yet transgenic mice that overexpress mouse **apoA-II**, another major HDL protein, develop more and larger fatty streak lesions than their nontransgenic counterparts. Since the plasma HDL-cholesterol levels in the latter transgenic mice are significantly elevated, it appears that both the composition and the level of plasma HDL are important atherosclerotic mediators. Similarly, transgenic mice that express high levels of human apoE or human LDLR resist the elevation in plasma LDL levels that would otherwise be brought on by a cholesterol-rich diet, whereas mice in which the gene encoding apoE has been knocked out rapidly develop atherosclerotic lesions.

Cholesteryl ester transfer protein (CETP) is a plasma protein that exchanges neutral lipids (e.g., cholesteryl esters and triacylglycerols) among lipoproteins and hence functions analogously to phospholipid exchange proteins (Section 12-4Ab). Since VLDL and LDL are triacylglycerol-rich whereas HDL are cholesteryl ester-rich (Table 12-6), CETP mediates the net transport of cholesteryl esters from HDL to VLDL and LDL (and of triacylglycerols in the opposite direction). Consequently, animals that express CETP have higher cholesterol levels in their VLDL and LDL and lower cholesterol levels in their HDL than animals that do not express CETP. Mice of a strain that normally have little or no CETP activity were made transgenic for CETP and fed an atherogenic (high-fat, high-cholesterol) diet. These transgenic mice developed atherosclerotic lesions far more rapidly than their similarly fed nontransgenic counterparts. Since the two types of mice had similar total plasma cholesterol levels, these results suggest that *the progression of atherosclerotic lesions is more a function of how cholesterol is partitioned between lipoproteins than it is of the total plasma cholesterol level.*

Increased risk of atherosclerosis in humans is also associated with elevated plasma levels of lipoprotein **Lp(a)**, a variant of LDL in which apoB-100 is tightly associated with the 4259-residue plasma protein **apo(a)**. Rodents and most other nonprimate mammals lack the gene for apo(a). However, mice transgenic for human apo(a) rapidly develop fatty streak lesions when given a high-fat diet (approximating human diets in industrialized Western countries).

Apo(a) mainly consists of repeated segments that are homologous to **plasminogen**, a plasma protein that, when activated, functions to proteolytically dismantle blood clots (Section 35-1Fa). The normal function of apo(a) in humans is unknown, although it has been hypothesized that it participates in healing blood vessel wounds.

d. Tangier Disease Eliminates HDL Synthesis

Most cells do not consume cholesterol by converting it to steroid hormones or bile acids, for example, but all cells require cholesterol to maintain membrane fluidity. Cholesterol in excess of this requirement can be esterified by the action of ACAT and stored as cholesteryl esters in intracellular deposits. Cholesterol can also be eliminated from cells by a mechanism illuminated through studies of individuals with **Tangier disease**. In this recessive inherited disorder, almost no HDL is produced, because cells have a defective transport protein, known as **ATP-cassette binding protein A1 (ABCA1)**. In normal individuals, ABCA1 functions as a flippase (Section 12-4Aa) that transfers cholesterol, cholesteryl esters, and other lipids from the inner to the outer leaflet of the plasma membrane, from where they are captured by apoA-I to form HDL. Cells lacking ABCA1 cannot dispose of their excess cholesterol and therefore accumulate cholesteryl esters in their cytoplasm. Macrophages thus engorged with lipids contribute to the development of atherosclerosis and consequently individuals with Tangier disease exhibit symptoms similar to those with FH.

e. ApoE4 Is Implicated in Both Cardiovascular Disease and Alzheimer's Disease

There are three common allelic variants of apoE in humans: **apoE2** (occurring in 15% of the population), which has Cys at positions 112 and 158; **apoE3** (78% occurrence), in which these residues are Cys and Arg, respectively (Fig. 12-92 shows the structure of apoE3 with residues 112 and 158 magenta and white); and **apoE4** (7% occurrence), in which these residues are both Arg. These differences have medical significance: ApoE3 has a preference for binding to HDL, whereas apoE4 has a preference for binding to VLDL, which is probably why apoE4 is associated with elevated plasma concentrations of LDL and thus an increased risk of cardiovascular disease. Evidently, changes in apoE's N-terminal domain can affect the function of its C-terminal lipoprotein-binding domain.

ApoE4, as we have seen in Section 9-5B, is also associated with a greatly (16-fold) increased incidence of Alzheimer's disease (AD). This observation is perhaps less surprising when it is realized that apoE is expressed by certain nerve cells and is present in the cerebrospinal fluid, where it functions in mediating cholesterol transport, much as it does in blood plasma (cholesterol is abundant in nerve cell plasma membranes, which mediate neurotransmission; Section 20-5B).

Brain tissue from AD victims reveals numerous extracellular amyloid plaques, which consist of fibrillar deposits of amyloid β ($A\beta$) peptide that arises through proteolysis of the normally occurring amyloid precursor protein (Section 9-5B). Amyloid plaques appear to be AD's pathogenic

agent. Immunochemical staining indicates that apoE is associated with amyloid plaques. *In vitro* experiments demonstrate that both apoE3 and apoE4 form SDS-stable complexes with A β peptide that, after long incubation times, aggregate and precipitate from solution as a matrix of fibrils that closely resemble those in amyloid plaques. ApoE4 forms this complex more readily than apoE3 and yields a denser, more extensive matrix.

Comparison of the X-ray structures of apoE4 and apoE3 reveals that there are only minor differences in their backbone conformations, which are restricted to the immediate vicinity of their site of difference (residue 112: Cys in ApoE3 and Arg in ApoE4). The only two side chains in apoE4 that undergo changes in conformation relative to those in apoE3 are Glu 109, which swings around in apoE4 to form a salt bridge with Arg 112, and Arg 61 (orange in Fig. 12-92), which contacts Cys 112 in apoE3 but swings away to accommodate the new salt bridge in apoE4. Thus, both Glu 109 and Arg 61 are candidates for mediating the functional differences between apoE3 and apoE4. However, the mutagenic substitution of Ala for Glu 109 in apoE3 does not significantly alter its preference for binding to HDL over VLDL. In contrast, the substitution of Thr for Arg 61 in apoE4 gives this protein an apoE3-like preference for HDL over VLDL. Evidently, the position of Arg 61 is critical in determining the HDL/VLDL preference of apoE. This hypothesis is supported by the observation that residue 61 is invariably Thr in the 10 apoEs of known sequences from other species. None of these species exhibits the complete pathology of AD, although it remains to be

demonstrated that Arg 61 actually contributes to the differential binding of apoE3 and apoE4 to A β peptide.

f. ApoE2 Has a Low Affinity for LDL Receptor

ApoE2 binds to LDLR with only 0.1% of the affinity of apoE3 or apoE4. Thus the presence of apoE2 is the underlying cause of **familial type III hyperlipoproteinemia**, which is characterized by elevated plasma cholesterol and triglyceride levels and hence accelerated coronary artery disease.

The defective binding of apoE2 to LDLR is caused by the substitution of Cys for Arg 158, a position (gray in Fig. 12-92) that lies outside the previously identified receptor-binding region, residues 136 to 150 (located in the bottom half of the C-terminal helix in Fig. 12-92). In apoE3, Asp 154 forms a salt bridge with Arg 158 (which is situated one turn farther along the α helix). In apoE2, since Arg 158 is replaced with Cys, this salt bridge cannot form. Rather, as the X-ray structure of apoE2 reveals, Asp 154 forms a salt bridge with Arg 150 (which is situated one turn earlier on the α helix), thereby altering the side chain conformation of this LDLR-binding residue. In fact, the disruption of this abnormal salt bridge by the mutagenic replacement of Asp 154 in ApoE2 with Ala restores LDLR binding affinity to a nearly normal level.

Individuals with type III hyperlipoproteinemia are particularly responsive to a low-fat, low-calorie diet and to a reduction in body weight. It is therefore postulated that the altered lipid composition of lipoproteins under such a regimen causes significant amounts of apoE2 to assume a receptor-active conformation, leading to normal or near-normal rates of lipoprotein clearance from the circulation.

CHAPTER SUMMARY

1 Lipid Classification Fatty acids are long-chain carboxylic acids that may have one or more double bonds that are usually *cis*. Their anions are amphiphilic molecules that form micelles in water. Fatty acids rarely occur free in nature but rather are components of lipids. The most abundant class of lipids, the triacylglycerols or neutral fats, are nonpolar molecules that constitute the major nutritional store of animals. The lipids that occur in membranes are the phospholipids, the sphingolipids, and, in eukaryotes, cholesterol or similar sterols. Sphingolipids such as cerebrosides and gangliosides have complex carbohydrate head groups that act as specific recognition markers in various biological processes.

2 Properties of Lipid Aggregates The molecular shapes of membrane lipids cause them to aggregate in aqueous solution as bilayers. These form closed vesicles known as liposomes that are useful model membranes and drug delivery systems. Bilayers are essentially impermeable to polar molecules, except for water. Likewise, the flip-flop of a lipid in a bilayer is an extremely rare event. In contrast, bilayers above their transition temperatures behave as two-dimensional fluids in which the individual lipid molecules freely diffuse in the bilayer plane. Cholesterol decreases membrane fluidity and broadens the temperature range of its order–disorder transition by interfering with the orderly packing of the lipids' fatty acid side chains.

3 Biological Membranes Biological membranes contain a high proportion of proteins. Integral proteins, for example, bacteriorhodopsin, the photosynthetic reaction center, porins, and fatty acid amide hydrolase, have nonpolar surface regions that hydrophobically associate with the bilayer core. Peripheral proteins, for example, cytochrome *c*, bind to integral proteins on the membrane surface or to phospholipid head groups via polar interactions. Specific integral proteins are invariably associated with a particular side of the membrane or, if they are transmembrane proteins, have only one orientation. Lipid-linked proteins contain covalently attached isoprenoid, fatty acyl, and/or glycosylphosphatidylinositol (GPI) groups that serve to anchor these proteins to membranes and to mediate protein–protein interactions. According to the fluid mosaic model of membrane structure, integral proteins resemble icebergs floating on a two-dimensional lipid sea. These proteins, as observed by the freeze-fracture and freeze-etch techniques, are randomly distributed in the membrane. Certain lipids and/or proteins may form specific aggregates on one leaflet of a membrane.

The erythrocyte cytoskeleton is responsible for the shape, flexibility, and fluidity of the red cell. Spectrin, the major constituent of the cytoskeleton, is a wormlike ($\alpha\beta$)₂ heterotetramer that is cross-linked by actin oligomers and band 4.1 protein. The resulting protein meshwork is anchored to the

membrane by the association of spectrin with ankyrin, which, in turn, binds to band 3 protein, a transmembrane protein that forms an anion channel.

The erythrocyte surface bears the various blood group antigens. The antigens of the ABO system differ in the sugar at a nonreducing end. The ABO blood group substances occur in the plasma membranes of many cells and in the secretions of many individuals.

Gap junctions are hexagonal transmembrane protein tubes that link adjoining cells. The gap junction's central channel, which closes at high intracellular levels of Ca^{2+} , allows small molecules and ions but not macromolecules to pass between cells. The connexin subunits of a gap junction's two face-to-face hexameric connexons each contain four transmembrane helices.

Bacterial channel-forming toxins such as α -hemolysin form oligomers on the outer surface of a target cell's plasma membrane. These insert themselves into the membrane to form pores through which small molecules and ions leak, thereby killing the cell.

4 Membrane Assembly and Protein Targeting New membranes are generated by the expansion of old ones. Lipids are synthesized by membrane-bound enzymes and are deposited on one side of the membrane. They migrate to the other side by flip-flops that are catalyzed by membrane-bound flippases and phospholipid translocases. In eukaryotes, lipids are transported between different membranes by lipid vesicles or by phospholipid-exchange proteins.

In the secretory pathway, transmembrane proteins and proteins destined for secretion are ribosomally synthesized with an N-terminal signal sequence. A signal peptide is bound by an RNA-containing signal recognition particle (SRP), which then arrests polypeptide synthesis. The SRP-ribosome complex binds to the SRP receptor (SR) in complex with the translocon on the endoplasmic reticulum (ER) membrane and, on GTP hydrolysis by both the SRP and SR, resumes polypeptide synthesis. As a protein destined for secretion passes through the translocon into the ER lumen, its signal peptide is removed by an ER-resident signal peptidase, its folding is facilitated through interactions with ER-resident chaperone proteins such as BiP, and its post-translational processing, mainly signal peptide excision and glycosylation, is initiated. Integral proteins, whose transmembrane (TM) segments each contain signal-anchor sequences, also enter the translocon, which laterally installs these TM segments into the ER membrane. The orientation of TM helices in membranes usually obeys the positive-inside rule. Some proteins are wholly synthesized in the cytoplasm before being translocated into the ER.

Proteins are transferred between the ER, the Golgi apparatus (where further post-translational processing takes place), and their final destinations via membranous vesicles that are coated with clathrin, COPI, or COPII. Clathrin-coated vesicles also participate in endocytosis. Polyhedral clathrin cages are formed by triskelions, which are trimers of heavy chains, each of which binds a light chain. Clathrin-coated vesicle formation is primed by the action of ARNO, a guanine nucleotide exchange factor (GEF) that induces the small GTPase ARF1 to exchange its bound GDP for GTP and then insert its myristoyl group into the membrane. ARF1 · GTP then recruits adapter proteins such as AP1 and

AP2, which simultaneously bind clathrin heavy chains and TM proteins that are cargo proteins or are receptors for soluble cargo proteins inside the vesicle. The formation of the clathrin cage drives vesicle budding, but its actual release from its parent membrane requires the action of the GTPase dynamin. Shortly after its release, the vesicle uncoats in a process mediated by the chaperone protein Hsc70. COPI- and COPII-coated vesicles undergo similar processes, although they do not require a dynamin-like protein to bud off from their parent membranes. The Sec13/31 components of COPII-coated vesicles form cuboctahedral cages. The receptors in coated vesicles bind their target cargo proteins through specific signals such as the mannose-6-phosphate group that directs proteins to the lysosome or the C-terminal KDEL sequence that retrieves normally ER-resident proteins from the Golgi to the ER.

The fusion of a vesicle with its target membrane is initiated when a Rab protein, a small GTPase, induces the loose tethering of the two membranes. The vesicle is then more firmly anchored (docked) to the membrane through interactions between cognate R-SNAREs on the vesicle and Q-SNAREs on the target membrane. In neurons, synaptic vesicles dock with the presynaptic membrane through the association of the R-SNARE synaptobrevin (VAMP) with the Q-SNAREs syntaxin and SNAP-25 to form a 4-helix bundle. These neuronal SNAREs are specifically cleaved by tetanus and botulinum neurotoxins. The bilayer fusion step probably occurs as a result of the mechanical stresses generated by the formation of the several SNARE complexes at the fusion site. The neuronal SM protein nSec1 binds to syntaxin with high affinity so as to prevent the formation of the SNARE complex. A Rab protein and/or its effectors apparently induce nSec1 to release syntaxin and thereby permit the formation of the SNARE complex. After vesicle fusion, the SNARE complex must be dissociated in order to be recycled. This occurs through the auspices of the ATP-driven molecular chaperone NSF, which binds to the SNARE complex through the intermediacy of a SNAP protein.

Nuclear-encoded mitochondrial proteins are synthesized by cytosolic ribosomes and enter the mitochondrion post-translationally. A protein can only pass through a membrane in its unfolded form and hence must first be unfolded by ATP-driven molecular chaperones such as Hsp70 and MSF. A matrix-directed protein is passed through the mitochondrial outer membrane via the TOM complex, which recognizes the protein's amphipathic and positively charged N-terminal signal sequence. The N-terminal presequence then crosses the intermembrane space to encounter the TIM23 complex, which translocates it through the inner membrane into the matrix. This latter process is driven both by the mitochondrial membrane potential, which electrophoretically draws the positively charged presequence into the matrix, and by the ATP-driven chaperone mtHsp70, which binds to Tim44 in the matrix and pulls the unfolded protein into the matrix via a Brownian ratchet mechanism. MPP then excises the N-terminal signal sequence from the protein, which subsequently folds to its native state as facilitated by a battery of resident chaperones including mtHsp70 and Hsp60/Hsp10. Metabolite carrier proteins, which lack N-terminal presequences but have internal targeting sequences, also enter the intermembrane space via the TOM complex. However, they are then escorted by the

Tim9–Tim10 complex to the TIM22 complex, which laterally inserts them into the inner mitochondrial membrane. Many TM proteins that occupy the inner mitochondrial membrane are inserted there from the matrix by the Oxa1 protein, an indirect pathway that is a relic of the mitochondrion's descent from a gram-negative bacterium. Likewise, proteins that form β barrels are translocated by the TOM complex into the intermembrane space, from which they are inserted into the outer membrane by the SAM complex.

5 Lipoproteins Lipids are transported in the circulation by plasma lipoproteins. These are essentially droplets of triacylglycerols and cholesteryl esters coated with a monolayer of phospholipids, cholesterol, and apolipoproteins. The amphiphilic apolipoprotein helices float on the lipoprotein surface in hydrophobic contact with its lipid interior. Chylomicrons and VLDL function to respectively transport triacylglycerols and cholesterol from the intestines and the liver to the tissues. HDL transports mainly cholesterol from

the tissues to the liver, the only organ capable of disposing of significant quantities of cholesterol. The triacylglycerols of chylomicrons and VLDL are degraded by lipoprotein lipase that lines the capillaries. LDL, the cholesterol-containing degradation product of VLDL, binds to cell-surface LDL receptors (LDLRs) and is taken into cells by receptor-mediated endocytosis. The presence of excess intracellular cholesterol inhibits the synthesis of both LDLR and cholesterol. A major cause of atherosclerosis is an excess of plasma LDL, a phenomenon that is particularly evident in individuals with familial hypercholesterolemia, who lack functional LDLRs. The excess LDL becomes oxidized and is taken up by the macrophages that inhabit atherosclerotic plaques via their scavenger receptors. Atherosclerosis, a multifactorial disease, is also correlated with a low concentration of HDL, which functions as a cholesterol scavenger. The apoE2 and apoE4 variants of apoE are implicated in cardiovascular disease, whereas apoE4 is also implicated in Alzheimer's disease.

REFERENCES

General

- Edidin, M., Lipids on the frontier: a century of cell-membrane bilayers, *Nature Rev. Mol. Cell Biol.* **4**, 414–418 (2003). [A short account of the history of the study of membranes.]
- Luckey, M., *Membrane Structural Biology*, Cambridge University Press (2008).
- Mellman, I. and Warren, G., The road taken: Past and future foundations of membrane traffic, *Cell* **100**, 99–112 (2000). [An intellectual history and review of membrane trafficking.]
- Tanford, C., *The Hydrophobic Effect: Formation of Micelles and Biological Membranes* (2nd ed.), Wiley–Interscience (1980). [An exposition of the thermodynamic properties of micelles and membranes.]
- Vance, D.E. and Vance J.E. (Eds.), *Biochemistry of Lipids, Lipoproteins, and Membranes* (5th ed.), Elsevier (2008).

Lipids and Bilayers

- Giles, C.H., Franklin's teaspoon of oil, *Chem. Ind.*, 1616–1624 (1969). [A historical account of Benjamin Franklin's investigations into the effect of oil on waves.]
- Gurr, M.I., Harwood, J.L., and Frayn, K.N., *Lipid Biochemistry: An Introduction* (5th ed.), Blackwell Science (2002).
- Lasic, D.D., Novel applications of liposomes, *Trends Biotech.* **16**, 307–321 (1998). [Reviews the uses of liposomes as delivery vehicles for drugs, vaccines, gene therapy agents, and cosmetic products.]
- Lasic, D.D. and Papahadjopoulos, D. (Eds.), *Medical Applications of Liposomes*, Elsevier (1998).
- Lopez, P.H.H. and Schnaar, R.L., Gangliosides in cell recognition and membrane protein regulation, *Curr. Opin. Struct. Biol.* **19**, 549–557 (2009).
- Nagle, J.F. and Tristram-Nagle, S., Lipid bilayer structure, *Curr. Opin. Struct. Biol.* **10**, 474–480 (2000). [Explains why it is difficult to quantitatively describe the structure of the lipid bilayer.]
- Munro, S., Lipid rafts: elusive or illusive, *Cell* **115**, 377–388 (2003).
- Scott, L.H., Modeling the lipid component of membranes, *Curr. Opin. Struct. Biol.* **12**, 495–502 (2002).
- van Meer, G., Voelker, D.R., and Feigenson, G.W., Membrane

lipids: where they are and how they behave, *Nature Rev. Mol. Cell Biol.* **9**, 112–124 (2008).

Membrane Proteins

- Bracey, M.H., Hanson, M.A., Masuda, K.R., Stevens, R.C., and Cravatt, B.F., Structural adaptations in a membrane enzyme that terminates endocannabinoid signaling, *Science* **298**, 1793–1796 (2002). [The X-ray structure of fatty acid amide hydrolase.]
- Deisenhofer, J. and Michel, H., High-resolution structures of photosynthetic reaction centers, *Annu. Rev. Biophys. Biophys. Chem.* **20**, 247–266 (1991); and Deisenhofer, J., Epp, O., Miki, K., Huber, R., and Michel, H., Structure of the protein subunits in the photosynthetic reaction centre of *Rhodospseudomonas viridis* at 3 Å resolution, *Nature* **318**, 618–624 (1985).
- Elofsson, A. and von Heijne, G., Membrane protein structure: prediction versus reality, *Annu. Rev. Biochem.* **76**, 125–140 (2007).
- Engelman, D.M., Membranes are more mosaic than fluid, *Nature* **438**, 578–580 (2005). [A brief review updating the classic model with more proteins and variable bilayer thickness.]
- Ford, R.C. and Holzenburg, A., Electron crystallography of biomolecules: mysterious membranes and missing cones, *Trends Biochem. Sci.* **33**, 38–43 (2008).
- Fujiyoshi, Y. and Unwin, N., Electron crystallography of proteins in membranes, *Curr. Opin. Struct. Biol.* **18**, 587–592 (2008).
- Grigorieff, N., Ceska, T.A., Downing, K.H., Baldwin, J.M., and Henderson, R., Electron-crystallographic refinement of the structure of bacteriorhodopsin, *J. Mol. Biol.* **259**, 393–421 (1996); and Belrhali, H., Nollert, P., Royant, A., Menzel, C., Rosenbusch, J.P., Landau, E.M., and Pebay-Peyroula, E., Protein, lipid and water organization in bacteriorhodopsin crystal: A molecular view of the purple membrane at 1.9 Å resolution, *Structure* **7**, 909–917 (1999).
- Grum, V.L., Li, D., MacDonald, R.I., and Mondragón, A., Structures of two repeats of spectrin suggest models of flexibility, *Cell* **98**, 523–535 (1999).
- Haupts, U., Tittor, J., and Oesterhelt, D., Closing in on bacteriorhodopsin: Progress in understanding the molecule, *Annu. Rev. Biophys. Biomol. Struct.* **28**, 67–99 (1999).

- Killian, J.A. and von Heijne, G., How proteins adapt to a membrane–water interface, *Trends Biochem. Sci.* **25**, 429–434 (2000).
- Lacapère, J.-J., Pebay-Peyroula, E., Neumann, J.M., and Etchebest, C., Determining membrane protein structures: still a challenge! *Trends Biochem. Sci.* **32**, 259–270 (2007).
- Liang, J., Adamian, L., and Jackups, R., Jr., The membrane–water interface region of membrane proteins: structural bias and the anti-snorkeling effect, *Trends Biochem. Sci.* **30**, 355–359 (2005).
- MacKenzie, K.R., Folding and stability of α -helical integral membrane proteins, *Chem. Rev.* **106**, 1931–1977 (2006).
- Palsdottir, H. and Hunte, C., Lipids in membrane protein structures, *Biochim. Biophys. Acta* **1666**, 2–18 (2004).
- Pebay-Peyroula, E., Rummel, G., Rosenbusch, J.P., and Landau, E.M., X-ray structure of bacteriorhodopsin at 2.5 angstroms from microcrystals grown in lipidic cubic phases, *Science* **277**, 1676–1681 (1997); and Gouaux, E., It's not just a phase: Crystallization and X-ray structure of bacteriorhodopsin in lipidic cubic phases, *Structure* **6**, 5–10 (1998).
- Popot, J.-L. and Engelman, D.M., Helical membrane protein folding, stability, and evolution, *Annu. Rev. Biochem.* **69**, 881–922 (2000).
- Raunser, S. and Walz, T., Electron crystallography as a technique to study structure on membrane proteins in a lipidic environment, *Annu. Rev. Biophys.* **38**, 89–105 (2009).
- Rees, D.C., De Antonio, L., and Eisenberg, D., Hydrophobic organization of membrane proteins, *Science* **245**, 510–512 (1989).
- Schulz, G.E., β -Barrel membrane proteins, *Curr. Opin. Struct. Biol.* **10**, 443–447 (2000).
- Sharom, F.J., and Lehto, M.T., Glycosylphosphatidylinositol-anchored proteins: structure, function, and cleavage by phosphatidylinositol-specific phospholipase C, *Biochem. Cell Biol.* **80**, 535–549 (2002). [Includes a discussion of the GPI anchor and its importance for protein localization and function.]
- Subramaniam, S., The structure of bacteriorhodopsin: An emerging consensus, *Curr. Opin. Struct. Biol.* **9**, 462–468 (1999). [Compares the six structures of bacteriorhodopsin that have been independently determined by electron or X-ray crystallography and finds them to be remarkably similar.]
- Weiss, M.S. and Schulz, G.E., Structure of porin refined at 1.8 Å resolution, *J. Mol. Biol.* **227**, 493–509 (1992).
- White, S.H. and Wimley, W.C., Membrane protein folding and stability: Physical principles, *Annu. Rev. Biophys. Biomol. Struct.* **28**, 319–365 (1999).
- Wimley, W.C., The versatile β -barrel membrane protein, *Curr. Opin. Struct. Biol.* **13**, 404–411 (2003). [Reviews the basic principles of construction for transmembrane β barrels.]
- Lipid-Linked Proteins**
- Clarke, S., Protein isoprenylation and methylation at carboxyl-terminal cysteine residues, *Annu. Rev. Biochem.* **61**, 355–386 (1992).
- Cross, G.A.M., Glycolipid anchoring of plasma membrane proteins, *Annu. Rev. Cell Biol.* **6**, 1–39 (1990).
- Englund, P.T., The structure and biosynthesis of glycosyl phosphatidylinositol protein anchors, *Annu. Rev. Biochem.* **62**, 65–100 (1993).
- Linder, M.E. and Deschenes, R.J., Palmitoylation: policing protein stability and traffic, *Nature Rev. Mol. Cell Biol.* **8**, 74–84 (2007).
- Marshall, C.J., Protein prenylation: A mediator of protein–protein interactions, *Science* **259**, 1865–1866 (1993).
- Schafer, W.R. and Rine, J., Protein prenylation: Genes, enzymes, targets, and functions, *Annu. Rev. Genet.* **30**, 209–237 (1992).
- Schlesinger, M.J. (Ed.), *Lipid Modification of Proteins*, CRC Press (1993).
- Tartakoff, A.M. and Singh, N., How to make a glycoinositol phospholipid anchor, *Trends Biochem. Sci.* **17**, 470–473 (1992).
- Zhang, F.L. and Casey, P.J., Protein prenylation: Molecular mechanisms and functional consequences, *Annu. Rev. Biochem.* **65**, 241–269 (1996).
- Membrane Structure**
- Brown, D.A. and London, E., Structure and function of sphingolipid- and cholesterol-rich membrane rafts, *J. Biol. Chem.* **275**, 17221–17224 (2000); and Function of lipid rafts in biological membranes, *Annu. Rev. Cell Dev. Biol.* **14**, 111–136 (1998).
- Edidin, M., Lipid rafts: From model membranes to cells, *Annu. Rev. Biophys. Biomol. Struct.* **32**, 257–283 (2003).
- Engleman, D.M., Membranes are more mosaic than fluid, *Nature* **438**, 578–580 (2005).
- Fielding, C.J. (Ed.), *Lipid Rafts and Caveolae*, Wiley-VCH (2006).
- Frye, C.D. and Edidin, M., The rapid intermixing of cell surface antigens after formation of mouse–human heterokaryons, *J. Cell Sci.* **7**, 319–335 (1970). [The classic demonstration of membrane fluidity.]
- Galbiati, F., Razani, B., and Lisanti, M.P., Emerging themes in rafts and caveolae, *Cell* **106**, 403–411 (2001).
- Kusumi, A., Nakada, C., Ritchie, K., Murase, K., Suzuki, K., Murakoshi, H., Kasai, R.S., Kondo, J., and Fujiwara, T., Paradigm shift of the plasma membrane concept from the two-dimensional continuum fluid to the partitioned fluid: High-speed single-molecule tracking of membrane molecules, *Annu. Rev. Biophys. Biomol. Struct.* **34**, 351–378 (2005).
- Marguet, D., Lenne, P.-F., Rigneault, H., and He, H.-T., Dynamics in the plasma membrane: how to combine fluidity and order, *EMBO J.* **25**, 3446–3457 (2006).
- Singer, S.J. and Nicolson, G.L., The fluid mosaic model of the structure of cell membranes, *Science* **175**, 720–731 (1972). [A landmark paper on membrane structure.]
- The Erythrocyte Membrane**
- Agre, P. and Parker, J.C. (Eds.), *Red Blood Cell Membranes*, Marcel Dekker (1989).
- Bennett, V., Ankyrins, *J. Biol. Chem.* **267**, 8703–8706 (1992).
- Davies, K.E. and Lux, S.E., Hereditary disorders of the red cell membrane, *Trends Genet.* **5**, 222–227 (1989).
- Elgsaeter, A., Stokke, B.T., Mikkelsen, A., and Branton, D., The molecular basis of erythrocyte shape, *Science* **234**, 1217–1223 (1986).
- Gallagher, P.G. and Benz, E.J., Jr., The erythrocyte membrane and cytoskeleton: Structure, function, and disorders, in Stamatoyannopoulos, G., Majerus, P.W., Perlmutter, R.M., and Varmus, H. (Eds.), *The Molecular Basis of Blood Diseases* (3rd ed.), Chapter 8, Elsevier (2001).
- Gilligan, D.M. and Bennett, V., The junctional complex of the membrane skeleton, *Semin. Hematol.* **30**, 74–83 (1993).
- Grum, V.L., Li, D., MacDonald, R.I., and Mondragón, A., Structures of two repeats of spectrin suggest models of flexibility, *Cell* **98**, 523–535 (1999); and Kusnoki, H., MacDonald, R.I., and Mondragón, A., Structural insights into the stability and flexibility of unusual erythroid repeats, *Structure* **12**, 645–656 (2004).
- Jennings, M.L., Structure and function of the red blood cell anion transport protein, *Annu. Rev. Biophys. Biomol. Chem.* **18**, 397–430 (1989).
- Liu, S.-C. and Derick, L.H., Molecular anatomy of the red blood cell membrane skeleton: Structure–function relationships, *Semin. Hematol.* **29**, 231–243 (1992).
- Luna, E.J. and Hitt, A.L., Cytoskeleton–plasma membrane interactions, *Science* **258**, 955–964 (1992).

- Michaely, P., Tomchick, D.R., Machius, M., and Anderson, R.G.W., Crystal structure of a 12 ANK repeat stack from human ankyrinR, *EMBO J.* **21**, 6387–6396 (2002).
- Reithmeier, R.A.F., The erythrocyte anion transporter (band 3), *Curr. Opin. Struct. Biol.* **3**, 513–515 (1993).
- Schofield, A.E., Reardon, R.M., and Tanner, M.J.A., Defective anion transport activity of the abnormal band 3 in hereditary ovalocytotic red blood cells, *Nature* **355**, 836–838 (1992).
- Sedgwick, S.G. and Smerdon, S.J., The ankyrin repeat: a diversity of interactions on a common framework, *Trends Biochem. Sci.* **24**, 311–319 (1999).
- Viel, A. and Branton, D., Spectrin: On the path from structure to function, *Curr. Opin. Cell Biol.* **8**, 49–55 (1996).
- Yawata, Y., *Cell Membrane. The Red Blood Cell As a Model*, Wiley-VCH (2003).
- Blood Groups**
- Vitala, J. and Järnefelt, J., The red cell surface revisited, *Trends Biochem. Sci.* **10**, 392–395 (1985).
- Watkins, H.M., Biochemistry and genetics of the ABO, Lewis and P group systems, *Adv. Human Genet.* **10**, 1–136 (1980).
- Yamamoto, F., Clausen, H., White, T., Marken, J., and Hakomori, S., Molecular genetic basis of the histo-blood group ABO system, *Nature* **345**, 229–233 (1990).
- Gap Junctions**
- Goodenough, D.A., Goliger, J.A., and Paul, D.L., Connexins, connexons, and intercellular communication, *Annu. Rev. Biochem.* **65**, 475–502 (1996).
- Maeda, S., Nakagawa, S., Suga, M., Yamashita, E., Oshima, A., Fujiyoshi, Y., and Tsikihara, T., Structure of the connexin 26 gap junction channel at 3.5 Å resolution, *Nature* **458**, 597–602 (2009).
- Sosinsky, G.E. and Nicholson, B.J., Structural organization of gap junction channels, *Biochim. Biophys. Acta* **1171**, 99–125 (2005). [A detailed review.]
- Wei, C.-J., Xu, X., and Lo, C.W., Connexins and cell signaling in development and disease, *Annu. Rev. Cell Dev. Biol.* **20**, 811–838 (2004).
- Yeager, M. and Harris, A.L., Gap junction channel structure in the early 21st century: facts and fantasies, *Curr. Opin. Cell Biol.* **19**, 521–528 (2007).
- Channel-Forming Proteins**
- Gouaux, J.E., Channel-forming toxins: Tales of transformation, *Curr. Opin. Struct. Biol.* **7**, 566–573 (1997).
- Song, L., Hobaugh, M.R., Shustak, C., Chesley, S., Bayley, H., and Gouaux, J.E., Structure of staphylococcal α -hemolysin, a heptameric transmembrane pore, *Science* **274**, 1859–1866 (1996).
- Lipid Asymmetry in Membranes**
- Devaux, P.E., Protein involvement in transmembrane lipid asymmetry, *Annu. Rev. Biophys. Biomol. Struct.* **21**, 417–439 (1992).
- Op den Kamp, J.A.F., Lipid asymmetry in membranes, *Annu. Rev. Biochem.* **48**, 47–71 (1979).
- Wirtz, K.W.A., Phospholipid transfer proteins, *Annu. Rev. Biochem.* **60**, 73–99 (1991).
- Secretory Pathway**
- Alberts, B., Johnson, A., Lewis, J., Raff, M., Roberts, K., and Walter, P., *The Molecular Biology of the Cell* (5th ed.), Chapter. 12, Garland Science (2008).
- Alder, N.N. and Johnson, A.E., Cotranslational protein biogenesis at the endoplasmic reticulum, *J. Biol. Chem.* **279**, 22787–22790 (2004).
- Bowie, J.U., Solving the membrane protein folding problem, *Nature* **438**, 581–589 (2005).
- Cross, B.C.S., Sinning, I., Luirink, J., and High, S., Delivering proteins for export from the cytosol, *Nature Rev. Mol. Cell Biol.* **10**, 255–264 (2009).
- Doudna, J.A. and Batey, R.T., Structural insights into the signal recognition particle, *Annu. Rev. Biochem.* **73**, 539–557 (2004).
- Dowhan, W. and Bogdanov, M., Lipid-dependent membrane protein topogenesis, *Annu. Rev. Biochem.* **78**, 515–540 (2009).
- Driessen, A.J.M. and Nouwen, N., Protein translocation across the bacterial cytoplasmic membrane, *Annu. Rev. Biochem.* **77**, 643–667 (2008).
- Fewell, S.W., Travers, K.J., Weissman, J.S., and Brodsky, J.L., The action of molecular chaperones in the early secretory pathway, *Annu. Rev. Genet.* **35**, 149–191 (2001).
- Halic, M., Becker, T., Pool, M.R., Spahn, C.M.T., Grassucci, R.A., Frank, J., and Beckmann, R., Structure of the signal recognition particle interacting with the elongation-arrested ribosome, *Nature* **427**, 808–814 (2004).
- Halic, M. and Beckmann, R., The signal recognition particle and its interaction during protein targeting, *Curr. Opin. Struct. Biol.* **15**, 116–125 (2005).
- Halic, M., Gartmann, M., Schlenker, O., Mielke, T., Pool, M.R., Sinning, I., and Beckmann, R., Signal recognition particle receptor exposes the ribosomal translocon binding site, *Science* **312**, 745–747 (2006).
- Hegde, R.S. and Bernstein, H.D., The surprising complexity of signal sequences, *Trends Biochem. Sci.* **31**, 563–571 (2006).
- Kornfield, S. and Sly, W.S., I-cell disease and pseudo-Hurler polydystrophy disorders of liposomal enzyme phosphorylation and localization, Chapter 138 in Valle, D. (Ed.), *The Online Metabolic & Molecular Bases of Inherited Disease*, <http://ommbid.com/>.
- Lippincott-Schwartz, J., Roberts, R.H., and Hirschberg, K., Secretory protein trafficking and organelle dynamics in living cells, *Annu. Rev. Cell Dev. Biol.* **16**, 557–589 (2000).
- Lodish, H., Berk, A., Kaiser, K.A., Krieger, M., Scott, M.P., Bretscher, A., Ploegh, H., and Matsudaira, P., *Molecular Cell Biology* (6th ed.), Chapter 13, Freeman (2008).
- Ménétret, J.-F., Hegde, R.S., Aguiar, M., Gygi, S.P., Park, E., Rapoport, T.A., and Akey, C.W., Single copies of Sec61 and TRAP associate with a nontranslating mammalian ribosome, *Structure* **16**, 1126–1137 (2008). [A cryo-EM study.]
- Osborne, A.R., Rapaport, T.A., and van den Berg, B., Protein translocation by the Sec61/SecY channel, *Annu. Rev. Cell Dev. Biol.* **21**, 529–550 (2005).
- Rapoport, T., Protein translocation across the eukaryotic endoplasmic reticulum and bacterial plasma membranes, *Nature* **450**, 663–669 (2007).
- Schaffitzel, C., Oswald, M., Berger, I., Ishikawa, T., Abrahams, J.P., Koerten, H.K., Koning, R.I., and Ban, N., Structure of the *E. coli* signal recognition particle bound to a translating ribosome, *Nature* **444**, 503–505 (2006).
- van den Berg, B., Clemons, W.M., Jr., Collinson, I., Modis, Y., Hartmann, E., Harrison, S.C., and Rapoport, T.A., X-ray structure of a protein-conducting channel, *Nature* **427**, 36–44 (2004). [The X-ray structure of SecY.]
- von Heijne, G., Membrane-protein topology, *Nature Rev. Mol. Cell Biol.* **7**, 909–917 (2006).
- Wickner, W. and Schekman, R., Protein translocation across biological membranes, *Science* **310**, 1452–1456 (2005).
- Coated Vesicles**
- Brodsky, F.M., Chen, C.-Y., Knuehl, C., Towler, M.C., and Wakeham, D.E., Biological basket weaving: Formation and function

- of clathrin-coated vesicles, *Annu. Rev. Cell Dev. Biol.* **17**, 515–568 (2001).
- Collins, B.M., McCoy, A.J., Kent, H.M., Evans, P.R., and Owen, D.J., Molecular architecture and functional model of the endocytotic AP2 complex, *Cell* **109**, 523–535 (2002).
- Donaldson, J.G. and Lippincott-Schwartz, J., Sorting and signaling at the Golgi complex, *Cell* **101**, 693–696 (2000).
- D'Souza-Schorey, C. and Chavrier, P., ARF proteins: roles in membrane traffic and beyond. *Nature Rev. Mol. Cell Biol.* **7**, 347–358 (2006).
- Edeling, M.A., Smith, C., and Owen, D., Life of a clathrin coat: insights from clathrin and AP structures, *Nature Rev. Mol. Cell Biol.* **7**, 32–44 (2006).
- Evans, P.R. and Owen, D.J., Endocytosis and vesicle trafficking, *Curr. Opin. Struct. Biol.* **12**, 814–821 (2002).
- Fath, S., Mancius, J.D., Bi, X., and Goldberg, J., Structure and organization of coat proteins in the COPII cage, *Cell* **129**, 1325–1336 (2007).
- Fotin, A., Cheng, Y., Grigorieff, N., Harrison, S.C., Kirchhausen, T., and Walz, T., Molecular model for a complete clathrin lattice from electron cryomicroscopy; and Structure of an auxilin-bound clathrin coat and its implications for the mechanism of uncoating, *Nature* **432**, 573–579 and 649–643 (2004).
- Gürkan, C., Stagg, S.M., LaPointe, and Balch, W.E., The COPII cage: unifying principles of vesicle coat assembly, *Nature Rev. Mol. Cell Biol.* **7**, 727–738 (2006); and Stagg, S.M., LaPointe, and Balch, W.E., Structural design of cage and coat scaffolds that direct membrane traffic, *Curr. Opin. Struct. Biol.* **17**, 221–228 (2007).
- Heymann, J.B., Iwasaki, K., Yim, Y.-I., Chang, N., Belnap, D.M., Greene, L.E., Eisenberg, E., and Steven, A.C., Visualization of the binding of Hsc70 ATPase to clathrin baskets, *J. Biol. Chem.* **280**, 7156–7161 (2005).
- Hinshaw, J.E., Dynamin and its role in membrane fusion, *Annu. Rev. Cell Dev. Biol.* **16**, 483–519 (2000).
- Kirchhausen, T., Clathrin, *Annu. Rev. Biochem.* **69**, 699–727 (2000).
- Lodish, H., Berk, A., Kaiser, K.A., Krieger, M., Scott, M.P., Bretscher, A., Ploegh, H., and Matsudaira, P., *Molecular Cell Biology* (6th ed.), Chapter 14, Freeman (2008).
- McNiven, M.A., Cao, H., Pitts, K.R., and Yoon, Y., The dynamin family of mechanoenzymes: Pinching in new places, *Trends Biochem. Sci.* **25**, 115–120 (2000).
- McNiven, M.A., and Thompson, H.M., Vesicle formation at the plasma membrane and trans-Golgi network: the same but different, *Science* **313**, 1591–1594 (2006).
- Neufeld, E.F., Lysosomal storage diseases, *Annu. Rev. Biochem.* **60**, 257–280 (1991).
- Owen, D.J., Collins, B.M., and Evans, P.R., Adaptors for clathrin coats: structure and function, *Annu. Rev. Cell Dev. Biol.* **20**, 151–191 (2004).
- Pelham, H.R.B., Maturation of Golgi cisterna directly observed, *Trends Biochem. Sci.* **31**, 601–604 (2006).
- Pfeffer, S.R., Unsolved mysteries in membrane traffic, *Annu. Rev. Biochem.* **76**, 629–645 (2007).
- Robinson, M.S., Adaptable adaptors for coated vesicles, *Trends Cell Biol.* **14**, 167–174 (2004).
- Roth, M.G., Snapshots of ARF1: Implications for mechanisms of activation and inactivation, *Cell* **97**, 149–152 (1999).
- Stagg, S.M., Gürkan, C., Fowler, D.M., LaPointe, P., Foss, T.R., Potter, C.S., Carragher, B., and Balch, W.E., Structure of the Sec13/31 COPII coat cage, *Nature* **439**, 234–238 (2006); and Stagg, S.M., LaPointe, P., Razvi, A., Gürkan, C., Foss, T.R., Potter, C.S., Carragher, B., and Balch, W.E., Structural bases for cargo regulation of COPII coat assembly, *Cell* **134**, 474–484 (2008).
- ter Haar, E., Musacchio, A., Harrison, S.C., and Kirchhausen, T., Atomic structure of clathrin: A β propeller terminal domain joins an α zigzag linker, *Cell* **95**, 563–573 (1998).
- Traub, L.M., Ticket to ride: selecting cargo for clathrin-regulated internalization, *Nature Rev. Mol. Cell Biol.* **10**, 583–596 (2009).
- Ybe, J.A., Brodsky, F.M., Hofmann, K., Lin, K., Liu, S.-H., Chen, L., Earnest, T.N., Fletterick, R.J., and Hwang, P.K., Clathrin self-assembly is mediated by a tandemly repeated superhelix, *Nature* **399**, 371–375 (1999). [The X-ray structure of the clathrin heavy chain proximal leg segment.]

Vesicle Fusion

- Alberts, B., Johnson, A., Lewis, J., Raff, M., Roberts, K., and Walter, P., *The Molecular Biology of the Cell* (5th ed.), Chapter 13, Garland Science (2008).
- Bonifacino, J.S. and Glick, B.S., The mechanisms of vesicle budding and fusion, *Cell* **116**, 153–166 (2004). [A historical review.]
- Brunger, A.T., Weninger, K., Bowen, M., and Chu, S., Single-molecule studies of the neuronal SNARE fusion machinery, *Annu. Rev. Biochem.* **78**, 903–928 (2009); and Brünger, A.T., Structure and functions of SNARE and SNARE-interacting proteins, *Q. Rev. Biophys.* **38**, 1–47 (2006).
- Chernomordik, L.V. and Kozlov, M.M., Membrane hemifusion: crossing a chasm in two leaps, *Cell* **123**, 375–382 (2005).
- Doherty, G.J. and McMahon, H.T., Mechanisms of endocytosis, *Annu. Rev. Biochem.* **78**, 857–902 (2009).
- Grosshans, B.L., Ortiz, D., and Novick, P., Rabs and their effectors: Achieving specificity in membrane traffic, *Proc. Natl. Acad. Sci.* **103**, 11821–11827 (2006).
- Hanson, P.I., Roth, R., Morisaki, H., Jahn, R., and Heuser, J.E., Structure and conformational changes in NSF and its membrane receptor complexes visualized by quick freeze/deep etch electron microscopy, *Cell* **90**, 523–535 (1997).
- Jahn, R. and Scheller, R.H., SNAREs—engines for membrane fusion, *Nature Rev. Mol. Cell Biol.* **7**, 631–643 (2006).
- Martens, S., and McMahon, H.T., Mechanism of membrane fusion: disparate players and common principles, *Nature Rev. Mol. Cell Biol.* **9**, 543–556 (2008).
- May, A.P., Whiteheart, S.W., and Weis, W.I., Unraveling the mechanism of the vesicle transport ATPase NSF, the *N*-ethylmaleimide-sensitive factor, *J. Biol. Chem.* **276**, 21991–21994 (2001).
- Mayer, A., Membrane fusion in eukaryotic cells, *Annu. Rev. Cell Dev. Biol.* **18**, 289–314 (2002).
- McNew, J.A., Parlati, F., Fukuda, R., Johnston, R.J., Paz, K., Paumet, F., Söllner, T.H., and Rothman, J.E., Compartmental specificity of cellular membrane fusion encoded in SNARE proteins, *Nature* **407**, 153–159 (2000).
- Misura, K.M.S., Scheller, R.H., and Weis, W.I., Three-dimensional structure of the neuronal-Sec1–syntaxin 1a complex, *Nature* **404**, 355–362 (2000).
- Montecucco, C., Schiavo, G., and Pantano, S., SNARE complexes and neuroexocytosis: how many, how close? *Trends Biochem. Sci.* **30**, 368–372 (2005).
- Niemann, H., Blasi, J., and Jahn, R., Clostridial neurotoxins: New tools for dissecting exocytosis, *Trends Cell Biol.* **4**, 179–185 (1994).
- Stenmark, H., Rab GTPases as coordinators of vesicle traffic, *Nature Rev. Mol. Cell Biol.* **10**, 513–525 (2009).
- Sutton, R.B., Fasshauer, D., Jahn, R., and Brünger, A.T., Crystal structure of a SNARE complex involved in synaptic exocytosis at 2.4 Å resolution, *Nature* **395**, 347–353 (1998).
- Ungermann, C. and Langosch, D., Function of SNAREs in intracellular membrane fusion and lipid bilyaer mixing, *J. Cell Sci.* **118**, 3819–3828 (2005).

- Yu, R.C., Hanson, P.I., Jahn, R., and Brünger, A.T., Structure of the ATP-dependent oligomerization domain of *N*-ethylmaleimide sensitive factor complexed with ATP, *Nature Struct. Biol.* **5**, 803–810 (1998); and Lenzen, C.U., Steinmann, D., Whiteheart, S.W., and Weis, W.I., Crystal structure of the hexamerization domain of *N*-ethylmaleimide-sensitive fusion protein, *Cell* **94**, 525–536 (1998).
- Zerial, M. and McBride, H., Rab proteins as membrane organizers, *Nature Rev. Mol. Cell Biol.* **2**, 107–119 (2001).
- Mitochondrial and Nuclear Protein Targeting**
- Abe, Y., Shodai, T., Muto, T., Mihara, K., Torii, H., Nishikawa, S., Endo, T., and Kohda, D., Structural basis of presequence recognition by the mitochondrial protein import receptor Tom20, *Cell* **100**, 551–560 (2000). [An NMR structure.]
- Ahting, U., Thun, C., Hegerl, R., Typke, D., Nargang, F.E., Neupert, W., and Nussberger, S., The TOM core complex: The general protein import pore of the outer membrane of mitochondria, *J. Cell Biol.* **147**, 959–968 (1999). [An electron microscopy study of the TOM core complex.]
- Bolender, N., Sickmann, A., Wagner, R., Meisinger, C., and Pfanner, N., Multiple pathways for sorting mitochondrial precursor proteins, *EMBO Rep.* **9**, 42–49 (2008).
- de Marcos-Lousa, C., Sideris, D.P., and Tokatlidis, K., Translocation of mitochondrial inner-membrane proteins: conformation matters, *Trends Biochem. Sci.* **31**, 259–267 (2006).
- Dolezal, P., Likic, V., Tachezy, J., and Lithgow, T., Evolution of the molecular machines for protein import into mitochondria, *Science* **313**, 314–318 (2006).
- Neupert, W. and Herrmann, J.M., Translocation of proteins into mitochondria, *Annu. Rev. Biochem.* **76**, 723–749 (2007).
- Lipoproteins**
- Beglova, N. and Blacklow, S.C., The LDL receptor: how acid pulls the trigger, *Trends Biochem. Sci.* **30**, 309–316 (2005).
- Berglund, L. and Ramakrishnan, R., Lipoprotein(a). An elusive cardiovascular risk factor, *Arterioscler. Thromb. Vasc. Biol.* **24**, 2219–2226 (2004).
- Borhani, D.W., Rogers, D.P., Engler, J.A., and Brouillette, C.G., Crystal structure of truncated human apolipoprotein A-I suggests a lipid-bound conformation, *Proc. Natl. Acad. Sci.* **94**, 12291–12296 (1997).
- Brown, M.S. and Goldstein, J.L., A receptor-mediated pathway for cholesterol homeostasis, *Science* **232**, 34–47 (1986). [A Nobel prize address.]
- Brown, M.S. and Goldstein, J.L., Koch's postulates for cholesterol, *Cell* **71**, 187–188 (1992).
- Gent, J. and Braakman, I., Low-density lipoprotein receptor structure and folding, *Cell Mol. Life Sci.* **61**, 2461–2470 (2004).
- Krieger, M., Charting the fate of the “good cholesterol”: Identification and characterization of the high-density lipoprotein receptor SR-BI, *Annu. Rev. Biochem.* **68**, 523–558 (1999).
- Lawn, R.M., Wade, D.P., Hammer, R.E., Chiesa, G., Verstuyft, J.G., and Rubin, E.M., Atherogenesis in transgenic mice expressing human apolipoprotein(a), *Nature* **360**, 670–672 (1992).
- Marotti, K.R., Castle, C.K., Boyle, T.P., Lin, A.H., Murray, R.W., and Melchior, G.W., Severe atherosclerosis in transgenic mice expressing simian cholesteryl ester transfer protein, *Nature* **364**, 73–75 (1993).
- Parthasarathy, S., Steinberg, D., and Witztum, J.L., The role of oxidized low-density lipoproteins in the pathogenesis of atherosclerosis, *Annu. Rev. Med.* **43**, 219–225 (1992).
- Rudenko, G., Henry, L., Henderson, K., Ichtchenko, K., Brown, M.S., Goldstein, J.L., and Deisenhofer, J., Structure of the LDL receptor extracellular domain at endosomal pH, *Science* **298**, 2353–2358 (2002); and Rudenko, G. and Deisenhofer, J., The low-density lipoprotein receptor: ligands, debates, and lore, *Curr. Opin. Struct. Biol.* **13**, 683–689 (2003).
- Valle, D. (Ed.), Part 12, Lipids, *The Online Metabolic & Molecular Bases of Inherited Disease*, <http://www.ommbid.com/>.
- Steinberg, D., Low density lipoprotein oxidation and its pathobiological significance, *J. Biol. Chem.* **272**, 20963–20966 (1997).
- Weisgraber, K.H. and Mahley, R.W., Human apolipoprotein E: The Alzheimer's disease connection, *FASEB J.* **10**, 1485–1493 (1996).
- Zhong, N. and Weisgraber, K. H., Understanding the association of apolipoprotein E4 with Alzheimer disease: clues from its structure, *J. Biol. Chem.* **284**, 6027–6031 (2009).

PROBLEMS

1. Explain the difference in melting points between *trans*-oleic acid (44.5°C) and *cis*-oleic acid (13.4°C).
2. Why do animals that live in cold climates generally have more polyunsaturated fatty acid residues in their fats than do animals that live in warm climates?
- *3. How many different isomers of phosphatidylserine, triacylglycerol, and cardiolipin can be made from four types of fatty acids?
4. Estimate the thickness of the surface layer formed by Benjamin Franklin's teaspoon of oil on Clapham pond (1 teaspoon = 5 mL and 1 acre = 4047 m²).
5. “Hard water” contains a relatively high concentration of Ca²⁺. Explain why soap is ineffective for washing in hard water.
6. Explain why pure hydrocarbons do not form monolayers on water.
7. Soap bubbles are inside-out bilayers; that is, the polar head groups of the amphiphiles, together with some water, are in apposition, whereas their hydrophobic tails extend into the air. Explain the physical basis of this phenomenon.
8. Describe the action of detergents in extracting integral proteins from membranes. How do they keep these proteins from precipitating? Why do mild detergents such as Triton X-100 bind only to proteins that form lipid complexes?
- *9. Is the transmembrane portion of glycophorin A (Fig. 12-21) α helical (use the Chou and Fasman rules; Section 9-3Aa)?
10. The symmetries of oligomeric integral proteins are constrained by the requirement that their subunits must all have the same orientation with respect to the plane of the membrane. What symmetries can these proteins have? Explain. (Protein symmetry is discussed in Section 8-5B.)
11. (a) How many residues must an α helix contain in order to span the 30-Å-thick hydrocarbon core of a lipid bilayer? (b) How many residues in a β sheet are required to span this bilayer core if it is inclined by 30° with respect to the normal to the membrane

plane? (c) Why do most transmembrane α helices and β strands have more than these minimum numbers?

12. Explain why antibodies against type A blood group antigens are inhibited by *N*-acetylgalactosamine, whereas anti-B antibodies are inhibited by galactose.

13. (a) Individuals with a certain one of the ABO blood types are said to be “universal donors,” whereas those with another type are said to be “universal recipients.” What are these blood types? Explain. (b) Antibodies are contained in blood plasma, which is blood with its red and white cells removed. Indicate the various compatibilities of blood plasma from an individual with one ABO blood type with an individual with a different ABO blood type. (c) Considering the answers to Parts a and b, why is it possible that there can be a universal donor and a universal recipient for a transfusion of whole blood?

14. Anti-H antibodies are not normally found in human blood. They may, however, be elicited in animals by the injection of human blood. How would such antibodies be expected to react with tissues from individuals with type A, type B, and type O blood groups?

15. *Thermus aquaticus* is a thermophilic bacterium that grows between the temperatures of 50 and 80°C. Although the signal peptide binding groove of its Ffh M domain is lined with hydrophobic groups, only three of them are Met side chains. In contrast, the binding grooves of mesophilic organisms (those that live at normal temperatures) are lined with numerous Met side chains (11 in *E. coli*). In addition, one wall of the binding groove is disordered in the X-ray structure of the *E. coli* M domain but ordered in that of *T. aquaticus* (both proteins were crystallized at room temperature). Suggest a reason for these evolutionary adaptations in *T. aquaticus*.

16. Influenza virus neuraminidase (Section 33-4Bd) is a type II protein in which three Arg residues are located just before the N-terminal end of its signal-anchor sequence. What is the likely effect of mutating all of these Arg residues to Glu?

***17.** In a genetically distinct form of familial hypercholesterolemia, LDL binds to the cell surface but fails to be internalized by endocytosis. Electron microscopy reveals that each mutant cell has its normal complement of coated pits but that ferritin-conjugated LDL does not bind to them. Rather, the bound LDL is uniformly distributed about the noncoated regions of the cell surfaces. Apparently the binding properties of the mutant LDL receptors are normal but they are in the wrong place. What do these data suggest about how LDL receptor is assembled into coated pits?

18. Table 12-6 indicates that the densities of lipoproteins increase as their particle diameters decrease. Explain.

19. Certain types of animal viruses form by budding out from a cell surface much like coated pits bud into the cytoplasm during endocytosis to form coated vesicles. In both cases, the membranous vesicles form on a polyhedral protein scaffolding. Sketch the budding of an animal virus and indicate the location of its membrane relative to its protein shell.

20. Why aren't chylomicrons taken up by LDL receptors?

21. Wolman's disease is a rapidly fatal homozygous defect characterized by a severe deficiency in **cholesteryl ester hydrolase**, the enzyme that catalyzes the hydrolysis of intracellularly located cholesteryl esters. Describe the microscopic appearance of the cells of victims of Wolman's disease.